University of Siena

DEPARTMENT OF BIOTECHNOLOGY, CHEMISTRY AND PHARMACY

PhD in Chemical and Pharmaceutical Sciences

Ciclo XXXIV

Coordinator: Prof. Maurizio Taddei

New reactions and substrates for orthogonal bioconjugation

Supervisor: Prof. Maurizio Taddei

CHIM/06 – Organic chemistry

PhD student: Elena Ermini

ANNO ACCADEMICO 2020/2021

Abstract

The search for new and more efficient ligand-targeted drugs is always a challenge to overcome the side effects of therapeutic treatments. In these systems, a stimuli sensitive linker plays a crucial role for stability under physiological conditions and for selective release.

Such structures are commonly used both for prodrug design and in more complex systems such as ADCs, where each component needs to be optimised for its therapeutic purpose and biological target. Several cleavable linkers can be found in the literature, but the main criticism of these molecules is the limited range of functional groups that can be bonded to them. Here we present the synthesis of novel self-immolative spacers that have demonstrated their generality in releasing of a wide range of functional groups using the NO_2 group as a trigger. This group provides selectivity for the hypoxic environment and/or for the enzyme nitroreductase, which is over-expressed under hypoxic conditions such as in solid tumour cells and in bacterially infected tissues, and whose activity drives the reduction of aromatic nitro moieties. The developed systems have also been applied to construct ADCs. In addition, two novel photosensitive scaffolds for the development of photolabile protecting groups (PPGs) are discussed and investigated through computational chemistry.

Contents

List of abbreviations

ADC	antibody-drug conjugates
ADEPT	antibody-directed enzyme prodrug therapy
Ala	alanine
AML	acute myeloid leukaemia
API	active pharmaceutical ingredients
Arg	arginine
Asn	asparagine
ATP	adenosine triphosphate
AzAbs	azide antibodies
Boc	*tert*-butoxycarbonyl
BODIPY	boro-dipyrromethane
bs	broad singlet
CBS	Corey-Bakshi-Shibata
Cbz	carboxybenzyl
CD	Crohn's disease
CDC	complement-dependent cytotoxicity
CDI	1,1'-carbonyldiimidazole
cH	heavy-chain constant
Cit	citrulline
CM1	calicheamicin γ1
COS	carbonyl sulfide
CPT	camptothecin
Cys	cysteine
CuAAC	copper(I)-catalyzed azide-alkyne cycloaddition
DAR	drug-to-antibody ratio
DABCO	1,4-Diazabicyclo[2.2.2]octane

DBU	1,8-diazabicyclo[5.4.0]undec-7-ene
DCC	*N*,*N*'-dicyclohexylcarbodiimide
d	doublet
dd	doublet of doublets
dq	doublet of quartets
ddd	doublet of doublets of doublets
DDQ	2,3-dichloro-5,6-dicyano-1,4-benzoquinone
dddd	doublet of doublets of doublets of doublets
DEA	diethylamine
DFT	density functional theory
DIAD	diisopropyl azodicarboxylate
DIPA	diisopropylamine
DIP-Cl	β-chlorodiisopinocampheylborane
DIPEA	*N*,*N*-diisopropylethylamine
DPPA	diphenylphosphoryl azide
DLL3	delta-like protein
DM1	mertansine
DMA	dimethylacetamide
DMAP	4-dimethylaminopyridine
DME	dimethoxyethane
DMF	dimethylformamide
DMSO	dimethyl sulfoxide
DNA	deoxyribonucleic acid
DTT	dithiothreitol
EDC	1-ethyl-3-(3-dimethylaminopropyl)carbodiimide
EGFR	epidermal growth factor receptor
EMA	European Medicines Agency

Fab	antigen-binding fragment
Fc	fragment constant
FDA	Food and Drug Administration
FRET	Förster Resonance Energy Transfer
FULC	frequency upon-conversion luminescence
GDEPT	gene-directed enzyme prodrug therapy
Glu	glutamic acid
Gly	glycine
GPNMB	glycoprotein NMB
GSH	reduced glutathione
HAT	histone acetyltransferase
HDAC	histone deacetylase
HDLP	histone deacetylase-like protein
HER2	human epidermal growth factor receptor 2
HOBt	hydroxybenzotriazole
HPLC	high-performance liquid chromatography
ICT	intramolecular charge transfer
IEDDA	inverse-electron-demand Diels-Alder
IgG	immunoglobulin G
IR	infrared
ISC	intersystem crossing
KI	kinase inhibitors
LD_{50}	median lethal dose
Leu	leucine
LG	leaving group
LR	linear respons
Lys	lysine

m	multiplet
mAbs	monoclonal antibodies
MAC	methylene-alkoxy carbamate
MALDI	matrix-assisted laser desorption/ionization
MBC	metastatic breast cancer
MBH	Morita-Baylis-Hillman
MC	maleidocaproic acid
MDR1	multidrug resistance protein 1
MEL	melanoma
MMAE	monomethyl auristatin E
MMAF	monomethyl auristatin F
MS	mass spectroscopy
MSLN	mesothelin
MT	melatonin
NAD	nicotinamide adenine dinucleotide
NAMPT	nicotinamide phosphoribosyltransferase
NBS	*N*-bromosuccinimide
NfkB	Escherichia Coli nitroreductase
NHS	*N*-hydroxysuccinimide
NKA	Na^+/K^+-ATPase
NMR	nuclear magnetic resonance
NSCLC	non-small cell lung cancer
NTR	nitroreductase
PABA	*p*-aminobenzyl alcohol
PABQ	*p*-aminobenzyl quaternary ammonium salt
PBS	phosphate-buffered saline
PC4'AP	photocaged C4'-oxidized abasic site

PD-1	programmed cell death protein 1
PDB	pyrrolobenzodiazepins
PDT	photodynamic therapy
PEG	polyethylene glycol
PET	photoinduced electron transfer
PG	protecting group
PGA	Penicillin-G-amidase
Phe	phenylalanine
PPG	photolable protecting group
Pro	proline
q	quartet
RNS	reactive nitrogen species
ROS	reactive oxygen species
NPs	nanoparticles
Rf	retention factor
RT	retention time
s	singlet
S1P	s phingosine-1-phosphate
SAHA	vorinostat, suberanilohydroxamic acid
SCLC	small-cell lung cancer
SCN	suprachiasmatic nucleus
SIS	self immolative spacer
SMCC	succinimidyl-4-(*N*-maleimidomethyl)cyclohexane-1-carboxylate
SMDC	small molecule-drug conjugates
SPAAC	strain-promoted azide-alkyne cycloaddition
SS	state specific
t	triplet

TBAB	*N*-tetrabutylammonium bromide
TBAF	*N*-tetrabutylammonium fluoride
TCO	*trans*-cyclooctene
TEA	triethylamine
TD-DFT	time dependent DFT
THF	tetrahydrofuran
Thr	threonine
TKI	thirosin chinase inhibitors
TLC	thin-layer chromatography
TMS	tetramethylsilane
TNBC	triple-negative breast cancer
tRNA	transfer ribonucleic acid
Trp	tryptophan
TTET	triplet-triplet energy transfer
Tyr	tyrosine
US	United States
UV/Vis	ultraviolet-visible spectroscopy
Val	valine
VEGF	vascular endothelial growth factor
vH	heavy-chain variable
vL	light-chain variable
XC	exchange correlation
ZBG	Zinc bounding group

Chapter I

General Overview

1.1 Antibody drug conjugate – briefly introduction

Antibody-drug conjugates (ADCs) are systems developed for the selective release of drugs that take advantage of the selectivity of monoclonal antibodies. In these systems, the recombinant monoclonal antibodies (mAbs) are bound to cytotoxic small molecule drugs through linkers, leading to an increase in selectivity and stability and giving a favorable pharmacokinetic profile to highly cytotoxic molecules. The development of ADCs began in the 1960s in animal models and the first clinical trials were conducted in the 1980s.[1]

During the last twenty years, more than 100 ADCs have been tested in clinical trials, and most of them have recently left phase I and entered phase II. In order for these ADCs to be useful drug delivery systems, they need to fulfil some characteristics, including high binding specificity and affinity, good internalisation rate and stable binding with the payload.[2] All these properties are required to reduce the side effects of cytotoxic drugs, many of which are intended for oncology indications[3], but the toxicity of ADC remains an important issue. Mylotarg® can be used as an example, a humanised antibody conjugate to calicheamicin, which was approved by the FDA in 2000 for the treatment of acute myeloid leukaemia.[4] This treatment was withdrawn from the market in 2010 after phase III results showed toxicity comparable to standard therapies, making its use of no longer interest.[5] To overcome this problem and increase the therapeutic potential, great efforts have been made to implement the different components of these systems, such as the target, the linker, the payload and the conjugation chemistry.[6]

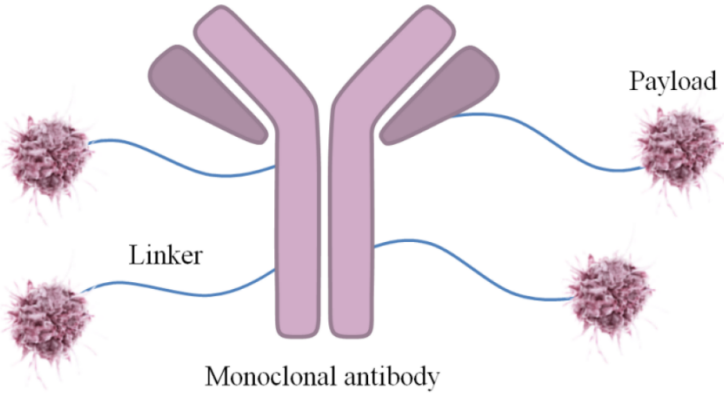

Figure 1: General structure of antibody-drug conjugate

The structure of an antibody-drug conjugate must be designed with the target of interest in mind. This involves not only the specific antigens that must be expressed on the cell, but also the choice of trigger to release the payload from the linker and how to bind the drug to the linker.

The payload must have peculiar properties to be employed in ADC systems. It must show very high potency (0.1 nM - 1 pM), stable in the bloodstream and during storage; it must be soluble, have a low immunogenic effect and have functional groups that can be used to bind the linker moiety. Many drugs failed as payloads because of their instability under hypoxic conditions, such as mitoxantrone and doxorubicin.[7] They must be highly toxic to destroy the majority of tumour cells, even with a minimal payload, since the antibody cannot carry many cytotoxic molecules and the rate at which mAb reaches and internalises cancer cells is quite low (less than 0.08% of the injection dose).[8] The hydrophobicity of the compound is another important property to consider. Extreme hydrophobicity may lead to aggregation during conjugation or alter the biological properties of the antibody, as its domain surface has a hydrophilic character.[9] However, high hydrophilicity can also be problematic for desolvation and transfer from aqueous media to protein binding sites, although increasing hydrophilicity may be associated with metabolic stability, less non-specific off-target effects and good solubility.[10] A look at cytotoxic drugs

currently used in ADC systems shows that they generally affect DNA synthesis or cell division.

An important and widely used class of drugs are the HDAC inhibitors, which is discussed in detail in this chapter and used in this thesis.

Last but not least, the literature reports many different types of linkers, which are essential for the development of ADC systems.

1.2 Linkers

Because of the important roles this structure has, special attention must be paid to the development of new linkers. The general structure requires two binding sites, one for the drug and one for conjugation with the antibody, possibly a self-immolating spacer, a moiety that allows the release of the drug after rearrangement, and a covalent bond that can be broken after internalisation inside the target cells and/or under certain conditions to trigger release of the payload as the drug. System stability is also critical to avoid uncontrolled release of the drug and thus undesirable systemic toxicity. In addition, the hydrophobicity of the linker is related to aggregation with the antibody and may affect pharmacokinetic parameters leading to potential side effects. Good linker polarity can compensate for the hydrophobic nature of the payload and allow optimisation of ADCs.[11] Therefore, it is an ongoing challenge to develop linkers with an optimal balance between appropriate stability and efficient cleavage. It is also an interesting area where much work remains to be done to obtain linkers that are useful for different targets.

Linkers are normally classified as:

- *Cleavable*: In this class we find linkers designed to release the payload after cleavage of the covalent bond triggered by a protease reaction, glutathione reduction or acidic conditions. They may be labile under extracellular or intracellular conditions. Release in the extracellular tumour microenvironment has the disadvantage of lower cell selectivity and off-target release. On the other hand, this could provide a bystander effect and increase the therapeutic efficacy

of the system. The bystander effect means that tumour cells that have or do not have the antigen on their surface or are too far from the vessel to be reached by ADC can also be killed. If the release occurs in the extracellular microenvironment of the tumour, endocytosis of the system is not required, which means that a wider range of antigens can be considered as targets. The same effect could be achieved if the payload is a small drug that can diffuse out of the cell due to its high membrane permeability.[12] However, most cleavable linkers focus on the traditional mechanism of action involving internalisation of the system prior to release of the cytotoxic payload.

They are divided into enzymatically cleavable linkers and chemically cleavable linkers.[13] The enzymatically cleavable class is the most advanced. It includes several structures that are substrates for several enzymes over-regulated in cancer cells, such as cathepsin B (the most commonly used)[14], lysosomal sulphatase enzymes[15], β-Galactosidase[16] and β-Glucuronidase[17,18]. These structures have good plasma stability and the great advantage that their release mechanism is well known. They can have very different structures, but the most popular are peptide-based linkers.

Chemically cleavable linkers have a labile bond that can be broken in different chemical environments. They are usually sensitive to reductive or acidic conditions and in some cases can release the drug into tumour tissue without internalising the system. Their structure is more versatile and can be greatly modified as they do not need to match the catalytic site of enzymes, but unfortunately they are associated with low plasma stability. This type of linker has led to the first clinical successes in this field: Pfizer's (Mylotargs,) gemtuzumab ozogamicin ADC (Figure 2), a system with a hybrid linker using a reducible disulphide and an acid-sensitive hydrazone. Release occurs at a pH of 4.5 by hydrolysis of the N-acylhydrazone moiety to the hydrazide payload structure.[19]

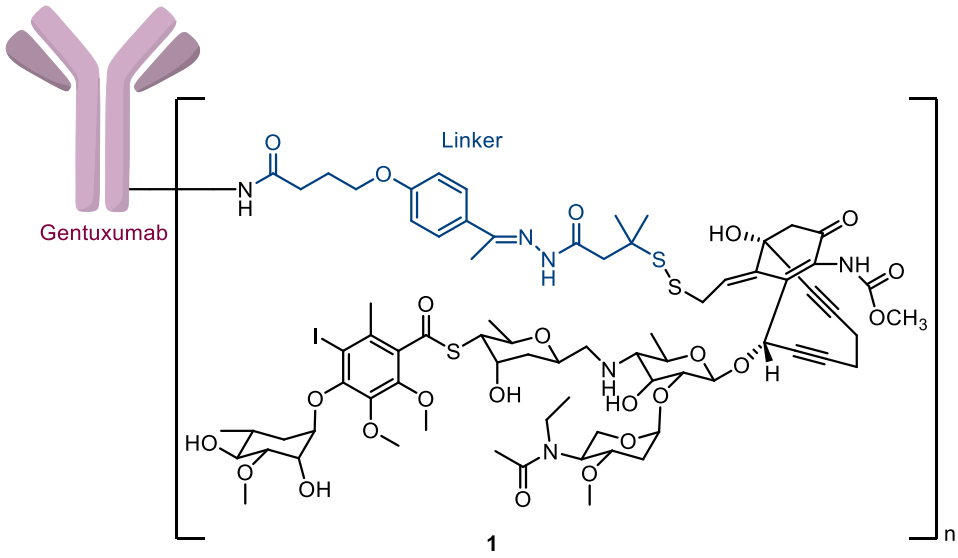

Figure 2: Pfizer's gemtuzumab ozogamicin (Mylotargs) ADC.[20]

Another interesting example was recently reported by Raabe and co-workers. They have managed to develop a ADC system with a new pH-sensitive and oxidation-sensitive linker.[21]

In summary, we can say that this class of molecules is usually preferred over non-cleavable linkers because their release mechanism is known and allows clearer preliminary studies. Nevertheless, they have raised more and more stability issues and off-target toxicities. However, to overcome this weakness, many efforts are being made to modify their structure.

- *Non-cleavable*: this type of linker requires internalisation of the system by endocytosis and complete degradation of the antibody within the lysosome to release the payload. In contrast to the discussion above on cleavable linkers, the main advantage of these structures is their high stability in human plasma and lower release of the drug at off-target sites, resulting in a low probability of damage to healthy cells. This also results in the loss of the bystander effect on neighboring tumour cells that we have with the other class. These linkers can be used to develop new systems to overcome multiple-drug resistance (MDR),

where tumour cells develop cross-resistance to multiple cytotoxic drugs. Many mechanisms of MDR have been reported, but the most common is overexpression of the P-glycoprotein (MDR1). Two mechanisms are known for resistance mediated by this protein. The first involves inhibition of drug efflux diffusing from the extracellular space into the plasma membrane, and the second involves extrusion of the drug outside the cell.[22] Therefore, rational design of linker-drug systems may result in free toxic payloads that are not substrates of MDR1. Cleavable linkers might avoid the first MDR1-mediated resistance mechanism, but once the linker-drug bond is cleaved, the drug may be subject to the second resistance mechanism. This problem might not occur with non-cleavable linkers, as the cytotoxic drug can remain bound to an amino acid residue via the linker after degradation in lysozyme, which does not affect its pharmaceutical activity.[23,24]

Most commonly, these linkers are used in cancers with high antigen expression because of their release mechanism. Their structure is usually based on a succinimide thioether group, which can be obtained by Michael addition from a thiol on maleimides. Proposed release mechanisms include a retro-Michael reaction, thiol exchange of the thioether succinimide in response to thiol-containing environments, or complete degradation of the antibody and release of the linker-drug moiety as a cytotoxic payload.[25,26] Examples include the thioether linker succinimidyl-4-(*N*-maleimidomethyl)cyclohexane-1-carboxylate linked to DM1, the drug, (SMCC– DM1), maleimidocaproic acid linked to MMAF (mc–MMAF) and linkers based on the *p*-mercaptobenzyl alcohol structure.[27,28]

Both cleavable and non-cleavable linkers are used in approved second- and third-generation ADCs, which are currently being investigated in clinical trials. In summary, rational design of the linker structure based on the target of interest and the drug to be delivered can help overcome many of the limitations that ADC systems have.

1.3 Self immolative spacers

Sometimes, when a drug release system or a prodrug is rationally designed for the selective delivery of highly cytotoxic payload, a spacer is inserted between the releasing trigger and the drug. For example, when either the protecting group or the drug itself has a high steric hindrance, or the covalent bond between them is particularly stable, complications in activating the complex can occur, resulting in poor drug release. One strategy to overcome this limitation is to synthetise a tripartite molecule with a self-immolative spacer (SIS) between the protecting group (PG) and the drug.[29] (Scheme 1)

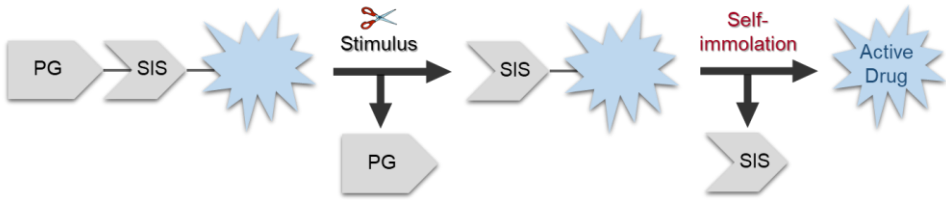

Scheme 1: general structure of prodrugs containing a self-immolative spacer.

In literature several self-immolative spacers have been reported and, since their appearance in 1981, their applications grow continuously. Several applications in pharmaceutical chemistry have been reported for the development of prodrugs[30–38], drug delivery systems (like ADC)[39–44] and sensors for enzymes.[45–47]

These systems can undergo to different immolation mechanisms depending on the structure of the spacer. The self-immolation must take place under defined physiological conditions, which is why the self-immolative spacers are masked in the molecule and are only activated by an endogenous or exogenous stimulus.

The first step requires activation of the system by the appropriate signal which causes the removal of the protective group. Once the protective group is removed, a series of intramolecular reactions are triggered leading to the release of the active compound. There are two types of self-immolation processes depending on the structure of the spacer: the first is based on electronic delocalisation, the second on

cyclization. In both cases, we start with a structure containing the inactive self-immolative spacer and we get the formation of a nucleophile, such as an amine, a thiol, or a hydroxyl group, which triggers the self-immolation process releasing of the active compound.

There are different types of stimuli, some of them similar to those previously discussed for the linkers:

- *Chemical*: most chemical triggers are associated with pH variation, which is an excellent stimulus to control drug release in various parts of the organism. Extracellular acidity is a key feature of many solid tumours and can be exploited to synthesise pH-dependent prodrugs.

  Groups sensitive to redox environments are also widely used, not only the common disulphide bridge but also the nitro group has been broadly employed to develop prodrugs sensitive to hypoxic conditions. The allyloxy and allylamino groups can also be removed by reducing agent containing metal, like $[Pd(PPh_3)_4]/NaBH_4$, $[Pd(PPh_3)_4]/(Bu)_3SnH$, $[PdCl_2(PPh_3)_2]/KBH_4$.[29]

  Many examples have been reported in the literature and there is no need to discuss them extensively as several reviews have been published recently.[48]

- *Enzymatic*: the classes of triggers that are substrate of enzymes for the self-immolative spacers are like the one discussed above for the linkers, and the enzymes used as targets are the same since they are the ones that provide selectivity for cancer cells. The most important family of enzymes used for the deprotection of prodrugs that need to be mentioned are the bacterial enzymes. As particular example, we find Penicillin-G-amidase (PGA), a microorganism's enzyme that have amide or ester as substrates. Several examples exploiting this enzyme have been reported, one of the most recent was developed by Redy and Shabat in 2012.[49] (Figure 3) They developed a new prodrug with a phenylacetamide moiety as the enzyme substrate, a self-immolative linker bearing a pair of FRET dyes and camptothecin as payload. Upon cleavage by PGA, self-immolation via cascade takes place followed by spontaneous decarboxylation, which ultimately delivers the free amino-aniline group of the

linker. Another self-immolative elimination leads to the release of the active drug and dye molecules that can be detected by their emitted fluorescent signal.

- *Photochemical*: photochemical activation is very appealing since it allows for the degradation of the spacer by an (remote) external stimulus. A precise temporal control is possible. Its application and examples are discussed in more detail in the dedicated chapter of this thesis.

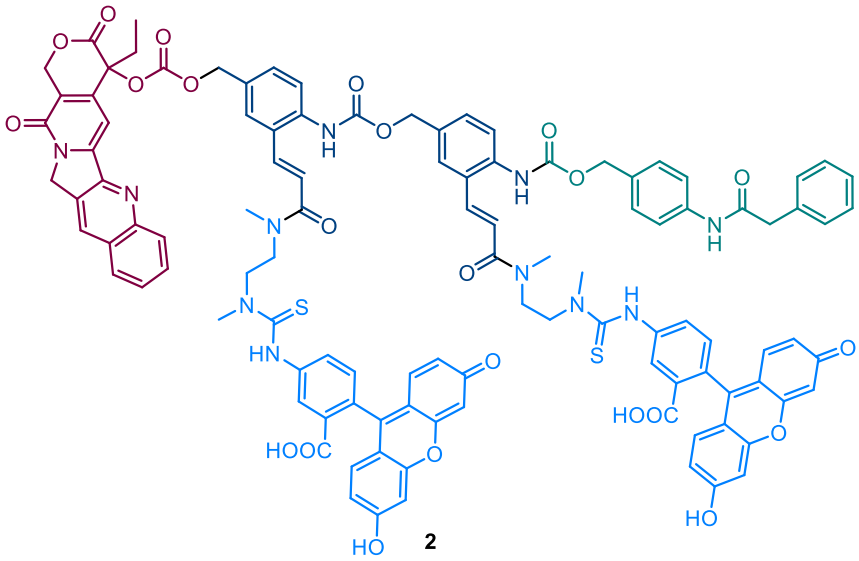

Figure 3: prodrug developed by Redy and Shabat.[49]

1.3.1 Self-immolative mechanisms:

The self-immolation mechanisms can involve elimination by electronic delocalisation or intramolecular cyclization, in both of which the reaction is spontaneous and irreversible. The speed of the process is structure-dependent, as well as being dependent on the trigger used and the reaction environment.

In the first case, the molecule has an aromatic ring with a nucleophilic group protected in *ortho* or *para* position to the group that have to be released. After activation, the nucleophile initiates the electronic cascade that dismantles the molecule leading to

the free drug. The mechanism of self immolation by electronic delocalisation involve a 1-4, 1-6 or 1-8 elimination and it is driven by an increase in entropy.

Examples of these systems are quite common and most of them are based on *p*-aminobenzyl alcohol (PABA) where the aromatic core and the masked nucleophile is an amine, a hydroxyl or a thiol group. Thus, after removal of the protecting moiety, these molecules form quinone or azaquinone methide as intermediates and carbon dioxide.

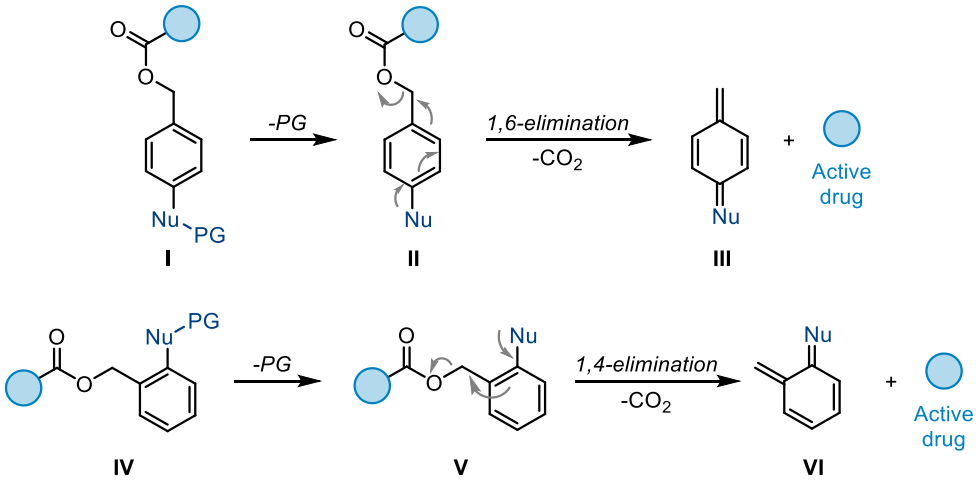

Scheme 2: self-immolative elimination mechanisms.

It has been demostrated that 1,8-elimination can only occur in *para*-amino (or hydroxy) cinnamyl alcohol or coumarinyl alcohol spacers.[50,51] However, due to its synthetic simplicity, the most widely used system is the PABA-based spacers, especially for common functional groups such as carboxylic acids, amines, acidic phenols and alcohols. Substituents in the aromatic ring may affect the elimination rate: electron-withdrawing group can destabilise the transient positive charge formed at the benzylic position during the elimination by inducing a drop in the electron density on the aromatic ring, resulting in a decrease in the rate of release. On the other hand, electron-donating group can have the opposite effect, facilitate the dearomatisation and increase the release rate.[52,53] The functional group used to link the drug to the specer also plays an important role, it must be a good leaving group

otherwise the intermediate with the free nucleophile will be too stable to release the active compound. For this reason, many functional groups cannot be used in the development of new prodrugs or delivery systems, most of which are not suitable for the release from the common PABA-like self-immolative spacer, and this has prompted the study of new structures that could generate less stable intermediates and consequently be used in this area.

Another key parameter is the nature of the aromatic ring, which determines the distance between the trigger and the leaving group, reducing, if necessary, the steric hindrance and favouring enzymatic cleavage. It may also contain heteroatoms that change the electronic distribution and decrease the aromaticity of the nucleus, which changes the rate of release. This has been reported for pyridine that has a lower resonance energy (142 kJ/mol) than benzene (about 150 kJ/mol).[54] Indeed, the decrease in resonance energy should accelerate the electronic cascade due to the dearomatisation involved in the mechanism but, in structures where the nitrogen is close to the benzylic position, the release may also be faster due to changes in electronic density on the benzyl carbon carrying the leaving group. A similar trend has also been observed in aromatic hydrocarbon compounds, wherein release from the phenanthrene spacer is five times faster than the naphthalene spacer, which is 10 times faster than the benzene spacer.[55]

The second self-immolation mechanism is an intramolecular cyclization that takes place when the protecting group is removed and the nucleophile can react with an electron-poor group within the structure, usually a carbonyl. The driving force of the reaction is the thermodynamically favoured formation of 5- and 6-membered rings.[56] An aliphatic amine is commonly used as a nucleophilic trigger due to its high nucleophilicity, and it can be masked as a carbamate and activated by enzymatic hydrolysis.

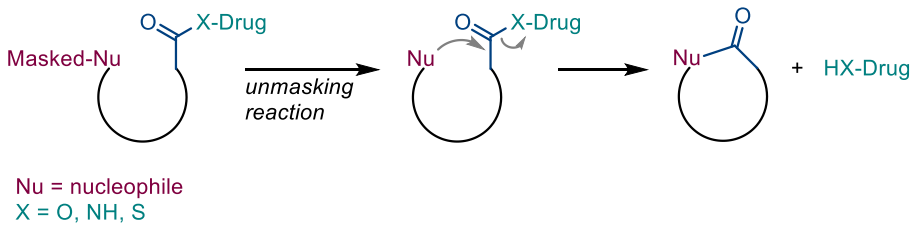

Scheme 3: intramolecular cyclization.

Self-immolative spacers that undergo elimination by cyclization may be made of:

- A linker with an alkyl chain
- A mono- or di-substituted *ortho* aromatic spacer.

For these systems, the conformational aspects and electrophilicity/nucleophilicity of the groups are very important for the kinetics of the process and, compared with elimination by electronic rearrangement, cyclization normally occurs with a slower kinetics. As with the previous series, the use of substituted carbamates/carbonates can influence the reaction rate. Furthermore, the insertion of the methyl group on the amine can increase its nucleophilicity and mono and di-substitutions at the α position in the alkyl chain can improve the reaction kinetics through the effect of angular compression (Thorpe-Ingold effect) and reactive rotameric effects.[57]
Self-immolative spacers involving alkyl chains are quite common in ADCs, while no current examples containing the *ortho*-substituted aromatic spacer are found in clinical trial phases.

1.3.2 Release of different functional groups

As mentioned, the nature of the functional group to be released influences the structure of the self immolative spacer that can be used. For this reason, different spacer structures have been developed and classified according to the payload of interest.

In this thesis, systems for which the release mechanism has not yet been elucidated are not discussed.

1.3.2.1 Self immolative spacers for releasing amino groups

The release of aliphatic or aromatic amines can be achieved by binding the nitrogen through a carbamate.[58,59] These amines, together with alcohols, are the functional group most commonly used to bind the payload to the spacer structure.

An example can be found in Adcetris (brentuximab vedotin), an ADC in which the antibody is bound to the drug via a cleavable cathepsin B substrate linker and a self-immolating spacer, based on *para*-amino benzyl alcohol. The release of the monomethyl auristatin payload, following internalization of the system, begins with the cleavage of the citrulline-*p*-hydroxymethyl aniline amide bond to generate the free aniline nucleophile, which undergoes a self-immolative 1,6-elimination and allows the formation of the active compound.[60,61]

In 2015, Genentech scientists developed an ADC with a rifamycin derivative as a payload that is bound via the amine group to the self-immolative spacer. The immolative mechanism is again the 1,6-elimination forming quinone intermediate.[62] Other examples of the same spacer were reported by Dubowchik in 2002[63] and Tiberghien in 2016[64], but several other can also be found in the literature.[65–67] A similar drug delivery system was developed with Mitomycin C (MMC) as payload in the work of Amitay and co-workers,[68] where they synthesised a lipid-based prodrug consisting of a lipophilic anchor bound via a dithiobenzyl bridge to MMC.

Recently, Staben *et al*. published a new protocol to bind tertiary and heteroaryl amines to the spacer for carrier drug delivery applications. They reported how this functional group is widely present in active pharmaceutical compounds and how the corresponding quaternary ammonium salt can be easily synthesised. Activation of the benzyl alcohol to a suitable leaving group is necessary to enable an efficient S_N2 displacement with tertiary-amine-containing drugs.[69]

In 2015, a novel anticancer prodrug activated by thiols with a mechlorethamine was published. In this case a 2,4-dinitrobenzenesulfonyl derivative was applied since it was shown that the phenyl sulfide bond can be cleaved by GSH efficiently. (Scheme 4)[70]

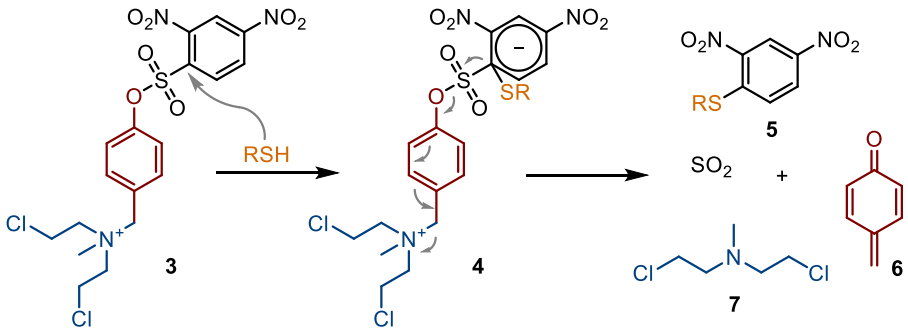

Scheme 4: release mechanism of 2,4-dinitrobensenesulfonyl prodrug.

Other reports with similar systems containing sulfonyl spacer for the release of amines or aliphatic and aryl alcohols can also be found in the literature, for example the self immolative linker published by Park *et al*. has *ortho*-hydroxy-protected aryl sulfate, that releases the drug by a concerted mechanism. The process starts with a cyclization by the deprotected phenol, followed by an electronic rearrangement resulting in elimination.[71]

An interesting ADC system with a drug containing a heterocyclic nitrogen, a highly potent cytotoxic pyrrolobenzodiazepine (PBD)-dimer, was reported by the group of Dragovich.[72] They successfully developed an ADC system in which one of the imines was masked as a carbamate group with a linker containing a disulfide bridge. The unmasked mechanism begins with the reductive cleavage of the disulfide bond and the free thiol leads to self-immolation through an electronic rearrangement with the formation of the free drug. A similar release mechanism for the same drug, reported by Pillow and coworkers[73], also contained a disulphide bridge in the spacer, although it relied on a different release mechanism. In this case, the imine-containing cycle is reformed after intramolecular cyclization, leading to the release of the active compound.[74]

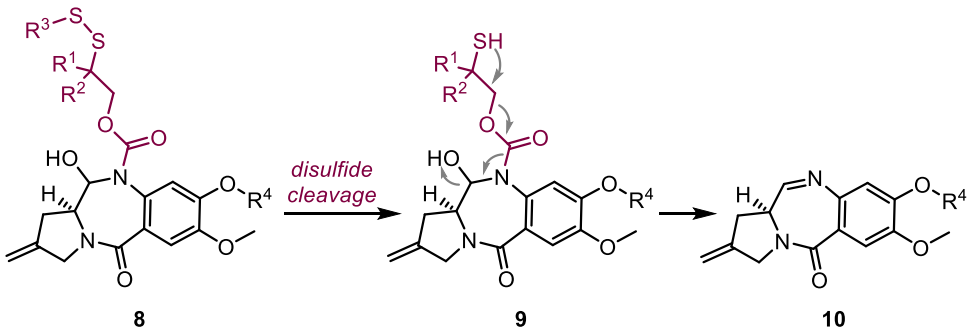

Scheme 5: self immolative mechanism of pyrrolobenzodiazepine (PBD)-dimer ADC.[72]

Additional examples exploiting the mechanism of intramolecular cyclization can be found, since the amide bond required to link the drug to the spacer is stable under physiological conditions.[75,76] An explanatory work combining the two mechanisms was published by Azoulay *et al*. They developed a self-immolative dendrimer prodrugs with a Staudinger linker, which involves intramolecular cyclization, followed by a 1,6 elimination, releasing quinone-methide species and Doxorubicin.[77] Finally, an inverse electron-demand Diels–Alder (IEDDA) reactions have been exploited for selective release of amine by Rossini and coworkers.[78] The IEDDA reaction between a doxorubicin-functionalized trans-cyclooctene (TCO) and a tetrazine leads to the formation of 4,5-dihydropyridazine, which usually tautomerize to 1,4-dihydropyridazine. The system, bearing a carbamate in allylic position, is prone to CO_2 and drug elimination via electronic cascade mechanism. Following this work, the same mechanism was applied later to release alcohols by Davies *et al*.[79]

1.3.2.2 Self immolative spacers for releasing carboxylic acids

This functional group are widely used for the construction of prodrugs due to the easy hydrolysis of the corresponding ester in cellular environment. As payload in drug delivery system with self immolative spacers, release of the carboxyl moiety can be achieved only through electronic rearrangement and elimination. In the work of Riber

and coworkers,[80] they studied disulfide linkers and self-immolative mechanisms triggered by the free thiol for several functional groups, among which are the carboxylic acids.

Additionally, few examples are reported for they use in *para*-amino benzyl based linkers due to the high instability of the corresponding benzyl ester in human plasma.[81–83] However, this group is suitable for design new prodrugs or for polymeric delivery systems.[84–86]

1.3.2.3 Self immolative spacers for releasing hydroxyl groups

Aliphatic alcohols are broadly common functional groups in active pharmaceutical compounds and widely studied as a binding site for delivery systems. In most examples, they are used in linkers together with a disulfide bridge that, upon reduction, can generate the free thiol as a nucleophile for the self-immolative intramolecular cyclization. The most commonly used drugs as payloads with this function are doxorubicin, dasatinib, camptothecin and gencitabine, which are highly cytotoxic compounds and can be bound to the spacer via an ester bond.[87–92] The same mechanism, but different trigger, has also been reported for the design of novel prodrugs or as self-immolative linkers.[89,93]

Several examples are also available regarding the elimination mechanism,[94,95] one interesting example, combining the 1,6 and 1,4 elimination for multiple drug delivery, was reported by Shabat, McGrath and Scheeren.[96–99] They developed a synthesis of dendrimers that disassemble into their building blocks via a self-immolative mechanism releasing two or three drug molecules.

Another delivery system that exploits the self-elimination mechanism via a photosensitive trigger is shown in scheme 6. The spacer has a photocaged C4′-oxidized abasic site (PC4AP) as a light-responsive moiety where hydroxyl or amine functional groups can be inserted through a carbonate or carbamate bond and the carrier of the system is a peptide. This prodrug is stable under physiological condition

and the photodecage generates an active species able to react with an amine in the carrier leading to drug release through an addition–elimination cascade.[100]

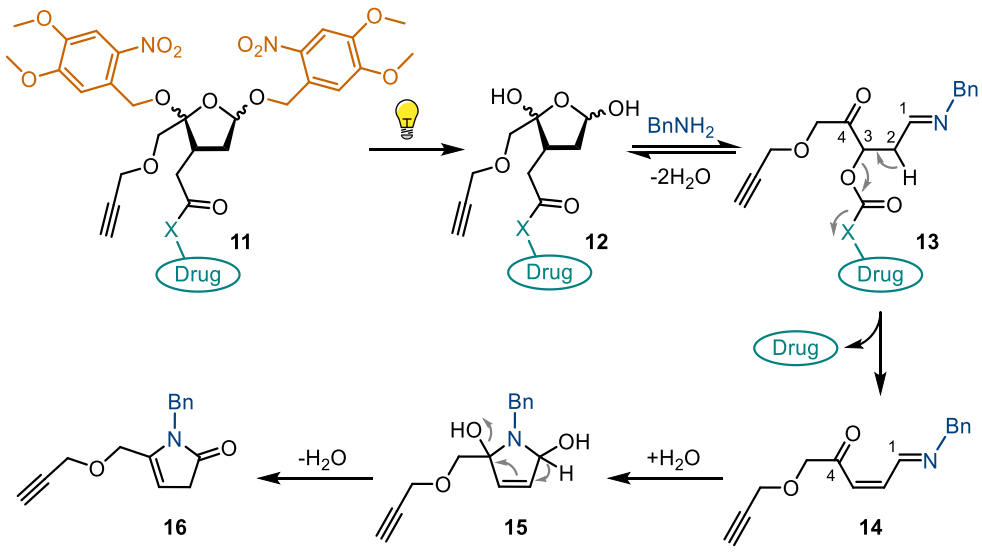

Scheme 6: photorelease of hydroxyl or amine groups (X = NH, O)

All of the examples and mechanisms discussed for the aliphatic alcohols can also be applied to release phenols.[101–104]

Recently, a new phosphorus-based self-immolative linker was synthetised for the delivery of two different drugs. This system was optimised by varying the substituents on the phosphorus atom and in the benzyl position to achieve rapid release of the cargo. Self-immolation is triggered by UV irradiation at 365 nm leading to a free carboxyl function that undergoes intramolecular cyclization on the phosphate group. This step releases the first drug of the system and hydrolysis of the cyclic intermediate leads to the release of the second. Simon and co-workers applied this system to a model phenol.[105]

1.3.2.4 Self immolative spacers for releasing thiols

The release of thiols is still an ongoing challenge as aliphatic thiols cannot be released from self-immolative PABA-like linkers due to the stability of the corresponding free aniline. Normally, the thiol moiety is protected as thioester, which undergoes enzymatic hydrolysis in a cellular environment or as a disulfide bridge that can be cleaved in the presence of glutathion.[106–110]

To the best of our knowledge, only one example has been reported for the release of aliphatic thiols. In 2020, Fernández and coworkers synthetised a library of thioalkyl- and thioarylpyridazinediones that can undergo addition–elimination mechanism in the presence of intracellular GSH to release free thiols. Thus, they investigated the stability and release in presence of high concentrations of GSH of the compounds concluding that the only suitable candidate for further studies was compound **19** bearing two aryl thiols.[111] (Scheme 7)

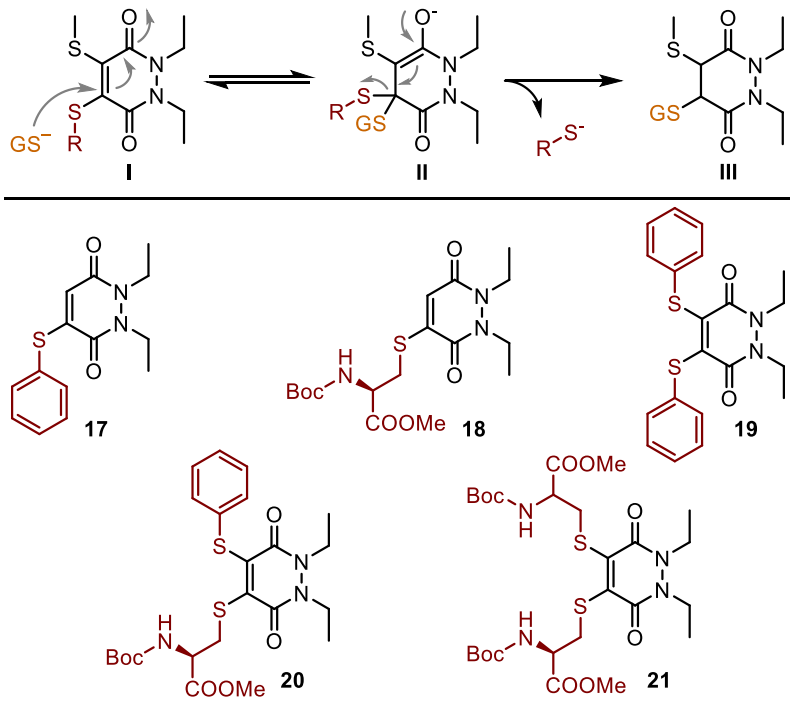

Scheme 7: prodrugs under study for the release of thiols reported by Fernàndez.[111]

Other examples of thiol release with self-immolative linkers involve aryl thiols and some examples of dithiocarbamates. For the release of aryl thiols, Thomson *et al*. studied the release of thiopurines from a linker containing a nitro group as a release trigger. After reduction and formation of the corresponding aniline, the system undergoes an immolative 1,6 elimination mechanism with release of the drug. The study focuses on the influence of the methyl substituents on the benzyl carbon to achieve rapid and efficient release.[112]

For tioguanidines, two different self immolative prodrugs have been reported and both undergo an elimination mechanism to release the active compound, however the spacer's structures and the triggers are different.[113] (Figure 4)

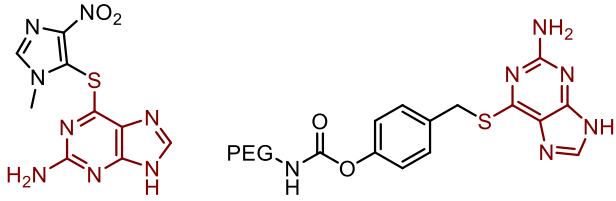

Figure 4

Finally, Franz's group reported a different prodrug bearing a dithiocarbamates bound to a self-immolative *para*-amino benzyl spacer, where release occurs after enzymatic cleavage promoted by γ-glutamyl transferase (GGT).[114,115]

1.3.2.5 Self immolative spacers for releasing uncommon groups

For the less commonly used functional groups in this field, not many examples have been reported, mainly due to the several difficulties encountered to link the self immolative spacers to the group itself. Most of them are suitable for developing efficient and stable prodrugs, like amides[116–122], ketones[123–125], esters[60,126], phosphates[127–129], and so on.

The release of hydroxamic acids cannot be achieved with self-immolative PABA-like system as proven by Cohen and coworkers.[130] However, in different study, they accomplished to develop a system for a HDAC-prodrug of SAHA where the hydroxamic group was directly attached to a thiol-sensitive promoiety. (Figure 5) The stability of the quinone promoiety used against other nucleophiles has been demonstrated, providing a prodrug that can only be activated in the presence of thiols. The release mechanism involves an addition-elimination with electronic rearrangement.[131]

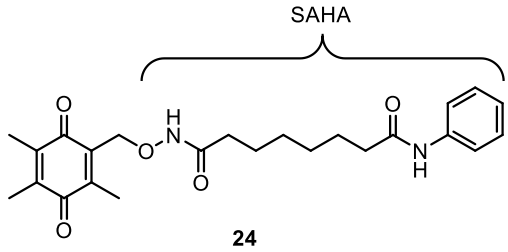

Figure 5: prodrug bearing hydroxamic acid (SAHA)

For the amide group, prodrugs involving a self immolative spacer contain an ester bond which can be broken by esterase enzymes leading to the formation of an unstable N-hydroxy methyl species which undergoes hydrolysis to release the free function.[116,119]

Additionally, Parveen and coworkers studied prodrugs containing heterocyclic system for releasing carboxamide active compound after reduction of a nitro group.[132] H_2S, persulfides (R-SSH) and related sulfur species can be delivered in a controlled way through self-immolative prodrugs. Pluth and Chakrapani implemented a class of dual carbonyl sulfide (COS) / H_2S donors based on a benzyl thiocarbamate structure (R–OC(S)NH–R). The system is based on the reduction of aryl azides that leads to a self-immolative reaction resulting in the release of benzyl thiocarbamate, which is then converted into H_2S in the presence of the enzyme carbonic anhydrase.[133]

Another uncommon system has been developed for the release of hydrazine derivatives via a self-immolating linker taking advantage of a disulphide bridge cleavage and subsequent intramolecular cyclization.[134]

An interesting new immolative system for the release of sulfonate-containing compounds has been investigated. The system is pH-sensitive and is based on Grob fragmentation, which leads to excellent and fast release under basic conditions but is also able to release at physiological pH and in some cases even at acidic pH by controlling the pKa of the pushing group (an amine group).[135]

No many other examples are reported for different functional groups and most of the discussed works have limitations in their application, so finding a new self-immolative spacer that can be applied to a wide range of functional groups is of great interest.

Chapter II

New self-immolative spacers for the release of different functional groups under nitroreductase activation

2.1 Introduction

After the general overview of ADC systems and their different components, in order to better understand how these projects came into being and why they caught our interest, it is important to give a brief introduction of what is reported for nitro-prodrugs, how their activation is selective in cancer cells and the class of drugs in which we are more interested.

2.1.1 The nitroreductase

Nitroreductase (NTRs), which belong to a family of structurally homologous proteins, are cytosolic flavoenzymes that catalyse the reduction of aromatic nitro groups to amines using flavin mononucleotide (FMN) and flavin adenine nucleotide (FAD) as cofactors and NADH or NADPH as coenzymes and electron donors.[136,137]

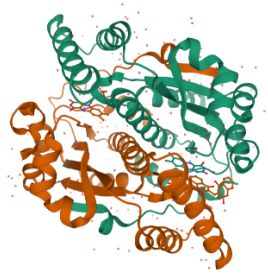

Figure 6: The structure of E. coli nitroreductase bound with the antibiotic nitrofurazone.[138]

Nitroreductase are divided into two subfamilies:

- *Oxygen-insensitive* or *Type I*: these catalyse the reduction by adding a pair of electrons taken from NAD(P)H and, before the formation of the final amine, two intermediates are formed: the hydroxylamine and the nitroso derivative. The

nitroso species cannot be observed due to its instability, but the hydroxylamine could be found in the final molecule instead of the corresponding aniline.

- *Oxygen-sensitive* or *Type II*: these catalyse the reduction by adding a single electron to the nitro group, forming an anion radical that could be re-oxidised in the presence of oxygen resulting in the formation of the superoxide anion, which is why this type can only completely reduce NO_2 in the absence of oxygen.[139–141]

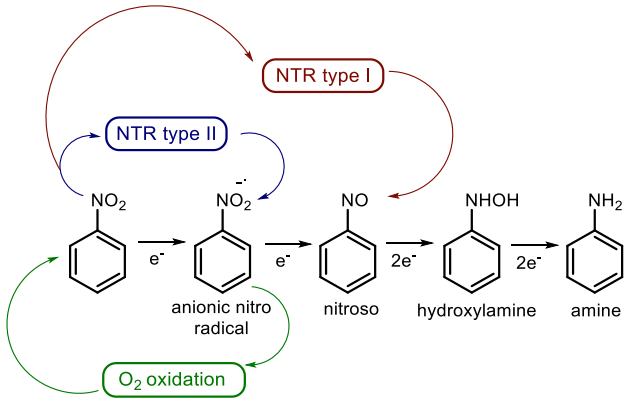

Scheme 8: reduction mechanism of the two types of nitroreductases.[141]

Type I nitroreductase are overexpressed in prokaryotic and eukaryotic cells but only under hypoxic conditions, and consequently in many tumour tissues.

2.1.2 Nitro-prodrugs

Hypoxia is a feature of several diseases. The condition of hypoxia in tumour cells can influence the effectiveness of radiotherapy. Since the work of Gray *et al*[142], in which they hypothesised the importance of oxygen in radiotherapy, many efforts have followed to overcome hypoxia-induced radiotherapy resistance, such as clinical trials of treatment with hyperbaric oxygen and chemical radiosensitizers.[143] Several studies currently demonstrate the hypoxic condition in tumour cells and the relationship between hypoxia and radiotherapy success.

In this field, the nitro group is very versatile and has a strong electron-attracting character which leads to electron-deficient regions in the molecule that may react with strong nucleophiles such as proteins, enzymes, or nucleic acids. This group is present in many drugs such as antibiotics, anticancer drugs, tranquillisers, antifungals, but also in herbicides and pesticides, and is considered an excellent candidate for the synthesis of anticancer prodrugs. Prodrugs with a nitro group in their structure can be applied in the development of 'bioreductive prodrugs', in which nitro aromatic or nitro heteroaromatic groups, precursors of the corresponding anilines, are inserted into the structure. These prodrugs rely for their efficacy on bioreduction to a reactive intermediate.[144]

Two types of prodrugs are possible: the first involves the reduction of a nitro-masking function to generate the bioactive compound, the second is based on the reduction of a nitro-trigger moiety, then releasing the bioactive agent. The latter found applications in the development of drug delivery systems and self-immolative spacers.

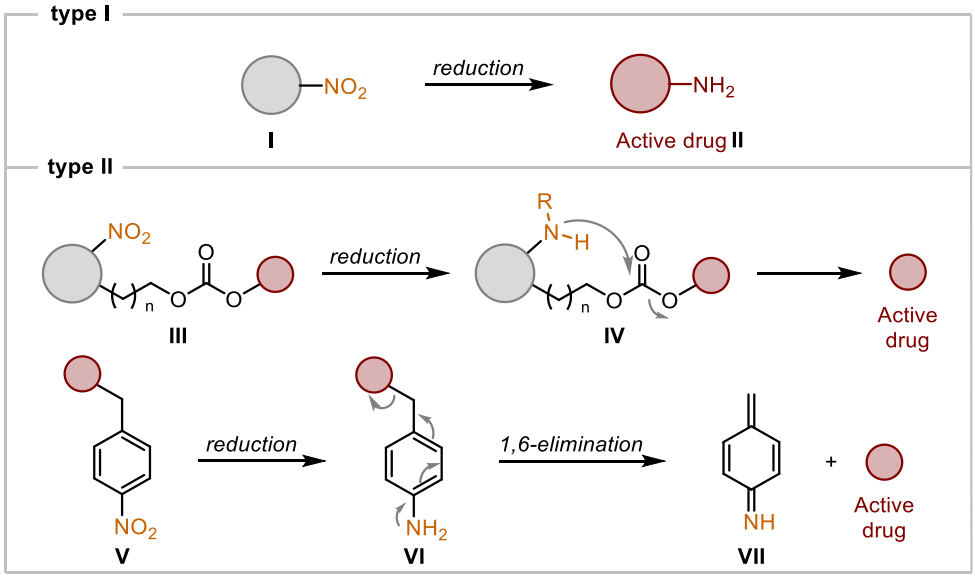

Scheme 9: the two types of nitro containing prodrugs.

These prodrugs gain selectivity for the targeted tissue, due to the hypoxia conditions or for the high level of bioreductive enzymes present in the intracellular environment, if compared to normal tissues. DT-diaphorase (NAD(P)H (quinone acceptor) oxidoreductase), aza-reductase, and nitroreductase are examples of reductive enzymes overexpressed in tumour cells. During the development of a new bioreductive prodrug, it is important to consider the steps in the process: the initial activation, the reactivity of the active intermediate with the biological target, the reactions with oxygen, and finally the consequences in case of the generation of oxidative stress and reactive oxygen radicals (ROS). [145]

The nitro group is widely used for the bioreductive therapy and it is generally reduced by nitroreductase, a family of enzymes whose substrates are compounds with an aromatic nitro group.

An application involving nitro prodrugs and nitroreductase is the development of antibacterials that can only be activated by specific enzymes in bacterial cells. Such prodrugs are often designed to overcome antibiotic resistance, which is frequently due to drug abuse. An important example is the use of this enzyme, more specifically the type I, to release nitric oxide from prodrugs containing the NO_2 functional group.[146,147] Nitric oxide is a potent antimicrobial agent that reacts with oxygen leading to reactive nitrogen species that alkylate DNA. Sharma *et al.* published in 2013 a new prodrug (Figure 7) containing the diazeniumdiolate group as a nitric oxide donor and the nitro group as a trigger for activation in the presence of Escherichia Coli nitroreductase (NfkB). Reduction to amine or hydroxylamine leads to electronic rearrangement and release of the diazeniumdiolate anion and subsequent formation of active nitric oxide.[148]

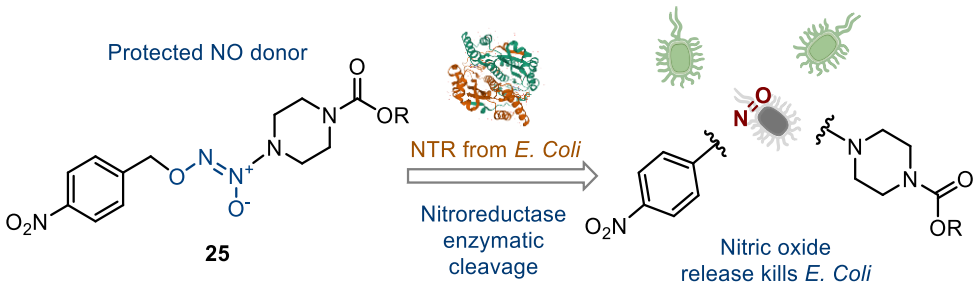

Figure 7: release of nitric oxide from the prodrug developed by Sharma *et al.*[148]

In solid tumours, the hypoxic condition of cells is correlated with tumour progression and recent studies have also shown that the concentration of nitroreductase is directly related to hypoxia. This allows the use of these enzymes as direct biomarkers in tumour diagnosis possible.

An example of biomarker development is the use of fluorescent probes to determine the concentration of nitroreductase in tissue. Fluorescent probes have a fluorophore in the structure, which typically is a positively charged molecule that can be excited and emit fluorescence when irradiated with UV-Vis light. The nitro group, as strong electron withdrawing group, modulates the fluorophore properties of the probe through photoinduced electron transfer (PET) from the excited fluorophore to the nitro group. Nitroreductase, when reducing the NO_2 to an amine, block the photoinduced electron transfer of the molecule. This strategy is also being employed to identify the presence of pathogens in the organism.[137]

Nitroreductase is also the most used enzyme for two different type of therapy involving nitro-prodrugs: the antibody-directed enzyme prodrug therapy (ADEPT) and the gene-directed enzyme prodrug therapy (GDEPT).

These therapies were developed to overcome the problems of prodrugs requiring enzymes not expressed in healthy human cells. These enzymes, when selectively expressed in tumour cells, allow precise release of the drug, resulting in high concentrations of the active molecule even at low dosages.

In ADEPT, the enzyme is bound to an antibody with a covalent bond or through the recombinant DNA technique. This therapy allows the activation of hundreds of molecules by a single enzyme but, if the active drug is a small molecule, it can spread to nearby healthy cells and give side effects. One example is 5-fluorouracil (5-FU), which can pass through molecular membranes by passive diffusion and affect neighbouring cells. Another limitation of ADEPT is the enzyme-antibody immunogenicity, resolved by using the human antibody instead of the murine antibody.

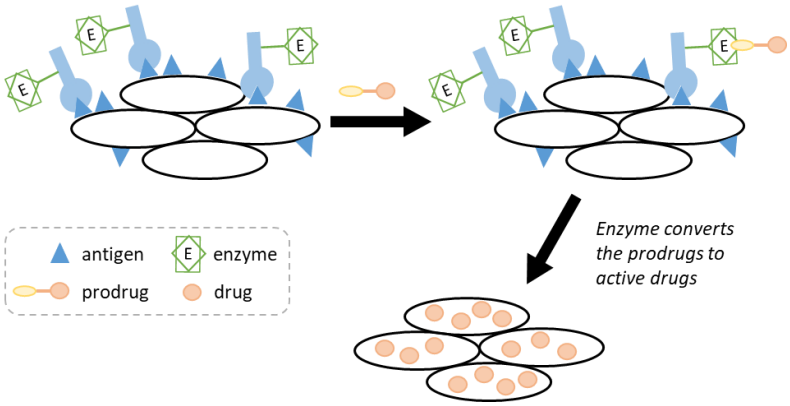

Figure 8: ADEPT mechanism.[149]

The second therapy, GDEPT or VDEPT or GPAT (gene prodrug activation therapy), delivers the gene coding for the enzyme into the tumour cells, followed by administration of the inactive drug. In both ADEPT and GDEPT, a non-endogenous enzyme is used, but the difference lies in the site of activation: in ADEPT the drug is activated outside the cellular environment, while in GDEPT it is activated inside the target cell, since the synthesis of the protein is required.[149]

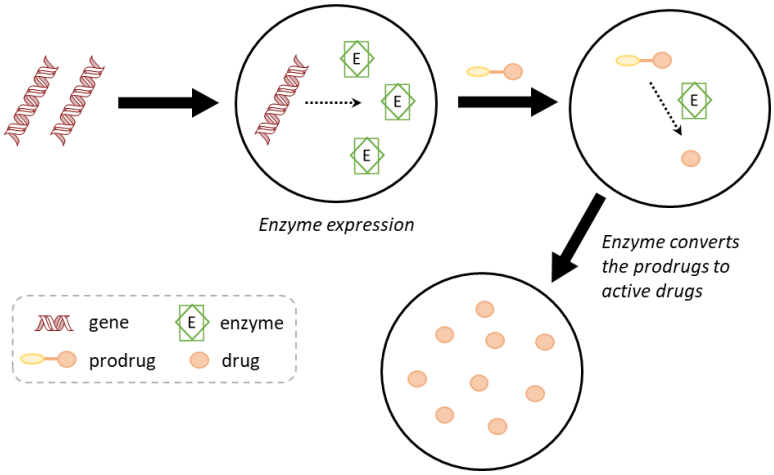

Figure 9: GDEPT mechanism[149]

NTRs are good candidates for EP therapies, especially for GDEPT. The nitro-benzyl alcohol linker is a key promoiety for many drugs such as doxorubicin, mitomycin C and nitrate mustards. Therefore, prodrugs containing the nitro group may be extremely useful not only for the selective presence of the enzyme under hypoxic conditions, but also for co-administration with nitroreductase, leading to high activation/release specificity only in neoplastic cells.

An example is the prodrug containing Paclitaxel bonded to (*E*)-4-nitrostyryl carbonate. (Figure 10) When this system finds the enzyme nitroreductase, the NO_2 is reduced to an anionic radical and subsequently the corresponding amine or hydroxylamine is formed, which undergoes 1,4 elimination releasing the drug. The process can be reverted in the presence of oxygen.[150]

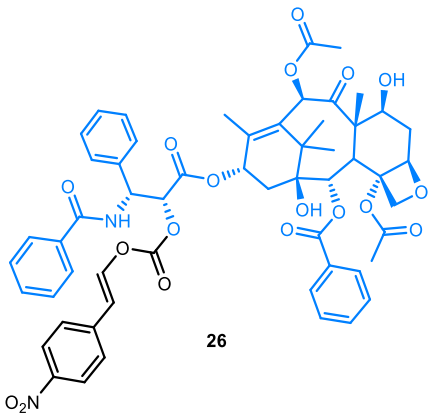

Figure 10: Prodrug of Paclitaxel®

Other examples that take advantage of a different self-immolation mechanism are reported by Ikeda *et al*., who developed two new anticancer prodrugs containing a 2-nitroimidazole moiety as the self-immolating group. The release involves intramolecular cyclization with formation of a six-membered ring and further release of Doxorubicin and Gemcitabine. They found that these systems are selectively activated in hypoxia, leading to reduced adverse effects in normotoxic tissues and improved survival rates in mice.[151]

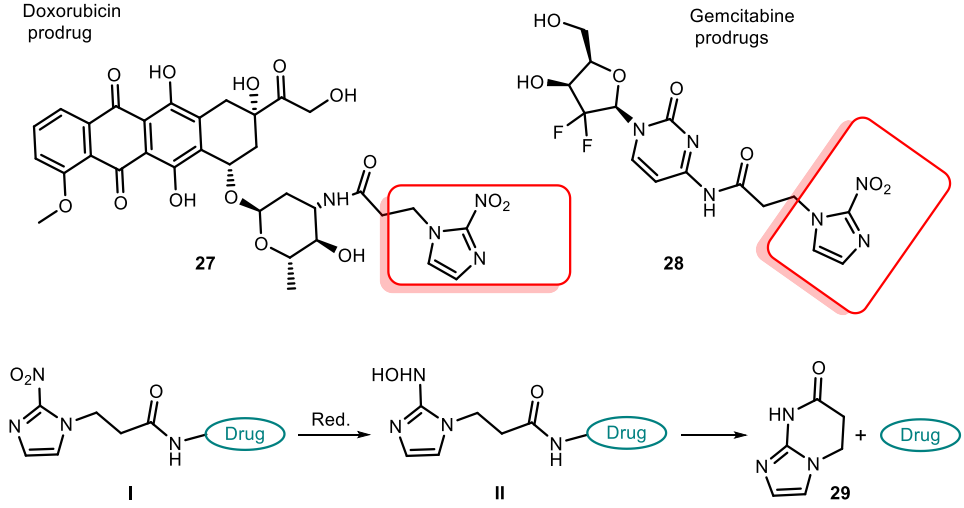

Scheme 10: prodrugs of Doxorubicin and Gencitabine and the release mechanism.

Another important application of self-immolative spacers bearing the NO_2 group was the synthesis of prodrugs inhibiting the enzyme tyrosine kinase, a family of enzymes overexpressed in many tumours. In recent years, several tyrosine kinases inhibiting drugs have been investigated, the majority of which targets the vascular endothelial growth factor receptor (VEGFR) and the epidermal growth factor receptor (EGFR), whose tyrosine residues are phosphorylated, leading to an increase in cell proliferation. Although tyrosine kinase inhibitors have a better therapeutic window than classic chemotherapeutic drugs, several adverse effects are caused by the inhibition of VEGFR and EGFR in healthy organs. In order to reduce the toxicity of these drugs, a study was carried out to see whether it was possible to use tyrosine kinase inhibitor prodrugs under hypoxic conditions.

Sunitinib, a VEFGR inhibitor approved for the treatment of gastrointestinal tumours, and Erlotinib, an EGFR inhibitor approved for the treatment of non-small cell lung cancer (NSCLC), were chosen for this study. The 2-nitroimidazole-5-yl unit was linked as hypoxic trigger through a carbamate linkage on important nitrogen which, if derivatized, should lead to the inactivated compound. For Erlotinib aniline and for Sunitinib the oxindole nitrogen were selected.

Drug release occurs by a 1-6 elimination mechanism after the reduction of the nitro group. In order to further reduce the interaction of the two drugs with tyrosine kinases in healthy tissues, a variant has been synthesised with a second self-immolating spacer *p*-amino benzyl (linked to 2-nitroimidazole by a carbamic bond). In this case, the release involves two steps: the first is the reduction of the nitro group, which undergoes electronic rearrangement, leading to the breaking of the aromatic amine bond; the second is always a 1-6 elimination with subsequent release of the drug.[152]

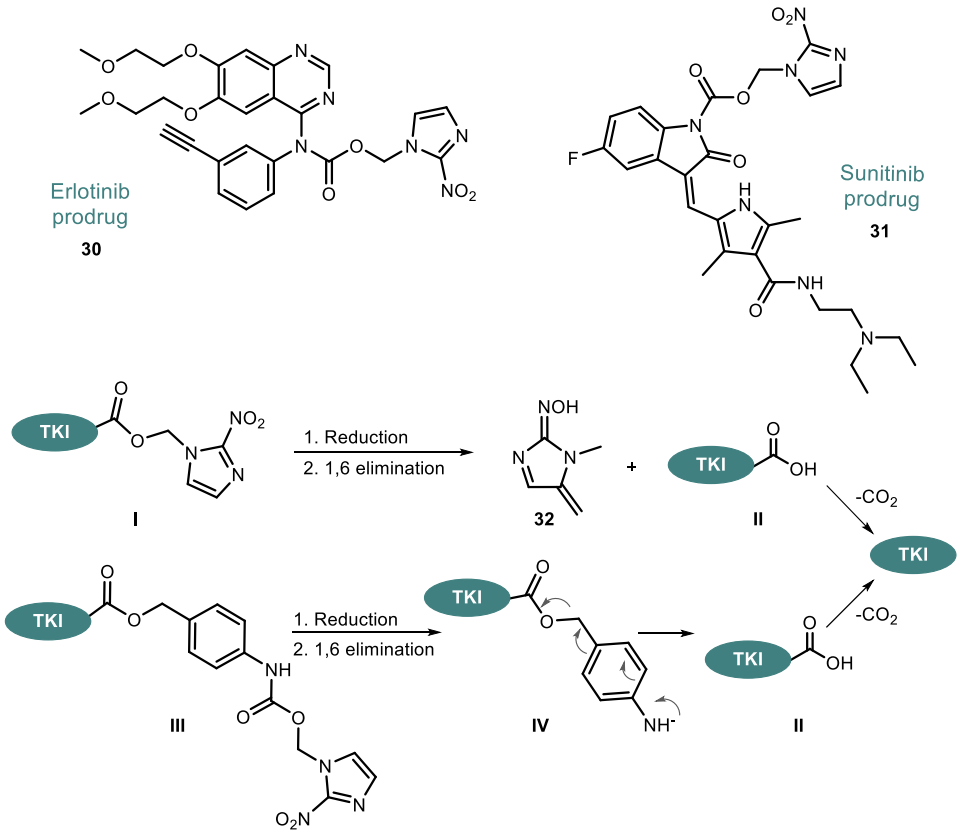

Scheme 11: release mechanisms of the tyrosine kinase inhibiting prodrugs.

2.1.3 HDAC

In eukaryotic cells, the genetic material is enclosed in chromatin, a complex structure of DNA, histone proteins and non-histone proteins, organised in nucleosomes. Each nucleosome is made up of 146 DNA base pairs wrapped around an octamer of histones, which is composed of two H3-H4 dimers and two H2A-H2B dimers. Histones are basic proteins characterised by an apolar central domain with a globular structure and N-terminal and C-terminal regions containing a larger amount of basic amino acids, the most abundant of which are lysine and arginine. The basic N-terminal regions of histones H2A, H2B, H3 and H4 are very flexible, protrude from the nucleosome and are the main sites of interaction with DNA; the non-polar zones

and C-terminal regions are involved in both histone-to-histone and histone-to-DNA interactions.[153]

H1 histones, which wrap around the octamer on the outside, stabilise the final structure through the interaction of their positively charged C-terminal domains with the linker DNA strands that connect one nucleosome to another. Depending on the structure of the nucleosomes, two types of chromatin are distinguished: euchromatin (relaxed), which promotes the entry of transcription factors, and heterochromatin (condensed), which prevents gene transcription processes.[154]

The gene transcription is regulated through the two different chromatin states by enzymes, including histone deacetylase (HDAC) and histone acetyltransferase (HAT), whose substrates are the ε-amino groups of the lysine residues of the N-terminal histone portions. Histone deacetylase removes the acetyl group from histones, which are allowed to interact closely with the negatively charged phosphate groups in the DNA. These interactions give chromatin a compact structure. Acetylation neutralises the charge and the tails are released from the DNA, allowing it to be more accessible for transcription.[155]

Thus, HATs enable gene transcription by acetylating the histone tails, which makes the DNA more approachable to transcription factors. (Scheme 12)

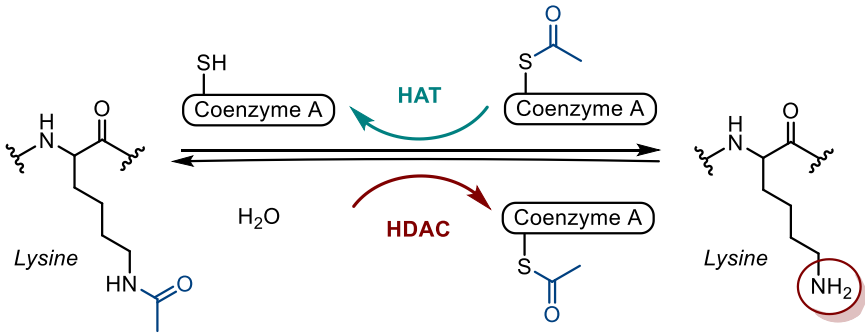

Scheme 12: HDAC and HAT in the transcription regulation.

The enzymatic activity of histone deacetylase was first reported in 1969. In humans, there are four different classes of the enzyme that differ in structure, enzymatic

function and subcellular localisation. Most of these enzymes are zinc proteins, which means they have a Zn^{2+} ion in the catalytic site that is essential for their function.

- Class I: HDAC1, HDAC2, HDAC3 and HDAC8. They are ubiquitous and mainly located in the nucleus where they are involved in cell cycle regulation. Structurally, they retain the deacetylase domain with short amine and carboxyl extensions.
- Class IIa: HDAC4, HDAC5, HDAC7 and HDAC9. They are located in the nucleus and have a domain similar to that of class I but larger than these. They possess large N-terminal extensions with binding sites for the transcription factor MEF2 (family of proteins that regulate gene expression) and the chaperone protein 14-3-3 (family of proteins). These enzymes are mainly expressed in the heart, muscle and brain.
- Class IIb: HDAC6 and HDAC10. HDAC6 acts on cytoskeletal proteins, transmembrane proteins and chaperone proteins. It is characterised by the presence of two domains with deacetylase activity.
- Class III: The mammalian genome also encodes for a further class of deacetylases, the Sirtuins (they show a sequence homologous to the Sir2 protein in yeast), which use the cofactor NAD^+ instead of the Zn^{2+} ion.
- Class IV: HDAC11. It is composed of a deacetylase domain that shows similarities to class I and II and has a small N- and C- terminal extension.[156]

In order to perform their function, these enzymes need to be in the cell nucleus where their substrate is present in high amounts.

The HDAC mechanism of classes I and II is assumed to be the same as the enzyme histone deacetylase-like protein (HDLP), a bacterial enzyme from Aquifex aeolicus whose structure was determined by X-ray in 1999. The crystal structure reveals that HDLP contains a single catalytic domain composed of α and β regions. At the carboxyl ends of the β-filaments there are loops which together with the α-helices, that are not part of the core, are associated with the core structures creating two main 3-D structures: a long, narrow pocket and an inner cavity adjacent to it. The pocket has a tubular shape, the width decreases towards the middle of its length but increases

at the end. The inner walls are structurally composed of hydrophobic and aromatic residues, identical to those of HDAC1. The zinc ion is located at the end of the hydrophobic pocket and is coordinated with Asp168, His170, Asp258 and a water molecule.[157]

The deacetylation mechanism, shown in the scheme 13, begins with nucleophilic attack of the metal-bound water molecule on the carbonyl carbon of the substrate, the acetyl of the lysine of the histone tail, which is made more electron-poor by interactions with the zinc and the phenol of the aminoacid Y306. In addition, the coordination with the metal gives greater nucleophilicity to the water molecule, making the oxygen pair more available. The oxyanion of the tetrahedral intermediate is stabilised by two coordination bonds with the metal cation and a hydrogen bond with the Tyrosine297 hydroxyl moiety. H143 is used as a general acid catalyst to facilitate the breaking of the amide bond and the release of acetate and L-lysine.[157,158]

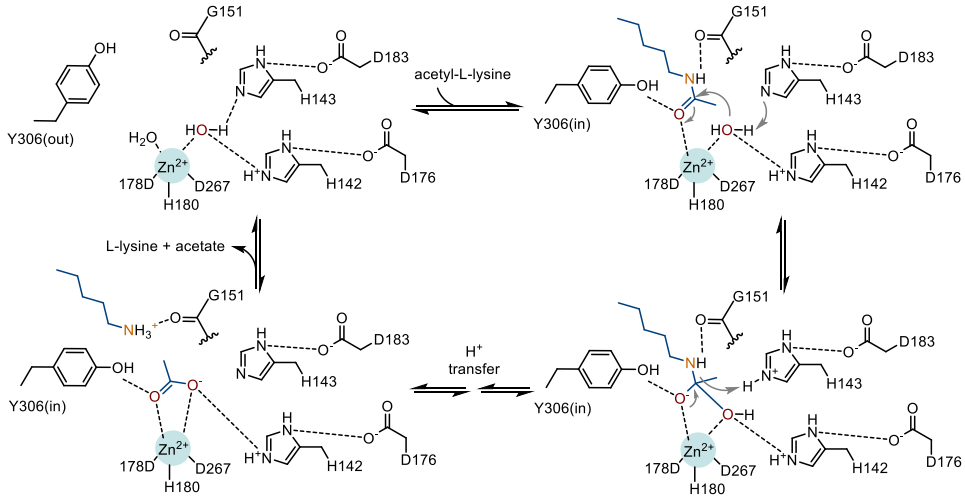

Scheme 13: HDAC-catalysed deacetylation mechanism.[158]

2.1.4 HDAC inhibitors

HDAC inhibitors (HDACi) are a class of molecules that reversibly or irreversibly obstruct access to the enzyme's active site by chelating the cation present at its

bottom. Although these inhibitors can be differentiated into 7 classes, it is possible to identify a common pharmacophore with three necessary structural features for optimal inhibitory activity:

- An aromatic group that allows interaction with the pocket entrance, called a cap group.
- A terminal group coordinating the Zn^{2+} ion at the bottom of the active site, also known as the zinc binding group (ZBG).
- A lipophilic linker positioned between the two groups mentioned above, the optimal length of which is 7-8 carbon atoms.[159]

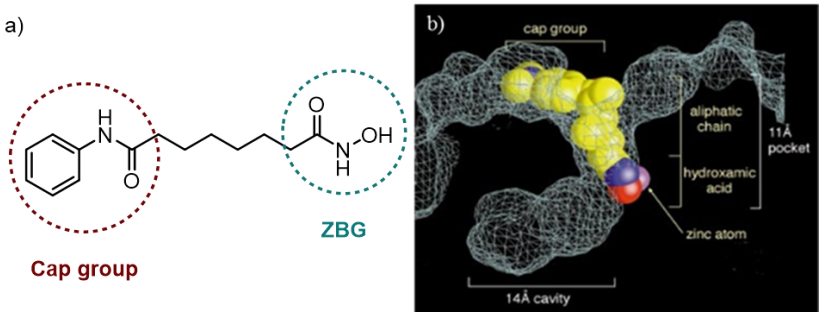

Figure 11: a) example of HDACi b) 3D structure of inhibitor into the enzymatic pokect.[157]

The most interesting classes of compounds for the synthesis of HDACi are hydroxamic acids, benzamides and thiols, as they have a functional group capable of efficiently coordinating the Zn^{2+}. Much of the biological activities of hydroxamic acids are due to their ability to chelate metals such as Zinc, Nickel and Iron, which are found in many enzymes, through the interaction of both the N-hydroxy and carbonyl groups.[141] Two FDA approved inhibitor belonging to these classes are Vorinostat and Romidepsin. (Figure 12)

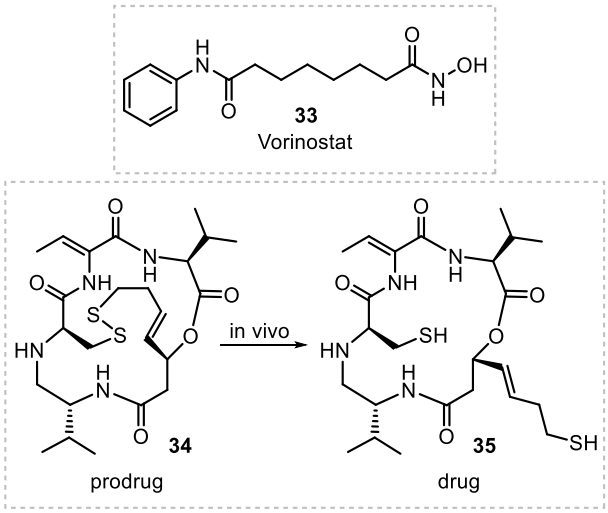

Figure 12: Examples of HDACi.

However, these molecules show many metabolic and kinetic problems that may lead to reduced efficacy in clinic, in spite of their have promising preclinical efficacy.[160] They also exhibit dose-limiting toxicity and lack selectivity because they do not discriminate between HDAC isoforms. HDACs induce a wide range of effects on cells, including cell cycle arrest, autophagy, apoptosis via both the intrinsic and extrinsic pathways, and anti-angiogenic effects by suppressing HIF-1α (a factor that regulates cell transcription and proliferation under hypoxic conditions) and VEGF (vascular endothelial growth factor).[161] Synthesising HDAC inhibitors specific to individual isoforms would enable to better understand which role the isoforms play in healthy cells and in tumour cells.[162] In order to achieve better pharmacological selectivity, structural modifications can be made to the pharmacophore to improve selectivity towards the target enzyme.

Sigma Tau (currently Alfa Sigma), in collaboration with M. Taddei and co-workers, studied HDACi, with particular focus on the zinc chelating group. Taking into account the interesting profile of Romidepsin, compounds containing thiols that could be used as inhibitors of the enzyme were studied and starting from the structure of Vorinostat, modifications were made to both the ZBG and the aliphatic chain. The

hydroxamic acid was replaced with an -SH group, protected as an acetal, and a lactam carbamide was added as the ω-substituent of the methyl chain, giving the molecule greater inhibitory power. The thioacetal derivative (ST7612AA1 shown in figure 13) demonstrated high selectivity for cytotoxicity against NCI-H460 and HCT116 cell lines, together with high inhibitory activity for tubulin and histone H4 acetylation.[163]

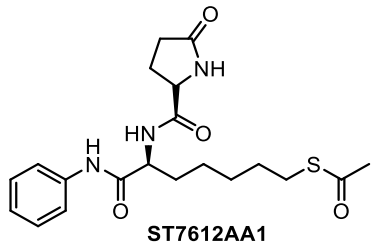

Figure 13: structure of ST7612AA1.

However, this compound, like the other inhibitors reported in the literature, cannot eliminate intrinsic toxicity because the target enzyme is ubiquitous, which obviously results in poor selectivity for tumour cells. To overcome this limitation, it is necessary to use prodrugs specifically designed to be activated only in the target cells, or selective delivery systems, such as ADCs.

Recently, ADC systems containing HDAC inhibitors have been developed, including the active thiol corresponding to the prodrug ST7612AA1[164] and drugs containing hydroxamic acids, such as Vorinostat and Dacinostat.[28].

Two linkers were chosen for these systems:

- a maleimide linker on which the thiol is bound through Michael addition, this binding will then be cleaved into the target cell via catabolism
- a cleavable linker based on the Val-Cit dipeptide bound to a *p*-aminobenzyl group (PAB) acting as a self-immolative spacer.

Both linkers were attached to the EGFR-specific monoclonal antibody Cetixumab (Ctx) (Figure 14) and studies have shown that after conjugation the properties of the antibody remain unchanged.

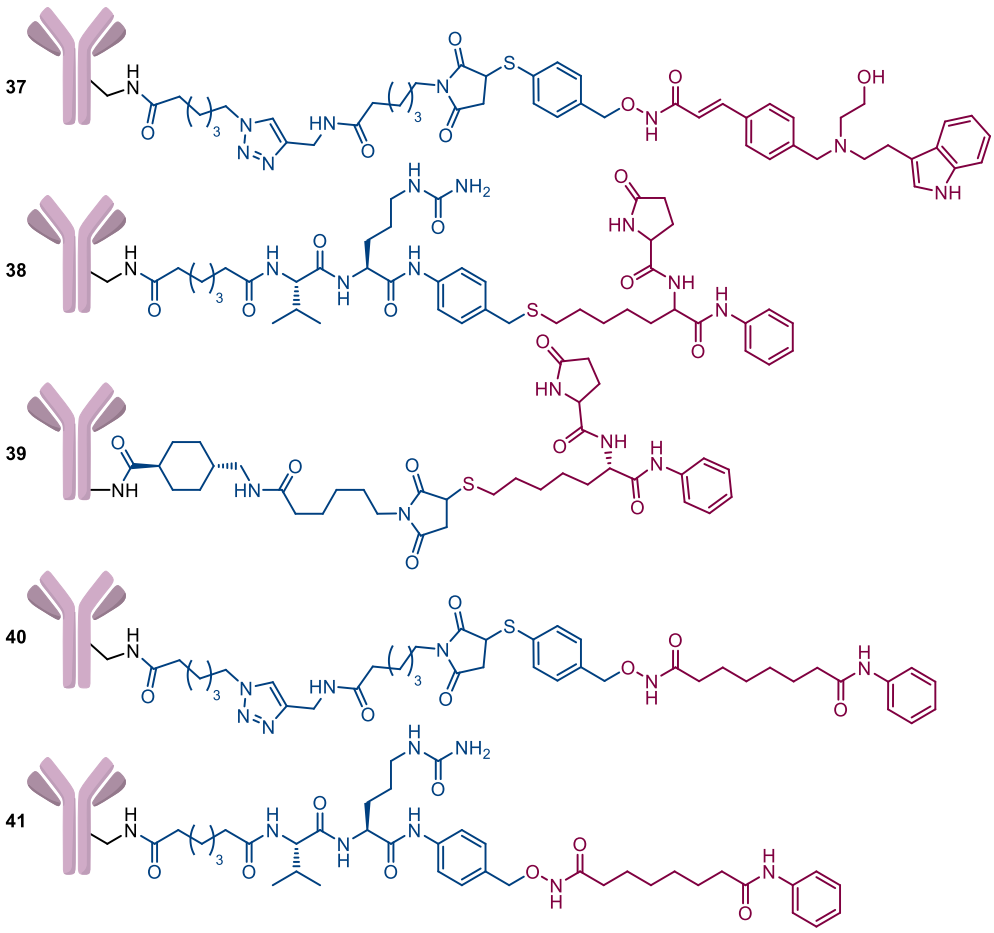

Figure 14: HDACi ADCs reported.

Internalisation of ADCs was studied in tumour cell lines expressing EGFR Capan-1, such as NCI-H1975 and A549, and in EGFR-negative cells; the two inhibitors were successfully internalised and then translocated into the lysosomal compartment. Inhibitor activity was demonstrated by increased acetylation levels of α-tubulin, histone H3 and H4 (resulting from direct inhibition of HDAC6 and HDAC class 1). Despite numerous studies, the mechanism of the inhibitor's release from the non-cleavable linker is still unclear.

2.2 Release of thiol containing compounds from heterocyclic systems and development of new heterocyclic self-immolative spacer

2.2.1 Heterocyclic self-immolative spacer

Many different self-immolative spacers have been developed in recent years and most of them use *para*-amino benzyl alcohol as the core structure. Heterocyclic systems are less common since PABA is commercially available, but some functional groups need a change in spacer structure to allow the formation of a sufficiently unstable intermediate that can go through self-immolative mechanisms. Here we can find the heterocyclic self-immolative spacers, to be specific the 5-membered aromatic ring heterocycles. They are less aromatic than benzene and this leads to an easier release for these groups. Examples can be found in the literature using furan, thiophene, pyrrole (less common) and imidazole.

To the best of our knowledge, the examples are few and most of them use the nitro group as a trigger for release into hypoxic cells.

The only reported example that has a different group for activation was recently developed by Skarbek and co-workers.[165] They synthetised 3 different prodrugs bearing arylboronic esters using Doxorubicin as payload, one being the unsubstituted benzeneboronate, one being a fluorinated benzene homologue and the third being the furan ring. Their cytotoxic proprieties were studied in 6 different cell lines and the results showed that the most effective was the unsubstituted benzene boronic ester.

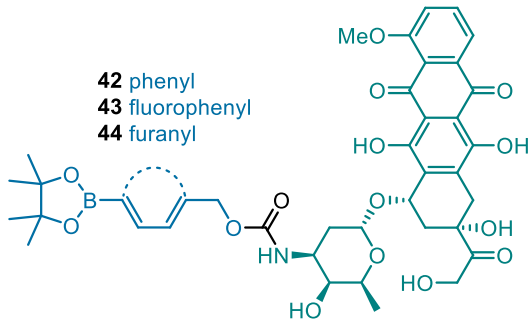

Figure 15: structure of the three prodrugs reported by Skarbek.

The other self-immolating systems reported have the nitro group in position 5 of the heterocyclic ring.

In the study by Parveen *et al.* in 1999, the first example of nitroimidazole prodrugs applied in the release of a cytotoxic agent was reported. Previously, the same research group had developed a nitrofuran derivative carrying the same drug. (Figure 16) Taking into account the results obtained for that compound, they claim that the redox potential of 2-nitrofuran is relatively high (E^{1}_{7} = -325 mV for a 5-nitrofuran-3-carboxamide) for this application, whereas the potential of 2-nitroimidazole is more appropriate for selective bioreduction in hypoxic tumour tissue (E^{1}_{7} = -389 mV for 1-alkyl-2-nitroimidazole). Release from the imidazole derivative was obtained after reduction with $NaBH_4$ and palladium on carbon in aqueous alcohol as a solvent. The amine passes through a 1,6-elimination mechanism and, under these reaction conditions, complete release of the active drug was obtained after 10 minutes, when reduction was carried out with tin(II) chloride the release occurred in 5 minutes.[132,166]

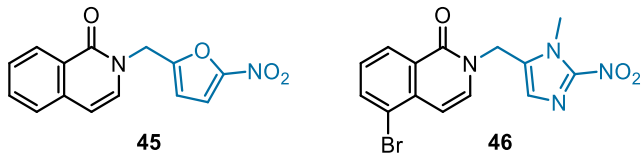

Figure 16: furan and imidazole prodrugs.

A few years later, Tercel and co-workers reported an interesting paper in which they synthesised and compared different aromatic heterocyclic prodrugs to optimise the nitroheterocyclic system for masking mustard. Starting with the benzyl derivative, they reported imidazole, pyrrole, thiophene and their regioisomers with the associated one-electron reduction potential. These prodrugs were tested on different cell lines to measure toxicity under normoxic conditions and pharmaceutical activity and selectivity in a hypoxic environment. It was found that the benzene derivative was the least toxic, but this characteristic was not directly related to the reduction potential of the compound. Thiophene was the most toxic and least selective, and pyrazole

derivatives were the most selective. Finally, they concluded that these deviations were quite variable and there was no obvious correlation with reduction potential or structure. All these prodrugs are too unstable and toxic for application, although they are less toxic than free mechlorethamine in vitro and all were more toxic under hypoxic than aerobic conditions.[167]

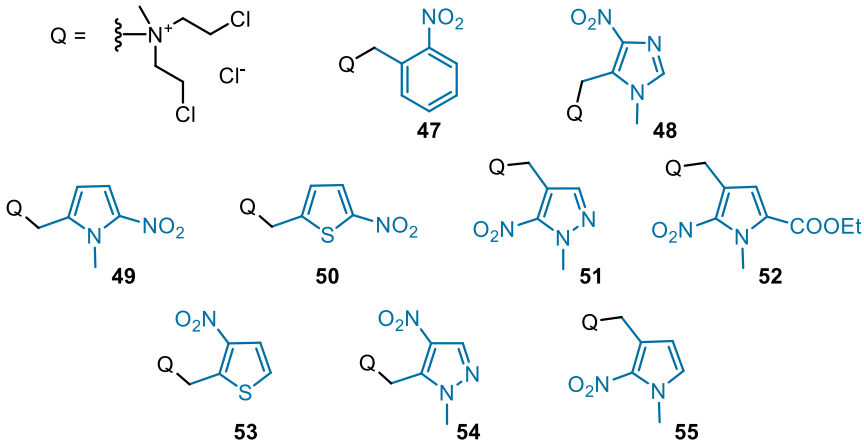

Figure 17: heterocyclic prodrugs bearing mustard as payload.

An important feature of the compounds reported in these two papers is that the spacer was bound directly to the drug via the amine functional groups. In 2003, two further papers with similar systems were published, but in these cases it was necessary to use a carbamate or ester bond between the spacer and the drug.[168,169]

Other examples that should be mentioned have been published more recently, such as that of Winn *et al*. They studied *nor*-, *mono*-, and *gem*-dimethyl nitro-thiophene, -furan, -imidazole and -benzylic systems. The cytotoxic drug was bound to the phenol moiety via an ether bond to the spacers and enzymatic cleavage was tested in the presence of NADPH and cytochrome P450 oxidoreductase. The best results were given by *gem*-dimethyl nitrothiophene and *gem*-dimethyl nitrofuran, which show good inhibitor activity under hypoxic condition compared with the anticancer agent phenstatin.[170]

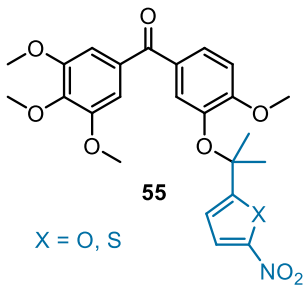

Figure 18: prodrugs reported by Winn *et al*.

A comprehensive review on nitro-containing prodrugs was published in 2019 and also reported the latest developments in the field of self-immolative spacers bearing the nitro group.[144]

Lastly, various strategies for the introduction of the bioreductive nitro group have been studied by O'Connor *et al*. They propose various reactions during the study of a new prodrug, such as the alkylation of nitrobenzyl halides, reductive amination, the formation of carbonate/carbamate from nitrobenzyl carbonbrominates and the esterification of nitroaryl halides. [171]

From all these examples and their results, it is possible to assume that when comparing bioreductive groups to each other, since oxygen-dependent reduction in cells apparently occurs via a single-electron mechanism, the propensity of a particular group to undergo bioreduction does not seem to be directly related to the electrochemical reduction potential of a compound.

2.2.2 Aim of the project

As the aromaticity of the system has been thought to influence on the disassembly kinetics of self-immolative spacer groups,[172,173] we supposed that poorly aromatic five membered heterocycles[174] could be useful as scaffolds for the release of low acidity compounds.

Following our interest in selective drug release systems, we chosen to focus on these structures. Such systems should lead to more unstable intermediates and thus be able to release functional groups that are not good leaving groups.

Among these groups are thiols, a class of molecules that play a variety of roles both in biological systems and in several classes of drugs. They have important biological roles in controlling redox homeostasis and as scavengers for ROS and RNS (reactive oxygen and/or nitrogen species). Moreover, they are excellent electron donors, which means that they can easily complex metals present in proteins, working as potent metal-enzyme inhibitors.[107,114,175,176]

Indeed, except for thiol release via reversible disulfide linkage, there are very few examples of thiol prodrugs.[176,177] They are not released by PABA-like systems, while the choice of binding via thiocarbonate or thiocarbamate is not applicable due to the instability of these functional groups in water/organic media such as plasma.[115]

A potent HDAC pan-inhibitor (ST7612AA1, structure reported in Chapter 2.1.3, Figure 13)[163] was developed by Prof. Taddei research group, containing a thiol as the zinc chelating group. It has shown excellent activity in vitro and significant anti-tumour activity in vivo.[178] The thiol group is masked as thioester, which is rapidly hydrolysed into the active compound, this drug was also bioconjugated to form an ADC system.[179] However, release through a chemical or enzymatic stimulus was sluggish. Strong lysosomal metabolism was responsible for the degradation of the bioconjugates producing the active inhibitor within the cell. Although effective for conjugation with internalising antibodies, this approach prevents any extracellular delivery of thiol-containing drugs or other applications for non-oncological purposes.[180]

Assuming that a stimuli sensitive system for release of thiol-containing compounds may be very useful for a controlled delivery of drugs containing the extremely reactive sulfhydryl group, we decided to investigate the potential of different heteroaromatic scaffolds as self-immolative spacers for the conjugation of thiols.

Thus, the structures studied are furan, thiophene and pyrrole, and the nitro group was used as a trigger for the release.

We also set out to develop a spacer that could be used in ADC systems. In addition, to verify the generality of these structures, we wanted to test the system that best released the thiols for other functional groups.

2.2.3 Result and discussion

2.2.3.1 Procedure for the selective reduction of nitro group

In order to verify the release of the systems, we needed to have a procedure to reduce the nitro group to the corresponding amine or hydroxylamine. The reduction conditions needed to be mild and biocompatible to obtain reliable and translatable results in physiological conditions and to avoid releases due to too harsh conditions. After an extensive literature research, the procedure reported by Lipshutz in 2016 was selected, which involves the use of Palladium dispersed in Iron nanoparticles (NPs), in aqueous micellar reaction environment, room temperature and $NaBH_4$ as reducing agent.[181]

NPs are synthesised from anhydrous $FeCl_3$, $Pd(OAc)_2$ and MeMgCl, under anhydrous conditions and Argon flow. The formation of the nanoparticles is characterised by their distinctive yellow-brown colour and, once dried, they must be stored under inert gas at low temperatures.

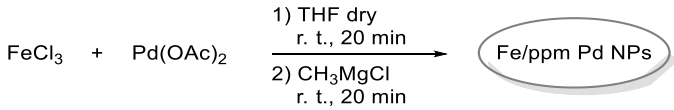

Scheme 14: synthesis of nanoparticles.

The described nanoparticles in combination with $NaBH_4$ do not reduce other unsaturations present in the molecule, such as the double bonds or the *tert*-butyl esters. The reaction is carried out in a micellar environment, constituted by water the

surfactant TPGS-750-M at 2% w/w. The micelle acts as a hydrophobic nanoreactor capable of incorporating, in the lipophilic core, both the nanoparticles and the compound that has to be reduced; however, THF (in a low percentage) is also used as a co-solvent to facilitate the solubilisation of the starting material. TPGS-750-M is composed of Vitamin E and succinic acid, with a chain of MPEG-750M for substrate transport within the micelle.

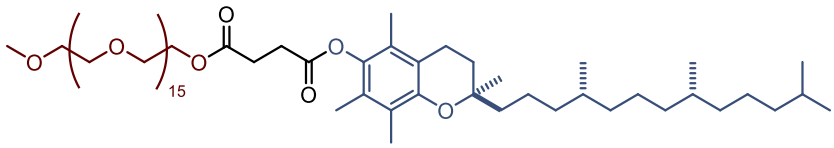

57 racemic Vitamine E

Figure 19: TPGS-750-M

The proposed reduction mechanism involves the release of hydride by $NaBH_4$ with the formation of Palladium hydride on the surface of the nanoparticles. The release of hydrogen is evident from the gas evolution in the reaction, such as the change in the oxidation state of palladium leading to the black coloration of the mixture. The palladium species acts as the reducing agent which, after formation of the nitrous and hydroxylamine intermediates, enables the desired amine to be obtained.

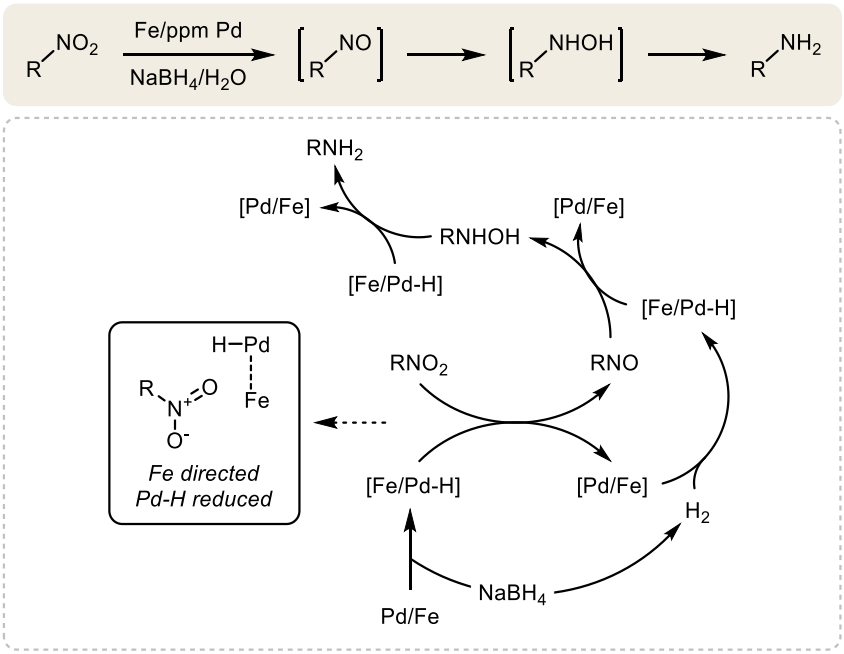

Scheme 15: proposed reported mechanism for the reduction of nitro group with nanoparticles of Pd/Fe.[181]

Performing the reaction in H_2O, using micelles, at room temperature and without the use of acidic conditions allows the physiological environment to be simulated as closely as possible, which is a prerequisite for demonstrating the effectiveness of the self-immolative spacer and avoiding non-reproducible results.

2.2.3.2 Study on the release of aliphatic thiols

Before starting the synthesis of the heterocyclic systems, we decided to test whether a PABA self-immolative spacer could release an alkyl thiol. Therefore, compounds **61** and **62** (shown in Scheme 16) were prepared from the corresponding bromides **58** and **59** and 1-octanthiol (**60**), which was used as a model for a lipophilic thiol containing drug. The reduction of the nitro group was carried out using the procedure reported by Lipshutz based on $NaBH_4$ in the presence of Fe/Pd nanoparticles (Nps) in an aqueous/micellar solution (2% wt.% TPGS-750-M) at room temperature.[181]

These conditions, previously described in chapter 2.2.3.1, seem to be the best "biocompatible" mimetic methodology for the nitroreductase enzyme. By subjecting compound **61** to this reduction reaction, the formation of the corresponding aniline **63** occurred without any trace of generation of free 1-octanthiol. Furthermore, the introduction of a methoxy in the *ortho* position, as with compound **62**, had no effect in facilitating the release of the free thiol, in fact benzyl sulfide **64** was isolated. (Scheme 16)

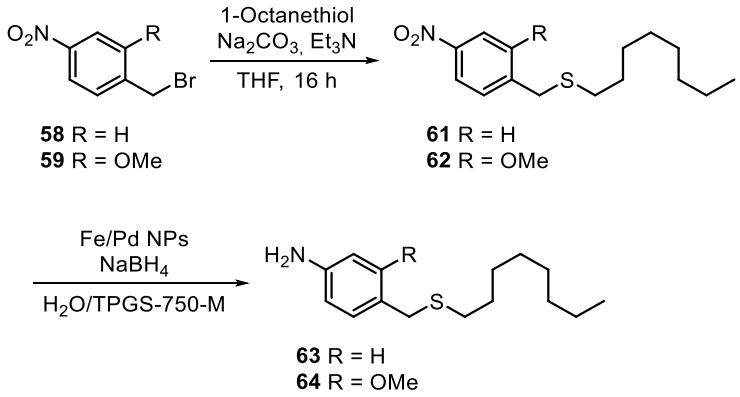

Scheme 16

Then, our investigation started with the preparation of 5-nitrofuran and 5-nitrothiophene having an octylthiomethyl group in position 2. We expected that the reduction of the nitro group to amine or hydroxylamine would results in the release of the model compound in solution. Thus, starting from aldehydes **65** and **66**, alcohols **67** and **68** were synthesized in good yields (Scheme 17). The corresponding bromides, obtained using PBr_3 as a brominating agent, were reacted with 1-octantiol to give products **69** and **70**, which were isolated in acceptable yields.

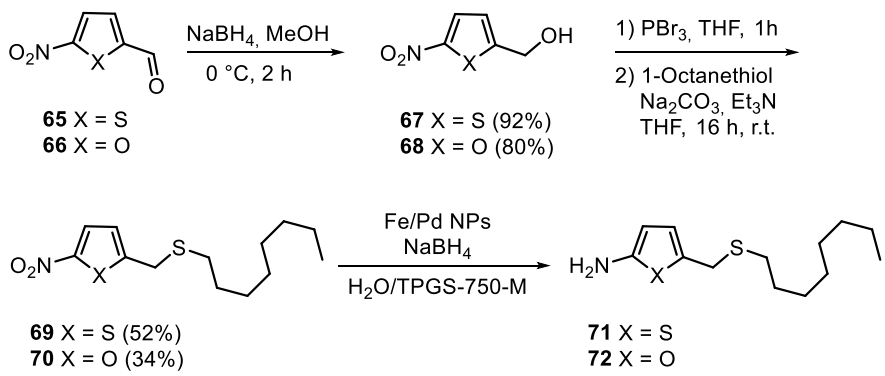

Scheme 17

After mixing **69** or **70** with the Fe/Pd nanoparticles and $NaBH_4$ in the micellar environment, aliquots of the solution were collected and analysed by HPLC-MS analysis. After 30 min, we observed the decrease of the nitro derivative **69** or **70** and the appearance of a peak corresponding to 5-aminofuran **71** or 5-aminothiophene **72**. The complete transformation into compounds **71** and **72** occurred after 2 h at room temperature, but free 1-octanethiol was not recorded in TLC, ESI/MS and HPLC/MS analysis. Despite the disappointment for the failed thiol release under these conditions, we decided to investigate the behaviour of the corresponding 5-nitro-2-octylthiomethylpyrrole. Surprisingly, only one example of nitro pyrrole triggers have been described so far, the system bearing a quaternary amine reported by Tercel *et al.*,[167] probably due to some difficulties to assembly this type of products.

After some test reactions with different starting material and nitration conditions, we developed an efficient 4-step synthesis of [5-nitro-1-(2-propynyl)-1*H*-pyrrol-2-yl]methanol **77** (NPyM) starting from commercially available 2-(trichloroacetyl)pyrrole **73** (Scheme 18). Nitration of **73** occurred with nitric acid in acetic anhydride at controlled temperature, affording product **74** in acceptable yield after chromatography separation from the 4-nitro isomer. The trichloroacetyl moiety was then converted into the methyl ester (**75**) and sequentially reduced to the corresponding alcohol **76** with DIBALH. Alkylation of nitrogen with propargyl bromide was carried out using Na_2CO_3 in DMF at 40 °C to give product **77** in

acceptable yield. Introduction of the alkyne in position 1 of the pyrrole ring was convenient for the introduction of an additional linker through click chemistry (Copper-Catalyzed Azide-Alkyne Cycloaddition, CuAACC). Starting from **77**, transformation of the alcohol into Br with PBr_3 followed by introduction of 1-octanthiol gave compound **78** in 68% yield. (Scheme 18)

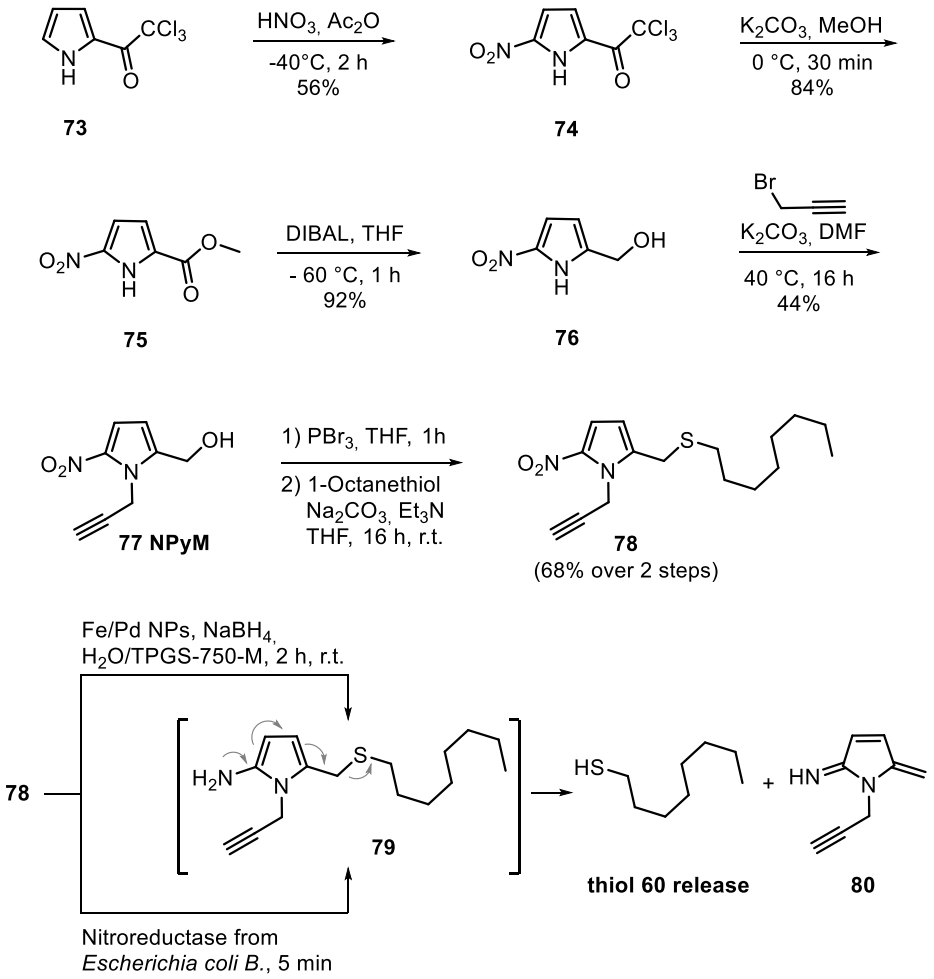

Scheme 18

When compound **78** was submitted to the Fe/Pd nanoparticle mediated reduction of the nitro group, we were pleased to observe the formation of free 1-octanthiol in solution with a complete conversion reached in almost 2 h from the addition of the

reducing agent. The potential of the nitro pyrrole trigger was confirmed by the rapid release of the thiol in 5 min after addition of the oxygen-insensitive nitroreductase (NTR) from *Escherichia coli B*, the standard model enzyme employed to mimic hypoxic environments.

Moreover, a careful inspection of the reaction mixture HPLC/MS trace, showed a peak at m/z 133 corresponding to the protonated form of the 5-methylene-3-pyrrolin-2-imine **80**, not stable enough for isolation. The presence of this product demonstrates that the release of the thiol occurs via a truly 1-6 elimination passing through the undetected 2-aminoderivative **79**. These data clearly demonstrated that 5-nitro-1*H*-pyrrol-2-yl-methanol (NPyM) linker is the first example of a platform for the release of free thiols induced by nitroreductase enzymes.

2.2.3.3 Introduction of a pharmacologically active thiol

The NPyM linker was than applied to the delivery of a pharmacologically active thiol, present in ST7612AA1 (Scheme 19). After removal of the acetyl group with sodium methyl thiolate, the solution containing the free thiol **81** was mixed with the solution containing the bromide **82** obtained from alcohol **77**. After stirring at room temperature overnight, compound **83** was isolated in 22% of yield.

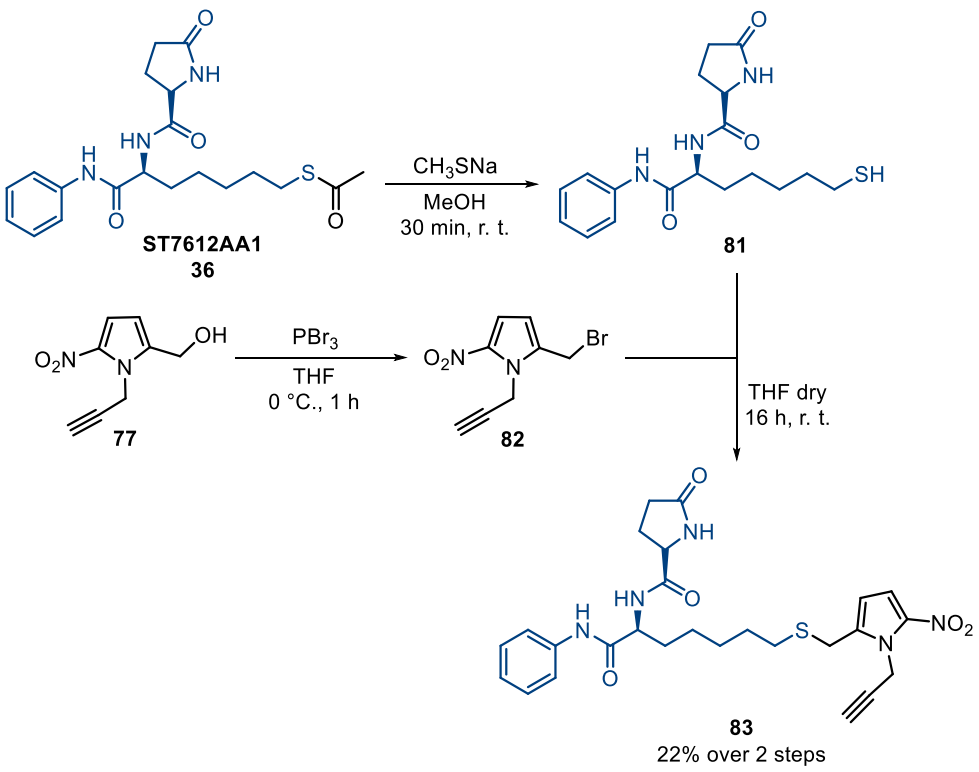

Scheme 19

Fe/Pd nanoparticle catalyzed reduction of compound **83** with $NaBH_4$ released in solution thiol **81**, the active principle of antitumoral prodrug ST7612AA1.

We determined the concentrations of the released product, the byproducts and the conversion of the starting materials by HPLC-MS at predetermined time intervals. Chromatograms were obtained using an eluent mixture H_2O/CH_3CN with a gradient of CH_3CN 5-95%. Reactions were set up on small amounts of nitro derivatives and sampling was carried out at 5 times: 0.0 h (t_0), 0.25 h (t_1), 0.5 h (t_2), 1 h (t_3), 1.5 h (t_4), 2 h (t_5). In order to determine the released active thiol more accurately, a calibration curve was made and is shown in the experimental section (see Chapter IV).

After 1 h, 92% of the free thiol was delivered in solution, while after 2 h the HPLC/MS profile showed a decrease in the concentration of **81** and the appearance of a signal associated to the m/z of the corresponding disulfide. (Figure 20) The

triggering of **81** was also evaluated using NTR reduction. An aqueous solution of **83** mixed with the enzyme (2 µg/mL) and NADH (1 mM) was incubated at 37 °C. The structure behaved as substrate for NTR and was readily reduced after 5 minutes giving a completely release of the active thiol **81**.

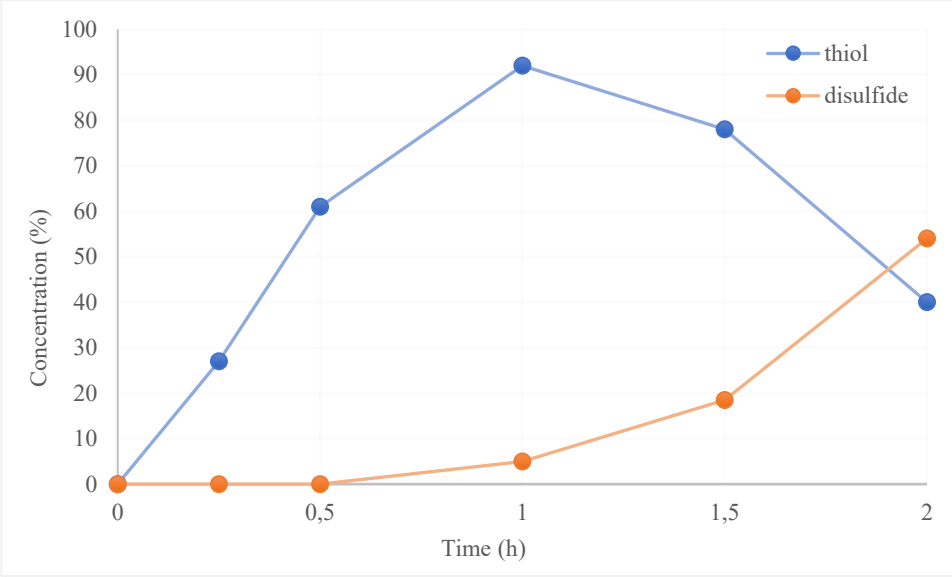

Figure 20: Kinetic curve for the release of active compound after reduction of **83** with nanoparticles. Blue line is the concentration of the free thiol **81**, orange line is the concentration of the corresponding disulfide. The concentrations were determined with HPLC-MS and calculated with calibration curves.

To develop a new ADC system containing this nitro pyrrole self-immolative spacer, we decided to synthesise an azide bearing the carboxylic acid group and a TEG tail to increase the solubility of the final system.

Azide **87** (Scheme 20) was prepared from *tert*-butyl 5-bromopentanoate (**84**) which was reacted with triethylene glycol (TEG) in the presence of NaH. The hydroxyl group of **85** was activated with *p*-toluenesulfonyl chloride and subjected to substitution with NaN_3 to obtain azide **86** in moderate yield. Subsequent hydrolysis of the ester gave the desired carboxylic acid **87**.

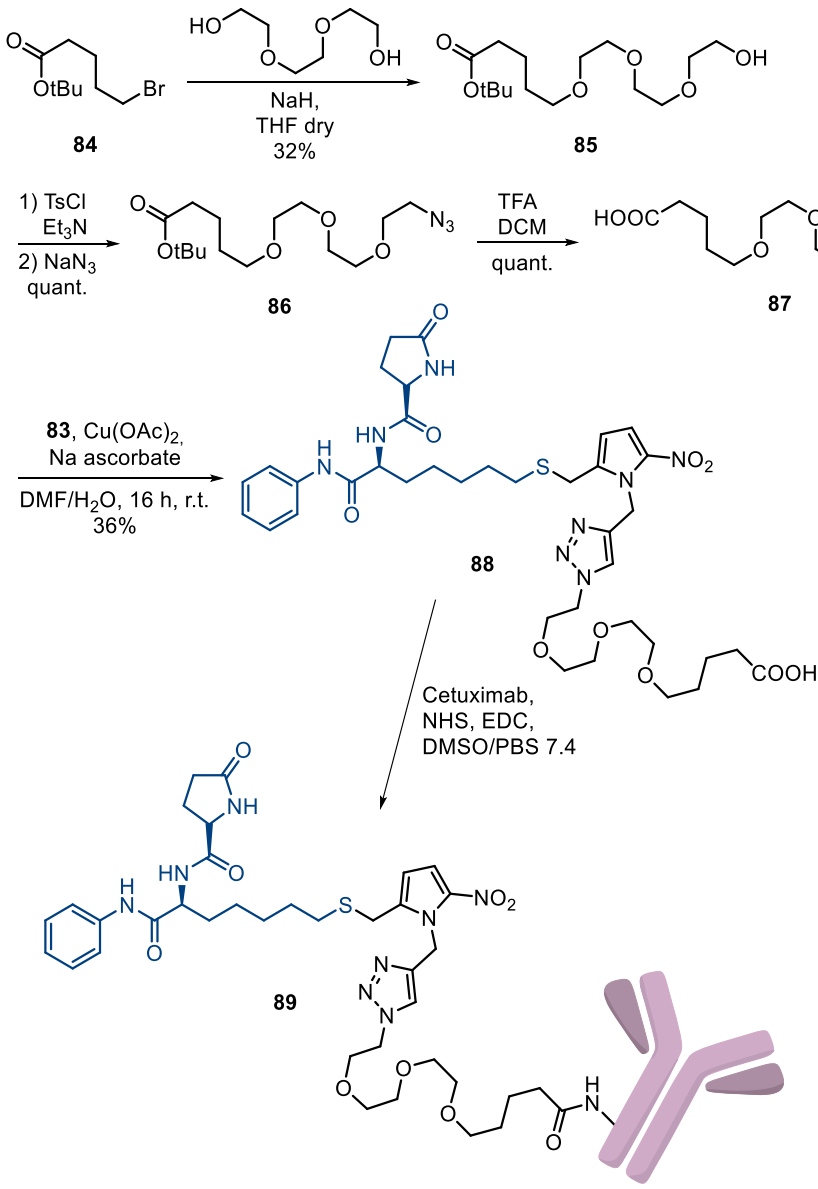

Scheme 20

The further CuAACC reaction with azide **87** gave triazole **88** as free carboxylic acid in acceptable yields. The introduction of the TEG fragment in the product increased the solubility in water of our compound and the presence of a free carboxylic function provided the further conjugation point for the carrier molecule (Scheme 20).

Furthermore, molecule **88** was stable in PBS (pH 7.4 and pH 6.5) and in mouse plasma for more than 36 h.

Table 1 Stability tests of payload **88**

Compound	H_2O	Buffer pH 7.4[a], $t_{1/2}$[b]	Buffer pH 6.5[a], $t_{1/2}$[b]	Plasma[a], $t_{1/2}$[b]
88	99%	96%, >36 h	96%, >36 h	94, 8.3 h

[a]Expressed as percentage of unmodified compound after 36 hours of incubation.
[b]Half-life ($t_{1/2}$) expressed as the amount of time it takes before half of the compound is hydrolyzed/degraded.

With a $t_{1/2}$ of 30 min with the nanoparticles and approximately 2 min in the presence of NTR, compound **88** seemed an ideal system for the costruction of ADC.
The conjugation of **88** with Cetuximab (ctx), a monoclonal antibody targeting epidermal growth factor receptor (EGFR), was then pursued to verify if our product could be a suitable cargo to delivery thiols for histone deacetylase (HDAC) inhibition. Anchoring to ctx was done through activation with DCC and NHS and further incubation in DMSO/H_2O/PBS buffer (pH 7.4) with the antibody using a 20-molar fold excess of the linker respect to ctx. Purification of conjugate **89** was carried out by dialysis and DAR was determined by MALDI analysis that showed a DAR of 4.03.
The anti-proliferative activity (MTT assay) of the conjugate **89** is still under investigation.

2.2.3.4 Introduction of different functional groups

In order to verify the generality of the nitro pyrrole system, we decide to test it for the release of other functional groups: phenol, aniline, amide and hydroxamic acid were used and their model compounds were chosen.
The synthetized products are reported in scheme 21.

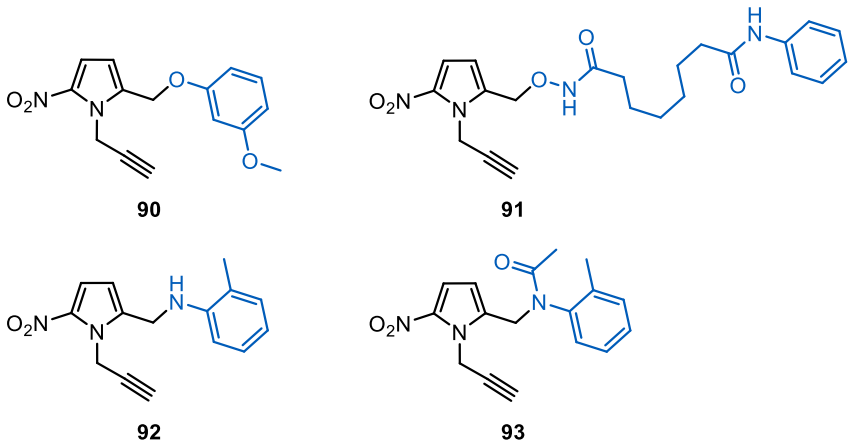

Scheme 21

The reactions for compounds **90**, **91**, **92** involve the bromine derivative **82**, obtained from **77** and PBr_3 as described above, and the nucleophile in presence of a base. For each product different conditions had to be used, which are summarized in Table 2. The procedure for hydroxamic acid involves an aqueous solution of NaOH to deprotonate the starting and lead to the product, however the reaction time has to be short to avoid conversion of the reactive bromine **82** into the parent alcohol **77**.

The preparation of **93**, obtained in good yield, was done by acylation of compound **92** due to the difficulties found in the direct use of a model amide.

Table 2: Reaction conditions and yields of the compounds under study.

Compound	Reaction conditions	Yield
90	**82**, K_2CO_3, Et_3N, THF, 16 h, r.t.	40%
91	**82**, NaOH, MeOH, 5 min, r.t.	32%
92	**82**, Et_3N, THF, 16 h, r.t.	24%
93	**92**, acetyl chloride, Et_3N, THF, 1 h, r.t.	75%

We underwent the reductions of all the compounds under the same conditions (Fe/Pd NPS and $NaBH_4$ in micellar environment H_2O/TPGS-750-M at room temperature), and we determined the concentrations of the released products, the reduced byproducts (when no release took place) and the conversion of the starting materials by HPLC-MS at predetermined time intervals. Chromatograms were obtained using an eluent mixture H_2O/CH_3CN with a gradient of CH_3CN 5-95%.

Reactions were set up on small amounts of nitro derivatives and sampling was carried out at 5 times: 0.0 h (t_0), 0.25 h (t_1), 0.5 h (t_2), 1 h (t_3), 3 h (t_4), 8 h (t_5). With the increase in the concentration of the model compounds it was possible to represent the kinetic curve for each of the systems tested. (Figure 21)

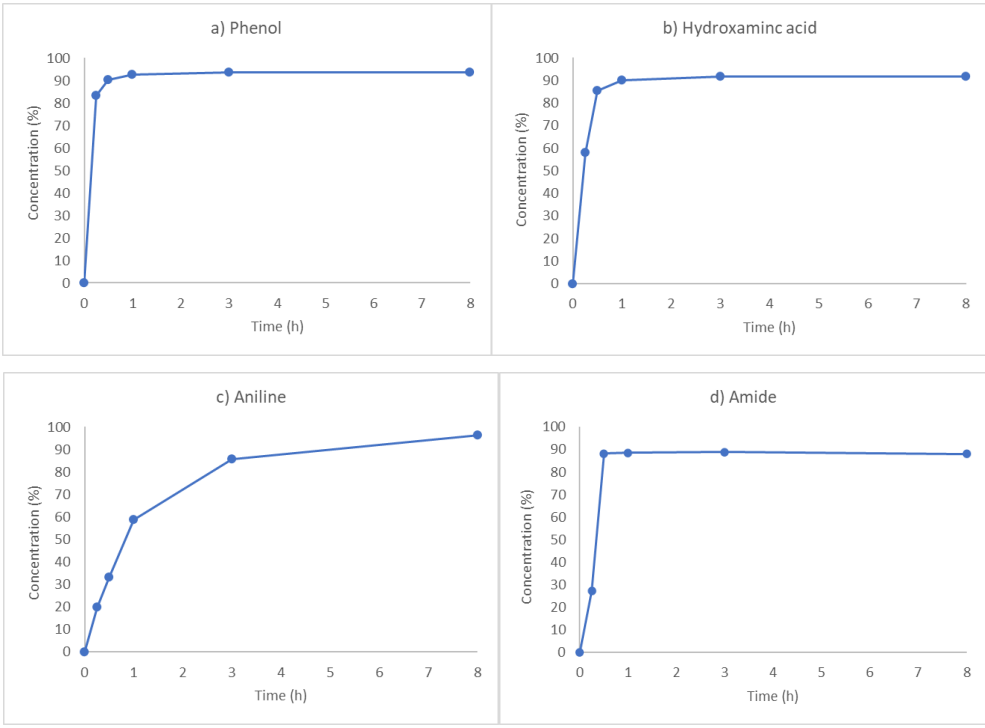

Figure 21: Kinetic curves of the release of a) 3-methoxyphenol, b) SAHA, c) *o*-toluidine, d) N-(*o*-tolyl)acetamide. Concentrations are reported as a percentage of the free compound detected by HPLC-MS.

The release of the phenolic group ended after 0.5 h, leading to the complete disappearance of the starting, in which case the corresponding reduced compound

was never identified. The release of the hydroxamic acid also took place with relatively fast kinetics, and after 1h the plateau was already reached. However, in this case the formation of the corresponding reduced amine was detected 15 minutes after the start of the reaction. As for the release of aniline, this occurred more slowly, it took 8 h for the complete release of *o*-toluidine and the disappearance of compound **92**. Lastly, the release of the amide exhibited comparable kinetics to those of the phenol and the formation of the reduced compound was not identified in this case either.

Table 3: $t_{1/2}$ (h) values obtained for the release of different functional groups from the pyrrole system after reduction with Fe/Pd NPs.

	ST	**50**	**51**	**52**	**53**
$\mathbf{t_{1/2}}$ (h)	0.54	0.15	0.22	0.85	0.28

2.2.4 Conclusions

In conclusion, we demonstrated that the 5-nitro-1*H*-pyrrol-2-yl-methanol spacer can be employed for drug delivery of thiols in hypoxic biologic environments and the cargo is suitable for conjugation of cytotoxic drugs with an antibody carrier. The NPyM linker is stable in plasma and possess all the features for the preparation of different reduction responsive materials based on a thiol/sulfide function. Orthogonal reactivity is also possible introducing azides, alkynes, tetrazines or other fragments for click chemistry, to access easy conjugation with macromolecular carriers.

The pyrrole based self-immolative spacer is also suitable for releasing a wide range of functional groups that are not commonly released by PABA-like spacers and they can be stably bonded to the core structure.

2.3 New Morita-Baylis-Hillman adducts for the selective Nitroreductase-mediate drug release

Before introducing this project, it is necessary to give a very short introduction of the reaction which gives the name to the chapter: the Morita-Baylis-Hillman reaction. It is also important explore its reported application in the fields of organic synthesis and medicinal chemistry.

2.3.1 Morita-Baylis-Hillman reaction and its applications

The Morita-Baylis-Hillman reaction (MBH reaction, Scheme 22) is widely used in organic synthesis and medicinal chemistry. MBH reaction was reported for the first time in 1968 by K. Morita,[182] and it was further explored in a patent published in 1972 by Baylis and Hillman. This reaction is one of the simplest and most useful methods to form a new allylic alcohol by forging a new carbon-carbon bond, combining an aldol and an elimination reaction in a single step, providing structures widely employed in the synthesis of pharmaceutical compounds.[183]

The product is obtained by reacting together an aldehyde with activated alkene, like alkyl vinyl ketones, alkyl (aryl) acrylates, vinyl-sulphones, acrylamides, allylic esters, vinyl sulfonate and vinyl phosphates, in the presence of a tertiary amine as catalyst. The most commonly used amine is 1,4-Diazabicyclo[2.2.2]octane (or DABCO), but various tertiary amines have been reported. The reaction conditions are very mild although reaction times are quite long and several days are needed to obtain a good yield. Conventional or MW dielectric heating have been reported to accelerate MBH reactions.

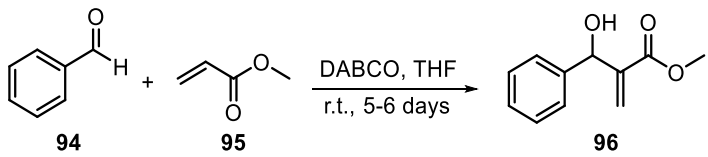

Scheme 22: Morita-Baylis-Hillman reaction.

The mechanism (Scheme 23) involves an initial nucleophilic attack by the tertiary amine on the double bond of the Michael acceptor, leading to the formation of a zwitterionic intermediate. The α-carbon of this charged intermediate has electron-rich character and can react with the carbonyl group of the aldehyde to generate the following intermediate which spontaneously undergoes intramolecular proton transfer, resulting in the generation of the final MBH adduct, releasing the catalyst by elimination. All these species are in equilibrium, thus accounting for the slow reaction kinetics.[184]

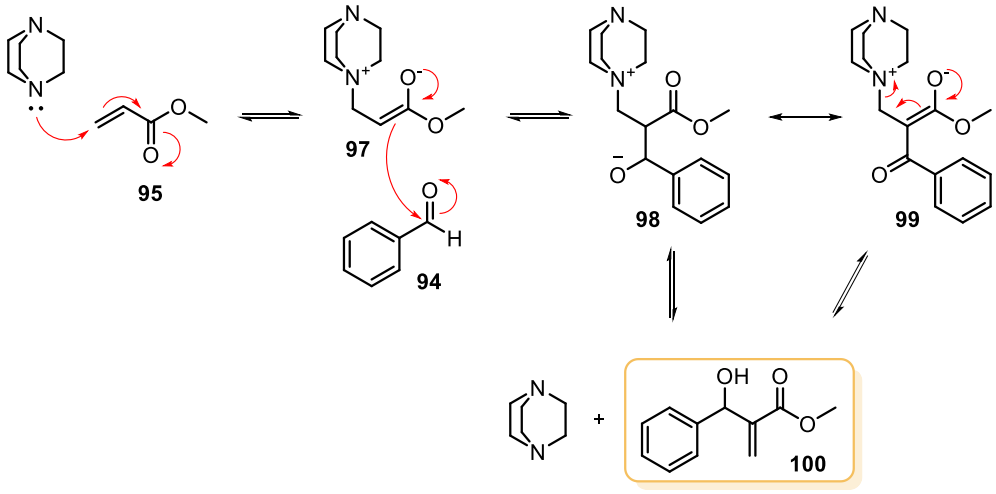

Scheme 13: mechanism of Morita-Baylis-Hillman reaction

In medicinal chemistry, this reaction is used for the synthesis of quinolines, heterocyclic aromatic compounds that can be found in several drug classes, such as synthetic antimalarials, antibacterials (ciprofloxacin and norfloxacin are some examples) and HIV-1 protease inhibitors.[185,186] Quinolines are synthesised from 2-nitro benzaldehyde and acrylic esters or ketones, using DABCO as catalyst. The wide-ranging applications of this reaction prompt to research for conditions to improve the yield and increase stereochemical control. Since a pro-chiral electrophile is involved, ultimately leading to the formation of a new stereogenic centre, asymmetric synthesis can be employed in order to control its configuration. It was observed that the yield decreases when the steric hindrance increases on the Michael

acceptor. In addition, electron-donating substituents on the aromatic ring decrease the reactivity of the aldehyde, increasing the electron density of the molecule, and thus adversely affect the reaction kinetics; while electron-withdrawing groups, such as the nitro group, promotes reactivity.

After obtaining the MBH adduct, reduction of the nitro group in *ortho* position leads to the formation of the corresponding aniline, which may undergo cyclization and form the quinoline core. Cyclization may occur on the double bond, by conjugate addition, or on the carbonyl group, by nucleophilic attack. (Scheme 24) Substitution on the carbonyl and the nature of the leaving group may have an influence on the obtained product.

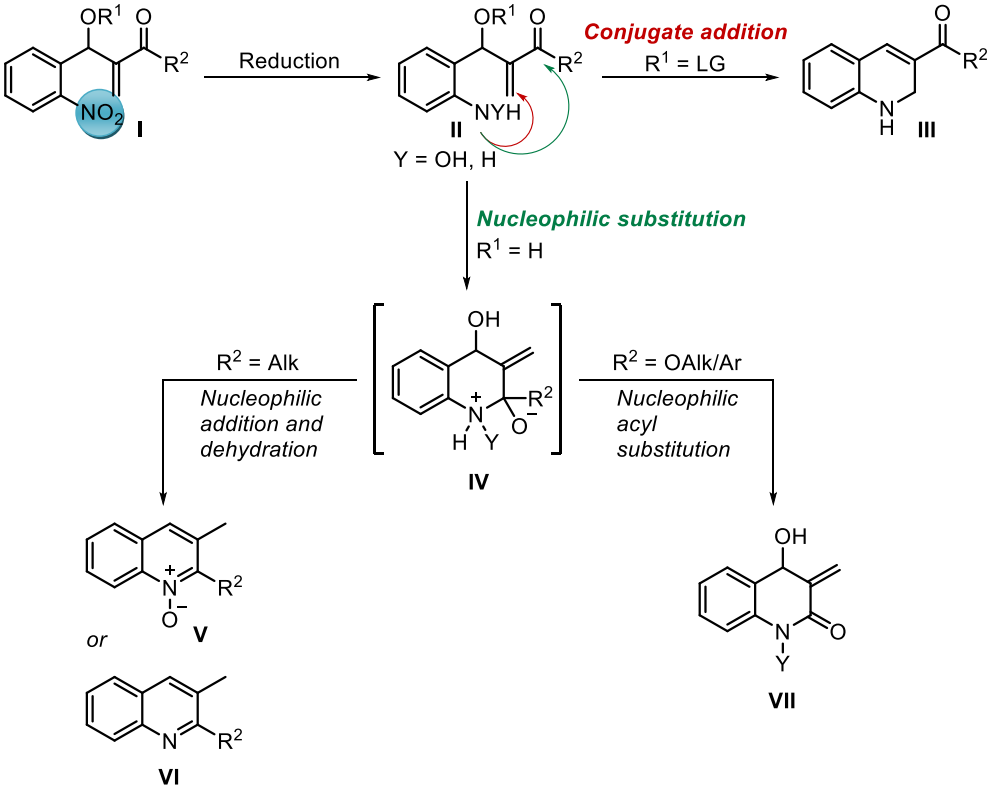

Scheme 24: reduction of the nitro group and possible cyclization via nucleophilic substitution or conjugate addiction on generic MBH adduct.

When reduction of the NO_2 group is carried out with H_2 and Pd/C, nucleophilic substitution is favoured, forming quinolines if Michael acceptor is a vinylketone, or quinolones when the substrate is an acrylic ester. If the reduction leads to the formation of a hydroxylamine, or the cyclization has very fast kinetics, the product is a quinoline N-oxide.[187] On the other hand, reduction with tin(II) chloride proved to be substrate-dependent, e.g. if the starting material is an ester, conjugate addition on the double bond will be favoured instead of nucleophilic attack on the carbonyl group. However, in all cases, an increase in steric hindrance on the acrylic ester leads to cyclization by conjugate addition.[188,189]

The secondary alcohol obtained from the MBH reaction can be modified and functionalized on the allylic carbon with other nucleophiles. As shown in Scheme 25, upon synthesis of the bromine derivative, a nucleophilic substitution with DABCO can be carried out, forming a charged intermediate that can react with a nucleophile by S_N2', giving the final substituted product. This mechanism resembles that of the Morita-Baylis-Hillman reaction.[190]

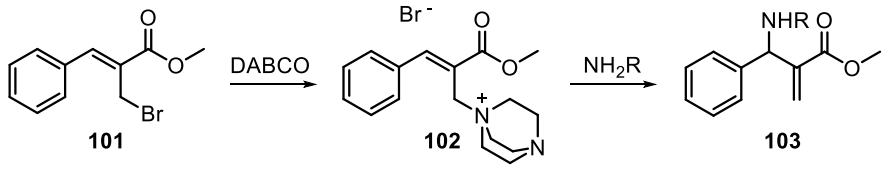

Scheme 25: introduction of nucleophile in allyl position.

The products of the MBH reaction have also found multiple applications in organic chemistry as valuable substrates for various reactions, such as the Friedel-Craft,[191] Heck coupling,[192] Diels-Alder reaction,[193] radical reactions,[194] cycloaddition reactions,[195] hydrogenation,[196] photochemical transformations,[197] Claisen rearrangement,[198] dihydroxylation,[199] epoxidation,[200] aziridination,[201] aminohydroxylation[202] and so on; leading to the discovery of various new pathways and strategies with high levels of stereochemical control. Several natural products and biologically active molecules were also synthesised using the Baylis-Hillman

methodology.[185] Finally, this reaction became an innovative source for combinatorial chemistry and for the synthesis of molecules exhibiting liquid-crystalline properties.[183]

2.3.2 Aim of the work

As mentioned before, the development of a new self-immolative spacer that can release different functional groups is an ongoing challenge in the field of drug delivery systems.[48] Structures reported in the literature can release common functional groups such as amines, alcohols and acidic phenols, but for drugs that do not bear these groups, only a few strategies to bind them are available and they present many limitations. Intramolecular cyclization is the best choice when the intermediate with the free nucleophile is too stable to give elimination through the electronic cascade (for detailed mechanism see chapter 1.3.1), but this strategy has the limitation of needing an electron-poor group and consequently the most used are the same common functional groups carbamate or carbonate already reported.

To develop a new self-immolating spacer that could overcome these limitations, we needed to find a structure that would allow us to obtain an intermediate that was sufficiently unstable to undergo intramolecular cyclization even when the bound drug functional group was not an optimal leaving group. The formation of a six-membered ring could be sufficiently thermodynamically favoured, so we thought that product **I**, where the precursor allyl alcohol can be obtained from an MBH reaction, could generate a reactive aniline **II** leading to the release of the group in the benzyl position. (Scheme 26)

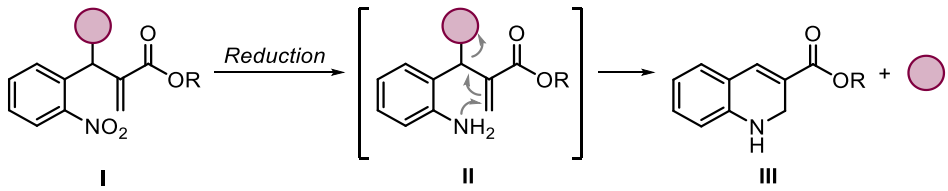

Scheme 26: intramolecular cyclization mechanism for a model structure.

The main challenge is to check whether the aniline intermediate can be sufficiently reactive to undergo intramolecular cyclization and which functional groups can be used being compatible with the carbonyl moiety present in the molecule.

2.3.3 Result and Discussion

2.3.3.1 Synthesis of the self-immolative spacer and introduction of different functional groups

The synthesis of the system was carried out by Morita-Baylis-Hillman reaction between *o*-nitro benzaldehyde and *tert*-butyl acrylate, in the presence of DABCO as a tertiary amine catalyst. The reaction took six days to be completed, however yields were high and side products absent. Even if the starting material was not completely consumed, it was recovered and the purification was simple. The *tert*-butyl ester was chosen to have a higher steric hindrance and a more electron-rich character, hoping to avoid amidation as a side reaction upon reduction of the nitro group.

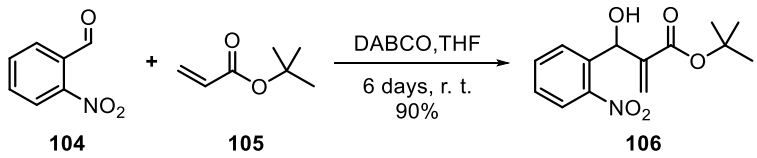

Scheme 27: MBH reaction between *o*-nitro benzaldehyde and *tert*-butyl acrylate.

With the allylic alcohol in hand, the hydroxyl group needed be converted into a good leaving group. Several procedures are reported in the literature to achieve this purpose, initially we decided to convert compound **106** into a chlorine derivative with $POCl_3$ and DMF. This reaction was carried out leading to a high yield, with the hypothesised mechanism, highlighted in scheme 28, involving the Vilsmeier intermediate (the chloroiminium ion) and subsequently the formation of an oxonium ion (structure **107**). The next step was the nucleophilic attack of the chlorine anion on the double bond leading to electronic rearrangement and release of DMF.[203]

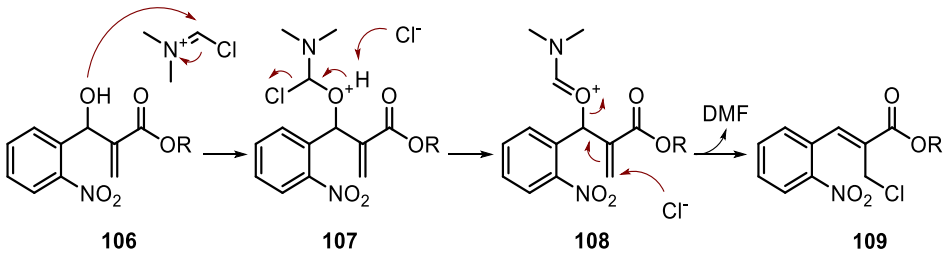

Scheme 28: Proposed mechanism for the synthesis of compound **109**.

Thus, **109** was submitted to nucleophilic displacement of the chlorine with 2-nitro benzyl sulfonamide, as a model. Unfortunately, this reaction showed the formation of a side product (**112**) due to the S_N2 substitution instead of the S_N2' on the double bond. (Scheme 29) The two products were also difficult to isolate, but no other side reactions or degradation of the starting materials was observed.

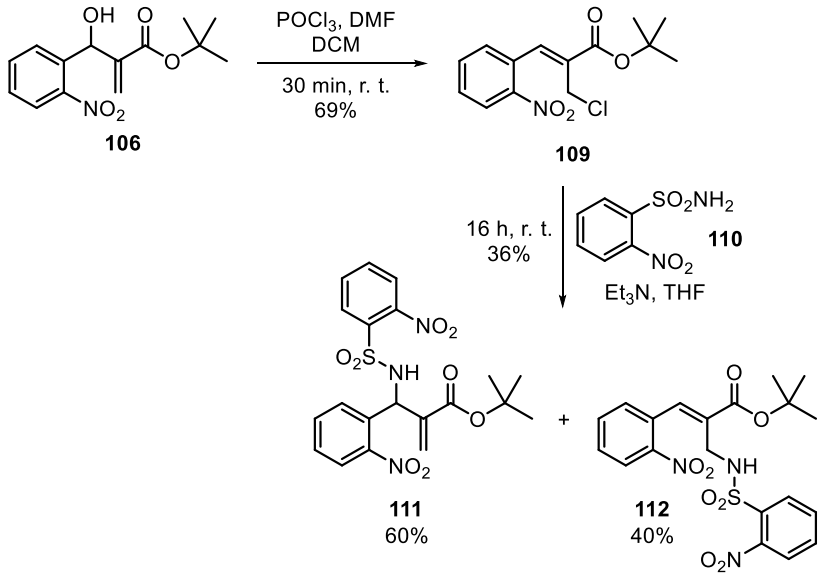

Scheme 29

Other reaction conditions were tested, a strong base such as NaH led to the formation of only the unwanted compound **112,** and the use of DMAP gives only a slight change in the relative amount of the regioisomers.

Then, the way of activating the allylic alcohol **106** was changed converting the hydroxyl group into a good leaving group through reaction with ethylchloroformate. (Scheme 30) The procedure involves the use of LiHMDS at low temperature leading to **114** in excellent yield. The sulphonamide nucleophile derivative was then changed to the more nucleophilic 4-methyl benzyl sulphonamide.

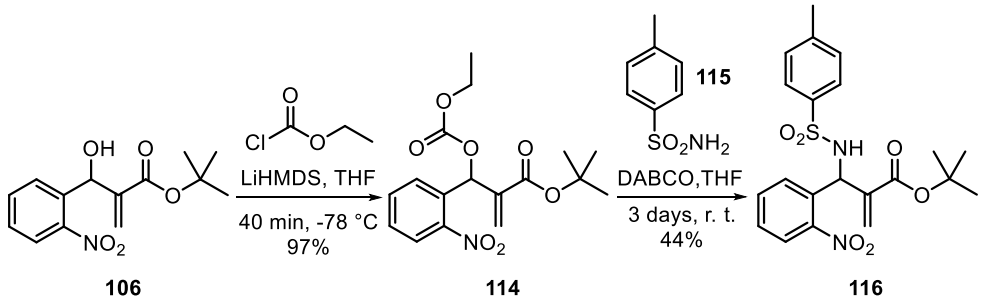

Scheme 30

For the introduction of sulphonamide, we used a reaction catalysed by a tertiary amine (DABCO in Scheme 30), with a similar mechanism to the Morita-Baylis-Hillman reaction, going through a charged intermediate between the amine and the unsaturated substrate, followed by the substitution by the nucleophile. (Scheme 31)

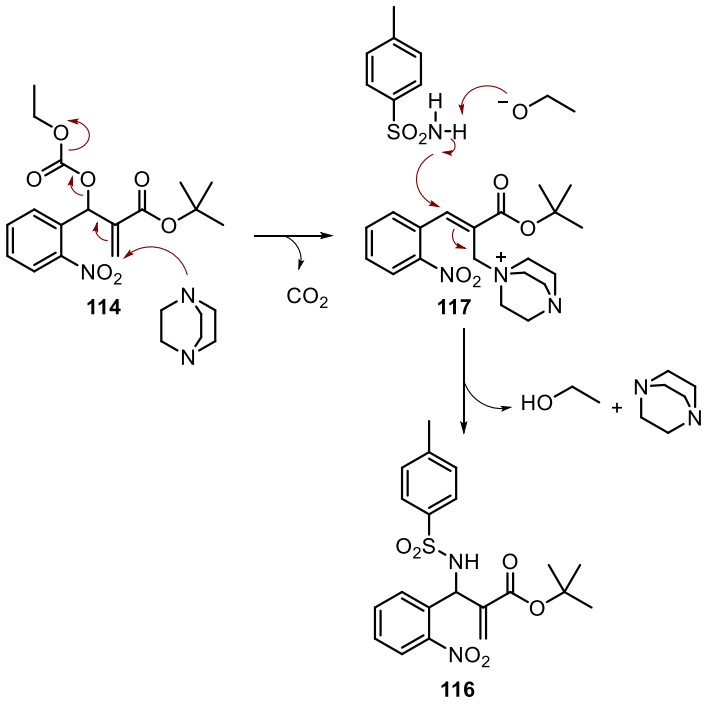

Scheme 31: proposed mechanism for the reaction MBH-like.

The reaction worked reasonably well, with no side products although in moderate yield. With this procedure different nucleophiles were introduced selectively in the benzylic position. The choice of groups used in this project was determined by the aim of testing the larger possible set of functional groups for the innovation of the designed delivery system.

Phenols are susceptible to extensive first-pass effects in the body and reduced absorption by passive diffusion, often due to their low lipophilicity, and these problems limit their use as active compounds.[204] In addition, for anticancer drugs such as Combretastatin A4 (Scheme 32), there is also reduced selectivity towards neoplastic cells. To overcome these limits, they are often bound to protective groups or to self-immolative spacers through the formation of a ester or sulfate, that show low metabolic stability.[102,205] In our system, however, we would like to achieve direct ether linkage to the delivery system.

Therefore, to study the reactivity of non-acidic phenols, we selected 4-*tert*-butylphenol as a model compound, a molecule which has an electron-donating group in *para* position. The reaction was carried out under the same conditions as for sulphonamide, resulting in product **119** in 49 % yield.

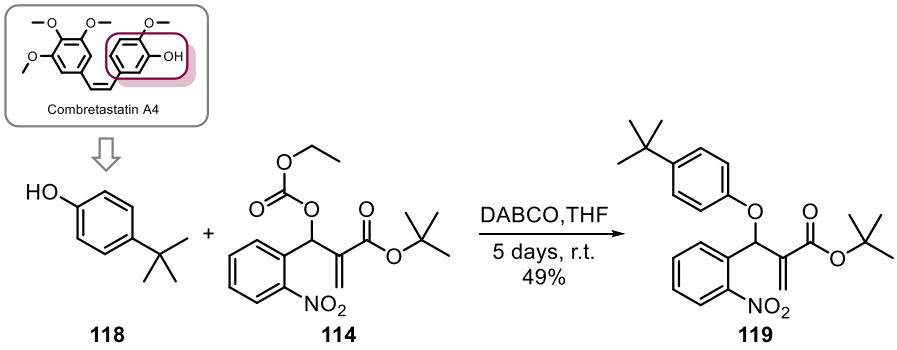

Scheme 32: insertion of phenol.

Indoles are present in numerous classes of drugs such as anti-hypertensives, analgesics, anti-HIV and anticancer drugs; one example is the anticancer drug Cediranib, an inhibitor of the tyrosine kinase enzyme.

This group is difficult to release from PABA-like self-immolative spacers and its use in controlled release systems is therefore extremely limited. In order to promote the nucleophilic attack by indole, it was necessary to slightly modify the reaction conditions, still using the MBH-type mechanism. Performing the reaction at 40 °C in DCM (Scheme 33), a yield of 27% was obtained, which is most likely due to the low nucleophilicity of the indole nitrogen and the low acidity of the proton bound to it.

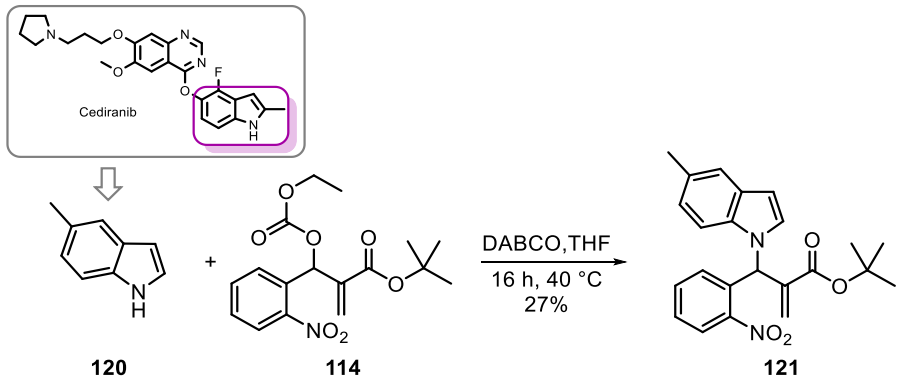

Scheme 33: insertion of indole.

Thiol-containing drugs are difficult to release from self-immolative spacers and the few examples in the literature employ a disulphide bridge, which is not particularly stable in a physiological environment, or an acetyl group as a protecting group.[176,177] Their possible release from a system to which they are bound as thioethers would be extremely advantageous as, to our knowledge, there are no reported examples. The molecule chosen for the study is *N*-acetyl-2-cysteine, a pharmacologically active compound.

As free carboxylic acid moiety could compete in the addition reaction of the molecule on compound **114**, it was protected by esterification with $SOCl_2$ in MeOH to obtain the corresponding methyl ester. Once the esterified derivative **122** was obtained, the next reaction was carried out under standard conditions with DCM as the solvent. The product was isolated in excellent yields as a mixture of the two diasteroisomers in a ratio 1:1, identified by ^{1}H NMR spectrum analysis. (Scheme 34)

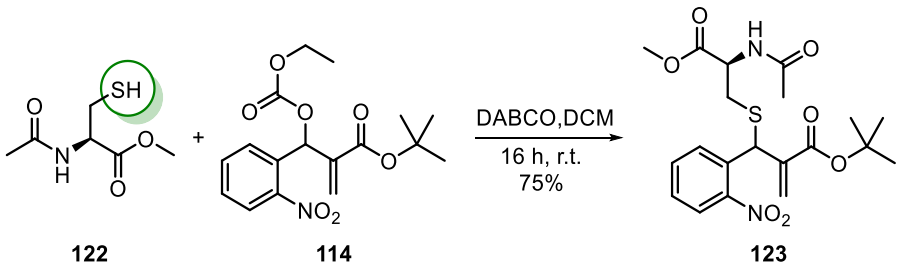

Scheme 34: insertion of aliphatic thiol.

The last two functional groups studied were a secondary amine and a hydroxamic acid, and two commercially available drugs were used as model compounds. Ciprofloxacin, an antibiotic belonging to the fluoroquinolones family and, as an antibiotic, of particular interest for the development of prodrugs that can be activated by the nitroreductase enzyme expressed in prokaryotic cells, was chosen for the amine. The NH group of piperazine has a high basicity and nucleophilicity but, as with *N*-acetyl-2-cysteine, it was necessary to methylate the carboxylic acid to avoid the formation of by-products.

Esterification was performed, as reported in the literature,[206] by suspending Ciprofloxacin in MeOH and treating it with *p*-toluenesulphonic acid. The methylated compound **124** was obtained in quantitative yield and no purification was required. The protected Ciprofloxacin was then reacted with compound **114** under standard reaction conditions and the product was obtained in moderate yield (52%).

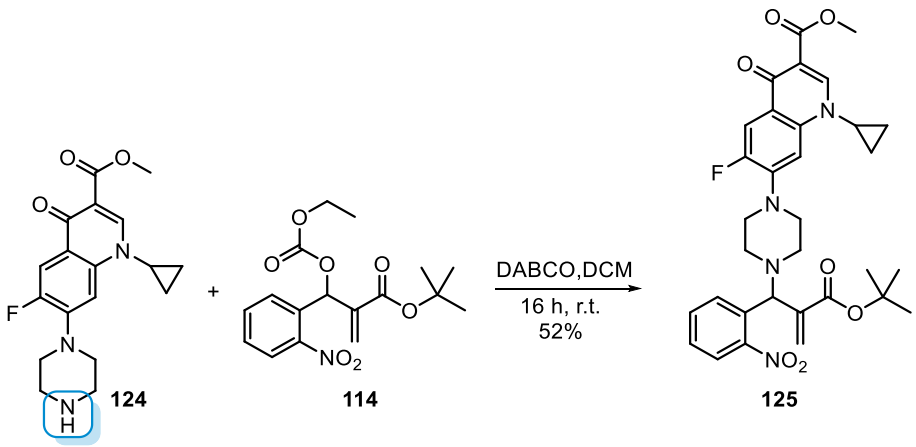

Scheme 35: insertion of secondary amine.

For the last class of molecules, the hydroxamic acids, Vorinostat (**33**, SAHA), an HDAC inhibitor currently in use for the treatment of malignant tumours, was used. It has several side-effects due to its non-selectivity towards tumour cells, so synthesising a prodrug of SAHA that can only be activated in specific targeted tissues would reduce its toxicity.[207] The reaction with the carbonate made it possible to obtain the product, even if in low yield.

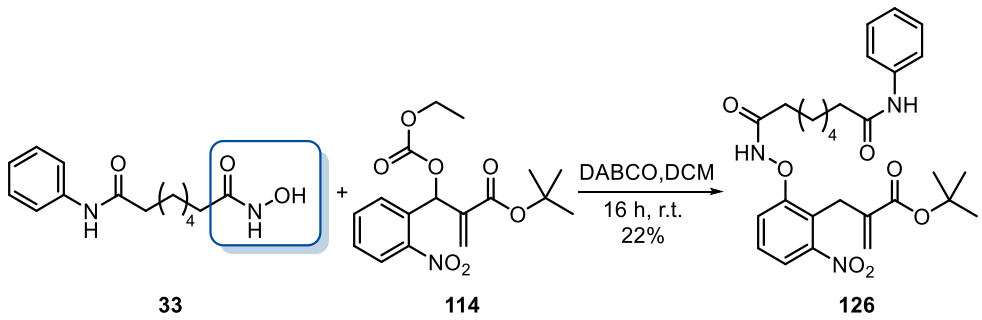

Scheme 36: insertion of hydroxamic acids

Summarizing, the functional groups successfully introduced were sulphonamide, phenol, indole, hydroxamic acid, thiol and secondary amine. The products obtained are collected in Scheme 37.

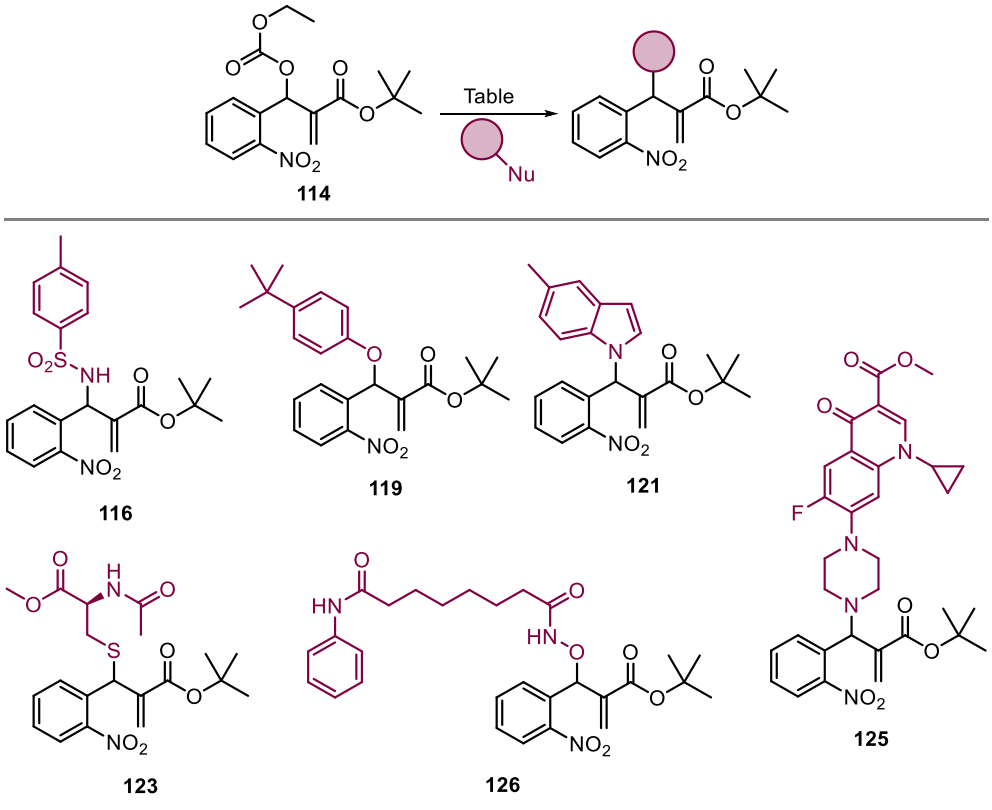

Scheme 37: product obtained with the different functional groups for testing the release with the self-immolative spacer.

2.3.3.2 Kinetic study of the releases

The proposed release mechanism involves intramolecular cyclization with the formation of a 6-terminal cycle that should be thermodynamically favoured.

We carried out the reductions of all the compounds under the same conditions, and we determined the concentrations of the released products, the reduced byproducts (when no release took place) and the conversion of the starting materials by HPLC-MS at predetermined time intervals. Chromatograms were obtained using an eluent mixture H_2O+HCOOH 0.1% /CH_3CN+HCOOH 0.1% with a gradient of CH_3CN 20-95%.

Reactions were set up on small amounts of nitro derivatives and sampling was carried out at 6 times: 0.0 h (t_0), 0.25 h (t_1), 0.5 h (t_2), 1 h (t_3), 2 h (t_4), 6 h (t_5), 8 h (t_6). With the increase in the concentration of the model compounds it was possible to describe the kinetic curve for each of the systems tested. (Figure 22)

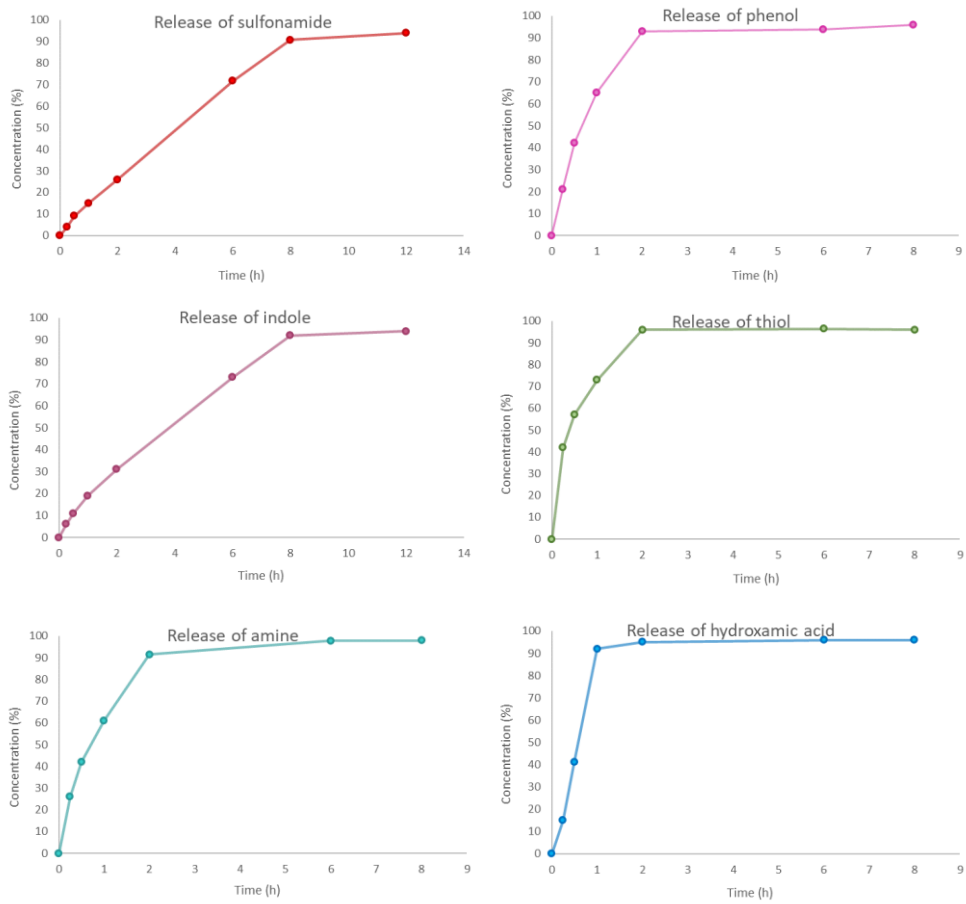

Figure 22: Kinetic curves of the release of 4-methyl benzyl sulphonamide (red line), 4-*tert*-butyl phenol (pink line), 5-methyl indole (violet line), methyl acetyl-cysteinate (green line), methyl ciprofloxacin (light green line) and SAHA (blu line). Concentrations are reported as a percentage of the free compound detected by HPLC-MS.

The first case was the one bearing a sulphonamide, the free functional group was detected after 15 min together with the dihydroquinoline derivative. As it is highlighted in the graphic in figure 22, the release time was 8 h, then the plateau was reached and the starting material completely consumed.

The second compound studied was the phenolic-derivative **119**. In this case the release was faster than the previous one, as showed in the kinetic curve (Figure 22).

After the first hour, the concentration of the phenol was already high, and after 2 h the reaction was complete.

For the compound bearing the alkylated indole, the reduction of the nitro group was fast and it finished after 1 h, but the release was slow. This led to the identification of the corresponding aniline before the intramolecular cyclization in the HPLC-MS chromatograms. The concentration of the 5-methyl indole kept increasing until 8 h making necessary another analysis after 12 h, where the release was finished.

We were gladly surprised by the release of the thiol kinetic profile. After 15 minutes the concentration of the free compound **122** was already high, even with the reduction of the nitro group not completely finished, and the corresponding amine was never detected. After 2 h, methyl-acetyl-cysteine was completely released and the starting material consumed.

For the release of the secondary amine **124**, we expected that the release of amine should be fast due to its good group leaving capacity. After 1 h, two picks in the chromatogram, corresponding to the free drug and to the dihydroquinoline derivative, were already clearly evident and the release finished in the next hour. (Figure 22)

The last case studied was the hydroxamic acids. In this case, the reduction was fast and after only 30 min the starting material **126** was already consumed, detecting both the drug and the aniline derivative. The intramolecular cyclization required another 30 minutes, after which the pick of the aniline disappeared resulting in the fastest release obtained.

Table 4: $t_{1/2}$ (h) values obtained for the release of different functional groups from the MBH system after reduction with Fe/Pd NPs.

	116	**119**	**121**	**123**	**126**	**125**
$\mathbf{t_{1/2}}$ (h)	4.41	1.07	4.34	0.44	0.61	0.81

Analysing the results, it is possible to observe how fast the phenol, hydroxamic acid and secondary amine were released, but surprisingly the fastest was the release of the aliphatic thiol. Slower kinetics were obtained for sulphonamide and indole, but all the functional groups tested were released unmodified within a reasonable time.

2.3.3.3 Synthesis of new functionalized self-immolative spacer

Following the good results obtained for the model system with several functional groups, the introduction of a terminal alkyne into the structure of self-immolative spacers was considered for its application in more complex delivery systems such as ADCs.

For the new molecule, we chose to start with vanillin, which is commercially available, cheap and has a phenol that could be functionalized to introduce the unsaturation of interest.

Thus, the synthesis started with the alkylation of the hydroxyl group with propargyl bromide and potassium carbonate as a base. The reaction works well and the product **127** was obtained in high yield. The second step was nitration under standard conditions, the sulphonitric mixture allows the regioisomer **128** of interest to be isolated in acceptable yield after column chromatography, and sequentially the MBH reaction was carried out under the same conditions as previously described. Finally, the alcohol **129** was activated as carbonate. (Scheme 38)

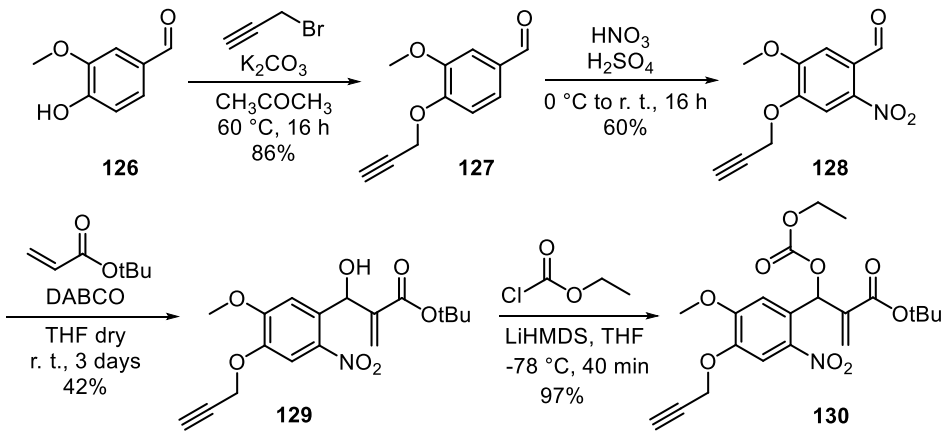

Scheme 38

A model drug, Ciprofloxacin methyl ester (**124**, CpxMe) was then introduced into the final structure to test the applicability of the system and in particular its stability under physiological conditions. Our biggest concern was the possible nucleophilic attack

on the double bond by plasma proteins or free thiols, which could result in the uncontrolled release of the payload.

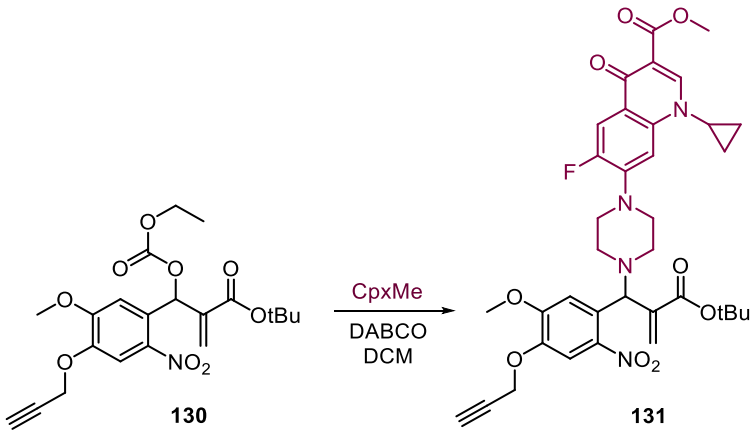

130 131

Scheme 39

Initial tests were unsuccessful since compound **131** was completely insoluble in water. Samples were prepared with DMSO as cosolvent in different amounts, the last of which was 1:1 (DMSO:plasma) and again the compound precipitated. To increase the solubility, a TEG tail was introduced on the alkyne through a click reaction. The azide **134** was synthesized according to literature procedures and obtained with moderate yield.

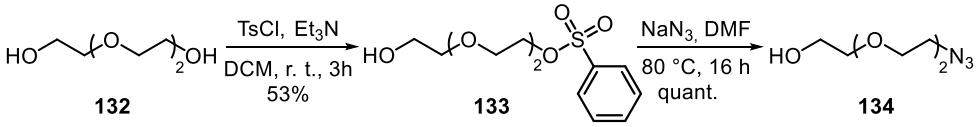

132 133 134

Scheme 40: synthesis of the azide

The click reaction was carried out at room temperature using $Cu(OAc)_2$ and sodium ascorbate as catalysts, in a mixture of DMF and water as solvents. The crude reaction mixture was purified, allowing to obtain the compound **135**.

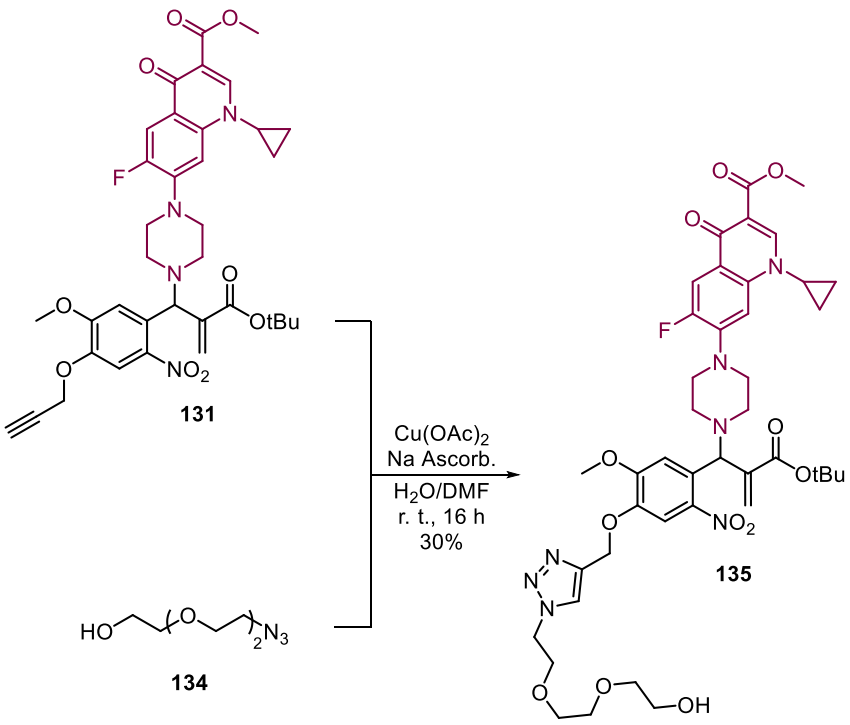

Scheme 41

With the final product in hands, we were able to test the plasma stability and we were glad to find that the system was more stable than expected, 89.9% of unmodified compound was found after 24 hours of incubation and the half-life ($t_{1/2}$), expressed as the amount of time it takes before half of the drug is hydrolysed/degraded, is more than 48 h.

Table 5 Stability tests of compound **135.**

Compound	H_2O	Buffer pH 7.4,[a] $t_{1/2}$[b]	Buffer pH 6.5,[a] $t_{1/2}$[b]	Plasma[a], $t_{1/2}$[b]
135	99%	94%, >48 h	94%, >36 h	89.9%, >48 h

[a]Expressed as percentage of unmodified compound after 24 hours of incubation.
[b]Half-life ($t_{1/2}$) expressed as the amount of time it takes before half of the compound is hydrolysed/degraded.

2.3.4 Conclusions

A new self-immolative spacer has been synthesised and successfully applied to the release of different functional groups present in many drug classes. The release trigger involves the reduction of the nitro group, which allows its use in conditions of tissue hypoxia or for therapies involving the nitroreductase enzyme. This system can be used for the synthesis of prodrugs. We further developed a derivative containing a functionalized terminal alkyne to expand the application to more complex delivery systems. The starting compounds employed in the synthesis of the prodrugs are cheap and easy to find, and the synthetic steps are simple and not difficult to purify, which highlights the potential of the new releasing system in higher scales. Finally, the stability of the system in plasma was successfully verified.

Chapter III

Design of new photolabile protecting groups for the selective release of drugs in the NIR region of UV-Vis spectra

3.1 Introduction

3.1.1 Photoremovable protecting groups

In chemistry, a protecting group is the moiety that masks a functional group to protect it from undesired reactions. Photoremovable protecting groups belong to the category of light-sensitive substances that allow to mask functionalities and subsequently uncaging after irradiation with a light of a suitable wavelength. The light is a reagent leaving no traces in the process, the removal occurs in mild conditions and does not require additional chemical reagents. Photoremovable protecting groups were introduced in organic chemistry in 1962 by Barltrop[208] and Barton[209] followed by Engels[210] and Kaplan[211] who first reported the photoactivation of cyclic adenosine monophosphate (cAMP) and adenosine triphosphate (ATP), using the photolabile 2-nitrobenzyl and (2-nitrophenyl)ethyl groups. Since then, photolabile groups have been a keystone in optochemical biology. They have been used for the light regulation of many biomolecules,[212] providing precise spatio-temporal control over biological processes in the cellular environment.[213]

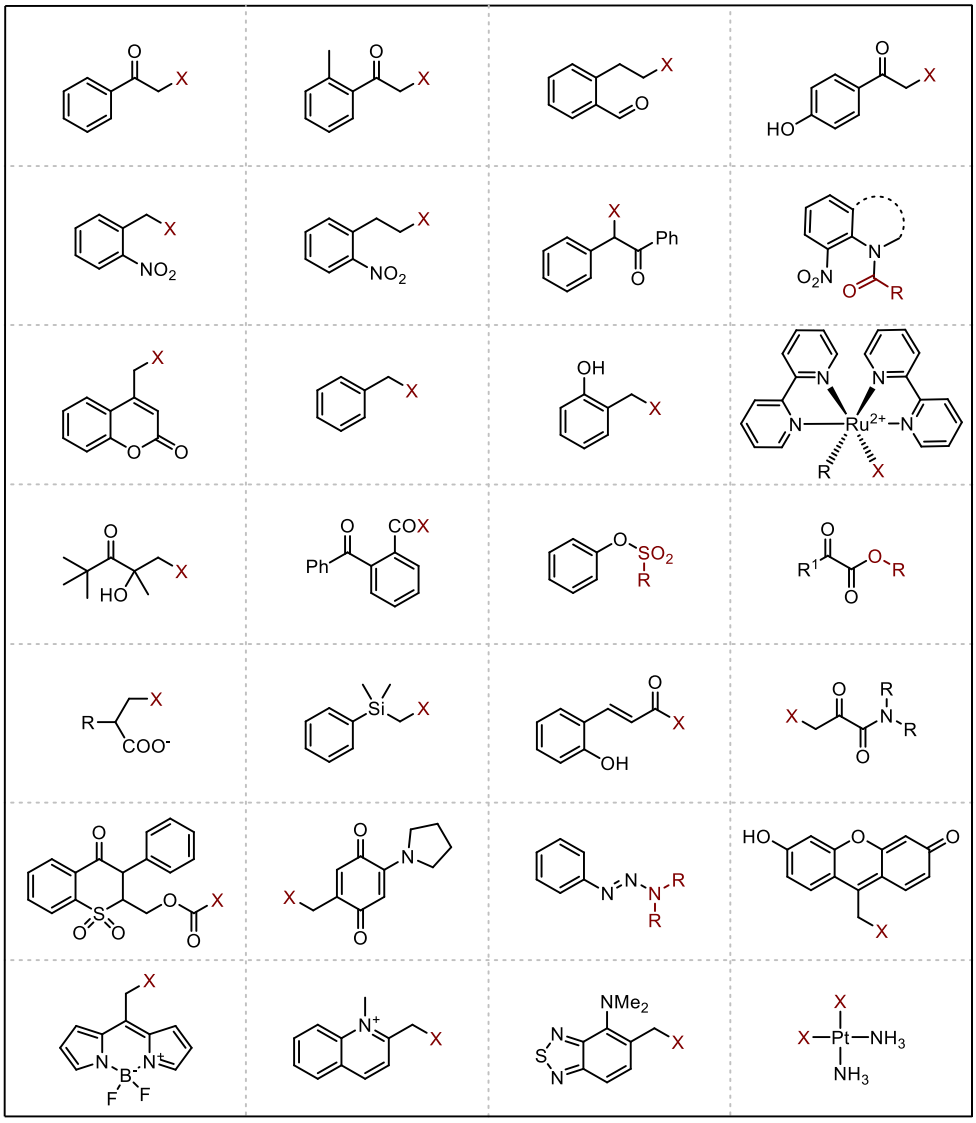

Figure 23: some class of photoremovable protecting group.

The development of an efficient PPG is related to its application, but there are some general features that must be respected.

In general, a PPG should have a high quantum release yield (Φ), and a high value of molar extinction coefficient (ε). The molar extinction coefficient expresses the ability of a light-sensitive compound to capture photons, while the quantum yield is a measure of the compound's ability to translate this absorption into a chemical event.

The quantum yield is given by the number of moles of product formed divided by the moles of photons absorbed.[214] The product of these two parameters yields the quantum efficiency (εΦ), which is used to measure the reactivity of the photosensitive compound.[215,216]

A PPG also needs to be pure, have low intrinsic activity and be thermodinamically stable before and after the photorelease. Their byproducts accompanying the release cannot absorb at the wavelength used for deprotection to prevent competitive absorption and the PPG and the byproducts must not react with other molecules present in the reaction environment. Furthermore, it is essential that the PPG should not cause the formation of radical species.[217]

In order to be applied in the biological field, PPGs must not only fulfil all the characteristics listed above, but also need to be biocompatible and not be reactive with the biological target. They have to absorb a wavelength greater than 350 nm, to avoid the undesired breaking of covalent bonds, that can occur due to the high energy of light at shorter wavelengths, and the interaction with biological macromolecules or tissue damage. They should also be soluble in aqueous media, not interfere with the pharmacodynamics of the system and the byproducts, in addition to being transparent at the irradiation wavelength, need to be non-toxic.[218]

Lots of different class of PPGs were developed but most of them are not suitable for in vivo application. The ones that have the right features became part of photocleavable linkers for the design of new prodrugs and drug delivery systems.[219]

3.1.2 Photocleavable linkers

In medicine and pharmacology, selective drug delivery is a topic of increase interest that includes a wide range of different approaches. In this context, one of the most common problems in drug therapies is the low accumulation rate of drug molecules in the targeted area.[2,220]

The two main types of stimuli considered for selective drug release are:

- Endogenous stimuli (pH, enzymes, redox reactions, etc.)
- Exogenous stimuli (light, magnetic field, ionising radiation, etc.)

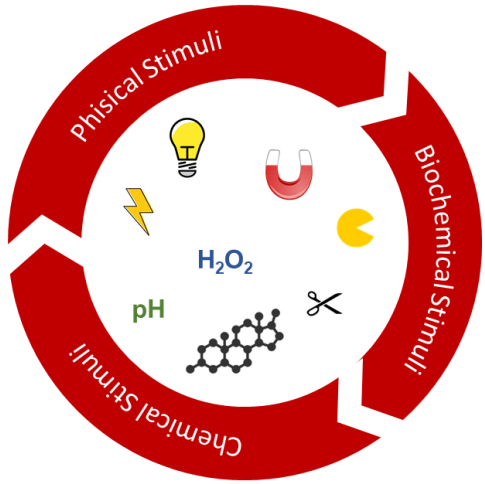

Figure 24: 3 stimuli subclasses: chemical, physical, biochemical.

In recent years, research has increasingly focused on the development of photosensitive drug delivery systems to achieve targeted drugs that can only be activated after a light stimulus. In this field, photosensitive systems have been designed to be cleaved only with a specific wavelength, allowing spatial and temporal control over the release of the active compound. Spatial control enables greater accumulation of the drug in the target cell, on the other hand, temporal control gives precise regulation of the amount of drug to be released into the cell. The efficiency of these systems depends on the external light properties used.[221]

The parameters to be taken into account are light intensity, absorption and irradiation time.

Light interacts with tissues by diffusion and/or absorption since the depth of light penetration is inversely proportional to the attenuation coefficient. The power and wavelength can be precisely adjusted for different photoreactive systems to achieve tissue, cellular or subcellular release.

For in vivo drug delivery, the wavelengths that can be used should be in the range of 400 - 900 nm, shorter wavelengths have been shown to be damaging to cellular tissues whereas excitation in the near-infrared can lead to tissue heating.[222,223]

The light spectrum is divided into UV (200-280 nm UVC, 280-320 nm UVB and 320-400 nm UVA), Vis (visible, 400 - 650 nm) and NIR (near infrared, 650 - 2500 nm).

Systems that respond to UV and visible radiation can be used for topical treatments; radiation below 600 nm cannot penetrate deeper than 1 cm into the tissue due to high scattering and absorption by haemoglobin, oxyhaemoglobin and water, indeed UV radiation from the sun is one of the main factors behind skin cancer. This limitation in the wavelength and the difficulties in developing new structures with a high absorption maximum are partly responsible for the intense interest in two- photon excitation.[224]

Near-infrared light between 650 and 900 nm can reach up to 10 cm into tissues and causes minimal damage to the target tissue, making it preferable to other types of light for triggering the release of a drug into a biological system.[225]

The ability of tissues to penetrate light is dictated by several parameters. First, the nature of the tissue plays a key role, as some tissues are more transparent to light than others. In addition, the parameters and technology of light delivery can also modulate tissue penetration and when the tissue depth is an issue, new alternative technologies such as biodegradable fibre optics or small wireless light sources can be employed.[226,227]

Regarding the wavelength, if too short, it is impossible to penetrate the tissue and damage is possible. However, the main limitation is the ability to generate the photon flux required to trigger the desired effect. Two parameters are generally used, the molar extinction coefficient (ε) and the quantum yield (Φ).

They are parameters introduced to evaluate the reactivity of PPGs but obviously used also to determine the efficiency of photosensitive drugs. The product of theme, the quantum efficiency ($\varepsilon\Phi$), is the most used in phototherapy to measure the reactivity of the photosensitive drug.[215,216]

As a consequence of all these limitations, only recently the attention has been focused on the development of novel high-wavelength activated photorelease systems that can be used in vivo and many efforts have been made in this regard. Numerous nanostructures such as liposomes, polymeric nanoparticles, micelles, and polymer-drug conjugates have been recently developed.[228–233]

Two strategies are usually employed to construct a photolabile therapeutic agent. The first requires a function, essential for the pharmacological activity, bounded to a photolabile group. The compound becomes inactive and, after irradiation, release of the native structure occurs reactivating the biological activity. The second strategy involves the use of a carrier to which the compound is attached by a photolabile bond that can be cleaved by irradiation to release the drug. This approach does not deactivate the compound through a structural modification but by preventing its interaction with the biological target.[234]

Since phototherapy started to attract general attention, several reviews, on nanocarriers[220,235], photolabile protective groups[219,225,236], prodrugs and mechanisms involved in the release of the active compound[221,234], have been published. Therefore, in this thesis we will discuss only the topics strictly related to the projects.

3.2 Rational design of a new BODIPY derivative for photosensitive drug delivery systems

3.2.1 BODIPY

Boro-dipyrromethene (BODIPY), a fluorescent dye whose structure resembles that of porphyrins, has been extensively studied in recent decades.

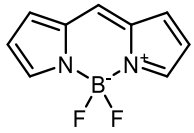

136

Figure 25: structure of BODIPY

In 1968, the synthesis was first reported by Treibs and Kreuzer[237], but it is only in recent years that the focus has been on studying its properties and the various applications in different fields of research. They noted that the acylation of 2,4-dimethylpyrrole with acetic anhydride and boron trifluoride, as Lewis acid, led to the formation of a highly fluorescent compound.

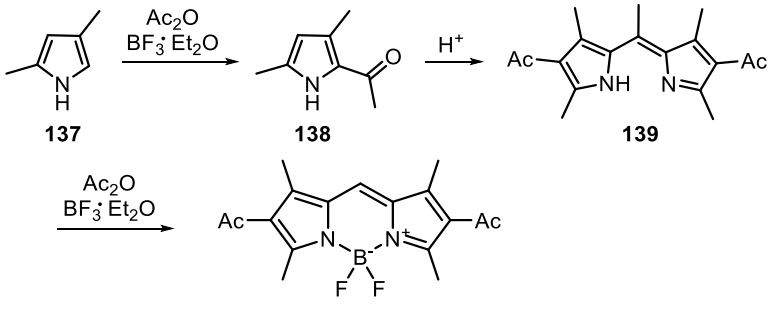

137 **138** **139** **140**

Scheme 42: first reported synthesis of BODIPY.

The core structure consists of two pyrrole rings connected by a methylene and a BF_2 group, in which the boron atom coordinates the heteroatoms. In analogy to porphyrin systems, position 8 is called the *meso* position. The coordination of the boron atom is responsible for the rigid, planar structure. In addition, this molecule has frontier

molecular orbitals similar to those of long-established PPGs (such as coumarins and xanthenes).[214]

Over time, the boron-dipyrromethene dye (BODIPY) is finding increasing use in numerous fields thanks to the versatility of its chemical and physical properties, which can be modulated through changes in the core structure. It has been used in the pharmaceutical field as drug delivery agents[238], as a sensitiser for photodynamic therapy (PDT)[234], as a PPG (photolable protecting group), but also as a fluorescent indicator, chemosensors,[239], electroluminescent agents[240], solar cell sensitisers[241], etc. The BODIPY core can be functionalised in various ways, providing great versatility in terms of structure and photochemical properties.[242]

Initially, the major problem that slowed down the research on potential PPGs, capable of absorbing in the visible or even in the NIR, was the lack of a robust relationship structure-reactivity regarding the heterolysis that PPGs must undergo in the excited state. In other words, it is difficult to predict which structure, once irradiated with light, will undergo efficient photo-heterolysis reactions.[243]

It has been proven that photo-heterolysis of a C-LG bond (LG = leaving group) must generate two low-energy carbocations.[244] In the work published by Goswami and coworkers, as a result of a computational study using TD-DFT theory, they found that the energy gap for the S_0-S_1 transition of the carbocation generated by C-O cleavage is only 8 kcal/mol, suggesting a near-degenerate diradical configuration.[243] For this reason, since it is easy to induce C-O bond cleavage, the *meso* carbon of BODIPY can be functionalised with a CH_2OH group upon which a drug can possibly be bonded. In this way, the drug is masked by covalent bonds and is inert until it reaches the site of action, achieving a photocleavable prodrug. The deprotection mechanism takes place with irradiation at wavelengths in the visible spectrum, inducing the formation of carbocation on the BODIPY with consequent release of the drug (Scheme 43). The functional groups that can be bound are carboxylic acids, alcohols and amines.[242]

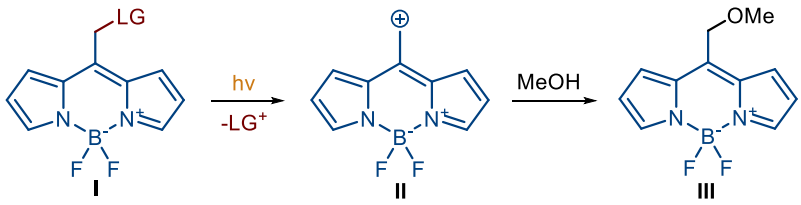

Scheme 43: deprotection mechanism.

BODIPY has further advantages: it is very easy to synthesise and soluble in most of the organic solvents, has a compact structure, is photostable, is compatible with biological systems[245] and has very high absorption in the visible range (located within the UV/Visible region at approximately 490/550 nm).[246]

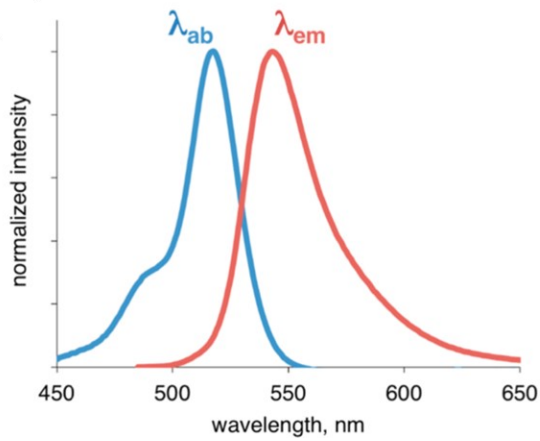

Figure 26: absorption (blue line) and emission (red line) spectra of BODIPY.

This molecule absorbs in the visible region, but it is still possible to modify the core structure to raise the wavelength even further. The ideal situation would be to create a structure that is compatible with biological systems and absorbs in the therapeutic window of light, meaning at a wavelength of 600 to 900 nm.

3.2.1.1 Functionalization of BODIPY structure to increase absorption wavelength

Several strategies have been employed to modify the structure of BODIPY. The simplest approach is to introduce atoms or functional groups onto the starting pyrrole rings. Indeed, the versatility of this core allows a wide variety of substituents to be introduced, giving rise to countless structures whose photochemical properties are often studied with the support of computational chemistry.[247–249]

Alkylation and arylation in the *meso* position have no significant effect on the absorption and emission wavelengths. For example, the difference between compounds **141** and **142** in figure 27 can be attributed to the presence of methyl groups in positions 1 and 7 which block the phenylic free rotation, there is no conjugation between the aryl substituents and the BODIPY core as both groups adopt twisted conformation to minimise steric hindrance.
This was proved by performing computational study where it was found that methyl substitution in that positions leads to a nearly perpendicular configuration due to geometrical restrictions.[250]

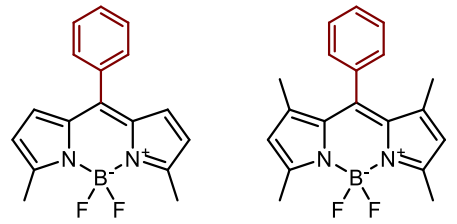

Figure 27: examples of meso aryl substituted BODIPY compounds.[250]

The introduction of halogens into the core structure increases the maximum absorption and maximum emission values. Since the first halogenated derivative (2,6-dibromo)[251] was assembled, various halogen-substituted compounds have been prepared. The first 3,5-dihalogenated derivative was reported in 2005[252], attracting

interest due to the wide distribution of HOMO and LUMO at these positions, as well as the less commonly used 8-halogen derivative.[253]

There are various synthetic strategies for introducing halogens, either by direct halogenation of the nucleus or by introducing halogens on the pyrrole precursor, as the higher electronic density of pyrrole makes it suitable for halogenation. The most used is the direct halogenation on the BODIPY structure that allows to obtain mono- or di-halogenated derivatives.

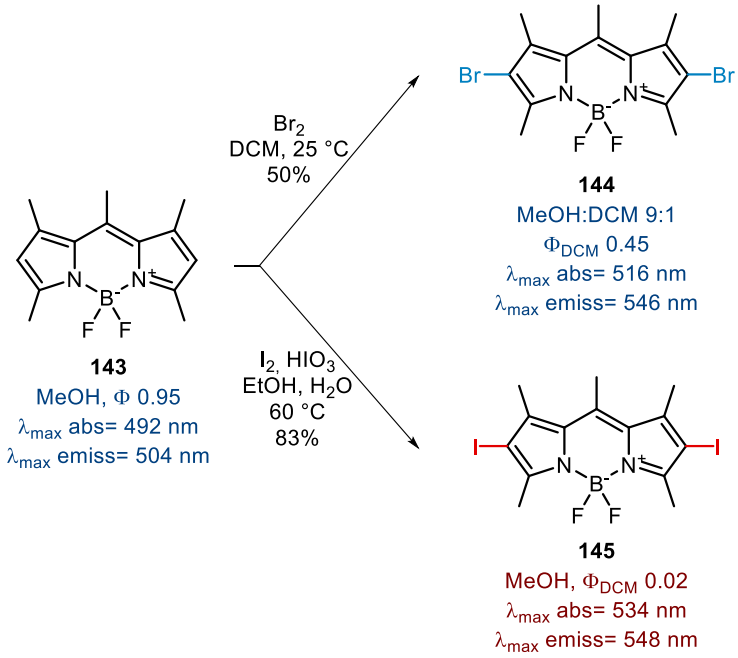

Scheme 44: example of direct 2,6 bromination and iodination of BODIPY.[254]

Halogenated derivatives can be used as precursors in subsequent functionalisation reactions, such as Suzuki and Stille arylation reactions, Heck reaction, Sonogashira alkynylation and nucleophilic substitutions.[255,256]

Among the various strategies applied, the introduction of substituents in position 3 and 5 is particularly useful to obtain an extension of the π-system conjugation, as 3,5-dimethyl derivatives, like other electronically poor heteroaromatic systems, are very acidic and this allows condensation with aromatic aldehydes leading to higher conjugate system via a Knoevenagel reaction. The use of aromatic aldehydes with

electron-donor substituents leads to an additional bathochromic shift in both absorption and fluorescence spectra, especially if they are in the para position to the aldehyde function. This approach has been identified as one of the best strategies for generating BODIPY derivatives that absorb in the NIR region.[257]

However, to increase the absorption wavelength, the simplest method remains the extension of the π-conjugation of the molecule, usually achieved by aromatic ring condensation.[250,258] The introduction of aromatic rings on the *a* or *b* bond produces a reduction in the HOMO-LUMO energy gap and in addition rigid, coplanar structures are obtained.[259]

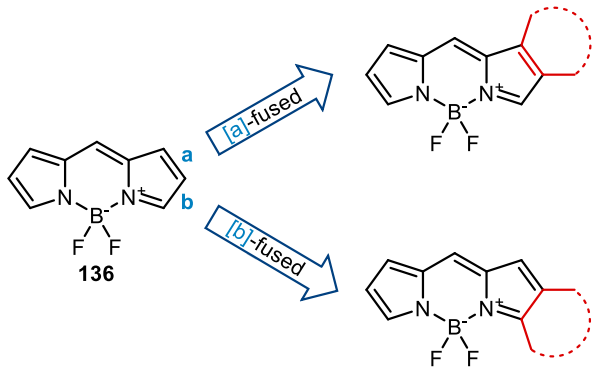

Scheme 45

Recently, five-member aromatic heterocyclics were used for substitution or condensation, such as furan, thiophene and pyrrole, instead of simple benzyl aromatic rings. These rings not only lead to an extension of the π-system but also maintains the rigidity and planarity of the structure.[250,259]

Benzofuran fusion can lead to an increase in the wavelength of absorption and fluorescence. There may be differences between 2,6-dioxy-benzofuran and 3,5-dioxy-benzofuran, for example for the last one there is a larger red shift in the absorption and emission bands.[257]

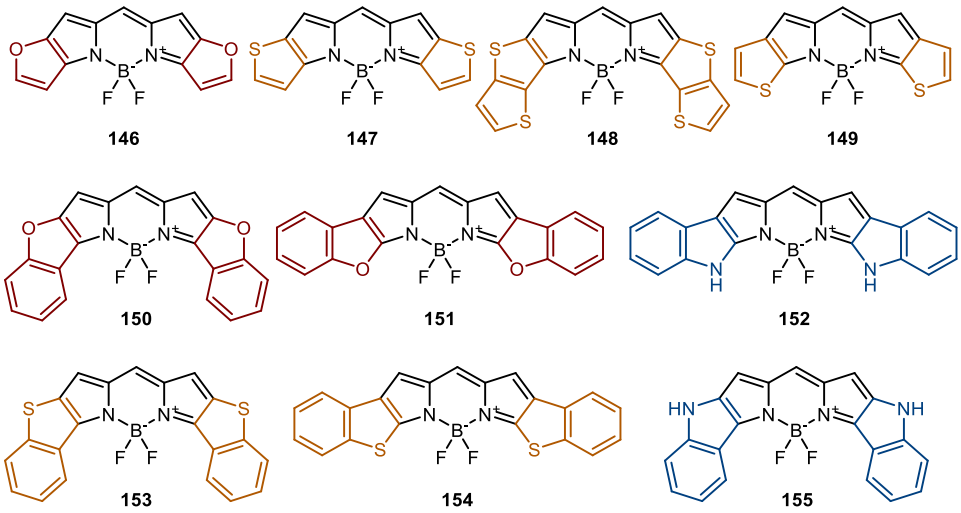

Figure 28: some examples of heterocyclic fused BODIPY derivatives.

There are many thiophene-fused BODIPY structures on the *a*- and *b*-bonds (Figure 28) that exhibit a broad bathochromic shift due to the inductive electron-donating effect of the heteroatom, which further reduces the energy gap between the frontier molecular orbitals. These structures can be additionally functionalised with the use of other substituents, leading to molecules that absorb over a very wide range due to the combination of the effects of extended π-conjugation, the presence of electron-attracting and/or electron-donating groups and the heteroatom.

In a work by Awuah et al., they developed BODIPY fused with thieno-pyrroles that show very high absorption (between 650-900 nm). Among the structures that have been synthesised, those with the lowest λ_{max} values are structures **157** and **156** (Figure 29). This decrease in absorption wavelength seems to be consequence of the interruption of π-conjugation by the oxygen between the core and the peripheral phenyl groups, while the presence of a sulphur atom in the same position leads to a smaller decrease in the λ_{max}. (Structure **158**, Figure 29)[260]

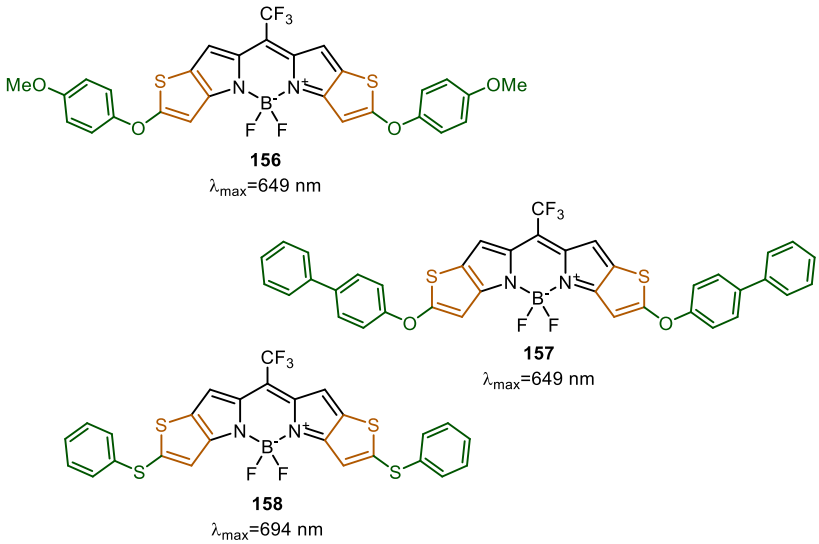

Figure 29: derivatives of BODIPY reported by Awuah *et al*.[260]

A systematic study of the optical properties of the BODIPY nucleus and the dependence on the nature and position of the substituent was published.[261] By analysing the different combinations, the different nature of the substituents and their positions, a trend in the spectral shift was observed, which can be explained by the delocalisation of π-electrons within the core. The greatest influence on the photophysical properties occurs for moieties with a mesomeric effect.

In summary, they report that for the blue shift acceptor substituents should be inserted in positions 2 and 6 or donor substituents in position 8. For the red shift, acceptor substituents should be placed in positions 8, 3 and 5 and donor substituents in positions 2 and 6.

The explanation for these data is given by the analysis of frontier molecular orbital energies. Donor groups should lead to a decrease in the excitation energy due to an increase in the energy of the HOMO, while acceptors should have the opposite behaviour, leading to a decrease in the energy of the HOMO and a consequent increase in the excitation energy. The results obtained show that the acceptor substituents not only increase the energies of the HOMO orbitals but also act by decreasing the energies of the LUMO orbitals. It is well known that an increase in the

delocalisation of the π-system leads to an increase in the stability of the ground state. The distribution of π-electrons in the unsubstituted BODIPY core can be altered by the electronic effect of the substituent. If the "new" charge distribution is more delocalised than in the unsubstituted BODIPY, a blue shift is observed and, conversely, if the charge distribution is more localised, a red shift occurs.[261]

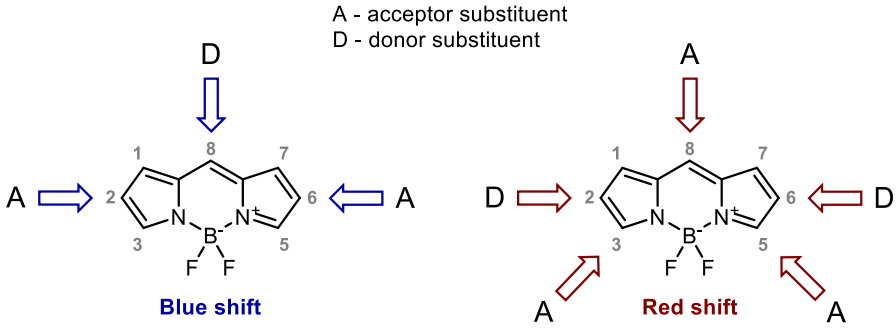

Scheme 46

In summary, in order to functionalize BODIPY derivatives to achieve light absorption in the NIR, the most commonly used strategies are:

- fusion of aromatic rings/heterocycles at the a- or b-bond
- functionalising positions 3 and 5 by further extending the π-system, e.g. by introducing styrene derivatives
- insertion of electron-donator groups in positions 3 and 5.[250]

In addition to structural modifications, there are other ways of carrying out a low-energy photolytic reaction.

Generally, photochemical reactions proceed via a "multi-photon" mechanism involving the absorption of two photons. One reported approach to limit the energy required to achieve photolysis is through triplet-triplet energy transfer (TTET), which involves a photosensitiser and a photolabile molecule. In the work published by Lv and coworkers, Platinum(II) tetraphenyltetrabenzoporphyrin (PtTPBP) was chosen as the photosensitiser and a prodrug bearing BODIPY as the photocleavable molecule. Photolysis of the system is achieved by a TTET mechanism following

excitation of PtTPBP around 625 nm. The release efficiency was higher than with direct excitation of the photolabile prodrug at 530 nm. Therefore, it was hypothesised that the system could be excited in the S_1 state of the photosensitiser, which then, via an intersystem crossing process (ISC), arrives in an excited T_1 triplet state that has a higher energy than the T_1 of the photolabile molecule. This leads to TTET to the T_1 state of the prodrug, resulting in the release of the active compound. (Figure 30) Due to the lower-energy excited S_1 state of PtTPBP, it is possible to use low-energy light radiation to induce a high-energy photolysis reaction.[262]

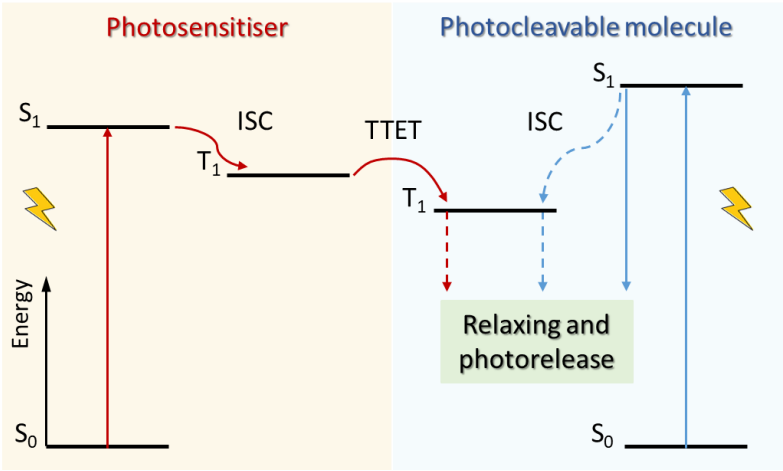

Figure 30: photorelease through a TTET process (red line) and phtorelease through direct excitation of photocleavable molecule (blue line).

3.2.1.2 Benchmark studies on BODIPY derivatives

The valuable optical properties of BODIPY core structures are often studied using computational chemistry. Comparative studies, or benchmark studies, are usually carried out to test the accuracy of the theories available in computational chemistry and to understand their applicability in different fields. The reciprocal interaction between experiment and theory and the reproducibility of experimental data through

theoretical calculations allows the validation of theoretical models and their use for predictive purposes.

In 2019, Matulis and co-workers[261] carried out a study of 11 BODIPY derivatives (Figure 31) exhibiting absorptions in the 491-793 nm range, using TD-DFT theory to investigate the accuracy of 8 DFT functionals in which the effects of solvation on the excitation energy were assessed via the Linear Response (LR) scheme and the State Specific (SS) scheme.[263,264]

The studied functionals are:

- B3LYP, M062X and PBE0, the most used hybrid functionals
- CAM-B3LYP, wB97XD, LC-WPBE
- LC-M06L
- BMK

They construct a linear correlation curve between the calculated data and the experimental data. In general, the analysis of linear regression coefficients and maximum deviations reveals which functionals have the best performance.

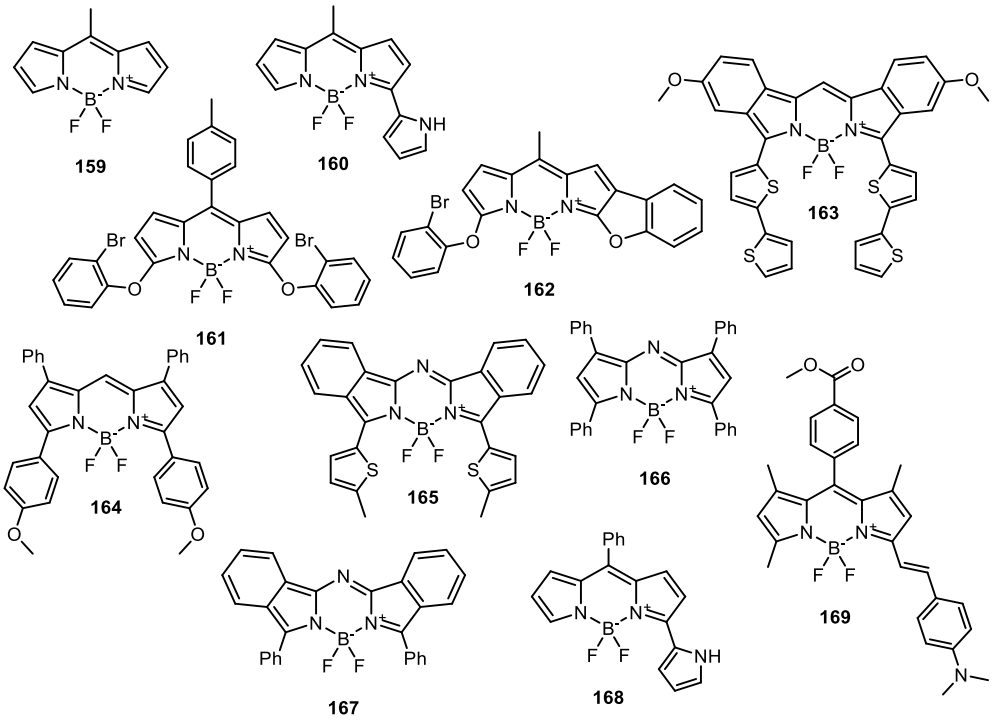

Figure 31: the studied structures reported by Matulis *et al.*[261]

Their results showed that the functionals giving the most reliable data in the calculation of the absorption spectrum were M062X, wB97XD and CAM-B3LYP. Of particular note, M062X offers better performance in the LR scheme while wB97XD offers better performance in the SS scheme.

Another study, carried out on various BODIPY derivatives (Figure 32), compares BMK and CAM-B3LYP functionals. In this work, the wavelengths of maximum absorbance were calculated using BMK/6-311+G(2d,p) and CAM-B3LYP/cc-pVTZ as levels of theory and the values obtained with both deviate from the experimental values with an average of approximately 73 nm. Applying a linear empirical correction, it was observed that the value of R^2 is optimal, (R^2 = 0.92 for BMK and R^2 = 0.94 for CAM-B3LYP). The vertical excitation energies showed an overestimation of the experimental values of 0.29 eV for CAM-B3LYP and 0.30 eV for BMK.[263]

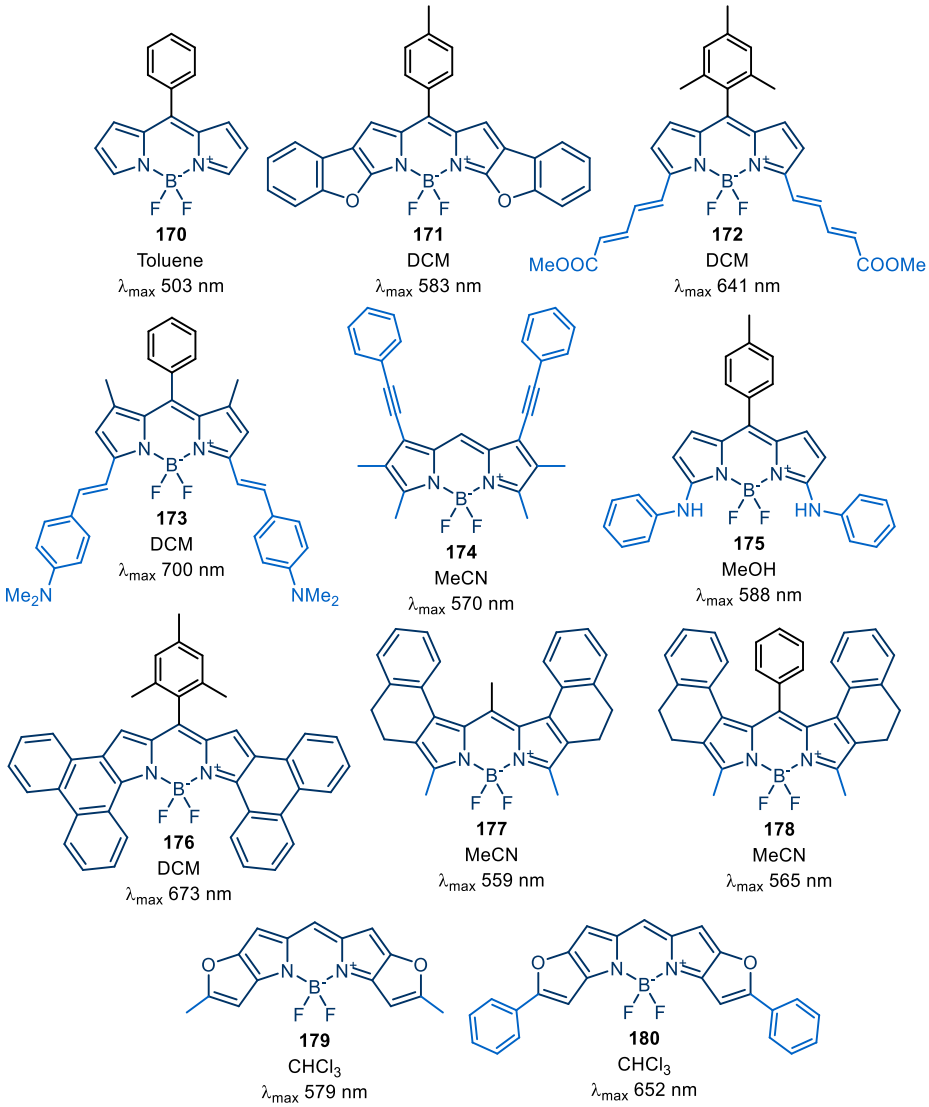

Figure 32: BODIPY structures studied by Rose *et al*. [263]

Since there is no approach that allows to choose a priori one level of theory over another, many benchmark studies can be found in the literature.

Chibani, Jacquemin and co-workers carried out a study on the calculation of vertical energies with various functionals on a set of 24 molecules absorbing in the rage between 400-750 nm. The functionals tested were B3LYP, PBE0, BMK, M062X, CAM-B3LYP, wB97X-D. The obtained mean absolute errors (MAE) were high for

TD-DFT calculations, B3LYP and PBE0, resulting in mean deviations below the 0.3 eV limit and a weak R^2. Even though some of the data calculated with B3LYP and PBE0 are very close to the experimental value, they are not suitable for robust predictions. Particularly surprising is the performance of M062X, which provides a standard deviation of 0.06 eV and an R^2 of 0.98, resulting as the most adequate and performing functional even when tested on very different molecules, giving optimal results for MAE, SD and R^2.[264]

Any comparative analysis of DFT functionals needs to rely on basis sets that produce convergent results or at least mitigate typical errors that occur between experimental and calculated values. In general, increasing the size of the basis set slightly reduces the excitation energy but this does not have a significant impact on the results. According to a study reported in the literature examining basis sets such as cc-pVDZ, aug-cc-pVDZ, cc-pVTZ, aug-cc-pVTZ, def2-TZVPP, def2-QZVPP, adding diffusion and polarisation functions to the cc-pVDZ basis set to form aug-cc-pVDZ reduced the excitation energy of S1 by only 0.079 eV, while switching from cc-pVDZ to def2-QZVPP produced a reduction of 0.074 eV. These results led them to choose cc-pVDZ as the basis set to use in their work.[265]

In general, optimisations of geometries and vibrational parameters can be achieved using 6-31G* without a significant loss of accuracy.[266] In contrast, transition energies are much more dependent on the choice of basis set and the use of larger basis sets is recommended.[267]

One example is a study of isoindole-BODIPY derivatives for which their photophysical properties were theoretically determined, focusing on the calculation of absorption wavelengths. The performance of four exchange-correlation (XC) functionals was evaluated by comparing both geometrical parameters and electronic absorption spectra with available experimental data. Molecular ground-state optimisations were calculated using M06, M062X, wB97XD and PBE0 in combination with 6-31+G* as a basis set, each functional being able to accurately reproduce the geometrical parameters. Regarding the calculation of absorption

wavelengths, M06 provided satisfactory results in predicting maximum absorption with errors around 0.1 eV.[268]

Summarizing, from the works reported in the literature, we can conclude that the functionals with the most accurate results have a significant Hartee-Fock term,[269,270] so including this parameter also in the long-range functionals gives a more reliable result. For basis sets, the addition of diffuse functions does not bring a high improvement in the accuracy of the λ_{max} calculation.

3.2.2 Aim of the project

There is a growing interest in photocleavable drug release systems, which is why we have set ourselves the aim of studying, through computational chemistry, new structures derived from BODIPY that have an absorption wavelength that allows them to be used as photolabile protecting groups (PPGs) in cellular environment.
In order to predict the absorption maximum of new molecules with good accuracy by calculating vertical excitation energies using time-dependent density functional theory (TD-DFT), it was necessary to select a significant number of BODIPY derivatives for which the experimental absorption data were reported. Ten molecules were chosen with the absorption λ_{max} in the range between 600 nm and 900 nm, the therapeutic window. (Figure 33)

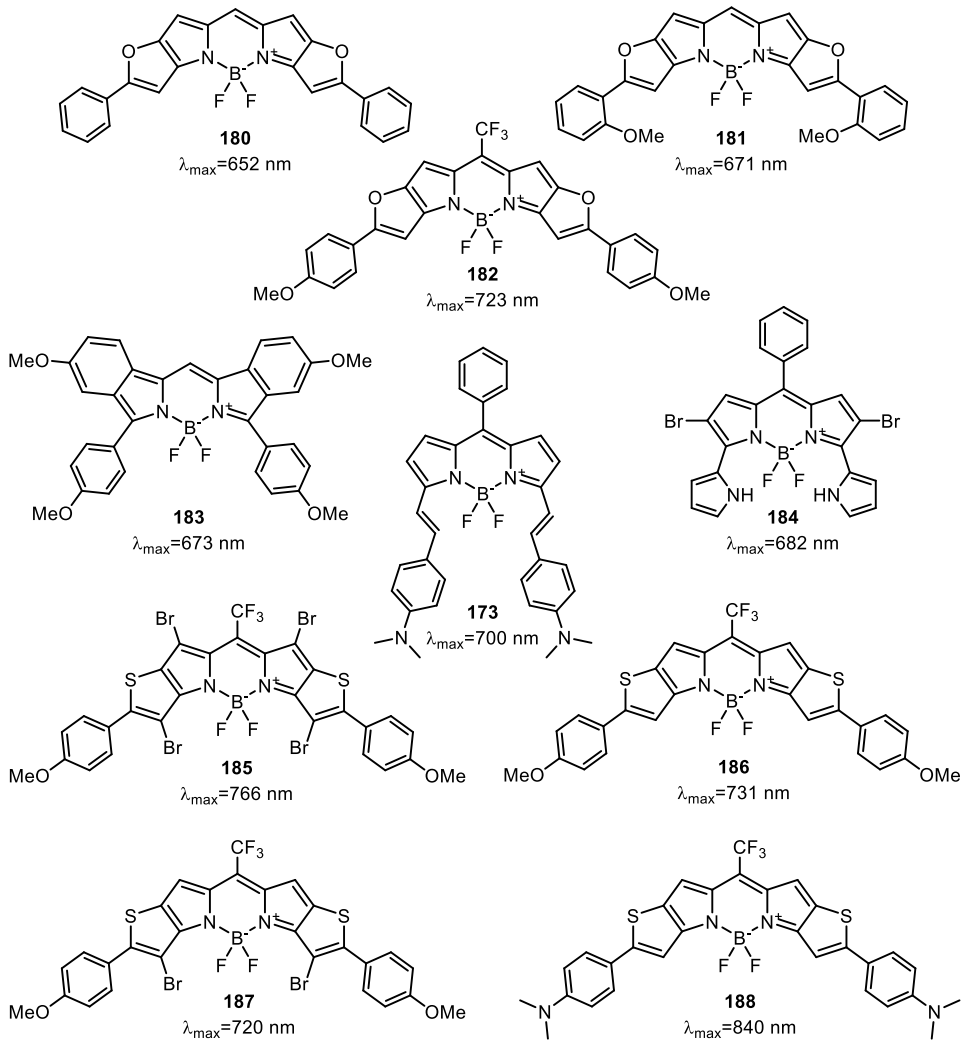

Figure 33: structures of the 10 chosen molecules.[250,260,263,271]

Vertical excitation energies obtained in TD-DFT are not physically observable and cannot be directly compared with experimental spectra, but trends in both are the same, so calculated vertical excitation energies are widely used for predicting experimental spectra.

Therefore, our first goal was to find a computational model capable of reproducing, with reasonable accuracy, the absorption maxima reported for this library of compounds.

Subsequently, new BODIPY derivatives have been designed and functionalized in various ways to achieve absorptions with λ_{max} values inside the therapeutic window. The core of these new structures will be the *meso*-methylhydroxy-BODIPY, where the hydroxyl function is required for the insertion of the drug to be released as the CH_2-LG bond has been proven to undergo photolytic cleavage. (see Scheme 43, Chapter 3.2.1)

Figure 34

3.2.3 Results and discussion

3.2.3.1 Study of the BODIPY derivatives in the ground state

The structures of the selected molecules (shown in chapter 3.2.2, Figure 33) were constructed with Avogadro and then the ground state geometry was optimised with Gaussian 16 using B3LYP/6-31G* as level of theory. The minimal geometries are reported in the experimental section (Chapter 4.6.1.1) together with the bond distances in Å and the angles in degrees.

In order to have the most appropriate levels of theory for the chosen molecules, a thorough literature search was carried out on benchmark studies using the TD-DFT for calculating the maximum absorption. Four levels of theory were selected:

- M062X/cc-pVDZ
- CAM-B3LYP/6-311+G(2d,p)
- M062X/6-311+G(2d,p)
- CAM-B3LYP/ cc-pVDZ

M062X is the most widely used functional for this type of structure and is reported to be the most reliable. CAM-B3LYP was selected from a previous work done by the

research group in which this project was carried out and is a large and widely used functional for calculating vertical excitation energies.[261,263,267] The effect of the solvent was included using the PCM model, taking the dielectric constant of the solvent in the experimental reference data. The values obtained for the vertical excitation energies, for the lowest-energy excited state for all the molecules examined, are shown in tables in the experimental chapter (Chapter 4.6.1.2).

In order to understand the linearity and reproducibility of the four levels of theory, linear correlation curves were constructed (Figure 35), as linear correlation coefficient (R^2) analysis is often used to evaluate the performance of the levels of theory by allowing the goodness of correlation between the experimental and calculated data to be established.[261,263]

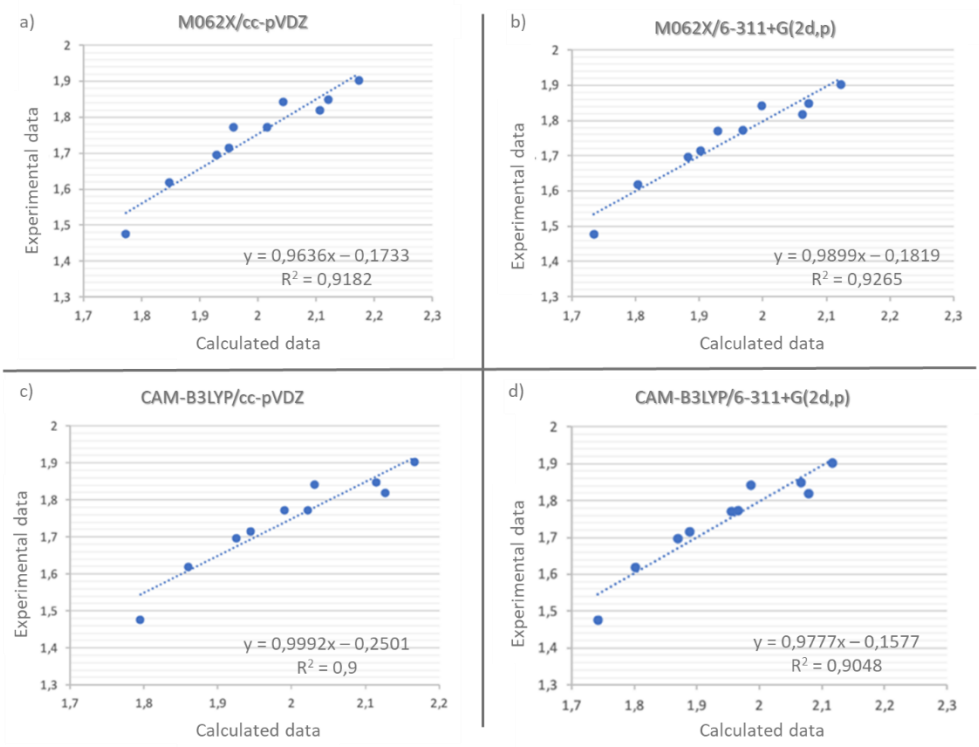

Figure 35: linear correlation curves for a) M062X/cc-pVDZ, b) M062X/6-311+G(2d,p), c) CAM-B3LYP/cc-pVDZ, d) CAM-B3LYP/6-311+G(2d,p).

In an ideal case the different levels of theory should give the same values of the vertical excitation energies and an ideal correlation between the experimental results and the calculated ones should be described by an equation like y = x, obviously this ideal condition is unattainable. However, all the above four levels of theory have sufficiently high R^2.

Analysing the obtained data, we observed that M062X has a slightly higher R^2 when associated with 6-311+G(2d,p) as a basis set than the R^2 value of cc-pVDZ. The same behaviour was found for the functional CAM-B3LYP.
The CAM-B3LYP/6-311+G(2d,p) level of theory seems to reproduce more accurately the maximum absorption for high λ_{max}, as in the case of compounds **185** and **188**.
In conclusion, the level of theory that has the highest R^2 and therefore reproduces the maximum absorptions more linearly is M062X/6-311+G(2d,p).

3.2.3.2 Rational design and study of new BODIPY derivatives

Having selected the best level of theory, among those studied, to be used to reproduce the experimental data, new molecules were designed that could have a suitable structure to be used as PPGs in drug delivery. For the rational design of the new derivatives, the compound **189** was taken as the scaffold and the various positions were functionalised with the aim of obtaining high absorption maxima that would fall into the therapeutic window.

189

Figure 36

The experimental aspect, in other words their synthetic feasibility, was taken into account when designing the new structures. In general, for the introduction of the various functional groups, it was found that palladium-catalysed reactions are very efficient on the BODIPY core.[250,272] In addition, fusion with aromatic rings such as benzene, naphthalene, thiophene and furan has been evaluated as conjugated systems will exhibit a smaller HOMO-LUMO energy gap, thus leading to a longer absorption length. The molecules we have designed are highlighted in the figure 37.

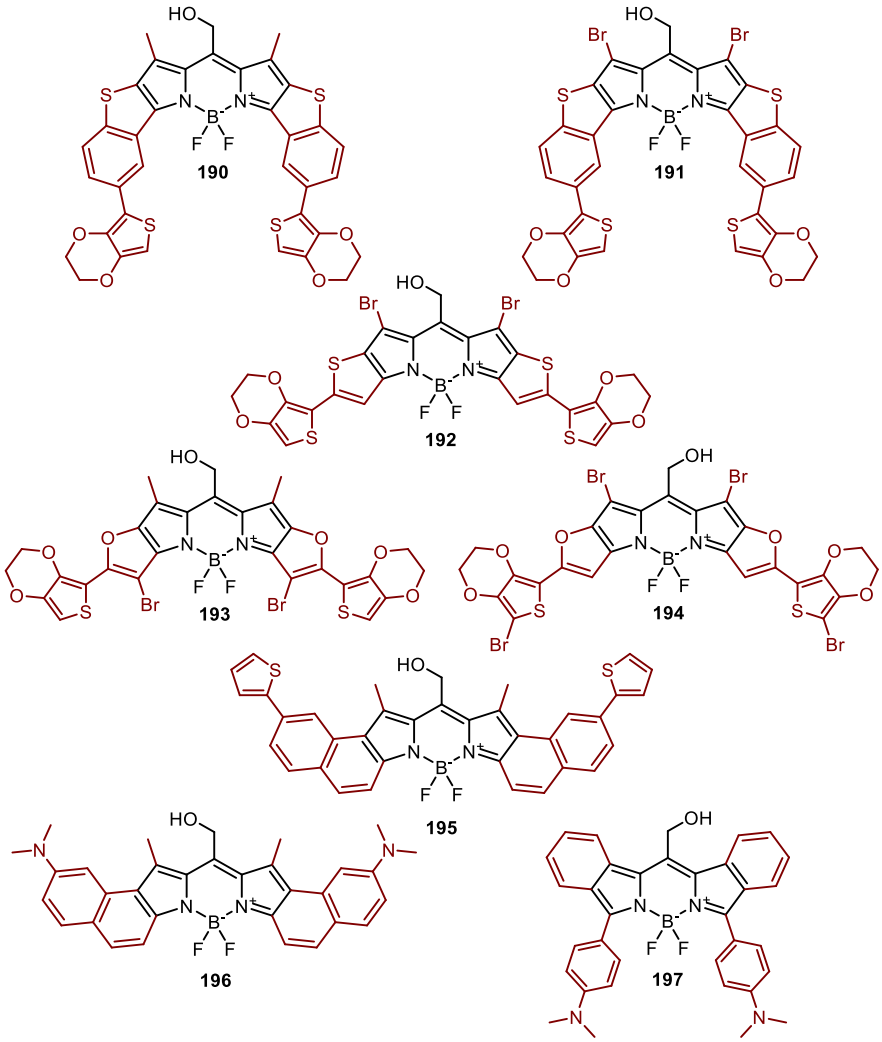

Figure 37: designed structures.

For compounds **190** and **191**, positions 1 and 7 were functionalised with two methyl and bromine atoms respectively, so as not to create steric hindrance at the carbon in position 8. The BODIPY core for these two structures was fused with aromatic rings to have a further extension of the π-system and two EDOT groups were inserted as substituents.[272]

For molecule **192** there is a thieno[3,2-*b*]-BODIPY core with good physicochemical properties[273], positions 1 and 7 have been functionalised with bromine atoms and position 5 of the thiophene with EDOT groups.

In molecules **193** and **194**, the main core consists of furan[3,2-*b*]-BODIPY, positions 1 and 7 have been functionalised with methyl groups, bromine atoms have been introduced in position 4 of the furan and position 5 has been substituted with EDOT groups.[274]

Molecule **197** has an isoindole BODIPY core[275] where positions 3 and 5 have been functionalized with an N-dimethylaniline.

In molecules **195** and **196**, we have a naphtho[*b*]-BODIPY core, functionalized with thiophenes and dimethylamine groups.

The structures of the new BODIPY derivatives (Figure 37) were constructed using Avogadro, the ground state minimum geometry was obtained using Gaussian 16 and B3LYP /6-31G* as a level of theory, in the same way of the molecules reported for the benchmark study. The optimised geometries are shown in the experimental chapter (Chapter 4.6.1.1) together with the bond distances in Å and the dihedral angles in degrees.

Taking into account the good results obtained for all four levels of theory used for the structures reported in the literature, we decided to use all of them to calculate the vertical excitation energies of the lowest-energy excited state for the designed molecules. All calculations were performed for solution with chloroform as solvent since it is the most used for experimental adsorption on BODIPY derivatives. Solvation effects upon excitation were considered using the PCM model.

Table 6 below shows the values obtained from the calculation with the M062X/6-311+G(2d,p) level of theory and the value obtained from the calibration line, as this was the level of theory with the best correlation between the calculated data and the experimental value. The data from the other levels of theory are reported in Chapter 4.6.1.2.

Table 6: values obtained with M062X/6-311+G(2d,p), vertical excitation energies ($E_{ecc.}$), calculated absorption maxima (λ_{max} calc.), absorption maxima obtained from the calibration line (λ_{max} expt.), oscillator strength (f).

Compound	E_{ecc} (eV)	λ_{max} calc. (nm)	$\lambda_{max.}$ expt. (nm)	f
190	2,15	579	639	0,7558
191	2,18	569	623	0,7962
192	1,90	652	733	1,7648
193	1,90	653	734	1,9025
194	1,86	666	751	2,0399
195	1,87	663	744	1,5084
196	2,03	612	681	1,7686
197	1,95	637	713	0,9651

Molecules **192**, **193**, **194** and **195** show an absorption more shifted to the red, falling within the therapeutic window (650-900 nm).

The calculated value of λ_{max} of molecule **194** is lower than that of compound **182**, which is structurally similar. This may be due to the different nature of the substituent present on the *meso* carbon, which is involved in the LUMO orbital, as can be seen in Figure 38 where the frontier molecular orbitals of the two compounds are compared.

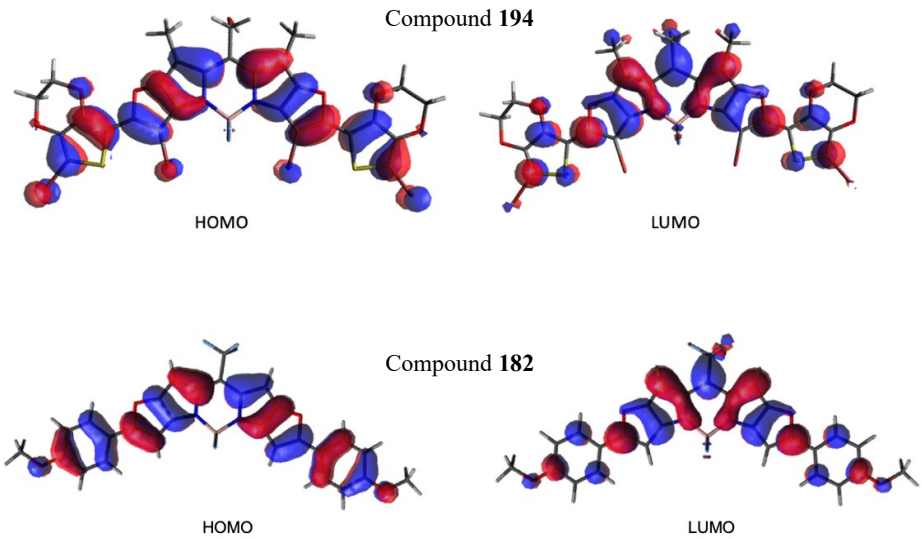

Figure 38: frontier molecular orbitals of compound **194** (on the top) and **182** (below)

Structures **197** and **195** are very similar but have fused aromatic rings in different positions. From the λ_{max} data obtained, it can be seen that aromatic fusion at the 2-3 position (compound **195**) leads to a greater bathochromic shift than aromatic systems fused at the 1-2 position (compound **197**). This supports the literature where it has been observed that the fusion of benzenes at bond 1-2 in the BODIPY structure increases the HOMO energy level, whereas the fusion of benzenes at bond 2-3 affects both frontier molecular orbitals, leading to a decrease in LUMO energy along with an increase in HOMO.[261]

Molecules **190** and **191** did not show a decisive shift towards red as we expected, we can see that position 1 and 7 substituted with bromine atoms do not make a substantial contribution if we compare the results with compound **191** which has methyl groups in the same positions.

The bromination of furan position 4 (structure **193** and **194**) appears to contribute more to the bathochromic shift than the bromination in 1 and 7.

The introduction of the dimethyl amine electron donating group has a significant effect on the absorption wavelength. If the calculated data between molecules **195** and **196** are compared, we can assume that the amine is able to influence the bathochromic shift by about 50/60 nm.

In conclusion, we chose to study the synthesis of molecule **195** and the proposed synthetic pathway are based on previously reported reactions on similar substrates.

3.2.4 Conclusions

Through the study of a small library of molecules, we verified the goodness of 4 levels of theory selected for their performance reported in the literature. For these the correlation curve was constructed and the R^2 coefficient defined.

New structures were then designed carrying the CH_2OH function on the meso carbon of the BODIPY core in order to use the alcohol group as a functional group for drug insertion. For them, the vertical excitation energies were calculated with the four levels of theory and the values obtained were interpolated on linear regression curves to obtain a more reliable value.

Among the various compounds hypothesised, compounds **192**, **193**, **194** and **195** showed very promising results, with absorption maxima falling within the therapeutic window (650-900 nm), indicating their possible application as protective groups or photolabile vehicles for substances with therapeutic activity.

3.3 Study of a dye for the development of a photosensitive drug delivery system.

3.3.1 Application of dyes in pharmaceutical field

Dyes are coloured substances which are soluble or dissolvable during the application process and give colour to the medium they are in by selective absorption of light. Unlike pigments, whose properties depend on the characteristics of their particles, the properties of dyes are defined almost exclusively by their chemical structure.[276]
There are two types of dyes: synthetic and natural. Synthetic dyes are based on petroleum derivatives, while natural dyes are obtained from plant, animal and mineral materials.[277]
The properties of dyes are due to the absorption of electromagnetic radiation in the UV and visible regions, which causes the excitation of an electron towards a higher energy level. This process occurs for all compounds that contain unsaturations, but what characterises a dye is the absorption of radiation in the visible region (400-800 nm).[278]

The pharmaceutical industry uses various inorganic and, mainly, organic dyes to give colour to products. The priority of the colouring agent is to improve the aesthetics and allow easier identification of the drug by the consumer. Thus, dyes can be considered to be the makeup of pharmaceutical products.[279] The colour, shape and appearance of drug are studied and tested extensively, almost as much as the drugs themselves.[280] These colour additives are natural pigments or synthetic chemical compounds. However, most colourants obtained from natural dyes are unstable and can easily undergo degradation during product processing. Aspects affecting stability include light, oxidising and reducing agents, heat, pH and microbial contamination. Synthetic dyes have an important technological superiority over most natural dyes since they can be designed to give bright colours, be resistant to light, oxidising and reducing agents and pH changes.[217] Therefore, synthetic dyes are widely used, not only because of their stability, but also because of their low production cost compared to the natural ones.[281] The European Union has authorised 43 dyes as food additives,

each of which has been assigned a number. Of these, 17 are synthetic dyes and 26 are naturally derived, synthesised to match their naturally occurring counterparts, or are inorganic pigments that occur freely in nature.[282]

In the pharmaceutical industry, colour is used:

- as an indicator of quality,
- to distinguish between drugs,
- to indicate test results,
- as part of a brand identity
- as an indicator of degradation and loss of potency over time.

Therefore, dyes are widely studied in the pharmaceutical field, but mainly as additives; there are few examples of dyes used for therapeutic purposes. In both cases, they have to fulfil all safety, stability and non-toxicity regulations. The use as a therapeutic agent or as photolabile protecting groups (PPGs) in drug delivery systems of a dye already studied in this area could lead to faster development for its use in vivo and eliminate the uncertainty of the possible toxicity of the structure before its synthesis.

3.3.2 Aim of the project

The starting point of this project was the search for dyes that have a conjugation to absorb in the near-infrared region, with benzyl functions or related functional groups in their structure and that are reported to be non-toxic in cells, in order to study, through computational chemistry, their possible use as photolabile protective groups (PPGs) and to explore their application in drug delivery systems. For being able to insert the functional group to be released, the benzyl function is of crucial importance. To assess whether this function can undergo homolytic cleavage after irradiation, the involvement of this group in the molecular orbitals that participate in the energy transition of interest must be evaluated. Therefore, after a thorough bibliographical search, two molecules of interest were selected, PH-1 and ND-1. (Figure 39).

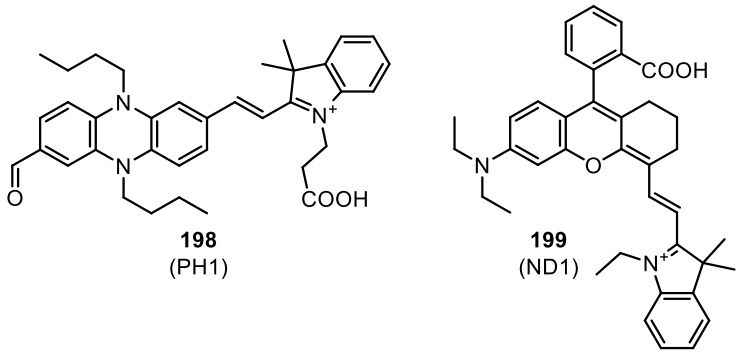

Figure 39: structures of PH-1 and ND-1

For the computational study of these two structures, we used density functional theory (DFT) and its time-dependent extension (TD-DFT). As there is no computational data in the literature on these compounds, our first concern was to assess the best level of theory to use in order to predict the absorption data with a reasonable accuracy and to determine the delocalization of the molecular orbitals. This is necessary for applying the best performed level of theory to two derivatives, modified on the aldehyde and carboxyl positions of the dyes, in order to predict, with a sufficient degree of confidence, the shift of the absorption λ_{max} and to verify the involvement of the modified functionalities in the molecular orbitals of interest.

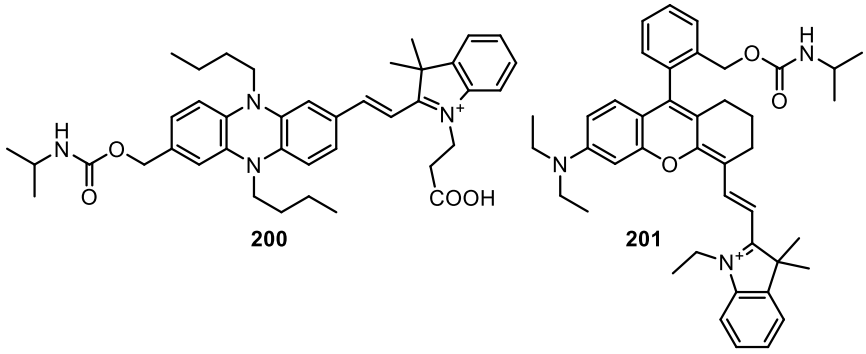

Figure 40: new compounds.

3.3.3 PH-1

Compound PH-1 is a synthetic dye reported by Yongchao Yan *et al*.[283] that belongs to the category of phenazine-cyanine dyes.

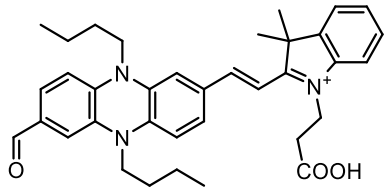

198
(PH1)

Figure 41: PH-1 structure.

Reduced phenazines have many modification sites, strong electron-donor proprieties and excellent stability, due to which they have been used to design fluorescent probes.[284–286] When nitrogen atoms have n-butyl groups as substituents, the originally electron-deficient phenazine group becomes an electron-rich group. Within the structure of this dye, there is also a positively charged indole and an aldehyde group, both of which are electron-withdrawing group. All of these functionalities result in an acceptor-donor-acceptor (A-D-A') structure.

Although no solubility problems were found for this dye, its bioavailability is low. Therefore, with the aim of improving the latter property, PH-1 was assembled with human serum albumin (HSA) to form nanoparticles called PH-1@HSA that showed excellent solubility in water. In addition, the PH-1@HSA compound showed a slight bathochromic effect, caused by molecular aggregation, with a red-shift of 40 nm compared to the pure dye. The therapeutic effect of these nanoparticles arises from the heating they cause after irradiation at a specific wavelength. Their efficacy was tested in solutions at various concentrations (0, 5, 10, 20, 40 and 80 μM), and after 300 s of irradiation, the temperature of the 20 μM solution reached 49.3 °C, a temperature high enough to kill tumour cells. Photothermal stability was also studied by laser irradiation at 808 nm for 3 minutes followed by 3 minutes of cooling, demonstrating constancy in the various absorption peaks and consequently stability

of both the dye and the nanoparticles. Cytotoxicity was also examined. The studies were carried out in 4T1 cells divided into two groups: control group (laser only) and experimental group (PH1@HSA + laser). In the control group was observed that almost all the cells had survived, while in the experimental groups the death cells increase with irradiating time. When the cells were incubated with NPs and exposed to laser for 0 min, the phenomenon was similar with that of the control group, which also indicated the low toxicity in dark condition. After exposure for 2, 6 and 10 min, the death cells increase drastically. These results confirmed that PH-1@HSA with measurable concentration indeed damaged cells only in the presence of a laser.

3.3.4 ND-1

Compound ND-1 is an organic dye that is produced by a ring-opening reaction from compound FUC-1. FUC-1 is a near-infrared rhodamine derivative reported by Huiran Yang *et al.*[287] as a chemodosimiter for mercury (II) or methylmercury. This dye has a monothiospirolactone group which is converted from the non-fluorescent cyclic thiolactone to the open fluorescent derivative (ND-1), with a carboxyl function, in the presence of mercury (II) due to the strong interaction between mercury and sulphur.

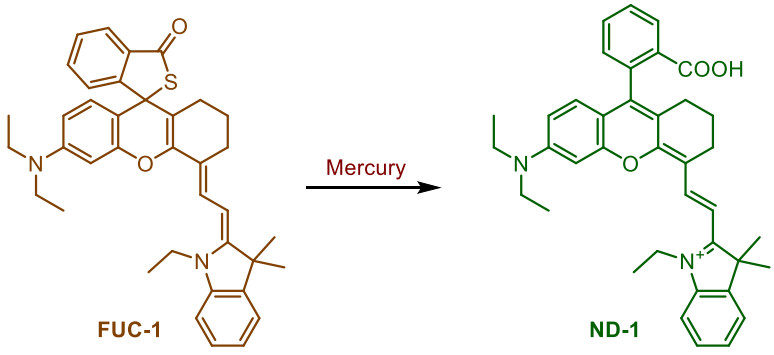

Figure 42: ring-opening reaction that occurs in presence of mercury (II).[287]

Pure FUC-1 displayed no absorption and fluorescence in the NIR region due to its structure, on the other hand, ND-1 has a sharp absorption band at 710 nm and the

emission maximum occurs at 745 nm. Moreover, ND-1 exhibits unique single-photon frequency upconversion luminescence (FUCL).

Normal Stroke luminescence go through an excitation from the zero-point vibrational level of the ground state to the first excited electronic state (S_0-S_1). FULC needs an excitation of the compound to reach the thermally excited vibrational-rotational energy level of the ground state, from which, upon continuous optical pumping, can get to the first electronic excited state. The resulting fluorescence will be the same for both energy processes, but dyes that can undergo through FULC require a much lower excitation power.[288–290]

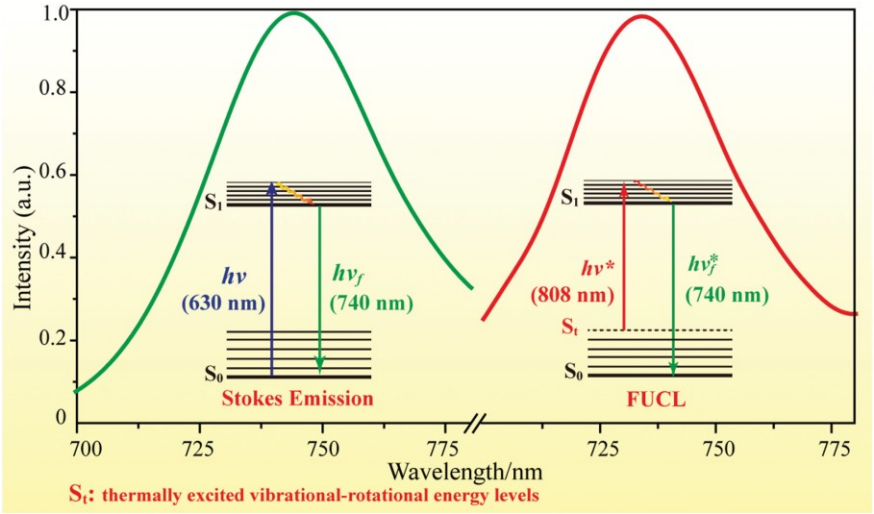

Figure 43: mechanism of Stokes luminescence emission and anti-Stokes frequency upconversion luminescence emission.[287]

ND-1 exhibits an anti-Stokes FUCL at a wavelength of 745 nm when irradiated at 808 nm and is therefore used to monitor mercury concentrations in vivo and ex vivo. In addition, the cytotoxicity of these two compounds towards Hela cells was investigated by a 24-hour treatment at different concentrations, after which cell viability was found to be between 90% and 100%.

3.3.5 Results and discussion

3.3.5.1 Study of PH-1 and ND-1 in the ground state

The structures of cis and trans isomer of PH-1 and ND-1 were constructed with Avogadro and then the ground state geometry was optimised with Gaussian 16 using B3LYP/6-31G* as level of theory.

The minimal geometries of the lower energy isomers are reported in Figure 44, while the energies of the minimal geometries of all the calculated isomers are reported in the experimental section (Chapter 4.6.2.1). The first single excited state geometries were also computed with the same level of theory.

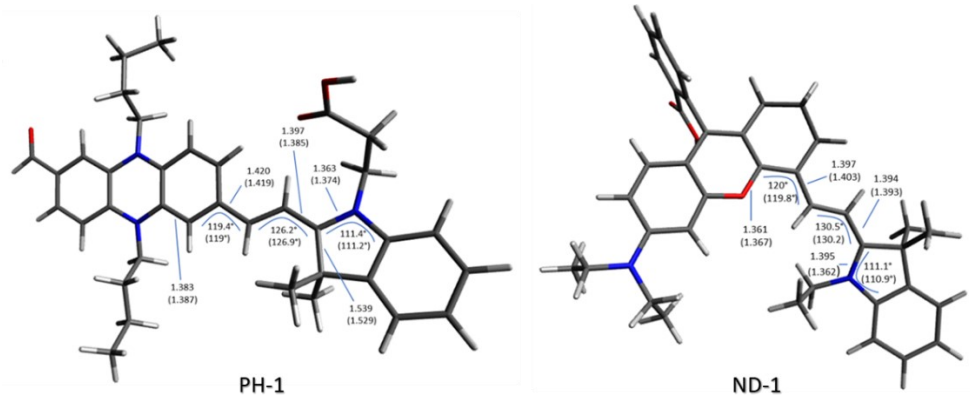

Figure 44: minimal ground state geometries of compound **PH-1** and **ND-1** obtained with B3LYP/6-31G* as level of theory. The bond distances are reported in Å and the dihedral angles in degrees. In brackets the values for the S_1 geometry.

Using the previously minimised geometries, TD-DFT calculations were carried out to determine the vertical excitation energies in the solvents reported in the literature. The effect of the solvent was considered through the PCM (Polarizable Continuum Model). Several functionals were used to calculate the absorptions in order to verify which one reproduced the experimental data with the best degree of accuracy. The following functionals were evaluated: B3LYP, PBE0, CAM-B3LYP, LC-ωPBE and ωB97XD, combined with the basis set 6-311+G(2d, p). The results of the calculations for the first excited state are given in Tables 7 and 8.

Table 7: results for **PH-1** in DMSO: Vertical excitation energies ($E_{ecc.}$), calculated absorption maxima (λ_{max} calc.), experimental absorption maxima reported (λ_{max} exp. = 690 nm), oscillator strength (f), difference between experimental data and calculated data (ΔE) and percentage involvement of HOMO-LUMO orbitals in the electronic transition $S_0 \rightarrow S_1$ (H→L).

Level of theory	E_{ecc} (eV)	λ_{max} calc.	H→L	ΔE (eV)	f
B3LYP/311+G(2d,p)	1,80	689 nm	98%	0,003	0,78
PBE0/311+G(2d,p)	1,74	713 nm	98%	0,058	0,73
CAM-B3LYP/6-311G(2d,p)	2,06	601 nm	94%	0,264	0,99
LC-ωPBE/6-311+G(2d,p)	2,12	585 nm	91%	0,324	1,02
wB97XD/6-311G(2d,p)	2,27	546 nm	84%	0,475	1,16

Table 8: results for **ND-1** in EtOH: Vertical excitation energies ($E_{ecc.}$), calculated absorption maxima (λ_{max} calc.), experimental absorption maxima reported (λ_{max} exp. = 630 nm), oscillator strength (f), difference between experimental data and calculated data (ΔE) and percentage involvement of HOMO-LUMO orbitals in the electronic transition $S_0 \rightarrow S_1$ (H→L).

Level of theory	E_{ecc} (eV)	λ_{max} calc.	H→L	ΔE (eV)	f
B3LYP/311+G(2d,p)	2,05	605 nm	99%	0,080	1,11
PBE0/311+G(2d,p)	2,09	594 nm	99%	0,118	1,15
CAM-B3LYP/6-311G(2d,p)	2,17	572 nm	96%	0,199	1,26
LC-ωPBE/6-311+G(2d,p)	2,18	568 nm	94%	0,214	1,27
wB97XD/6-311G(2d,p)	2,20	564 nm	81%	0,232	1,33

The calculation of the vertical excitation energies for both molecules was also performed with a smaller basis set than reported, but a larger error was observed when comparing the data with the experimental ones. The complete tables with the results of the calculation of the first excitation states at the different levels of theory are provided in the experimental chapter. (Chapter 4.6.2.2)

In figures 45, the ground state frontier molecular orbitals involved in the $S_0 \rightarrow S_1$ transition are shown. For compound PH-1, comparing the molecular orbitals, an intramolecular charge transfer (ICT) involving the aldehyde function is clearly visible, passing from the initial situation (HOMO), in which the electronic density is located on the phenazine ring, to that in which the electronic density is located on the indole ring (LUMO).

For compound ND-1, although much less obvious, there is always an intramolecular charge transfer from the indole ring to the benzene ring, but without the involvement of the carboxyl group.

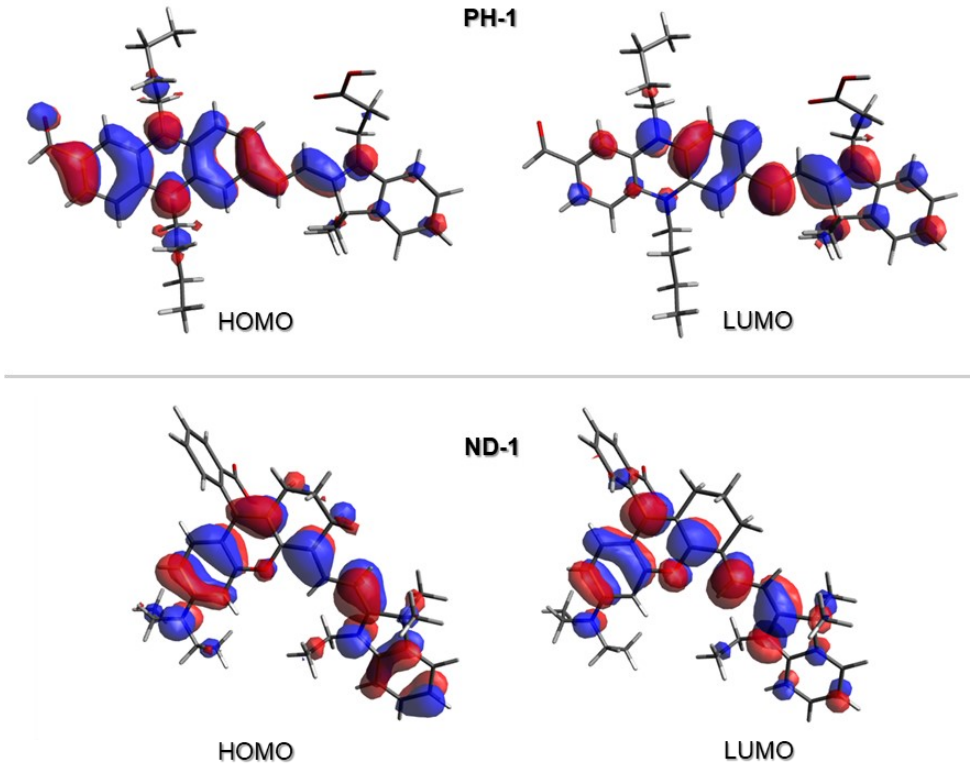

Figure 45: HOMO and LUMO orbitals of PH-1 and ND-1.

The results of the calculations of the absorption maxima show a good correspondence with the experimental data. The best results were obtained with B3LYP and PBE0, but acceptable results were also observed with the long-range corrected CAM-B3LYP functional.

This may be since intramolecular charge transfer is present in the two molecules but is not very pronounced. Therefore it is possible to assume that the B3LYP/6-311+G(2d,p) level of theory can reproduce with reasonable reliability the vertical excitation energies of structures similar to the two dyes under investigation.

3.3.5.2 Study of the PH-1 derivative in the ground state

The structure of PH-1 was modified by insertion of a carbamate group in place of the aldehyde function to mimic the structural change that would occur after the binding of a generic drug molecule. For compound **200**, the energy of the fundamental state and the S_1 excited singlet state has been minimised using B3LYP/6-31G* as level of theory.

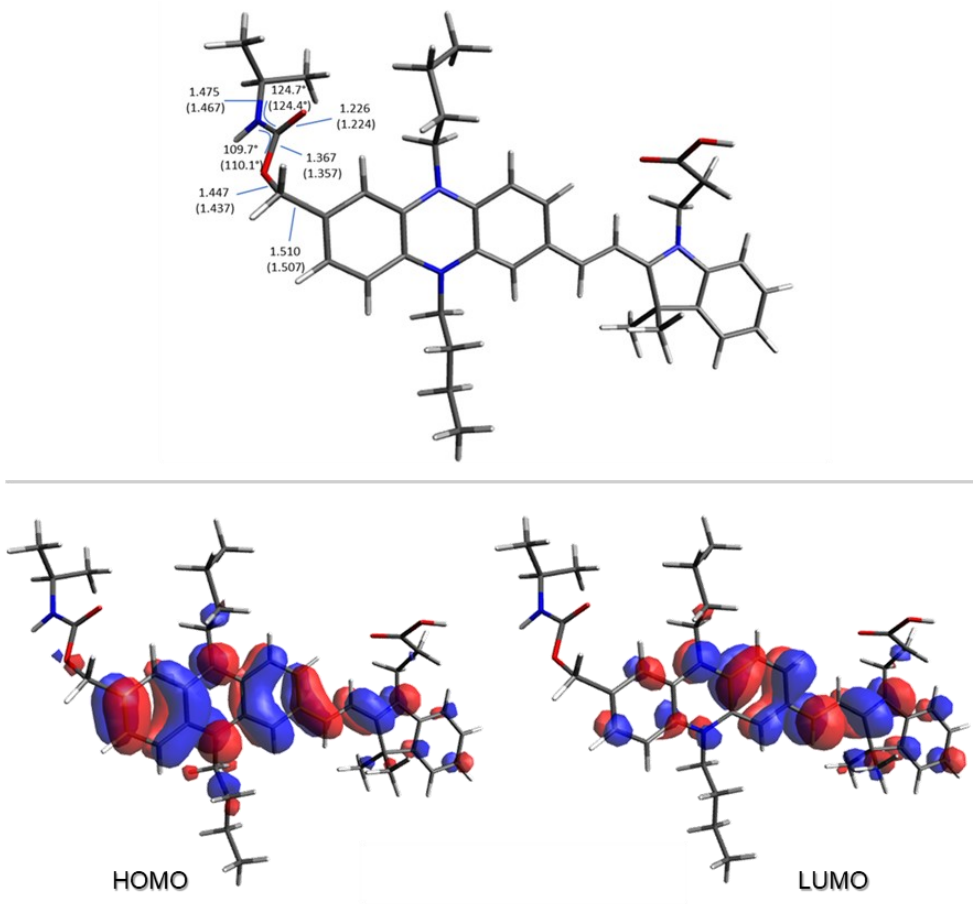

Figure 46: minimal ground state geometry and frontier molecular orbitals of compound **200** obtained with B3LYP/6-31G* as level of theory. The bond distances are reported in Å and the dihedral angles in degrees. In brackets the values for the S_1 geometry.

Using the B3LYP/6-311+G(2d,p) level of theory, the vertical excitation energies of the first excited states in dimethyl sulfoxide were calculated, as done for the parent compound PH-1. (Table 9, complete tables are given in Chapter 4.6.2.2)

Table 9: results for **200** in DMSO: Vertical excitation energies ($E_{ecc.}$), calculated absorption maxima (λ_{max} calc), oscillator strength (f)) and percentage involvement of HOMO-LUMO orbitals in the electronic transition $S_0 \rightarrow S_1$ (H→L).

Level of theory	E_{ecc} (eV)	λ_{max} calc.	H→L	f
B3LYP/311+G(2d,p)	1,62	765 nm	99%	0,68

From the analysis of the results obtained, it can be seen that there is a red shift of 76 nm in the λ_{max}, due to the introduction of the carbamate group, which is still involved in the frontier molecular orbitals. Using the output data from the absorption calculations, the UV-Vis spectrum was simulated with GaussSum software.

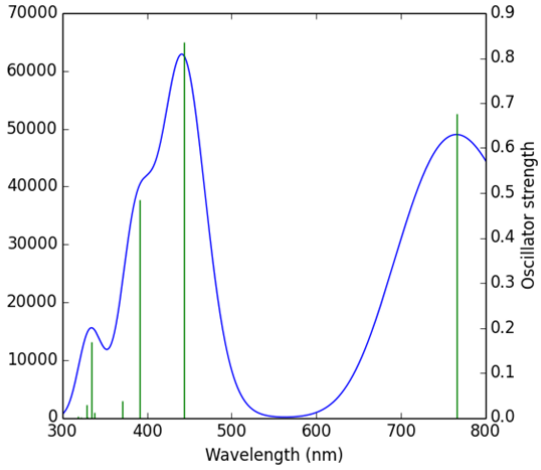

Figure 47: simulated UV-Vis spectra for compound **200** with the main transitions and their intensities in the range 300-800 nm using a Gaussian distribution with arbitrary linewidth of 0.3 eV.

3.3.5.3 Synthesis of the new PH-1 derivative

Recently, we started with the synthesis of derivative of compound **200**. (Scheme 46) The first steps involving reduction and alkylation of the phenazine core were carried out as reported[283] without any problems with acceptable yield. The subsequent

Vilsmeier-Haack reaction leads to the symmetric compound **205** after purification by silica gel flash chromatography. At this point, our aim was to obtain the reduction of only one of the two aldehydes but, even with low amounts of reducing agent or with slow addition, the desired product was always obtained in unsatisfactory yield recovering as the main product compound **206**. Therefore, it was decided to reduce both aldehyde functionalities, selectively protect one of the alcohols as silyl ether and reoxidise the free alcohol moiety. All these reactions gave acceptable yields and no by-products were formed, so the starting materials were always recovered and again subjected to the reaction conditions. The last Knoevenagel reaction was carried out with the previously synthesised positively charged derivative **209**, obtained as reported[283], leading to the formation of the protected compound **210**.

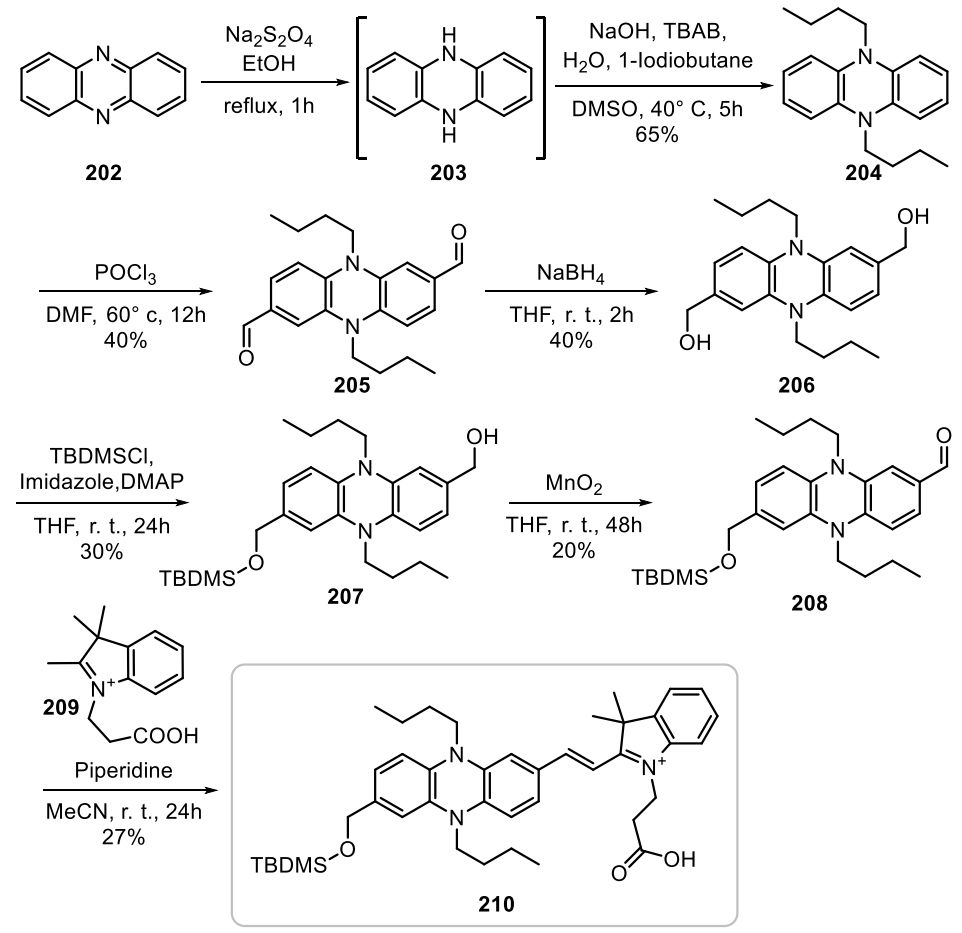

Scheme 46: synthesis of compound **210.**

Having the product **210** in hand, it will be subjected to UV-Vis spectra study and then irradiation in MeOH as a solvent to verify the cleavage of the C-O bond by identification of the corresponding methyl ester (as was previously done for BODIPY derivatives[243]).

3.3.6 Conclusions

For two dyes reported in the literature with an aldehyde and carboxyl function, the ground-state geometries were minimised and the distribution of the frontier molecular orbitals analysed to evaluate the involvement of these functional groups. It was observed that the aldehyde function of compound PH-1 is involved in the HOMO orbital, making it a possible scaffold for the design of photolabile protective groups that undergo photolytic cleavage of the bond between the benzyl carbon and the heteroatom. In order to obtain sufficiently reliable data for the prediction of λ_{max}, four levels of theory were used to reproduce the experimental data of the two starting molecules.

Once the best-performing level of theory had been selected, a new structure with the carbamate group in place of the aldehyde of the PH-1 dye was studied. For this new compound **200**, the minimum geometry, the geometry of the first excited electronic state and the vertical excitation energy for the first excited states were calculated. From the analysis of the frontier molecular orbitals was outlined that the new functional group is involved in the HOMO orbital, so we have therefore start the synthesis of a derivative, compound **210**, arriving to the silyl-derivatives that can be tested to verified the application as photosensitive release system and then deprotected in order to obtain the free hydroxyl moiety useful for further functionalization.

Chapter IV

Experimental part

4.1 General

All reagents were used as purchased from standard commercial suppliers without further purification, if not differently specified. Solvents were dried and purified by conventional methods prior to use or, if available, purchased in anhydrous form.[328]

For the reactions carried out under anhydrous conditions, all glassware and syringes were dried overnight in an oven thermostated ad 140 °C and allowed to cool in a desiccator. For the transfer of some reagents sterile packaged one-way plastic syringes were employed. Hypodermic needles for medicinal use were used together with metal needles (specially to transfer anhydrous solvents) and the latter dried in a oven as described previously. The inert gas used for all reactions were nitrogen or argon 4.8.

Vacuum distillations were accomplished with standard equipment using oil pumps. Flash column chromatography was performed with Merck silica gel 60, 0.040-0.063 mm (230-400 mesh). Merck aluminium backed plates pre-coated with silica gel 60 (UV254) were used for analytical thin layer chromatography (TLC) and were visualized by staining either with a $KMnO_4$ solution or a ninhydrin solution.

4.2 Analytical instruments

NMR. NMR spectra were recorded at 25 °C with a Bruker AC 400 or 600 MHz both for ^{1}H and ^{13}C. Deuterated solvents were used as purchased. The solvent is specified for each spectrum. Splitting patterns are designated as s, singlet; d, doublet; t, triplet; q, quartet; m, multiplet; bs, broad singlet. Chemical shifts (δ) are given in part-per-million (ppm) relative to the resonance of tetramethylsilane (TMS) as internal

standard. ^{13}C spectra are given only in case of new compounds with interest in their publication.

IR. Perkin-Elmer Spectrum BX.

GC/MS. GC/MS analysis were performed with a GC Varian 3900 coupled to a MS Varian Saturn 2000. The capillary column (stationary phase: VF-5 ms) has the following dimensions: 30 m x 0.25 mm x 0.25 nm (L x ID x OD).

MS. Mass spectra were recorded with a LC/ SD chromatographic system equipped with an inline UV detector, Agilent 1100 series. Test conditions: 95% MeOH + 5% H_2O, flow 0.4 mL/min, direct injection, ESI ionization, desiccant gas (N_2) flow equal to 9 l/min, temperature 350 °C, atomizing pressure 40 psi, fragmentation 70 eV.

HPLC/MS. HPLC/MS analysis were performed with Agilent 1260 Infinity II Preparative LC/MSD System Single Quadrupole (LC/MSD iQ), connected with UV detector (254 nm) using an InfinityLab Poroshell 120 EC-C18 column (2.1 x 50 mm, 2.7 µm), flow 0.4 mL/min, MeCN/H_2O gradient from 0.5:9.5 to 9.5:0.5 in 10 minutes. ESI ionization, flow of the drying gas (N_2) 9 L/min, temperature 350 °C, atomizing pressure 40 PSI, fragmentation. Melting points were determined in open capillary tubes and are uncorrected

4.3 Stability in Human Plasma

Pooled human plasma (0.9 mL, 55.7 µg protein/mL)[291], hepes buffer (1.0 mL, 25 mM, NaCl 140 mM, pH 7.4) and tested compound dissolved in DMSO (100 µL, 2.0 mM) were mixed in a test tube that was incubated at 37 °C under continuous mechanical agitation. At set time points (0.0, 0.25, 0.50, 1.0, 3.0, 5.0, 8.0, and 24.0 h), samples of 100 µL were taken, mixed with 400 µL of cold acetonitrile and centrifuged at 5000 rpm for 15 min.[292] The supernatant was collected and analysed by UV/LC-MS to monitor the amount of unmodified compound. For each compound, the determination was performed in three independent experiments.

UV/LC-MS methods

LC analyses of plasma stability tests were performed by using Agilent 1100 LC/MSD VL system (G1946C) (Agilent Technologies, Palo Alto, CA) constituted by a vacuum solvent degassing unit, a binary high-pressure gradient pump, an 1100 series UV detector, and an 1100 MSD model VL benchtop mass spectrometer. MSD single-quadrupole instrument was equipped with the orthogonal spray API-ES (Agilent Technologies, Palo Alto, CA). The pressure of the nebulizing gas and the flow of the drying gas (nitrogen used for both) were set at 40 psi, 9 L/min, respectively. The capillary voltage, the fragmentor voltage, and the vaporization temperature were 3000 V, 10 V, and 350 °C, respectively. MSD was used in the positive and negative ion mode. Spectra were acquired over the scan range m/z 100-2000 using a step size of 0.1. Chromatographic analyses were performed using a Phenomenex Kinetex EVO C18-100Å (150 x 4.6 mm, 5 µm particle size) at room temperature, at flow rate of 0.6 mL/min, and injection volume of 10 µL, operating with a gradient elution of A: water (H2O) and B: acetonitrile (ACN). Both solvents were acidified with 0.1% v/v of formic acid. UV detection was monitored at 254 nm. The analysis started with 0% of B, then B was increased to 80% (from t = 0 to t = 20 min), then kept at 80% (from t = 20 to t = 25 min) and finally return to 0% of eluent B in 5.0 min.

4.4 Computational details

All the calculations were carried out within density functional theory (DFT) for ground states and time-dependent density functional theory (TDDFT) for excited states. The structures were constructed with Avogadro and then the ground state geometry was optimised with Gaussian 16[293] using B3LYP/6-31G*[294,295] as level of theory. The vertical excitation energies were calculated using B3LYP[296], M062X[297], PBE0[298], CAM-B3LYP[299], LC-ωPBE[300] and ωB97XD[301] as functional, and 6-311+G(2d,p), 6-311G*[302] and cc-pVDZ[303] as basis set. Solvation effects upon excitation were considered using the PCM model[304].

.

4.5 Synthetic procedures

4.5.1 Release of thiol containing compounds from heterocyclic systems and development of new heterocyclic self-immolative spacer

4.5.1.1 General procedures

General procedure for bromination:

The alcohol (1 mmol) was solubilized in dry THF (5 mL) and cooled to 0 °C. PBr_3 (2 mmol) was added to the solution and the reaction was allowed to warm to room temperature for 1 h. The crude reaction mixture was concentrated in vacuo and filtered through a silica gel path with EtOAc to provide the bromo derivatives in quantitative yields as a bright orange oil identified by mass spectroscopy. The products were immediately used for the next steps due to their instability.

General procedure for the synthesis of thioethers:

1-Octanethiol (2.1 mmol) and K_2CO_3 (1.95 mmol) were added to dry THF (4 mL) in a round-bottomed flask and the suspension was stirred for 1 h under N_2 atmosphere at room temperature. The bromide derivative (1 mmol) and Et_3N (1,05 mmol) were added into the reaction and the mixture was leave under magnetic stirring for 16 h. After complete consumption of the starting material monitored by TLC, the reaction was taken up in EtOAc and washed with water and brine. The organic phase was dried over anhydrous Na_2SO_4, filtered and concentrated in vacuo. The crude reaction mixture was purified by silica gel flash chromatography (PE:EtOAc) to provide the desired compound.

General procedure for nitro group reduction:[181]

Iron-based nanoparticles (6 mg) was added to a round-bottomed flask. 0.5 mL aqueous solution of 2 wt. % TPGS-750-M was added via syringe and $NaBH_4$ (59.0 mg, 1.5 mmol) was added to the reaction mixture. Reaction flask was closed with septum and the reaction mixture turned black with evolution of hydrogen gas. After

2 minutes the nitro-containing compounds (0.5 mmol), pre-dissolved in mixture of 0.5 mL aqueous 2 wt. % TPGS-750-M and 0.1 mL THF, was added to the catalyst suspension and the reaction was vigorously stirred at room temperature. HPLC-MS traces were recorded at set time points (0.0, 0.25, 0.50, 1.0, 2.0 h, 4.0 h).

4.5.1.2 Synthesis of benzylic compounds

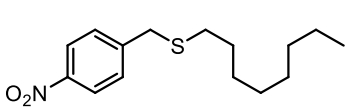

(4-Nitrobenzyl)(octyl)sulfane (61):

Following the general procedure for the synthesis of thioethers, 4-nitrobenzyl bromide (100 mg, 0.46 mmol) was reacted with 1-octanethiol (142 mg, 0.97 mmol), K_2CO_3 (125 mg, 0.90 mmol) and Et_3N (67 µL, 0.49 mmol) in dry THF (2 mL). The crude reaction mixture was purified by silica gel flash chromatography (PE:EtOAc 9:1) to provide compound **61** (130 mg, 0.45 mmol, 98 % yield).

MS (ESI): m/z calcd for $C_{15}H_{23}NO_2SNa$ $[M+Na]^+$: 304.1342; found: 304.1334.

^{1}H NMR (600 MHz, $CDCl_3$): δ 8.17 (d, J = 8 Hz, 2H), 7.48 (d, J = 8 Hz, 2H), 3.76 (s, 2H), 2.40 (t, J = 6.9 Hz, 2H), 1.59 – 1.48 (m, 2H), 1.37 – 1.12 (m, 12H), 0.87 (t, J = 6.9 Hz, 3H).

^{13}C NMR (150 MHz, $CDCl_3$): δ 146.66, 129.62, 123.74, 35.81, 31.79, 31.63, 29.14, 29.10, 28.80, 22.64, 14.10

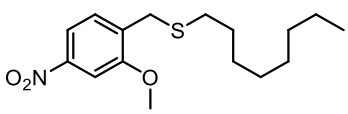

(2-Methoxy-4-nitrobenzyl)(octyl)sulfane (62):

Following the general procedures for bromination and for the synthesis of thioethers, (2-methoxy-4-nitrophenyl)methanol (40 mg, 0.22 mmol) was reacted with PBr_3 (62 µL, 0.66 mmol) in 2 mL of dry THF and the corresponding bromide **59** was obtained. The bromo derivative (38 mg, 0.15 mmol) was reacted with 1-octanethiol **60** (46 mg, 0.32 mmol), K_2CO_3 (40 mg, 0.29 mmol) and Et_3N (21.8 µL, 0.16 mmol) in dry THF (2 mL), following the general procedure. The crude reaction mixture was purified by silica gel flash chromatography (PE:EtOAc 9:1) to provide compound **62** (24 mg, 0.077 mmol, 52 % yield).

MS (ESI): m/z calcd for $C_{16}H_{25}NO_3SNa$ $[M+Na]^+$: 334.1447; found: 334.1441.

^{1}H NMR (600 MHz, $CDCl_3$): δ 7.82 (dd, J = 8.2, 2.0 Hz, 1H), 7.72 (d, J = 2.0 Hz, 1H), 7.41 (d, J = 8.3 Hz, 1H), 3.96 (s, 3H), 3.76 (s, 2H), 2.46 (m, 2H), 1.57 (m, 3H), 1.36 – 1.32 (m, 2H), 1.31 – 1.22 (m, 8H), 0.88 (t, J = 7.0 Hz, 3H).

^{13}C NMR (150 MHz, $CDCl_3$): δ 157.47, 148.04, 135.32, 130.18, 115.78, 105.54, 56.05, 32.10, 31.80, 30.11, 29.70, 29.32, 29.19, 29.17, 28.90, 22.64, 14.09.

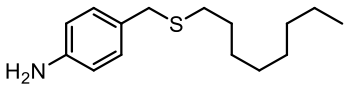

4-((Octylthio)methyl)aniline (63):

Following general procedure for the reduction of nitro group, the nanoparticles (2.4 mg) were activated with $NaBH_4$ (11 mg, 0.294 mmol) in 0.4 mL aqueous solution of 2 wt. % TPGS-750-M followed by the addition of nitro derivative **61** (55 mg, 0.196 mmol). The crude was purified by silica gel flash chromatography (DCM) to provide compound **63** (48 mg, 99% yield).

MS (ESI): m/z calcd for $C_{15}H_{25}NSNa$ $[M+Na]^+$: 274.1600; found: 274.1595.

^{1}H NMR (600 MHz, CD_3OD): δ 7.04 (d, J = 8.2 Hz, 2H), 6.67 (d, J = 8.2 Hz, 2H), 4.92 (s, 2H), 3.59 (s, 2H), 2.36 (t, J = 7.3 Hz, 2H), 1.57 – 1.47 (m, 2H), 1.38 – 1.22 (m, 16H), 0.90 (t, J = 7.0 Hz, 3H).

^{13}C NMR (150 MHz, CD_3OD): δ 146.01, 129.32, 128.05, 115.19, 35.13, 31.63, 30.48, 29.00, 28.92, 28.56, 22.36, 13.10.

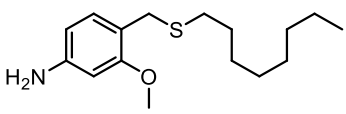

3-Methoxy-4-((octylthio)methyl)aniline (64):

Following general procedure for the reduction of nitro group, the nanoparticles (3.3 mg) were activated with $NaBH_4$ (15.5 mg, 0.41 mmol) in 0.4 mL aqueous solution of 2 wt. % TPGS-750-M followed by the addition of nitro derivative **62** (85 mg, 0.273 mmol). The crude was purified by silica gel flash chromatography (DCM) to provide compound **64** (75 mg, 99% yield).

MS (ESI): m/z calcd for $C_{15}H_{25}NSNa$ $[M+Na]^+$: 304.1706; found: 304.1690.

^{1}H NMR (600 MHz, CD_3OD): δ 6.94 (d, J = 8.0 Hz, 1H), 6.36 (d, J = 1.6 Hz, 1H), 6.26 (dd, J = 8.0, 1.9 Hz, 1H), 3.77 (s, 3H), 3.60 (s, 2H), 2.40 (t, J = 7.4 Hz, 2H), 1.57 – 1.51 (m, 2H), 1.39 – 1.24 (m, 12H), 0.90 (t, J = 7.0 Hz, 3H).

^{13}C NMR (150 MHz, CD_3OD): δ 158.17, 147.81, 130.49, 116.32, 106.98, 98.60, 54.34, 30.87, 29.38, 29.28, 28.93, 28.60, 22.31, 13.03.

4.5.1.3 Synthesis of heterocyclic systems

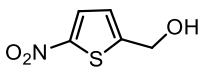

(5-Nitrothiophen-2-yl)methanol (67):

The product was prepared according to literature.[2]

5-Nitrothiophene-2-carbaldehyde (500 mg, 3.18 mmol) was solubilized in 10 mL of dry CH_3OH under an inert atmosphere of N_2 and magnetic stirring. The solution was cooled to 0 °C in an ice bath and $NaBH_4$ (145 mg, 3.82 mmol) was added ad portions. After 30 minutes the reaction was quenched with a solution of HCl 4N until pH = 7, then the crude was extracted with EtOAc (x2) and washed with H_2O and brine. The organic layer was dried over anhydrous Na_2SO_4, filtered and concentrated *in vacuo*. The crude reaction mixture was purified by silica gel flash chromatography (PE:EtOAc 2:1) to provide compound **67** (465 mg, 2.92 mmol, 92% yield).

^{1}H NMR (600 MHz, $CDCl_3$): δ 7.28 (d, *J* = 3.6 Hz, 1H), 6.56 (d, *J* = 3.6 Hz, 1H), 4.71 (s, 2H), 2.78 (sb, 1H).

^{13}C NMR (150 MHz, $CDCl_3$): δ 157.61, 112.67, 110.75, 57.30.

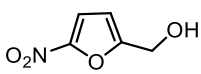

(5-Nitrofuran-2-yl)methanol (68):

Product prepared according to literature.[3]

5-nitrofuran-2-carbaldehyde (500 mg, 3.55 mmol) was solubilized in 10 mL of dry CH_3OH and cooled to 0 °C in an ice bath under atmosphere of N_2. $NaBH_4$ (161 mg, 4.25 mmol) was added, and the reaction was stirred for 1 h. The reaction was quenched with a solution of HCl 4N until pH = 7, the mixture was extracted with EtOAc (x2) and washed with water and brine. The organic layer was dried over anhydrous Na_2SO_4, filtered and concentrated *in vacuo*. The crude reaction mixture was purified by silica gel flash chromatography (PE:EtOAc 2:1) to provide compound **68** in 80% yield (405 mg, 2.54 mmol).

^{1}H NMR (600 MHz, $CDCl_3$): δ 7.28 (d, *J* = 3.6 Hz, 1H), 6.55 (d, *J* = 3.6 Hz, 1H), 4.70 (s, 2H), 2.97 (s, 1H).

^{13}C NMR (150 MHz, $CDCl_3$): δ 157.61, 112.67, 110.75, 57.28

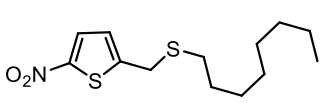

2-Nitro-5-((octylthio)methyl)thiophene (69):

Following the general procedures for bromination, the alcohol **67** (190 mg, 1.2 mmol) was reacted with PBr_3 (223 µL, 2.38 mmol) to provide 2-(bromomethyl)-5-nitrothiophene in 82% yield.

According with the general procedure for the synthesis of thioethers, the bromide (217 mg, 0.98 mmol) was reacted with 1-octanethiol (504 mg, 2.49 mmol), K_2CO_3 (320 mg, 2.32 mmol) and Et_3N (173 µL, 1,25 mmol) in dry THF (4 mL). The crude reaction mixture was purified by silica gel flash chromatography (PE:EtOAc 9:1) to provide compound **69** (150 mg, 0,521 mmol, 53% yield).

MS (ESI): m/z calcd for $C_{13}H_{21}NO_2S_2Na$ $[M+Na]^+$: 310.0906; found: 310.0911.

^{1}H NMR (600 MHz, $CDCl_3$): δ 7.77 (d, J = 4.1 Hz, 1H), 6.91 (d, J = 4.1 Hz, 1H), 3.86 (s, 2H), 2.53 (t, J = 7.4, 2H), 1.61 – 1.54 (m, 2H), 1.40 – 1.33 (m, 2H), 1.32 – 1.20 (m, 8H), 0.88 (t, J = 7.0 Hz, 2H).

^{13}C NMR (150 MHz, $CDCl_3$): δ 152.59, 128.65, 125.24, 32.12, 31.78, 31.04, 29.13, 29.12, 29.00, 28.76, 22.63, 14.08.

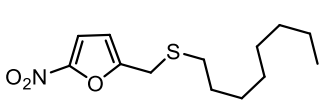

2-Nitro-5-((octylthio)methyl)furan (70):

Following the general procedures for bromination and for the synthesis of thioethers, the compound **68** (200 mg, 1.4 mmol) was reacted with PBr_3 (263 µL, 2.8 mmol) in dry THF (5 mL) to provide the bromo derivative in quantitative yield.

2-(bromomethyl)-5-nitrofuran was reacted with 1-octanethiol (409 mg, 2.8 mmol), K_2CO_3 (378 mg, 2.73 mmol) and Et_3N (156 mg, 1.54 mmol) in 4 mL of dry THF. The crude was purified by silica gel flash chromatography (PE:EtOAc 95:5) in order to obtain the product (114 mg, 0.42 mmol, 30% yield).

MS (ESI): m/z calcd for $C_{13}H_{21}NO_3SNa$ $[M+Na]^+$: 294.1134; found: 294.1152.

^{1}H NMR (600 MHz, $CDCl_3$): δ 7.26 (d, J = 3.6 Hz, 1H), 6.46 (d, J = 3.6 Hz, 1H), 3.74 (s, 2H), 2.57 (s, 2H), 1.61 – 1.55 (m, 2H), 1.40 – 1.33 (m, 2H), 1.28 (m, 8H), 0.87 (t, J = 7.0 Hz, 3H).

^{13}C NMR (150 MHz, $CDCl_3$): δ 157.05, 112.75, 110.55, 32.45, 31.78, 31.76, 29.13, 29.11, 20.07, 28.74, 28.27, 22.62, 14.06.

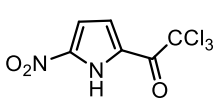

2,2,2-Trichloro-1-(5-nitro-1*H*-pyrrol-2-yl)ethan-1-one (74)

Product prepared according to literature.[4]

2,2,2-trichloro-1-(1H-pyrrol-2-yl)ethan-1-one (500 mg, 2.38 mmol) was solubilized in 2.5 mL of acetic anhydride under atmosphere of N_2. The solution was cooled to -40 °C and HNO_3 (210 µL) was added slowly into the reaction and the temperature was allowed to worm to room temperature in 2 h. After this time the mixture was cooled to -40 °C and water was added, the resulting suspension was extracted with EtOAc (x3) and the organic phase was washed with brine, dried with anhydrous Na_2SO_4, filtered and evaporated *in vacuo*. The crude was purified by silica gel flash chromatography (PE:EtOAc 2:1) to provide product (338 mg, 1.32 mmol, 56% yield).

^{1}H NMR (600 MHz, $CDCl_3$): δ 10.40 (s, 1H), 7.32 (d, J = 4.4 Hz, 1H), 7.13 (d, J = 4.4 Hz, 1H).

^{13}C NMR (150 MHz, $CDCl_3$): δ 173.30, 124,03, 119.85, 110.25, 22.19.

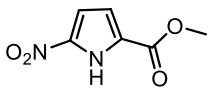

Methyl 5-nitro-1*H*-pyrrole-2-carboxylate (75)

Pyrrole **74** (479 mg, 1.87 mmol) was cooled at 0°C and 15 mL of anhydrous methanol and K_2CO_3 (494 mg, 3.74 mmol) were added. The reaction was maintained at 0°C under magnetic stirring for 1 h. After the disappearance of the starting material, the crude was concentrated *in vacuo*, diluted with DCM and washed with H_2O and Brine. The organic layer was dried with anhydrous Na_2SO_4, filtered and evaporated *in vacuo*. The crude was purified by silica gel flash chromatography (PE:EtOAc 4:1) to provide product (273 mg, 1.61 mmol, 86% yield).

^{1}H NMR (600 MHz, $CDCl_3$): δ 10.35 (s, 1H), 7.08 (d, J = 4.2 Hz, 1H), 6.90 (d, J = 4.2 Hz, 1H), 3.96 (s, 3H).

^{13}C NMR (150 MHz, $CDCl_3$): δ 160.06, 125.26, 115.32, 110,59, 52.68.

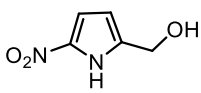

(5-Nitro-1*H*-pyrrol-2-yl)methanol (76)

Under atmosphere of N_2, compound **75** (318 mg, 1.87 mmol) was dissolved in 10 mL of anhydrous THF and cooled at -60 °C. Solution 1 M of DIBAL (5.6 mL, 5.61 mmol) was added carefully and, after the consumption of the starting material, the reaction was quenched with saturated aqueous solution of NH_4Cl. The crude was extracted with EtOAc (x3) and washed with H_2O and brine. The organic layer was dried over anhydrous Na_2SO_4, filtered and concentrated *in vacuo*. The reaction mixture was purified by silica gel flash chromatography (PE:EtOAc 2:1) to provide compound **76** (244 mg, 1.72 mmol, 92% yield).

MS (ESI): m/z calcd for $C_5H_6N_2O_3Na$ $[M+Na]^+$: 165.0276; found: 165.0283.

^{1}H NMR (600 MHz, CD_3OD): δ 7.03 (d, J = 4.0 Hz, 1H), 6.23 (d, J = 4.0 Hz, 1H), 4.56 (s, 2H)

^{13}C NMR (150 MHz, CD_3OD): δ 110.98, 108.53, 56.25

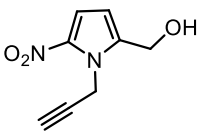

(5-Nitro-1-(prop-2-yn-1-yl)-1*H*-pyrrol-2-yl)methanol (77)

Compound **76** (110 mg, 0.775 mmol) was dissolved in 2 mL of anhydrous DMF under atmosphere of N_2 and K_2CO_3 (214 mg, 1.55 mmol) was added. The suspension was heated at 40 °C for 1 h, then propargyl bromide (59 µL, 0.775 mmol) was added and the reaction was stirred at 40 °C for 16 h. After cooled at room temperature, H_2O was added, and the crude was extracted with EtOAc (x3) and washed brine (x3). The organic layer was dried over anhydrous Na_2SO_4, filtered and concentrated *in vacuo*. The reaction mixture was purified by silica gel flash chromatography (PE:EtOAc 4:1) to provide compound **77** (62 mg, 0.341 mmol, 44% yield).

MS (ESI): m/z calcd for $C_8H_8N_2O_3Na$ $[M+Na]^+$: 203.0433; found: 203.0425.

^{1}H NMR (600 MHz, $CDCl_3$): δ 7.20 (d, J = 4.3 Hz, 1H), 6.22 (d, J = 4.3 Hz, 1H), 5.34 (d, J = 2.3 Hz, 3H), 4.76 (d, J = 5.7 Hz, 3H), 1.91 (t, J = 5.8 Hz, 1H).

^{13}C NMR (150 MHz, $CDCl_3$): δ 139.71, 138.62, 114.26, 109.61, 73.18, 56.94, 35.72.

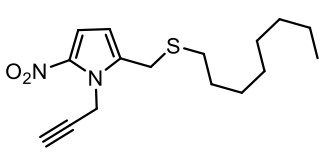

2-Nitro-5-((octylthio)methyl)-1-(prop-2-yn-1-yl)-1*H*-pyrrole (78)

Following the general procedures for bromination and for the synthesis of thioethers, compound **77** (15 mg, 0.083 mmol) was reacted with PBr_3 (16 µL, 0.17 mmol) in 2 mL of dry THF. The bromo derivative obtained (0.083 mmol) was immediately reacted with 1-octanethiol (24 mg, 0.17 mmol), K_2CO_3 (23 mg, 0.16 mmol) and Et_3N (12 µL, 0.08 mmol) in dry THF (2 mL). The crude reaction mixture was purified by silica gel flash chromatography (PE:EtOAc 9:1) to provide compound **78** (20 mg, 0.065 mmol, 78% yield).

MS (ESI): m/z calcd for $C_{16}H_{24}N_2O_2SNa$ $[M+Na]^+$: 331.1456; found: 331.1467.

^{1}H NMR (600 MHz, $CDCl_3$): δ 7.21 (d, J = 4.3 Hz, 1H), 6.13 (d, J = 4.3 Hz, 1H), 5.38 (d, J = 2.4 Hz, 2H), 3.80 (s, 2H), 2.47 (t, J = 7.2 Hz, 2H), 2.34 (s, 1H), 1.59 – 1.52 (m, 2H), 1.39 – 1.32 (m, 2H), 1.32 – 1.21 (m, 8H), 0.89 (t, J = 7.2 Hz, 3H).

^{13}C NMR (150 MHz, $CDCl_3$): δ 136.69, 114.48, 110.36, 73.15, 35.28, 31.78, 31.68, 29.14, 29.13, 29.09, 28.78, 27.36, 22.63, 14.08.

*4.5.1.4 Synthesis of compound **83***

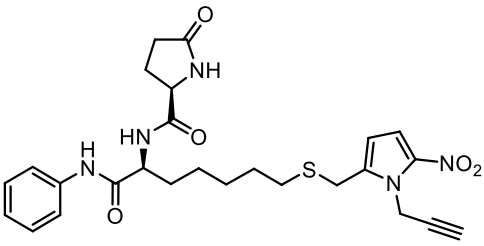

(S)-*N*-((S)-7-(((5-Nitro-1-(prop-2-yn-1-yl)-1*H*-pyrrol-2-yl)methyl)thio)-1-oxo-1-(phenylamino)heptan-2-yl)-5-oxopyrrolidine-2-carboxamide (83)

ST7612AA1 (50 mg, 0.123 mmol) was dissolved in 2.5 mL of MeOH in a round-bottom flask. The solution was degassed with three cycles of argon/*vacuum* and CH_3SNa (8.6 mg, 0.123 mmol, solution 1M in MeOH degassed with three cycles of argon/*vacuum*) was added. The reaction was stirred for 30 min then it was degassed with argon and evaporated *in vacuo* to lead the free thiol **81**.

Following the general procedure for bromination, compound **77** (24 mg, 0.133 mmol) was reacted with PBr_3 (25 µL, 0.26 mmol) in 2 mL of dry THF. The bromo derivative obtained (0.123 mmol) was solubilized in 2 mL of dry THF and added to thiol **81**. The reaction was stirred under argon for 16 h at room temperature. The crude was evaporated *in vacuo* and purified by silica gel flash chromatography (DCM:MeOH 8:2) to provide compound **83** (14 mg, 0.03 mmol, 22% yield).

MS (ESI): m/z calcd for $C_{26}H_{31}N_5O_5SNa$ $[M+Na]^+$: 548.1938; found: 548.1945.

^{1}H NMR (600 MHz, CD_3OD): δ 7.55 (d, J = 7.7 Hz, 2H), 7.31 (t, J = 7.9 Hz, 2H), 7.18 (d, J = 4.3 Hz, 1H), 7.11 (t, J = 7.3 Hz, 1H), 6.22 (d, J = 4.2 Hz, 1H), 5.33 (d, J = 2.3 Hz, 2H), 4.47 (dd, J = 8.3, 5.8 Hz, 1H), 4.27 (dd, J = 8.6, 4.7 Hz, 1H), 3.87 (s, 2H), 3.31 (s, 5H), 2.53 – 2.38 (m, 5H), 2.36 – 2.27 (m, 2H), 2.12 – 2.03 (m, 1H), 1.79 – 1.71 (m, 1H), 1.64 – 1.54 (m, 2H), 1.50 – 1.37 (m, 4H).

^{13}C NMR (150 MHz, CD_3OD): δ 180.12, 173.49, 171.13, 138.05, 137.54, 128.45, 124.09, 120.00, 113.83, 109.99, 77.21, 72.89, 56.59, 53.93, 45.99, 34.97, 31.86, 30.88, 29.15, 28.71, 27.93, 26.43, 25.98, 25.92, 25.42, 25.06.

4.5.1.5 Synthesis of azide

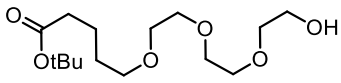

***tert*-Butyl 5-(2-(2-(2-hydroxyethoxy)ethoxy) ethoxy) pentanoate (85)**

To a suspension of NaH (24 mg, 1 mmol) in 5 mL of anhydrous THF at 0 °C was added triethylen glycol (300 mg, 2 mmol). The reaction was stirred for 1h, then *tert*-butyl 5-bromovalerate (116 mg, 0.5 mmol) was added at room temperature and the mixture was refluxed for 16 h. The reaction was quenched with 3 drops of water and after 5 minutes it was dried over anhydrous Na_2SO_4, filtered and concentrated *in vacuo*. The crude was purified by silica gel flash chromatography (DCM:MeOH 98:2) to provide compound **85** (38 mg, 0.16 mmol, 32% yield).

MS (ESI): m/z calcd for $C_{15}H_{30}O_6Na$ $[M+Na]^+$: 329.1935; found: 329.1924.

^{1}H NMR (600 MHz, CD_3OD): δ 3.67 – 3.63 (m, 8H), 3.59 – 3.56 (m, 4H), 3.49 (t, J = 6.1 Hz, 2H), 2.25 (t, J = 7.1 Hz, 2H), 1.64 – 1.58 (m, 4H), 1.45 (s, 9H).

^{13}C NMR (150 MHz, CD_3OD): δ 72.28, 70.41, 70.23, 70.17, 70.02, 69.73, 60.84, 34.72, 28.62, 26.95, 21.54.

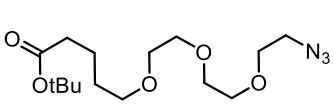

tert-Butyl 5-(2-(2-(2-azidoethoxy)ethoxy)ethoxy) pentanoate (86)

Compound **85** (100 mg, 0.327 mmol) was dissolved in 10 mL of anhydrous DCM under atmosphere of N_2 then Et_3N (49 µL, 0.654 mmol) and *p*-Toluenesulfonyl chloride (75 mg, 0.392 mmol) were added. The reaction was stirred at room temperature for 16 h, then the solvent was removed and the crude was filtered with a pad of silica (PE:EtOAc 3:1) to provide the desired intermediate that was used immediately for the next step due to its instability. The tosyl-activated compound (64 mg, 0.138 mmol) was dissolved in 7 mL of anhydrous DMF under inert atmosphere and NaN_3 (34 mg, 0.524 mmol) was added. The mixture was heated at 80 °C and stirred for 16 h. The crude was concentrated *in vacuo*, the resulted suspension was filtered and washed with DCM (10 mL x3). The solution was evaporated *in vacuo* to provide the product as light-yellow oil (<99% yield, 45 mg, 0.136 mmol).

MS (ESI): m/z calcd for $C_{15}H_{29}N_3O_5Na$ $[M+Na]^+$: 354.1999; found: 354.2005.

^{1}H NMR (600 MHz, CD_3OD): δ 3.68 – 3.64 (m, 8H), 3.59 – 3.58 (m, 2H), 3.49 (t, J = 6.2 Hz, 2H), 3.39 – 3.36 (m, 2H), 2.25 (t, J = 7.2 Hz, 2H), 1.67 – 1.56 (m, 4H), 1.45 (s, 9H).

^{13}C NMR (150 MHz, CD_3OD): δ 70.41, 70.28, 70.24, 70.17, 69.78, 69.76, 50.39, 34.73, 28.64, 26.96, 21.55.

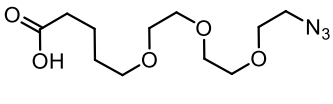

5-(2-(2-(2-Azidoethoxy)ethoxy)ethoxy)pentanoic acid (87)

Compound **86** (45 mg, 0.136 mmol) was dissolved in 5 mL of anhydrous DCM and trifluoroacetic acid (104 mL, 0.68 mmol) was added and the mixture was stirred at room temperature for 16 h. After the complete

consumption of the starting material the crude was evaporated *in vacuo* to provide the product as light-yellow oil (<99% yield, 37 mg, 0.135 mmol).

MS (ESI): m/z calcd for $C_{11}H_{20}N_3O_5$ $[M-1]^-$: 274.1408; found: 274.1406.

^{1}H NMR (600 MHz, CD_3OD): δ 3.68 – 3.61 (m, 8H), 3.59 – 3.58 (m, 2H), 3.50 (t, J = 6.2 Hz, 2H), 3.38 – 3.36 (m, 2H), 2.31 – 2.28 (m, 2H), 1.69 – 1.61 (m, 4H).

^{13}C NMR (150 MHz, CD_3OD): δ 70.47, 70.28, 70.23, 70.16, 69.78, 50.38, 29.34, 28.76, 22.81, 21.58.

4.5.1.6 Synthesis of conjugable system:

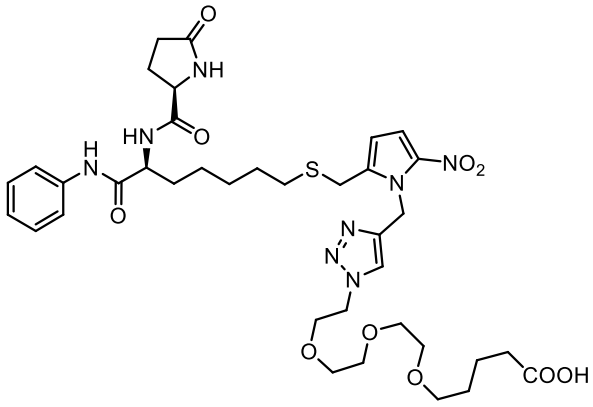

5-(2-(2-(2-(4-((2-Nitro-5-((((S)-7-oxo-6-((S)-5-oxopyrrolidine-2-carboxamido)-7-(phenylamino) heptyl)thio)methyl)-1*H*-pyrrol-1-yl)methyl)-1*H*-1,2,3-triazol-1-yl)ethoxy)ethoxy) ethoxy)pentanoic acid (88)

Compounds **83** (22 mg, 0.04 mmol) and azide **87** (11 mg, 0.04 mmol) were dissolved in dry DMF (2 mL) in a round-bottom flask under magnetic stirring and atmosphere of argon. The solution was degassed with three cycles of argon/*vacuum*. To this solution, a freshly prepared aqueous mixture (1 mL) of $Cu(OAc)_2$ (2.5 mg, 0.013 mmol) and sodium ascorbate (5 mg, 0.025 mmol), previously degassed by argon/*vacuum* cycles, was added dropwise. The reaction mixture was degassed and left to stir under argon at room temperature for 16 h. The solvent was evaporated and the crude reaction mixture was purified by silica gel flash chromatography (CH_2Cl_2:MeOH 8:2) to provide compound **88** (12 mg, 0.015 mmol) as a pale yellow oil (yield 36%).

MS (ESI): m/z calcd for $C_{37}H_{51}N_8O_{10}S$ $[M-1]^-$: 799.3454; found: 799.3463.

^{1}H NMR (600 MHz, CD_3OD): δ 7.93 (s, 1H), 7.55 (d, J = 7.8 Hz, 2H), 7.31 (t, J = 7.9 Hz, 2H), 7.19 (d, J = 4.3 Hz, 1H), 7.10 (t, J = 7.4 Hz, 1H), 6.25 – 6.23 (m, 1H), 5.8 (s, 1H), 4.53 (t, J = 4.9 Hz, 2H), 4.47 (dd, J = 8.5, 5.8 Hz, 1H), 4.30 – 4.27 (m, 1H), 4.01 (s, 2H), 3.84 (t, J = 4.9 Hz, 2H), 3.55 – 3.52 (m, 8H), 3.46 (t, J = 6.1 Hz, 2H), 2.53 (t, J = 7.2 Hz, 2H), 2.48 – 2.40 (m, 2H), 2.33 – 2.29 (m, 2H), 2.11 – 2.04 (m, 2H), 1.88 – 1.86 (m, 1H), 1.76 – 1.73 (m, 2H), 1.65 – 1.57 (m, 6H), 1.48 – 1.43 (m, 1H).

^{13}C NMR (150 MHz, CD_3OD): δ 138.23, 128.45, 128.45, 128.31, 124.07, 123.56, 120.01, 113.94, 110.02, 70.49, 70.16, 70.13, 70.09, 69.74, 68.96, 56.61, 53.99, 50.07, 48.44, 48.17, 48.02, 47.88, 47.73, 47.59, 47.45, 47.31, 47.17, 40.64, 31.85, 30.99, 29.36, 29.16, 28.84, 28.72, 27.93, 26.80, 26.71, 25.41, 25.08.

4.5.1.7 Synthesis with other functional groups:

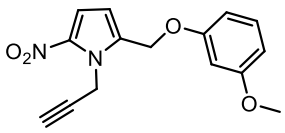

2-((3-Methoxyphenoxy)methyl)-5-nitro-1-(prop-2-yn-1-yl)-1*H*-pyrrole (90)

To a solution of 3-methoxyphenol (35 mg, 0.284 mmol) in THF (2 mL) was added K_2CO_3 (38 mg; 0.278 mmol) and the reaction was left a room temperature under magnetic stirring for 1 h. Then the bromide 42 (34.51 mg, 0.142 mmol, prepared according to the general procedure for bromination) and Et3N (15 mg, 0.149 mmol) were added and the mixture was stirred for 16 h. The crude was diluted with DCM then washed with H_2O and brine. The organic layer was dried over anhydrous Na_2SO_4, filtered and concentrated *in vacuo*. The reaction mixture was purified by silica gel flash chromatography purified by silica gel flash chromatography (PE:EtOAc 70:30) in order to obtain the product (30% yield).

MS (ESI): m/z calcd for $C_{15}H_{14}N_2O_4Na$ $[M+Na]^+$: 309.0851; found: 309.0867.

^{1}H NMR: (600 MHz, $CDCl_3$) δ 7.24 – 7.16 (m, 2H), 6.64 (dd, J = 8.2, 1.7 Hz, 1H), 6.62 – 6.59 (m, 1H), 6.57 (dd, J = 8.1, 1.7 Hz, 1H), 6.40 (d, J = 4.3 Hz, 1H); 5.30 (s, J = 2.3 Hz, 2H), 5.18 (s, 2H), 3.77 (s, 3H), 2.81 (s, J = 2.4 Hz, 1H).

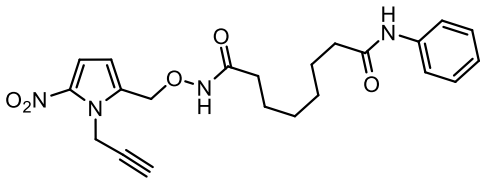

N^1-((5-Nitro-1-(prop-2-yn-1-yl)-1*H*-pyrrol-2-yl)methoxy)-N^8-phenyloctanediamide (91)

To a solution of SAHA (24 mg, 0.093 mmol) in MeOH (1 mL) was added an aqueous solution of NaOH 10N (11 mg; 0.279 mmol) and the reaction was left a room temperature under magnetic stirring for 10 min. Then a solution of the bromide **82** (19 mg, 0.08 mmol, prepared according to the general procedure for bromination) in THF (1 mL) was added and the mixture was stirred until consumpition of the bromide monitored by TLC. Then aqueous solution of HCl 1N (28 µL) was added in the reaction. The crude was diluted with DCM then washed with H_2O and brine. The organic layer was dried over anhydrous Na_2SO_4, filtered and concentrated *in vacuo*. The reaction mixture was purified by silica gel flash chromatography purified by silica gel flash chromatography (DCM:MeOH 95:5) in order to obtain the product (32% yield).

MS (ESI): m/z calcd for $C_{22}H_{25}N_4O_5$ $[M-1]^-$: 425.1830; found: 425.1837.

^{1}H NMR: (600 MHz, $CDCl_3$) δ 7.54 (d, J = 7.8 Hz, 2H), 7.29 (t, J = 7.9 Hz, 2H), 7.19 (d, J = 4.2 Hz, 1H), 7.08 (t, J = 7.4 Hz, 1H), 6.36 (d, J = 4.2 Hz, 1H); 5.49 (d, J = 2.0 Hz, 2H), 4.94 (s, 2H), 2.80 (s, 1H); 2.37 (t, J = 7.4 Hz, 2H), 2.11 – 2.01 (m, 2H), 1.73 – 1.65 (m, 2H), 1.65 – 1.57 (m, 2H), 1.41 – 1.32 (m, 4H).

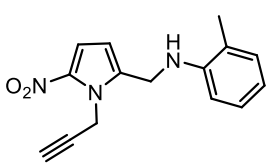

2-Methyl-*N*-((5-nitro-1-(prop-2-yn-1-yl)-1*H*-pyrrol-2-yl)methyl)aniline (92)

To a solution of *o*-toluidine (60 mg; 0.56 mmol) in THF (5 mL) was added the bromide **82** (68 mg, 0.28 mmol, prepared according to the general procedure for bromination) and Et3N (34 mg, 0.336 mmol), then the mixture was stirred for 16 h at room temperature. The crude was diluted with DCM then washed with H_2O and brine. The organic layer was dried over anhydrous Na_2SO_4, filtered and concentrated *in vacuo*. The reaction mixture was

purified by silica gel flash chromatography purified by silica gel flash chromatography (PE:EtOAc 60:40) in order to obtain the product (24% yield).

MS (ESI): m/z calcd for $C_{15}H_{15}N_3O_2Na$ $[M+Na]^+$: 292.1062; found: 292.1073.

^{1}H NMR: (600 MHz, $CDCl_3$) δ 7.24 (d, J = 3.8 Hz, 1H), 7.17 (t, J = 7.5 Hz, 1H), 7.12 (d, J = 7.1 Hz, 1H), 6.78 (t, J = 7.3 Hz, 1H), 6.69 (d, J = 7.9 Hz, 1H), 6.25 (d, J = 3.9 Hz, 1H); 5.33 (d, J = 1.5 Hz, 2H), 4.45 (s, 2H), 3.74 (s, 1H), 2.38 (s, 1H), 2.19 (s, 3H).

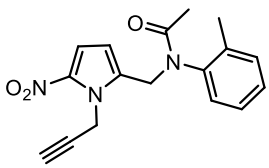

_N_-((5-Nitro-1-(prop-2-yn-1-yl)-1_H_-pyrrol-2-yl)methyl)-_N_-(_o_-tolyl)acetamide (93)

Compound **92** (6 mg, 0.022 mmol) was dissolved in hanydrous THF (3mL) and cooled to 0 °C with ice-bath under N_2 atmosphere and magnetic stirring. Et_3N (4.5 mg; 0.044 mmol) and acetyl chloride (2.6 mg, 0.033 mmol) were added into the reaction and the mixture was left at 0 °C for 1 h. Then the crude was diluted with DCM then washed with H_2O and brine. The organic layer was dried over anhydrous Na_2SO_4, filtered and concentrated *in vacuo*. The reaction mixture was purified by silica gel flash chromatography purified by silica gel flash chromatography (PE:EtOAc 70:30) in order to obtain the product (75% yield).

MS (ESI): m/z calcd for $C_{17}H_{17}N_3O_3Na$ $[M+Na]^+$: 334.1168; found: 334.1179.

^{1}H NMR: (600 MHz, $CDCl_3$) δ 7.36 – 7.13 (m, 2H), 7.11 – 6.78 (m, 2H), 5.79 (1, J = 22.1 Hz, 1H), 5.37 (ddd, J = 24.4, 19.9, 8.9 Hz, 3H); 4.36 (d, J = 15.4 Hz, 2H), 2.42 – 2.22 (m, 2H), 2.10 (d, J = 54.0 Hz, 3H), 1.82 (s, 3H), 1.63 (d, J = 73.3 Hz, 5H), 1.27 (d, J = 11.4 Hz, 2H).

*4.5.1.8 Calibration Curve for thiol **81***

Chromatographic analyses were performed at flow rate of 0.4 mL/min, injection volume of 5 µL, operating with a gradient elution of A: water (H_2O) and B: acetonitrile (ACN). UV detection was monitored at 254 nm. The analysis started with 5% of B, then B was increased to 95% (from t = 0 to t = 10 min), then kept at 95% (from t = 10 to t = 15 min) and finally return to 5% of eluent B in 1.0 min.

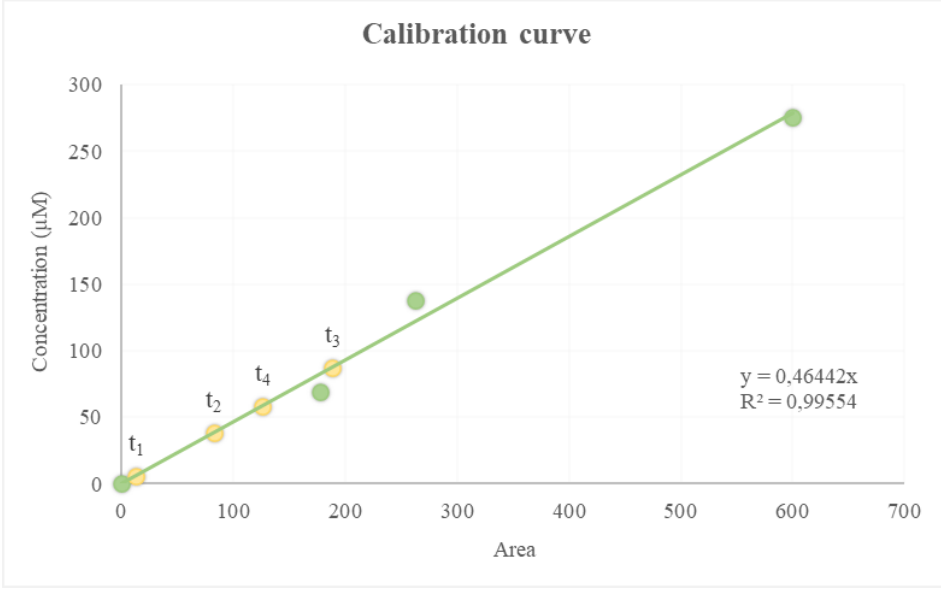

Figure 48: Calibration curve (green line and points, $R^2 = 0.99554$) for the compound **81** and its concentration monitored by HPLC-MS at different time during the reduction with nanoparticles (yellow points).

4.5.1.9 Determination of DAR (MALDI spectra)

The DAR was determined by MALDI mass spectrometry, using an Ultraflex III mass spectrometer (Bruker, GmbH), operating in positive linear mode. Briefly, 100 µL of unconjugated antibodies and products were desalted using PD spin trap G25 (GEHealthcare) eluting in water. A 10 mg/ml s-DHB MALDI matrix solution was prepared in 0.1%TFA dissolved in a mixture of water and acetonitrile (50:50, v/v). The sample solution (2 µL) was deposited on MALDI target using a double layer sample deposition method. The mass spectra were acquired in a mass range from 50 kDa to 180 kDa. The average DAR was calculated (over three experiments) dividing mass difference between unconjugated and conjugated antibodies by the MW of the linker-payload.

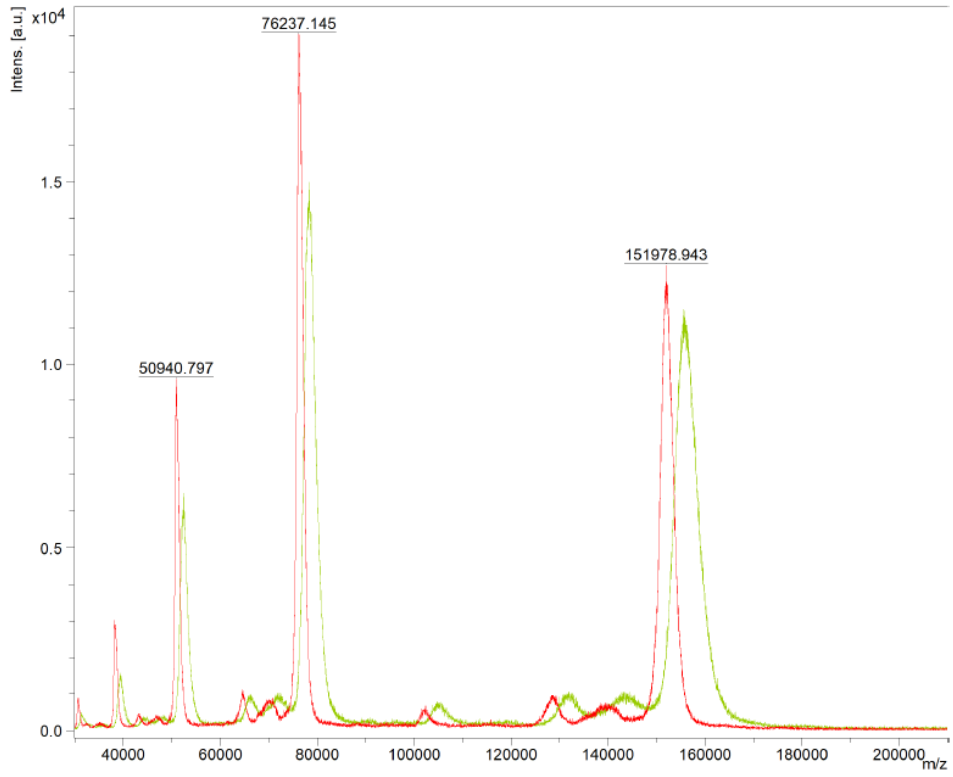

Figure 49: Comparison of MALDI spectra of ADC **89** (green line) and cetuximab alone (red line).

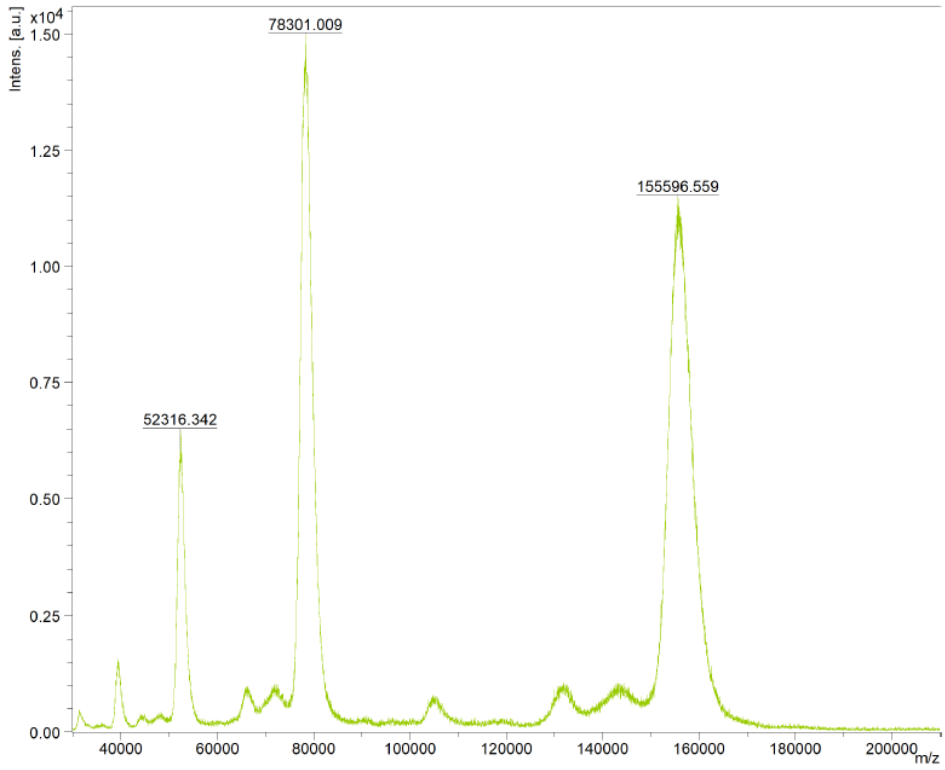

Figure 50: MALDI spectra of ADC **89** (green line).

4.5.2 New Morita-Baylis-Hillman Adducts for the selective Nitroreductase-mediated drug release

General procedure for nitro group reduction:[181]

Iron-based nanoparticles (6 mg) was added to a round-bottomed flask. 0.5 mL aqueous solution of 2 wt. % TPGS-750-M was added via syringe and $NaBH_4$ (59.0 mg, 1.5 mmol) was added to the reaction mixture. Reaction flask was closed with septum and the reaction mixture turned black with evolution of hydrogen gas. After 2 minutes the nitro-containing compounds (0.5 mmol), pre-dissolved in mixture of 0.5 mL aqueous 2 wt. % TPGS-750-M and 0.1 mL THF, was added to the catalyst suspension and the reaction was vigorously stirred at room temperature. HPLC-MS traces were recorded at set time points.

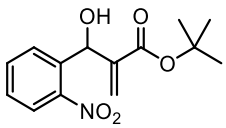

***tert*-Butyl 2-(hydroxy(2-nitrophenyl)methyl)acrylate (106)**

In an oven-dried flask under N_2 atmosphere, the 2-nitro benzaldehyde (1.5 g, 9.93 mmol) was solubilized in 1.5 mL of THF dry, successively *tert*-butyl acrylate (12.6 mL, 99.3 mmol) and DABCO (1.27 g, 9.93 mmol) were added. The reaction mixture was stirred at room temperature for 48 h. After concentration under vacuo, H_2O was added into the crude and extracted with EtOAc (3x 100 mL). The organic phase was washed with HCl 1N and brine, then was dried over anhydrous Na_2SO_4, filtered and concentrated in vacuo. The crude reaction mixture was purified by silica gel flash chromatography (PE:EtOAc 95:5) to provide the desired compound as yellow oil with 90% of yield.

MS (ESI): m/z calcd for $C_{14}H_{17}NO_5Na$ $[M+Na]^+$: 302.1004; found: 302.0992.

^{1}H NMR (600 MHz, $CDCl_3$): δ 7.86 (d, J = 8.1 Hz, 1H), 7.63 (d, J = 7.6 Hz, 1H), 7.56 (t, J = 7.5 Hz, 1H), 7.39 (dd, J = 11.3, 4.0 Hz, 1H), 6.23 (s, 1H), 6.03 (s, 1H), 5.64 (s, 1H), 1.29 (s, 9H).

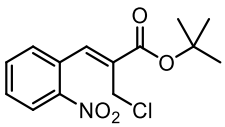

tert-Butyl (Z)-2-(chloromethyl)-3-(2-nitrophenyl)acrylate (109)

In a dried flask under N_2 atmosphere, $POCl_3$ (100 mg, 0.71 mmol) was added in 0.04 mL of dry DMF and left under magnetic stirring for 10 min. Then, a solution of compound 1 in DCM (1.5 mL) was added into the reaction. After 45 min, H_2O was used for quenched the excess of $POCl_3$ and the crude was extracted with DCM (10 mL x3). The organic phase was washed with brine and dried over anhydrous Na_2SO_4, filtered and concentrated in vacuo. The crude reaction mixture was purified by silica gel flash chromatography (PE:EtOAc 95:5) to provide the desired compound as yellow oil with 69% of yield.

MS (ESI): m/z calcd for $C_{14}H_{16}NO_4ClNa$ $[M+Na]^+$: 320.0666; found: 320.0682.

^{1}H NMR (600 MHz, $CDCl_3$): δ 8.20 (d, J = 8.2 Hz, 1H), 8.00 (s, 1H), 7.74 (d, J = 7.5 Hz, 1H), 7.66 (d, J = 7.5 Hz, 1H), 7.59 (d, J = 7.7 Hz, 1H), 4.20 (s, 2H), 1.58 (s, 9H)

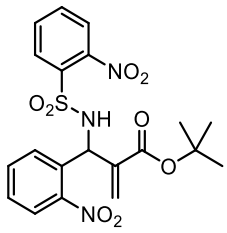

tert-Butyl 2-((2-nitrophenyl)((2-nitrophenyl)sulfonamido) methyl) acrylate (111)

A solution of 2-nitro benzyl sulfonamide (202 mg, 0.60 mmol) in 5 mL of THF was stirred under N_2 atmosphere in a round bottom flask, then Et_3N (87 µL, 0.64 mmol) and compound **109** (180 mg, 0.60 mmol) were added and the reaction was left at room temperature for 16 h. After, H_2O was added and the crude was extracted with DCM (x3). The organic phase was washed with brine and dried over anhydrous Na_2SO_4, filtered and concentrated in vacuo. The crude reaction mixture was purified by silica gel flash chromatography (PE:EtOAc 95:5) to provide the desired compound as yellow oil with 22% of yield.

MS (ESI): m/z calcd for $C_{20}H_{20}N_3O_8S$ $[M-1]^-$: 462.0977; found: 462.0971.

^{1}H NMR (600 MHz, $CDCl_3$): δ 7.94 (t, J = 8.1 Hz, 2H), 7.79 – 7.65 (m, 4H), 7.58 (t, J = 7.6 Hz, 1H), 7.46 (t, J = 7.7 Hz, 1H), 6.32 (s, 1H), 6.19 (s, 1H), 5.40 (s, 1H), 1.37 (s, 9H).

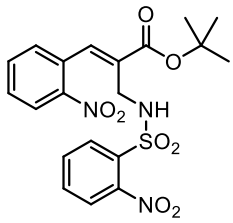

***tert*-Butyl 2-((2-nitrophenyl)((2-nitrophenyl)sulfonamido) methyl) acrylate (112)**

A solution of 2-nitro benzyl sulfonamide (202 mg, 0.60 mmol) in 5 mL of THF was stirred under N_2 atmosphere in a round bottom flask, then Et_3N (87 µL, 0.64 mmol) and compound **109** (180 mg, 0.60 mmol) were added and the reaction was left at room temperature for 16 h. After, H_2O was added and the crude was extracted with DCM (x3). The organic phase was washed with brine and dried over anhydrous Na_2SO_4, filtered and concentrated in vacuo. The crude reaction mixture was purified by silica gel flash chromatography (PE:EtOAc 95:5) to provide the desired compound as yellow oil with 14% of yield.

MS (ESI): m/z calcd for $C_{20}H_{20}N_3O_8S$ $[M-1]^-$: 462.0977; found: 462.0964.

^{1}H NMR (600 MHz, $CDCl_3$): δ 8.22 (d, J = 8.2 Hz, 1H), 7.97 (s, 1H), 7.86 (m, 2H), 7.79 (t, J = 7.6 Hz, 1H), 7.73 (t, J = 7.7 Hz, 2H), 7.64 (t, J = 7.9 Hz, 1H), 7.51 (d, J = 7.5 Hz, 1H), 3.91 (s, 2H), 1.48 (s, 9H).

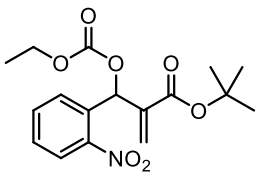

***tert*-Butyl 2-(((ethoxycarbonyl)oxy)(2-nitrophenyl) methyl) acrylate (114)**

In an oven-dried Schlenk under Ar atmosphere, compound **106** (150 mg, 0.53 mmol) was added in dry THF (2.5 mL) and the solution was cooled at -78 °C and LiHMDS (800 µL, 0.8 mmol) was added. After 30 min, ethyl chloroformate (163 µL, 1.59 mmol) was added and after 40 min the reaction was quenched with H_2O and extracted with EtOAc. The organic phase was washed with brine and dried over anhydrous Na_2SO_4, filtered and concentrated in vacuo. The crude reaction mixture was purified by silica gel flash chromatography (PE:EtOAc 95:5) to provide the desired compound as yellow oil with 56% of yield.

MS (ESI): m/z calcd for $C_{17}H_{21}NO_7Na$ $[M+Na]^+$: 374.1216; found: 374.1202.

^{1}H NMR (600 MHz, $CDCl_3$): δ 8.04 (d, J = 7.5 Hz, 1H), 7.71 – 7.57 (m, 2H), 7.49 (t, J = 6.8 Hz, 1H), 7.14 (s, 1H), 6.34 (s, 1H), 5.43 (s, 1H), 4.22 – 4.14 (m, 2H), 1.40 (s, 9H), 1.27 (m, 3H).

^{13}C NMR (150 MHz, $CDCl_3$): δ 14.20, 27.90, 64.70, 72.11, 81.91, 125.13, 127.20, 128.69, 129.32, 133.29, 133.63, 139.84, 153.85, 163.82.

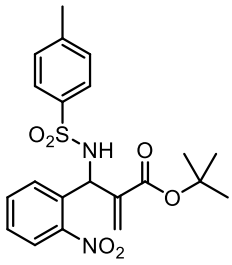

***tert*-Butyl 2-(((4-methylphenyl)sulfonamido)(2-nitrophenyl)methyl)acrylate (116)**

In a round bottom flask under N_2 atmosphere, compound **114** (200 mg, 0.57 mmol) was solubilized in 1 mL of THF and DABCO (255 mg, 2.29 mmol) was added. The solution was stirred for 10 min and after 4-toluensulfonamide (246 mg, 0.57 mmol) was added, then the reaction was leave at room temperature for 6 days. After concentration under vacuo, H_2O was added into the crude and extracted with DCM (3x 20 mL). The organic phase was washed with brine and dried over anhydrous Na_2SO_4, filtered and concentrated in vacuo. The crude reaction mixture was purified by silica gel flash chromatography (PE:EtOAc 70:30) to provide the desired compound as white solid with 31% of yield.

MS (ESI): m/z calcd for $C_{21}H_{23}N_2O_6S$ $[M-1]^-$: 431.1282; found: 431.1267.

^{1}H NMR (600 MHz, $CDCl_3$): δ 7.78 (dd, *J* = 8.1, 1.0 Hz, 1H), 7.63 (d, *J* = 8.2 Hz, 2H), 7.58 (d, J=7.7 Hz, 1H), 7.45 (td, J = 7.8 Hz, 1H), 7.37 – 7.32 (m, 1H), 7.17 (d, *J* = 8.1 Hz, 2H), 6.12-6.05 (m, 2H), 5.54 (s, 1H), 2.35 (s, 3H), 1.30 (s, 9H).

^{13}C NMR (150 MHz, $CDCl_3$): δ 21.5, 27.75, 54.47, 77.09, 82.18, 124.81, 127.08, 127.62, 128.56, 129.48, 130.13, 132.93, 133.63, 137.47, 139.02, 143.42, 164.37.

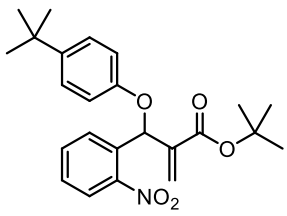

***tert*-Butyl 2-((4-(tert-butyl)phenoxy)(2-nitrophenyl) methyl) acrylate (119)**

In a round bottom flask under N_2 atmosphere and magnetic stirring, compound **114** (100 mg, 0.36 mmol) was solubilized in 1 mL of THF and DABCO (80 mg, 0.72 mmol) was added. The solution was stirred for 10 min and after 4-*tert*-butyl phenol (54 mg, 0.36 mmol) was added, then the reaction was leave at room temperature for 6 days. After concentration under vacuo, H_2O was added into the crude and extracted

with EtOAc (3x 20 mL). The organic phase was washed with brine and dried over anhydrous Na_2SO_4, filtered and concentrated in vacuo. The crude reaction mixture was purified by silica gel flash chromatography (PE:EtOAc 95:5) to provide the desired compound as yellow oil with 49% of yield.

MS (ESI): m/z calcd for $C_{24}H_{29}NO_5Na$ $[M+Na]^+$: 434.1943; found: 434.1920.

^{1}H NMR (600 MHz, $CDCl_3$): δ 8.06 (dd, *J* = 8.1, 0.9 Hz, 1H), 7.80 (d, *J* = 7.8 Hz, 1H), 7.64 (dd, *J* = 11.1, 4.0 Hz, 1H), 7.51 – 7.48 (m, 3H), 6.88 – 6.84 (m, 2H), 6.32 (s, 1H), 5.44 (s, 1H), 5.31 (s, 1H), 1.41 (s, 9H), 1.27 (s, 9H).

^{13}C NMR (150 MHz, $CDCl_3$):δ 27.89, 29.79, 31.47, 73.43, 77.07, 81.66, 115.16, 125.04, 126.28, 126.42, 128.88, 129.32, 133.59, 134.84, 141.35, 144.36, 155.56, 164.42.

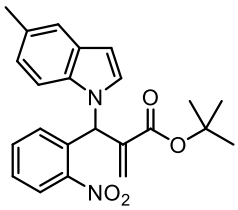

***tert*-Butyl 2-((1H-indol-1-yl)(2-nitrophenyl)methyl) acrylate (121)**

In a round bottom flask under N_2 atmosphere and magnetic stirring, compound **114** (50 mg, 0.14 mmol) was solubilized in 5 mL of DCM, then DABCO (1.5 mg, 0.014 mmol) and 5-methyl-1H-indole (18 mg, 0.14 mmol) were added. The solution was heated at 40 °C and stirred for 5 days, after H_2O was added into the crude and extracted with DCM (3x 20 mL). The organic phase was washed with brine and dried over anhydrous Na_2SO_4, filtered and concentrated in vacuo. The crude was purified by silica gel flash chromatography (PE:EtOAc 65:35) to provide the desired compound as orange solid with 17% of yield.

MS (ESI): m/z calcd for $C_{23}H_{24}N_2O_4Na$ $[M+Na]^+$: 415.1634; found: 415.1639.

^{1}H NMR (600 MHz, $CDCl_3$): δ 8.09 (dd, *J* = 7.8, 1.4 Hz, 1H), 7.53- 7.46 (m, 2H), 7.43 (s, 2H), 7.19 (d, *J* = 8.4 Hz, 1H), 7.00 (d, *J* = 3.1 Hz, 1H), 6.91 (d, *J* = 7.4 Hz, 1H), 6.49 (d, *J* = 3.1 Hz, 1H), 6.43 (s, 1H), 5.31 (s, 1H), 5.10 (s, 1H), 2.44 (s, 3H), 1.28 (s, 9H).

^{13}C NMR (150 MHz, $CDCl_3$) : δ 27.76, 29.71, 55.47, 81.90, 102.01, 109.44, 120.66, 123.82, 125.50, 125.75, 127.36, 129.06, 129.14, 133.75, 140.85.

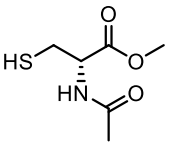

(*D*)-Methyl acetyl-cysteinate (122)

The compound was synthetised as reported.[305]

In a round bottom flask under N_2 atmosphere and magnetic stirring, N-acetyl-2-cysteine (500 mg, 3 mmol) was solubilized in 11 mL of MeOH and $SOCl_2$ (423 mg, 3.55 mmol) was added. The reaction was stirred for 90 min at room temperature and then concentrate in vacuo. The crude was diluited with EtOAc, washed with brine and dried over anhydrous Na_2SO_4, filtered and concentrated in vacuo. The crude was purified by silica gel flash chromatography (DCM:MeOH 99:1) to provide the desired compound as white solid with 37% of yield.

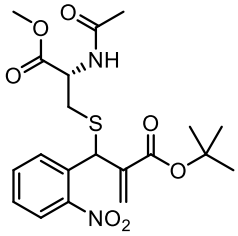

***tert*-Butyl 2-((((S)-2-acetamido-3-methoxy-3-oxopropyl) thio) (2-nitrophenyl)methyl)acrylate (123)**

In a round bottom flask under N_2 atmosphere and magnetic stirring, compound **114** (100 mg, 0.28 mmol) was solubilized in 5 mL of DCM, then DABCO (15 mg, 0.14 mmol) and methyl acetyl-cysteinate (46 mg, 0.28 mmol) were added. The solution was stirred at room temperature for 24 h, after this time H_2O was added into the crude and extracted with DCM (3x 20 mL). The organic phase was washed with brine and dried over anhydrous Na_2SO_4, filtered and concentrated in vacuo. The crude was purified by silica gel flash chromatography (PE:EtOAc 35:65) to provide the desired compound as a mixture of the two diasteroisomers (1:1) with 75% of yield.

MS (ESI): m/z calcd for $C_{20}H_{26}N_2O_7Na$ $[M+Na]^+$: 461.1358; found: 461.1372.

^{1}H NMR (600 MHz, $CDCl_3$): δ 7.93 (dd, *J* = 12.7, 8.3 Hz, 1H), 7.62 (t, *J* = 7.6 Hz, 1H), 7.55 (d, *J* = 3.2 Hz, 2H), 7.41 (ddd, *J* = 13.7, 12.5, 6.8 Hz, 3H), 6.44 (s, 1H), 6.21 (s, 1H), 5.96 (s, 1H), 5.87 (s, 1H), 5.79 (s, 1H), 5.47 (s, 1H), 5.28 (s, 1H), 4.95 (dd, *J* = 8.3, 4.1 Hz, 1H), 4.86 – 4.80 (m, 1H), 4.09 (q, *J* = 7.1 Hz, 1H), 3.72 (d, *J* = 5.9 Hz, 6H), 3.08 (ddd, *J* = 15.3, 11.4, 4.3 Hz, 1H), 2.94 (dd, *J* = 14.0, 4.4 Hz, 1H), 2.80 (dd, *J* = 14.3, 4.3 Hz, 1H), 1.44 (s, 6H), 1.33 (s, 18H).

^{13}C NMR (150 MHz, $CDCl_3$): δ 22.84, 22.98, 27.79, 27.87, 34.71, 34.86, 45.45, 46.22, 52.18, 53.37, 52.64, 52.72, 81.87, 82.15, 125.15, 125.28, 126.26, 127.36, 128.51, 128.51, 130.08, 130.91, 133.62, 141.23, 164.46, 165.03, 170.16, 170.41, 170.77, 170.78.

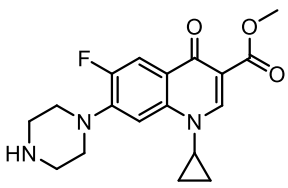

Methyl 1-cyclopropyl-6-fluoro-4-oxo-7-(piperazin-1-yl)-1,4-dihydroquinoline-3-carboxylate (CpxMe, 124)

The compound was synthetised as reported.[206]

In a round bottom flask under N_2 atmosphere and magnetic stirring, Ciprofloxacine (400 mg, 1.21 mmol) was suspended in 10 mL of MeOH dry and p-toluensolfonic acid (423 mg, 3.55 mmol) was added. The reaction was heated to 100 °C and stirred for 24. The crude was concentrated under vacuo and the solid mixture was washed with NaHCO3. The organic phase was extracted with DCM, washed with brine and dried over anhydrous Na_2SO_4, filtered and concentrated in vacuo. The desired compound as obtained without further purification as white solid with <99% of yield.

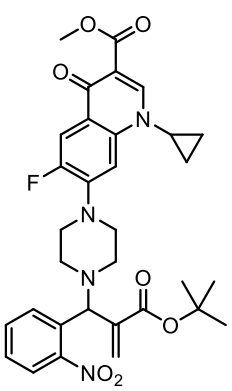

Methyl 7-(4-(2-(*tert*-butoxycarbonyl)-1-(2-nitrophenyl)allyl) piperazin-1-yl)-1-cyclopropyl-6-fluoro-4-oxo-1,4-dihydroquinoline-3-carboxylate (125)

In a round bottom flask under N_2 atmosphere and magnetic stirring, compound **114** (100 mg, 0.28 mmol) was solubilized in 10 mL of DCM, then DABCO (3 mg, 0.028 mmol) and compound **124** (97 mg, 0.28 mmol) were added. The solution was stirred at room temperature for 24 h, after this time H_2O was added into the crude and extracted with DCM (3x 20 mL). The organic phase was washed with brine and dried over anhydrous Na_2SO_4, filtered and concentrated in vacuo. The crude was purified by silica gel flash chromatography (DCM:MeOH 99:1) to provide the desired compound as yellow solid with 52% of yield.

MS (ESI): m/z calcd for $C_{32}H_{35}N_4O_7FNa$ $[M+Na]^+$: 629.2387; found: 629.2391.

^{1}H NMR (600 MHz, $CDCl_3$): δ 8.53 (s, 1H), 8.00 (d, *J* = 11.7 Hz, 1H), 7.82 (d, *J* = 38.1 Hz, 1H), 7.56 (d, *J* = 39.8 Hz, 2H), 6.41 (s, 1H), 5.82 (s, 1H), 5.29 (d, *J* = 11.3 Hz, 1H), 4.68 (s, 1H), 3.91 (s, 3H), 3.28 (s, 4H), 2.76 (d, *J* = 86.1 Hz, 4H), 1.42 (s, 9H), 1.28 (d, *J* = 35.6 Hz, 2H), 1.14 (s, 2H).

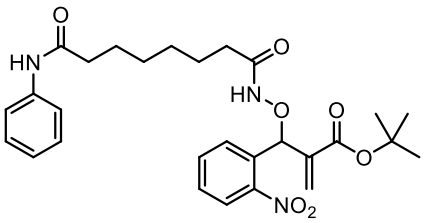

tert-Butyl 2-((2-nitrophenyl)((8-oxo-8-(phenylamino)octanamido)oxy) methyl) acrylate (126)

In a round bottom flask under N_2 atmosphere and magnetic stirring, compound **114** (100 mg, 0.28 mmol) was solubilized in 10 mL of dry DCM, then DABCO (3 mg, 0.028 mmol) and SAHA (74 mg, 0.28 mmol) were added. The solution was stirred at room temperature for 24 h, after this time H_2O was added into the crude and extracted with DCM (3x 20 mL). The organic phase was washed with brine and dried over anhydrous Na_2SO_4, filtered and concentrated in vacuo. The crude was purified by silica gel flash chromatography (DCM:MeOH 98:2) to provide the desired compound as yellow solid with 12% of yield.

MS (ESI): m/z calcd for $C_{28}H_{34}N_3O_7$ $[M-1]^-$: 524.2402; found: 524.2381.

^{1}H NMR (600 MHz, MeOD):δ 7.98 (d, *J* = 7.9 Hz, 1H), 7.83 (d, *J* = 7.6 Hz, 1H), 7.73 (d, *J* = 7.4 Hz, 1H), 7.54 (d, *J* = 7.7 Hz, 3H), 7.29 (t, *J* = 7.7 Hz, 2H), 7.08 (t, *J* = 7.0 Hz, 1H), 6.45 (s, 1H), 6.36 (s, 1H), 5.86 (s, 1H), 2.35 (dd, *J* = 17.7, 10.3 Hz, 4H), 1.69 – 1.62 (m, 2H), 1.57 (dd, *J* = 14.7, 7.3 Hz, 2H), 1.40 (s, 9H), 1.29 (s, 4H).

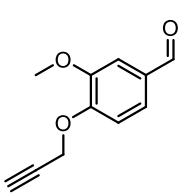

3-Methoxy-4-(prop-2-yn-1-yloxy)benzaldehyde (127)[306]

Vanillin (1.5 g, 9.86 mmol) was stirred with Cs_2CO_3 (3.213 g, 9.86 mmol) for five minutes in anhydrous DMF (25 mL). To the mixture was added propargyl bromide (3.742 mL,49.3 mmol). The reaction was stirred at room temperature for 24 hours. The reaction was then quenched with H_2O (30 mL) and extracted with EtOAc (3x30 mL) and washed with brine (3x80 mL). The organic layer was dried with Mg_2SO_4, filtered, and

concentrated by rotatory evaporation. The resulting solution was purified via flash chromatography (3:1 Hexanes: EtOAc), resulting in a white solid (86% yield).
^{1}H NMR (400 MHz, $CDCl_3$):δ 9.87 (s, 1H), 7.45 (dd, J = 1.9 Hz, J = 7.8 Hz, 1H), 7.43 (d, J = 1.9, 1H), 7.14 (d, J = 7.8 Hz, 1H), 4.85 (d, J = 2.4 Hz, 2H), 3.94 (s, 3H), 2.55 (t, J = 2.4 Hz, 1H)

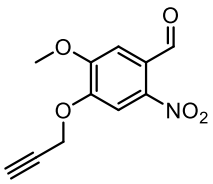

5-Methoxy-2-nitro-4-(prop-2-yn-1-yloxy) benzaldehyde (128)[306]

A flask was charged with **127** (1.5 g, 8.00 mmol, 1 eq), wrapped in aluminum foil and cooled at 0 °C. HNO_3 (50 mL, excess) was added to the flask and allowed to stir for 25 minutes at 0 °C. The reaction was then warmed to room temperature for 2 hours, then quenched with chilled H_2O (100 mL) and the precipitate was collected by vacuum filtration and washed with ice water (3x30 mL). The resulting product was a yellow solid (60% yield) and required no further purification.
^{1}H NMR (400 MHz, $CDCl_3$):δ 10.45 (s, 1H), 7.79 (s, 1H), 7.43 (s, 1H), 4.90(s, 2H), 4.02 (s, 3H), 2.62 (s, 1H).

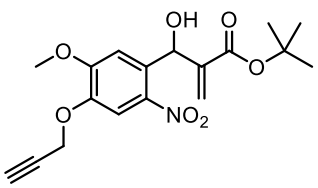

***tert*-Butyl 2-(hydroxy(5-methoxy-2-nitro-4-(prop-2-yn-1-yloxy)phenyl)methyl)acrylate (129)**

In an oven-dried flask under N_2 atmosphere, the compound **128** (90 mg, 0.38 mmol) was solubilized in 1.5 mL of THF dry, successively *tert*-butyl acrylate (0.55 mL, 3.8 mmol) and DABCO (43 mg, 0.38 mmol) were added. The reaction mixture was left at room temperature under magnetic stirring for 48 h. After concentration under vacuo, H_2O was added into the crude and extracted with EtOAc (3x 10 mL). The organic phase was washed with HCl 1N and brine, then was dried over anhydrous Na_2SO_4, filtered and concentrated in vacuo. The crude reaction mixture was purified by silica gel flash chromatography (PE:EtOAc 70:30) to provide the desired compound as yellow oil with 42% of yield.

MS (ESI): m/z calcd for $C_{18}H_{21}NO_7Na$ $[M+Na]^+$: 386.1216; found: 386.1211.

^{1}H NMR (600 MHz, MeOD): δ 7.76 (s, 1H), 7.20 (s, 1H), 6.19 (d, 2H), 5.51 (s, 1H), 4.80 (d, J = 2.3 Hz, 2H), 3.93 (s, 3H), 2.54 (t, J = 2.3 Hz, 1H), 1.40 (s, 9H).

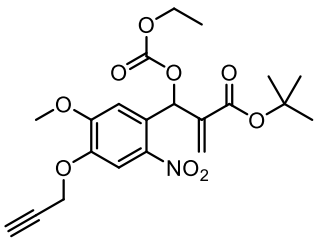

tert-Butyl 2-(((ethoxycarbonyl)oxy)(5-methoxy-2-nitro-4-(prop-2-yn-1-yloxy)phenyl)methyl)acrylate (130)

In an oven dried Schlenk under Ar atmosphere, compound **129** (130 mg, 0.36 mmol) was added in dry THF (10 mL) and the solution was cooled at -78 °C and LiHMDS (560 µL, 0.56 mmol) was added. After 30 min, ethyl chloroformate (111 µL, 1.08 mmol) was added and after 40 min the reaction was quenched with H_2O and extracted with EtOAc. The organic phase was washed with brine and dried over anhydrous Na_2SO_4, filtered and concentrated in vacuo. The crude reaction mixture was purified by silica gel flash chromatography (PE:EtOAc 95:5) to provide the desired compound as yellow oil with 97% of yield.

MS (ESI): m/z calcd for $C_{21}H_{25}NO_9Na$ $[M+Na]^+$: 458.1427; found: 458.1435.

^{1}H NMR (600 MHz, $CDCl_3$): δ 7.88 (s, 1H), 7.28 (s, 1H), 7.06 (s, 1H), 6.35 (s, 1H), 5.41 (s, 1H), 4.85 (d, J = 2.2 Hz, 2H), 4.28 – 4.19 (m, 2H), 3.95 (s, 3H), 2.59 (d, J = 1.2 Hz, 1H), 1.47 (s, 9H), 1.32 (t, J = 7.0 Hz, 3H).

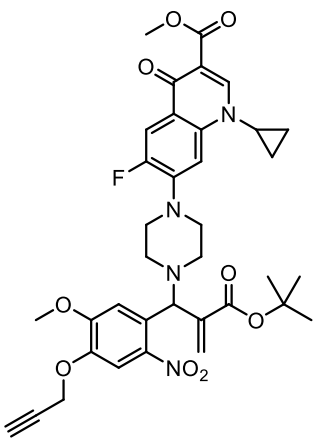

Methyl 7-(4-(2-(tert-butoxycarbonyl)-1-(5-methoxy-2-nitr-4-(prop-2-yn-1-yloxy)phenyl)allyl)piperazin-1-yl)-1-cyclopropyl-6-fluoro-4-oxo-1,4-dihydroquinoline-3-carboxylate (131)

In a round bottom flask under N_2 atmosphere and magnetic stirring, compound **130** (100 mg, 0.28 mmol) was solubilized in 10 mL of DCM, then DABCO (3 mg, 0.028 mmol) and CpxMe (**124**) (97 mg, 0.28 mmol) were added. The solution was stirred at room temperature for 24 h, after this time H_2O was added into the crude and extracted with DCM (3x 20 mL). The organic phase was washed with brine and dried over anhydrous Na_2SO_4, filtered and concentrated in vacuo. The crude was purified by silica gel flash chromatography (DCM:MeOH 99:1) to provide the desired compound with 38% of yield.

MS (ESI): m/z calcd for $C_{36}H_{39}N_4O_9FNa$ $[M+Na]^+$: 713.2599; found: 713.2604.

^{1}H NMR (600 MHz, MeOD): δ 8.63 (s, 1H), 7.83 (d, J = 13.3 Hz, 1H), 7.72 (s, 1H), 7.42 (s, 1H), 6.35 (s, 1H), 5.86 (s, 1H), 5.29 (s, 1H), 4.84 (s, 2H), 3.98 (s, 1H), 3.94 (s, 3H), 3.85 (s, 3H), 3.36 (bs, 4H), 2.91 – 2.84 (m, 2H), 2.74 – 2.66 (m, 2H), 2.53 (s, 1H), 1.44 (s, 9H), 1.33 – 1.27 (m, 2H), 1.19 – 1.14 (m, 2H).

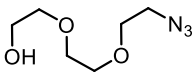

2-(2-(2-Azidoethoxy)ethoxy)ethan-1-ol (134)[307]

TEG (100 mg, 0.327 mmol) was dissolved in 10 mL of anhydrous DCM under atmosphere of N_2 then Et_3N (49 µL, 0.654 mmol) and *p*-Toluenesulfonyl chloride (63 mg, 0.327 mmol) were added. The reaction was stirred at room temperature for 16 h, then the solvent was removed and the crude was filtered with a pad of silica (PE:EtOAc 3:1) to provide the desired intermediate that was used immediately for the next step due to its instability. The tosyl-activated compound (64 mg, 0.138 mmol) was dissolved in 7 mL of anhydrous DMF under inert atmosphere and NaN_3 (34 mg, 0.524 mmol) was added. The mixture was heated at 80 °C and stirred for 16 h. The crude was concentrated *in vacuo*, the resulted suspension was

filtered and washed with DCM (10 mL x3). The solution was evaporated *in vacuo* to provide the product as light-yellow oil (<99% yield, 45 mg, 0.136 mmol).

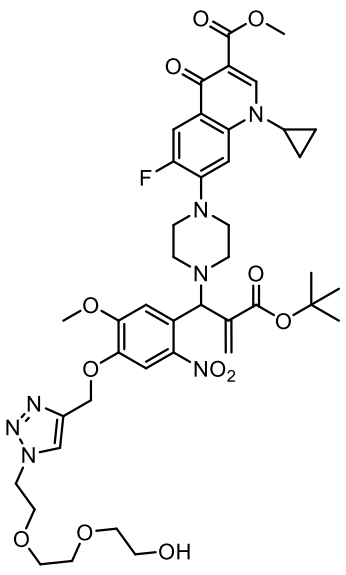

Methyl 7-(4-(2-(tert-butoxycarbonyl)-1-(4-((1-(2-(2-(2-hydroxyethoxy)ethoxy)ethyl)-1H-1,2,3-triazol-4-yl)methoxy)-5-methoxy-2-nitrophenyl) allyl)piperazin-1-yl)-1-cyclopropyl-6-fluoro-4-oxo-1,4-dihydroquinoline-3-carboxylate (135)

Compounds **131** (55 mg, 0.08 mmol) and azide **134** (11 mg, 0.06 mmol) were dissolved in dry DMF (6 mL) in a round-bottom flask under magnetic stirring and atmosphere of argon. The solution was degassed with three cycles of argon/*vacuum*. To this solution, a freshly prepared aqueous mixture (3 mL) of $Cu(OAc)_2$ (3.6 mg, 0.018 mmol) and sodium ascorbate (7.1 mg, 0.036 mmol), previously degassed by argon/*vacuum* cycles, was added dropwise. The reaction mixture was degassed and left to stir under argon at room temperature for 16 h. The solvent was evaporated and the crude reaction mixture was purified by silica gel flash chromatography (DCM:MeOH 96:4) to provide compound **135** as a pale yellow oil (yield 30%).

MS (ESI): m/z calcd for $C_{42}H_{52}FN_7O_{12}$ $[M+1]^+$: 866.3731; found: 866.3592.

4.5.3 Study of a dye for the development of a photosensitive drug delivery system

4.5.3.1 Synthetical procedures

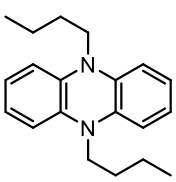

5,10-Dibutyl-4a,5,10,10a-tetrahydrophenazine (204)

Phenazine **202** (2.94 g, 16.3 mmol) was dissolved under Argon atmosphere in ethanol (70 mL) and was heated to 80°C. Solution of $Na_2S_2O_4$ (28.8 g, 16.5 mmol) in 250 mL of ultrapure water was prepared and added at the reaction flask. After the addition of the solution white precipitate was observed. The mixture was stirred for another hour, then the reaction was cooled to room temperature, filtered, washed with water and dried under vacuum atmosphere. 5,10-Dihydrophenazine **203** (2.81 g) was obtained as pale green solid and it was used directly for the next step due to its instability.

Under Argon atmosphere, compound **203**, NaOH (2.34 g, 58.6 mmol), 1mL of water and tetrabutylammonium bromide (0.4 g, 1.2 mmol) were dissolved in 25 mL of DMSO. The reaction was heated at 40° C and 1-iodobutane (4.0 mL, 35.2 mmol) was added. The reaction was stirred for other 5 hours, then it was cooled to room temperature and poured into water. The crude was extracted with DCM (3x50 mL), dried over anhydrous Na_2SO_4, filtered and concentrated in vacuo. The crude reaction mixture was purified with neutral aluminium oxide flash chromatography (PE as eluent). The purified product **204** was obtained with 65% yield.

MS (ESI): m/z calc for $C_{20}H_{28}N_2Na$ [M+Na]: 319.2150 found: 319.2173

^{1}H NMR (600 MHz, $CDCl_3$): δ 7.09 (d, *J* = 8 Hz, 2H), 6.82 (d, *J* = 8 Hz, 2H), 3.53 – 3.41 (m, 4H), 1.68 – 1.57 (m, 4H), 1.50 – 1.44 (m, 4H), 1.15 (t, *J* = 7.2 Hz, 6H)

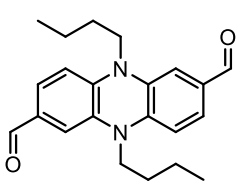

5,10-Dibutyl-5,10-dihydrophenazine-2,7-dicarbaldehyde (205)

Product **204** (2.9 g, 10 mmol) was dissolved in 20 mL of DMF under Argon atmosphere. The solution was cooled with ice bath and stirred for ten minutes. 2.5 mL of phosphorus oxychloride was added drop

by drop at the solution and the reaction was stirred for 30 minutes, then it was heated for 12 hours at 60°C. The reaction mixture was poured into ice water and the pH was adjusted to weakly basic. Dark orange precipitate was filtered, washed with ice water and dried. Product **205** (1.67 g, 40% yield) was obtained after silica flash chromatography with petroleum ether/EtOAc as eluent.

MS (ESI): m/z calc for $C_{22}H_{22}N_2NaO$ [M+Na]: 373.1892 found: 373.1864

^{1}H NMR (600 MHz, $CDCl_3$): δ 9.60 (s, 2H), 7.11 (d, *J* = 8.1 Hz, 2H), 6.73 (s, 2H), 6.28 (d, *J* = 8.1 Hz, 2H), 3.50 – 3.39 (m, 4H), 1.65 (dt, *J* = 15.6, 7.9 Hz, 4H), 1.53 – 1.46 (m, 4H), 1.05 (t, *J* = 7.3 Hz, 6H).

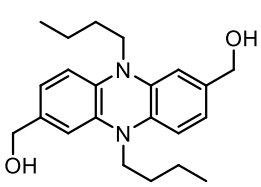

(5,10-Dibutyl-5,10-dihydrophenazine-2,7-diyl) dimethanol (206)

Compound **205** (500 mg, 1.425 mmol) was dissolved in THF dry under Argon atmosphere and was stirred in ice bath for ten minutes. Then $NaBH_4$ (54 mg, 1.425 mmol) was added at the solution and the reaction was stirred for 2 hours. The mixture was quenched with water, extracted with DCM (3x20 mL), dried over anhydrous Na_2SO_4, filtered and concentrated in vacuo. Product **206** (200 mg, 40% yield) was obtained after neutral aluminium oxide flash chromatography (PE/EtOAc).

MS (ESI): m/z calc for $C_{22}H_{30}N_2NaO_2$ [M+Na]: 377.2205 found: 377.2183

^{1}H NMR (600 MHz, $CDCl_3$): δ 7.57 (s, 2H), 7.09 (d, *J* = 8.1 Hz, 2H), 6.77 (d, *J* = 8.1 Hz, 2H), 4.46 (s, 2H), 3.52 – 3.40 (m, 4H), 1.55 – 1.52 (m, 4H), 1.49 – 1.46 (m, 4H), 1.15 (t, *J* = 7.3 Hz, 6H).

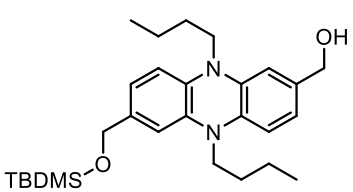

(5,10-Dibutyl-7-(((*tert*-butyldimethylsilyl)oxy) methyl)-5,10-dihydrophenazin-2-yl)methanol (207)

Product **206** (200 mg, 0.56 mmol), Imidazole (46 mg, 0.68 mmol) and DMAP (7.2 mg, 0.06 mmol) were dissolved in 10 mL of dry THF under Argon atmosphere. TBDMSCl (75 mg, 1.8 mmol) was dissolved in 1 mL

of dry THF and added in 1 hour at the reaction mixture. The reaction was stirred for 24 hours, after it was quenched with water and extracted with DCM (2x20 mL). The organic phase was washed with HCl 1N, NH_4Cl, brine and dried over anhydrous Na_2SO_4, filtered and concentrated in vacuo. Product **207** (80 mg, 30% yield) was obtained after purification with silica flash chromatography (PE/EtOAc).

MS (ESI): m/z calc for $C_{28}H_{44}N_2NaO_2Si$ [M+Na]: 491.3070 found: 491.3056

^{1}H NMR (600 MHz, DMSO): δ 7.35 (s, 2H), 7.12 (bd, *J* = 8.2, 2H), 6.61 (bd, *J* = 8.1 Hz, 2H), 4.59 (s, 2H) 4.44 (s, 2H), 3.45 – 3.38 (m, 2H), 3.31 – 3.29 (m, 2H), 1.59 – 1.50 (m, 4H), 1.43 – 1.40 (m, 4H), 0.90 (s, 6H), 0.85 (s, 9H), 0.10 (s, 6H).

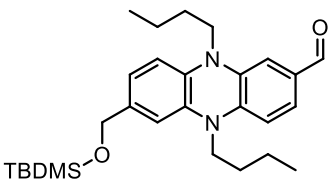

5,10-Dibutyl-7-(((*tert*-butyldimethylsilyl)oxy) methyl)-5,10-dihydrophenazine-2-carbaldehyde (208)

Compound **207** (160 mg, 0.33 mmol) and MnO_2 (34 mg, 0,4 mmol) were dissolved in DCM. The reaction was stirred at room temperature for 48h. Then the organic phase was washed with water (2x20 mL) and brine (1x20 mL), dried over anhydrous Na_2SO_4, filtered and concentrated in vacuo. Product **208** (25mg, 20% yield) was obtained after purification with after silica flash chromatography (PE/EtOAc).

MS (ESI): m/z calc for $C_{28}H_{42}N_2NaO_2Si$ [M+Na]: 489.2913 found: 489.2895

^{1}H NMR (600 MHz, DMSO): δ 9.53 (s, 1H), 7.10 (dd, *J* = 8.1, 1.3 Hz, 1H), 6.53 (d, *J* = 9.7 Hz, 2H), 6.40 (d, *J* = 8.2 Hz, 1H), 6.37 (s, 1H), 6.32 (d, *J* = 8.2 Hz, 1H), 4.46 (s, 2H), 3.47 – 3.40 (m, 2H), 3.39 – 3.33 (m, 2H), 1.57 – 1.46 (m, 4H), 1.40 (dt, *J* = 11.2, 7.3 Hz, 4H), 0.95 (dt, *J* = 11.5, 5.7 Hz, 6H), 0.89 (s, 9H), 0.06 (s, 6H).

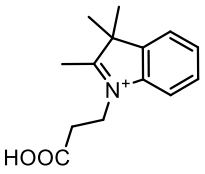

1-(2-Carboxyethyl)-2,3,3-trimethyl-3*H*-indol-1-ium (209)

2,3,3-Trimethylindolenine (3.18 g, 20 mmol) and 3-bromopropoinic acid (6.08 g, 40 mmol) were dissolved in MeCN (40 ml) under Argon atmosphere. The reaction mixture was refluxed for 12 h, then it was cooled to room temperature and the solvent was

removed under vacuum. The purple solid was crystallized in DCM, precipitate was filtered and washed with ice DCM. Product **209** (2.3 g, 50% yield) was obtained as a pale pink solid.

^{1}H NMR (600 MHz, DMSO): δ 8.01 – 7.94 (m, 1H), 7.84 – 7.78 (m, 1H), 7.61 (dd, *J* = 5.3, 3.3 Hz, 2H), 4.64 (t, *J* = 7.0 Hz, 2H), 2.97 (t, *J* = 7.0 Hz, 2H), 2.84 (s, 3H), 1.52 (s, 6H).

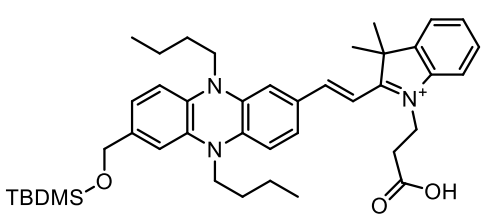

(*E*)-1-(2-Carboxyethyl)-2-(2-(5,10-dibutyl-7-(((*tert*-butyldimethylsilyl) oxy)methyl)-5,10-dihydrophenazin-2-yl)vinyl)-3,3-dimethyl-3*H*-indol-1-ium (210)

Product **7** (25 mg, 0.053 mmol) and product **209** (13 mg, 0.053 mmol) were dissolved in dry MeCN under Argon atmosphere in the dark. Then Piperidine was added in a catalytic amount and the reaction was stirred for 24 h at room temperature. Then the solvent was removed under vacuum and product **210** (10 mg, 27% yield) was obtained after silica flash chromatography (DCM/MeOH).

^{1}H NMR (600 MHz, DMSO): δ 8.31 (s, 2H), 8.02 (d, *J* = 15.5 Hz, 1H), 7.74 (d, *J* = 7.3 Hz, 1H), 7.67 (d, *J* = 7.8 Hz, 1H), 7.51 (t, *J* = 7.4 Hz, 1H), 7.44 (t, *J* = 6.9 Hz, 2H), 7.25 (d, *J* = 15.5 Hz, 1H), 6.74 (s, 1H), 6.63 (d, *J* = 7.8 Hz, 1H), 6.49 (d, *J* = 8.4 Hz, 2H), 6.43 (d, *J* = 8.1 Hz, 1H), 4.62 (s, 2H), 3.54 (d, *J* = 6.6 Hz, 4H), 2.65 (s, 2H), 2.07 (s, 6H), 1.02 – 0.92 (m, 9H), 0.91 – 0.81 (m, 15H), 0.07 (s, 6H).

4.6 Computational Appendixes

4.6.1 Rational design of a new BODIPY derivative for photosensitive drug delivery systems

4.6.1.1 Minimal geometries

The minimal geometries optimised with Gaussian 16 using B3LYP/6-31G* as level of theory.

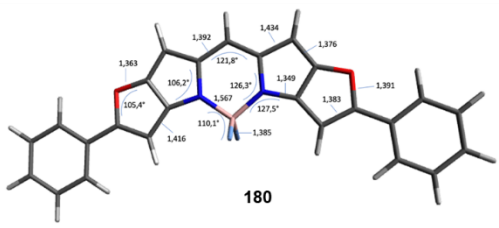

180

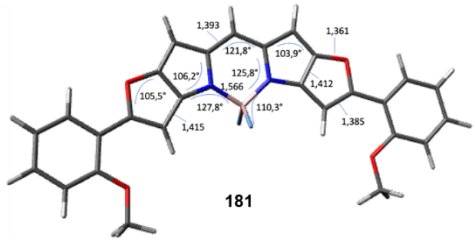

181

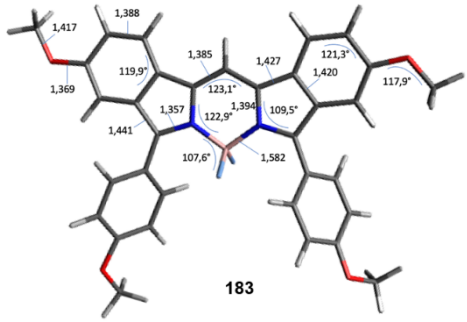

183

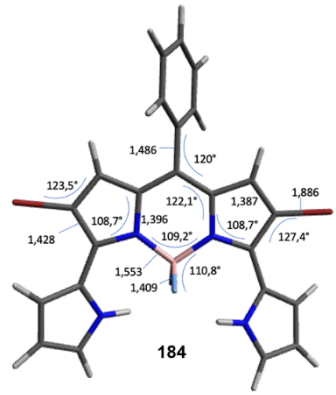

184

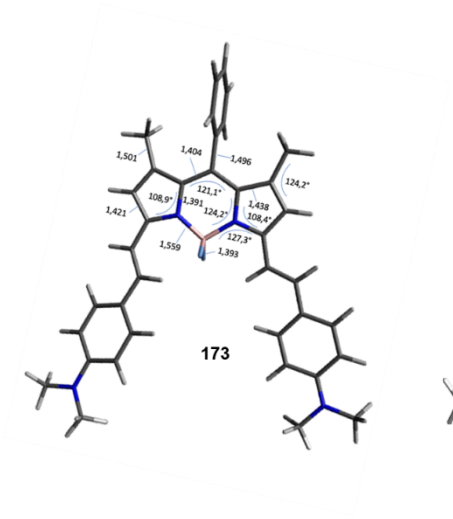

173

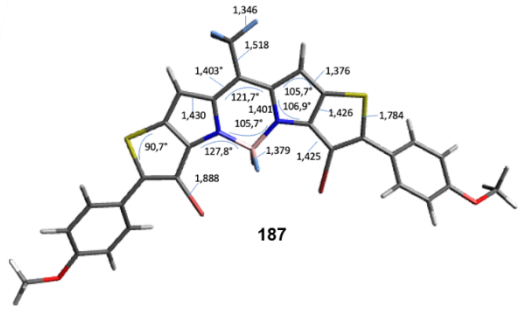

187

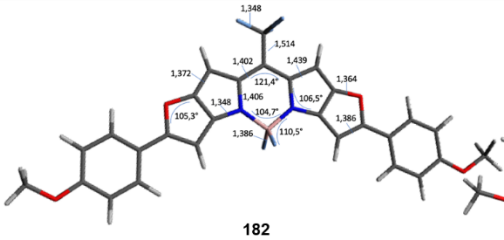

182

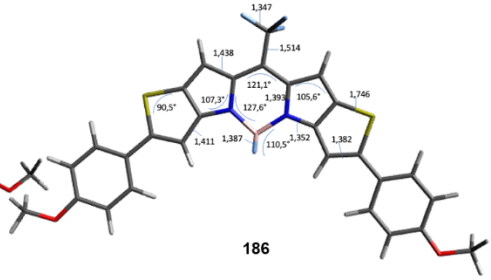

186

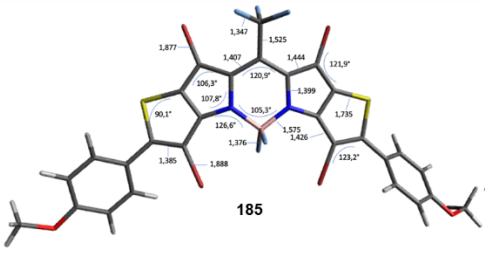

185

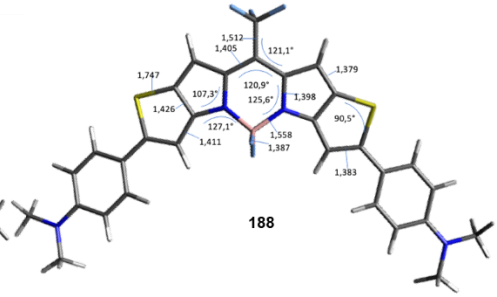

188

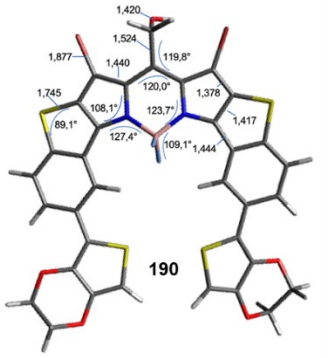

190

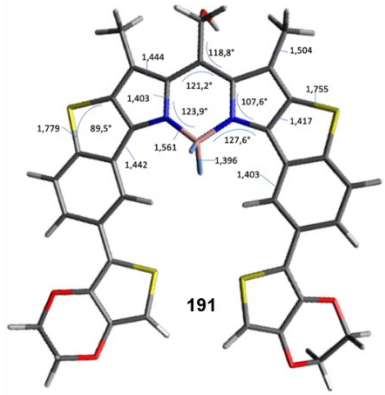

191

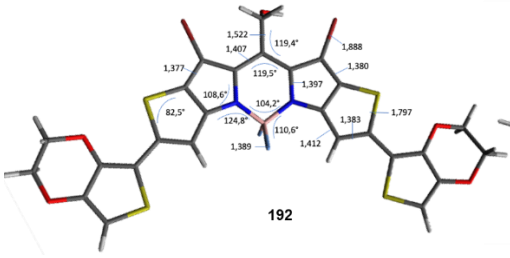

192

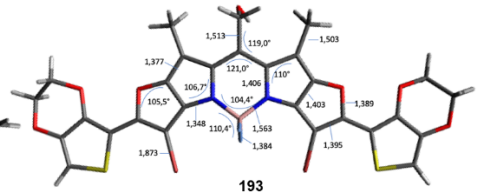

193

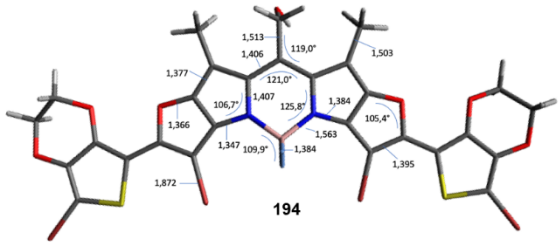

194

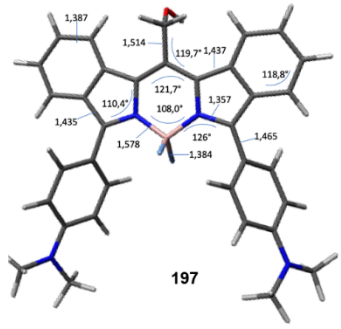

197

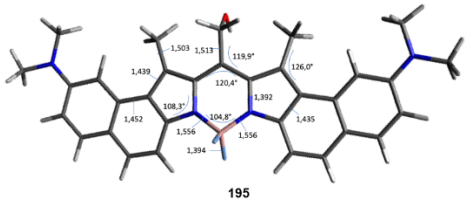

195

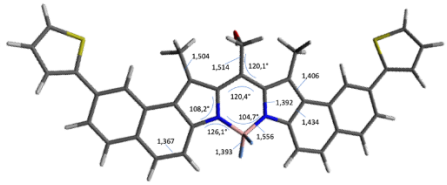

196

4.6.1.2 Tables of calculations of veritcal excitation energies

Vertical excitation energies ($E_{ecc.}$), calculated absorption maxima (λ_{max} calc.), experimental absorption maxima reported (λ_{max} exp.), absorption maxima obtained from the calibration line (λ_{max} expt.), oscillator strength (f), difference between experimental data and calculated data (ΔE).

Table 10: values obtained with M062X/cc-pVDZ.

Compound	E_{ecc} (eV)	λ_{max} calc. (nm)	$\lambda_{max.}$ exp. (nm)	ΔE (eV)	f
180	2,17	571	652	0,27	1,8963
181	2,12	585	671	0,27	1,8882
183	2,04	607	673	0,20	1,0029
184	2,11	589	682	0,29	0,7912
173	1,96	633	700	0,19	0,9335
187	2,02	615	720	0,24	1,6883
182	1,95	636	723	0,24	2,0167
186	1,93	643	731	0,23	1,8105
185	1,85	671	766	0,23	1,5056
188	1,77	699	840	0,29	1,8868

Table 11: values obtained with CAM-B3LYP/6-311+G(2d,p).

Compound	E_{ecc} (eV)	λ_{max} calc. (nm)	$\lambda_{max.}$ exp. (nm)	ΔE (eV)	f
180	2,12	586	652	0,21	1,9031
181	2,07	600	671	0,22	1,8929
183	1,99	624	673	0,14	0,9761
184	2,08	596	682	0,26	0,7925
173	1,96	634	700	0,24	0,9311
187	1,97	631	720	0,19	1,6720
182	1,89	656	723	0,17	1,9903
186	1,87	663	731	0,17	1,7971
185	1,80	688	766	0,18	1,5012
188	1,74	712	840	0,27	1,8764

Table 12: values obtained with M062X/6-311+G(2d,p).

Compound	E_{ecc} (eV)	λ_{max} calc. (nm)	$\lambda_{max.}$ exp. (nm)	ΔE (eV)	f
180	2,12	584	652	0,22	1,8933
181	2,07	598	671	0,22	1,8849
183	1,99	621	673	0,16	1,8849
184	2,06	601	682	0,24	0,7825
173	1,93	643	700	0,16	0,9189
187	1,97	630	720	0,20	1,6617
182	1,90	652	723	0,19	1,9901
186	1,88	659	731	0,19	1,7944
185	1,80	688	766	0,18	1,4822
188	1,73	715	840	0,26	1,8776

Table 13: values obtained with CAM-B3LYP/cc-pVDZ.

Compound	E_{ecc} (eV)	λ_{max} calc. (nm)	$\lambda_{max.}$ exp. (nm)	ΔE (eV)	f
180	2,17	572	652	0,27	1,8933
181	2,12	586	671	0,28	1,8961
183	2,03	610	673	0,19	1,0068
184	2,13	583	682	0,31	0,8016
173	1,99	623	700	0,22	0,9475
187	2,02	613	720	0,25	1,7044
182	1,94	638	723	0,23	2,0171
186	1,93	644	731	0,23	1,8159
185	1,86	667	766	0,24	1,5347
188	1,80	691	840	0,32	1,8884

Table 14: values obtained for compound **190**.

Level of theory	E_{ecc} (eV)	λ_{max} calc. (nm)	$\lambda_{max.}$ expt. (nm)	f
M062X/cc-pVDZ	2,21	561	632	0,7558
CAM-B3LYP/311+G(2d,p)	2,15	579	635	0,8511
M062X/6-311G(2d,p)	2,15	579	639	0,8511
CAM-B3LYP/cc-pVDZ	2,22	559	662	0,8548

Table 15: values obtained for compound **191**.

Level of theory	E_{ecc} (eV)	λ_{max} calc. (nm)	$\lambda_{max.}$ expt. (nm)	f
M062X/cc-pVDZ	2,23	557	626	0,7923
CAM-B3LYP/311+G(2d,p)	2,18	569	621	0,8352
M062X/6-311G(2d,p)	2,18	569	623	0,7962
CAM-B3LYP/cc-pVDZ	2,24	554	615	0,8392

Table 16: values obtained for compound **192**.

Level of theory	E_{ecc} (eV)	λ_{max} calc. (nm)	$\lambda_{max.}$ expt. (nm)	f
M062X/cc-pVDZ	1,96	634	728	1,7781
CAM-B3LYP/311+G(2d,p)	1,90	652	731	1,7768
M062X/6-311G(2d,p)	1,90	652	733	1,7648
CAM-B3LYP/cc-pVDZ	1,96	632	727	1,7963

Table 17: values obtained for compound **193**.

Level of theory	E_{ecc} (eV)	λ_{max} calc. (nm)	$\lambda_{max.}$ expt. (nm)	f
M062X/cc-pVDZ	1,95	637	732	1,9271
CAM-B3LYP/311+G(2d,p)	1,90	652	730	1,9150
M062X/6-311G(2d,p)	1,90	653	734	1,9025
CAM-B3LYP/cc-pVDZ	1,95	635	731	1,9424

Table 18: values obtained for compound **194**.

Level of theory	E_{ecc} (eV)	λ_{max} calc. (nm)	$\lambda_{max.}$ expt. (nm)	f
M062X/cc-pVDZ	1,91	649	748	2,0570
CAM-B3LYP/311+G(2d,p)	1,87	664	746	2,0475
M062X/6-311G(2d,p)	1,86	666	751	2,0399
CAM-B3LYP/cc-pVDZ	1,92	646	747	2,0681

Table 19: values obtained for compound **197**.

Level of theory	E_{ecc} (eV)	λ_{max} calc. (nm)	$\lambda_{max.}$ expt. (nm)	f
M062X/cc-pVDZ	1,99	624	712	0,9837
CAM-B3LYP/311+G(2d,p)	195	636	710	0,9786
M062X/6-311G(2d,p)	1,95	637	713	0,9651
CAM-B3LYP/cc-pVDZ	1,99	621	711	0,9974

Table 20: values obtained for compound **195**.

Level of theory	E_{ecc} (eV)	λ_{max} calc. (nm)	$\lambda_{max.}$ expt. (nm)	f
M062X/cc-pVDZ	2,06	601	685	1,7794
CAM-B3LYP/311+G(2d,p)	2,01	610	676	1,7871
M062X/6-311G(2d,p)	2,03	612	681	1,7686
CAM-B3LYP/cc-pVDZ	2,07	598	678	1,8022

Table 21: values obtained for compound **196**.

Level of theory	E_{ecc} (eV)	λ_{max} calc. (nm)	$\lambda_{max.}$ expt. (nm)	f
M062X/cc-pVDZ	1,89	655	755	1,5036
CAM-B3LYP/311+G(2d,p)	189	654	735	1,5605
M062X/6-311G(2d,p)	1,87	663	747	1,5084
CAM-B3LYP/cc-pVDZ	1,93	643	743	1,5658

4.6.2 Study of a dye for the development of a photosensitive drug delivery system

4.6.2.1 Energies of minimal geometries

The minimal geometries were optimised with Gaussian 16 using B3LYP/6-31G* as level of theory. Reported energies of the isomer ground states.

PH-1

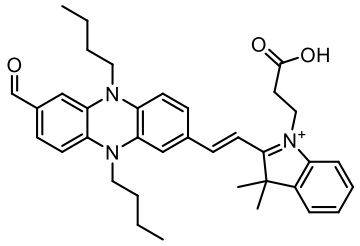

E = -1786.88895139 a.u.

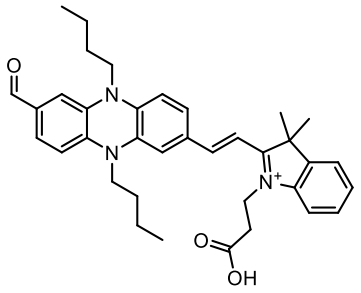

E = -1786.88648870 a.u.

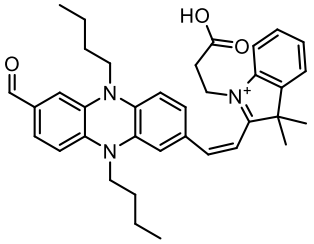

E = -1786.85977394 a.u.

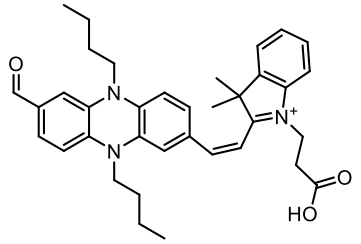

E = -1786.87012415 a.u.

ND-1

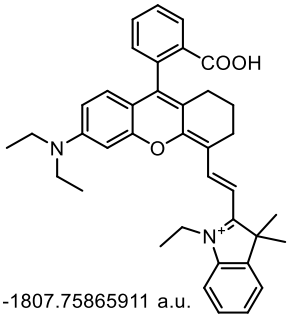

E = -1807.75865911 a.u.

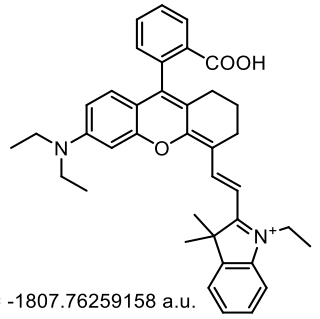

E = -1807.76259158 a.u.

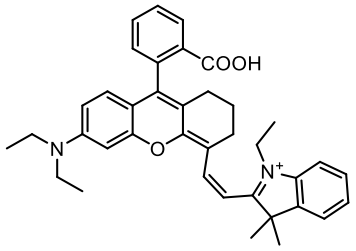

E = -1807.73938170 a.u.

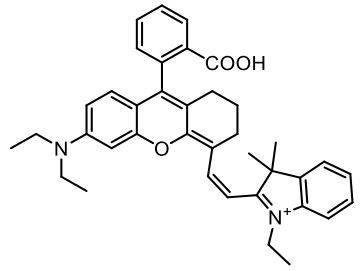

E = -1807.73326547 a.u.

4.6.2.2 Tables of calculations of veritcal excitation energies

Vertical excitation energies ($E_{ecc.}$), calculated absorption maxima (λ_{max} calc.), experimental absorption maxima reported (λ_{max} exp. = 690 nm), oscillator strength (f), difference between experimental data and calculated data (ΔE) and percentage involvement of HOMO-LUMO orbitals in the electronic transition $S_0 \rightarrow S_1$ (H→L).

Table 22: results for **PH-1** in DMSO with B3LYP/6-311+G(2d,p), ΔE = 0,0029

Exited state	E_{ecc} (eV)	λ_{max} calc. (nm)	Transition	f
1	1,7998	689	H→L 98%	0,7798
2	2,7628	449	H→L+1 94%	0,5590
3	2,9577	419	H-1→L 96%	0,7927
4	3,5628	348	H-2→L 89%	0,0291

Table 23: results for **PH-1** in DMSO with PBE0/6-311+G(2d,p), ΔE = 0,0579

Exited state	E_{ecc} (eV)	λ_{max} calc. (nm)	Transition	f
1	1,7390	713	H→L 98%	0,7304
2	2,6471	468	H→L+1 95%	0,4750
3	2,8577	434	H-1→L 96%	0,8602
4	3,4144	363	H-2→L 89%	0,0237

Table 24: results for **PH-1** in DMSO with CAM-B3LYP/6-311+G(2d,p), ΔE = 0,2649

Exited state	E_{ecc} (eV)	λ_{max} calc. (nm)	Transition	f
1	2,0618	601	H→L 94%	0,9897
2	3,1090	399	H→L+1 77%	0,9596
3	3,3375	371	H-1→L 80%	0,2666
4	3,9829	311	H-2→L 16%	0,0180

Table 25: results for **PH-1** in DMSO with LC-ωPBE /6-311+G(2d,p), ΔE = 0,3242

Exited state	E_{ecc} (eV)	λ_{max} calc. (nm)	Transition	f
1	2,1211	585	H→L 91%	0,7304
2	3,1610	392	H→L+1 71%	0,4750
3	3,4123	363	H-1→L 72%	0,8602
4	4,0350	307	H-2→L 14%	0,0237

Table 26: results for **PH-1** in DMSO with ωB97XD /6-311+G(2d,p), ΔE = 0,4752

Exited state	E_{ecc} (eV)	λ_{max} calc. (nm)	Transition	f
1	2,2721	546	H→L 85%	1,1654
2	3,3953	365	H→L+1 62%	1,0113
3	3,7194	333	H-1→L 58%	0,0582

Table 27: results for **ND-1** in DMSO with B3LYP/6-311+G(2d,p), ΔE = 0,0804

Exited state	E_{ecc} (eV)	λ_{max} calc. (nm)	Transition	f
1	2,0484	605	H→L 100%	1,1053
2	2,7514	451	H-1→L 95%	0,2261
4	3,4745	357	H→L+2 44%	0,1467

Table 28: results for **ND-1** in DMSO with PBE0/6-311+G(2d,p), ΔE = 0,1177

Exited state	E_{ecc} (eV)	λ_{max} calc. (nm)	Transition	f
1	2,0857	594	H→L 99%	1,1472
2	2,8618	433	H-1→L 96%	0,2423
4	3,6042	344	H→L+2 64%	0,2111

Table 29: results for **ND-1** in DMSO with CAM-B3LYP/6-311+G(2d,p), ΔE = 0,1997

Exited state	E_{ecc} (eV)	λ_{max} calc. (nm)	Transition	f
1	2,1677	572	H→L 96%	1,2598
2	3,3436	371	H-1→L 91%	0,3865
4	4,0638	305	H-2→L 3%	0,4161

Table 30: results for **ND-1** in DMSO with ωB97XD/6-311+G(2d,p), ΔE = 0,2147

Exited state	E_{ecc} (eV)	λ_{max} calc. (nm)	Transition	f
1	2,1827	568	H→L 94%	1,2736
2	3,4213	362	H-1→L 85%	0,4283
3	4,1160	298	H→L 71%	0,4342

Table 31: results for **ND-1** in DMSO with LC-ωPBE /6-311+G(2d,p), ΔE = 0,3242

Exited state	E_{ecc} (eV)	λ_{max} calc. (nm)	Transition	f
1	2,2001	564	H→L 91%	1,3291
2	3,6798	337	H-1→L 72%	0,6069
3	4,5264	274	H-2→L 22%	0,0392

Table 32: results for **X** in DMSO with B3LYP/6-311+G(2d,p)

Exited state	E_{ecc} (eV)	λ_{max} calc. (nm)	Transition	f
1	1,6198	765	H→L 99%	0,6761
2	2,7953	444	H-1→L 96%	0,8360
3	3,1710	391	H→L+1 78%	0,4842
4	3,3447	371	H-2→L 77%	0,0369
5	3,6647	338	H-4→L 32%	0,0112

Chapter V

Bibliography

(1) Beck, A.; Goetsch, L.; Dumontet, C.; Corvaïa, N. *Nat. Rev. Drug Discov.* **2017**, *16* (5), 315–337.

(2) Mckertish, C. M.; Kayser, V. *Biomedicines* **2021**, *9* (8).

(3) Fatima, S. W.; Khare, S. K. *J. Control. Release* **2022**, *341*, 555–565.

(4) ten Cate, B.; Bremer, E.; de Bruyn, M.; Bijma, T.; Samplonius, D.; Schwemmlein, M.; Huls, G.; Fey, G.; Helfrich, W. *Leukemia* **2009**, *23* (8), 1389–1397.

(5) Zaro, J. L. Mylotarg: Revisiting Its Clinical Potential Post-Withdrawal BT - Antibody-Drug Conjugates: The 21st Century Magic Bullets for Cancer; Wang, J., Shen, W.-C., Zaro, J. L., Eds.; Springer International Publishing: Cham, 2015; pp 179–190.

(6) Elgundi, Z.; Reslan, M.; Cruz, E.; Sifniotis, V.; Kayser, V. *Adv. Drug Deliv. Rev.* **2017**, *122*, 2–19.

(7) Sullivan, R.; Paré, G. C.; Frederiksen, L. J.; Semenza, G. L.; Graham, C. H. *Mol. Cancer Ther.* **2008**, *7* (7), 1961–1973.

(8) Nejadmoghaddam, M.-R.; Minai-Tehrani, A.; Ghahremanzadeh, R.; Mahmoudi, M.; Dinarvand, R.; Zarnani, A.-H. *Avicenna J. Med. Biotechnol.* **2019**, *11* (1), 3–23.

(9) Buecheler, J. W.; Winzer, M.; Weber, C.; Gieseler, H. *J. Pharm. Sci.* **2020**, *109* (1), 161–168.

(10) Leeson, P. D.; Springthorpe, B. *Nat. Rev. Drug Discov.* **2007**, *6* (11), 881–890.

(11) Lyon, R. P.; Bovee, T. D.; Doronina, S. O.; Burke, P. J.; Hunter, J. H.; Neff-Laford, H. D.; Jonas, M.; Anderson, M. E.; Setter, J. R.; Senter, P. D. *Nat. Biotechnol.* **2015**, *33* (7), 733–735.

(12) Burton, J. K.; Bottino, D.; Secomb, T. W. *AAPS J.* **2020**, *22* (1), 1–13.

(13) Bargh, J. D.; Isidro-Llobet, A.; Parker, J. S.; Spring, D. R. *Chem. Soc. Rev.* **2019**, *48* (16), 4361–4374.

(14) Anami, Y.; Yamazaki, C. M.; Xiong, W.; Gui, X.; Zhang, N.; An, Z.; Tsuchikama, K. *Nat. Commun.* **2018**, *9* (1), 2512.

(15) Bargh, J. D.; Walsh, S. J.; Isidro-Llobet, A.; Omarjee, S.; Carroll, J. S.; Spring,

D. R. *Chem. Sci.* **2020**, *11* (9), 2375–2380.

(16) Kolodych, S.; Michel, C.; Delacroix, S.; Koniev, O.; Ehkirch, A.; Eberova, J.; Cianférani, S.; Renoux, B.; Krezel, W.; Poinot, P.; Muller, C. D.; Papot, S.; Wagner, A. *Eur. J. Med. Chem.* **2017**, *142*, 376–382.

(17) Burke, P. J.; Hamilton, J. Z.; Jeffrey, S. C.; Hunter, J. H.; Doronina, S. O.; Okeley, N. M.; Miyamoto, J. B.; Anderson, M. E.; Stone, I. J.; Ulrich, M. L.; Simmons, J. K.; McKinney, E. E.; Senter, P. D.; Lyon, R. P. *Mol. Cancer Ther.* **2017**, *16* (1), 116–123.

(18) Lyon, R. P.; Bovee, T. D.; Doronina, S. O.; Burke, P. J.; Hunter, J. H.; Neff-Laford, H. D.; Jonas, M.; Anderson, M. E.; Setter, J. R.; Senter, P. D. *Nat. Biotechnol.* **2015**, *33* (7), 733–735.

(19) Hamann, P. R.; Hinman, L. M.; Hollander, I.; Beyer, C. F.; Lindh, D.; Holcomb, R.; Hallett, W.; Tsou, H. R.; Upeslacis, J.; Shochat, D.; Mountain, A.; Flowers, D. A.; Bernstein, I. *Bioconjug. Chem.* **2002**, *13* (1), 47–58.

(20) EMA. *CHMP Assess. Rep.* **2018**, *44* (February), 1–138.

(21) Raabe, M.; Heck, A. J.; Führer, S.; Schauenburg, D.; Pieszka, M.; Wang, T.; Zegota, M. M.; Nuhn, L.; Ng, D. Y. W.; Kuan, S. L.; Weil, T. *Macromol. Biosci.* **2021**, *n/a* (n/a), 2100299.

(22) Lehne, G. *Curr. Drug Targets* **2000**, *1*, 85–99.

(23) Shefet-Carasso, L.; Benhar, I. *Drug Resist. Updat.* **2015**, *18*, 36–46.

(24) Nasiri, H.; Valedkarimi, Z.; Aghebati-Maleki, L.; Majidi, J. *J. Cell. Physiol.* **2018**, *233* (9), 6441–6457.

(25) Wu, H.; Levalley, P. J.; Luo, T.; Kloxin, A. M.; Kiick, K. L. *Bioconjug. Chem.* **2018**, *29* (11), 3595–3605.

(26) Bessire, A. J.; Ballard, T. E.; Charati, M.; Cohen, J.; Green, M.; Lam, M. H.; Loganzo, F.; Nolting, B.; Pierce, B.; Puthenveetil, S.; Roberts, L.; Schildknegt, K.; Subramanyam, C. *Bioconjug. Chem.* **2016**, *27* (7), 1645–1654.

(27) Doronina, S. O.; Mendelsohn, B. A.; Bovee, T. D.; Cerveny, C. G.; Alley, S. C.; Meyer, D. L.; Oflazoglu, E.; Toki, B. E.; Sanderson, R. J.; Zabinski, R. F.; Wahl, A. F.; Senter, P. D. *Bioconjug. Chem.* **2006**, *17* (1), 114–124.

(28) Cianferotti, C.; Faltoni, V.; Cini, E.; Ermini, E.; Migliorini, F.; Petricci, E.; Taddei, M.; Salvini, L.; Battistuzzi, G.; Milazzo, F. M.; Anastasi, A. M.; Chiapparino, C.; De Santis, R.; Giannini, G. *Chem. Commun.* **2021**, *57* (7), 867–870.

(29) Alouane, A.; Labruère, R.; Le Saux, T.; Schmidt, F.; Jullien, L. *Angew.*

Chemie **2015**, *127* (26), 7600–7619.

(30) Schuster, H. J.; Krewer, B.; von Hof, J. M.; Schmuck, K.; Schuberth, I.; Alves, F.; Tietze, L. F. *Org. Biomol. Chem.* **2010**, *8* (8), 1833–1842.

(31) Toki, B. E.; Cerveny, C. G.; Wahl, A. F.; Senter, P. D. *J. Org. Chem.* **2002**, *67* (6), 1866–1872.

(32) Saari, W. S.; Schwering, J. E.; Lyle, P. A.; Smith, S. J.; Engelhardt, E. L. *J. Med. Chem.* **1990**, *33* (1), 97–101.

(33) Leu, Y.-L.; Chen, C.-S.; Wu, Y.-J.; Chern, J.-W. *J. Med. Chem.* **2008**, *51* (6), 1740–1746.

(34) Kratz, F.; Müller, I. A.; Ryppa, C.; Warnecke, A. *ChemMedChem* **2008**, *3* (1), 20–53.

(35) Alaoui, A. El; Saha, N.; Schmidt, F.; Monneret, C.; Florent, J.-C. *Bioorg. Med. Chem.* **2006**, *14* (14), 5012–5019.

(36) Ajaj, K.; Graeser, R.; Fichtner, I.; Kratz, F. *Cancer Chemother. Pharmacol.* **2009**, *64*, 413–418.

(37) Abu Ajaj, K.; Kratz, F. *Bioorg. Med. Chem. Lett.* **2009**, *19* (3), 995–1000.

(38) Grinda, M.; Clarhaut, J.; Renoux, B.; Tranoy-Opalinski, I.; Papot, S. *Medchemcomm* **2012**, *3* (1), 68–70.

(39) Yao, H.-P.; Zhao, H.; Hudson, R.; Tong, X.-M.; Wang, M.-H. *Drug Discov. Today* **2021**, *26* (8), 1857–1874.

(40) Shamis, M.; Lode, H. N.; Shabat, D. *J. Am. Chem. Soc.* **2004**, *126* (6), 1726–1731.

(41) Schmidt, F.; Florent, J. C.; Monneret, C.; Straub, R.; Czech, J.; Gerken, M.; Bosslet, K. *Bioorg. Med. Chem. Lett.* **1997**, *7* (8), 1071–1076.

(42) Mauger, A. B.; Burke, P. J.; Somani, H. H.; Friedlos, F.; Knox, R. J. *J. Med. Chem.* **1994**, *37* (21), 3452–3458.

(43) Liu, L.; Xie, F.; Xiao, D.; Xu, X.; Su, Z.; Wang, Y.; Fan, S.; Zhou, X.; Li, S. *Drug Deliv.* **2021**, *28* (1), 2603–2617.

(44) Burke, P. J.; Senter, P. D.; Meyer, D. W.; Miyamoto, J. B.; Anderson, M.; Toki, B. E.; Manikumar, G.; Wani, M. C.; Kroll, D. J.; Jeffrey, S. C. *Bioconjug. Chem.* **2009**, *20* (6), 1242–1250.

(45) Meyer, Y.; Richard, J.-A.; Delest, B.; Noack, P.; Renard, P.-Y.; Romieu, A. *Org. Biomol. Chem.* **2010**, *8* (8), 1777–1780.

(46) Louise-Leriche, L.; Păunescu, E.; Saint-André, G.; Baati, R.; Romieu, A.;

Wagner, A.; Renard, P.-Y. *Chem. – A Eur. J.* **2010**, *16* (11), 3510–3523.

(47) Richard, J.-A.; Jean, L.; Romieu, A.; Massonneau, M.; Noack-Fraissignes, P.; Renard, P.-Y. *Org. Lett.* **2007**, *9* (23), 4853–4855.

(48) Gonzaga, R. V.; do Nascimento, L. A.; Santos, S. S.; Machado Sanches, B. A.; Giarolla, J.; Ferreira, E. I. *J. Pharm. Sci.* **2020**, *109* (11), 3262–3281.

(49) Redy, O.; Shabat, D. *J. Control. Release* **2012**, *164* (3), 276–282.

(50) Shamis, M.; Shabat, D. *Chem. – A Eur. J.* **2007**, *13* (16), 4523–4528.

(51) Weinstain, R.; Segal, E.; Satchi-Fainaro, R.; Shabat, D. *Chem. Commun.* **2010**, *46* (4), 553–555.

(52) Alouane, A.; Labruère, R.; Le Saux, T.; Aujard, I.; Dubruille, S.; Schmidt, F.; Jullien, L. *Chem. – A Eur. J.* **2013**, *19* (35), 11717–11724.

(53) Weinert, E. E.; Dondi, R.; Colloredo-Melz, S.; Frankenfield, K. N.; Mitchell, C. H.; Freccero, M.; Rokita, S. E. *J. Am. Chem. Soc.* **2006**, *128* (36), 11940–11947.

(54) Richard, J.-A.; Meyer, Y.; Jolivel, V.; Massonneau, M.; Dumeunier, R.; Vaudry, D.; Vaudry, H.; Renard, P.-Y.; Romieu, A. *Bioconjug. Chem.* **2008**, *19* (8), 1707–1718.

(55) Schmid, K. M.; Phillips, S. T. *J. Phys. Org. Chem.* **2013**, *26* (7), 608–610.

(56) Jin, C.; Wen, S.; Zhang, Q.; Zhu, Q.; Yu, J.; Lu, W. *ACS Med. Chem. Lett.* **2017**, *8* (7), 762–765.

(57) Chen, E. K. Y.; McBride, R. A.; Gillies, E. R. *Macromolecules* **2012**, *45* (18), 7364–7374.

(58) Thomas, M.; Clarhaut, J.; Strale, P.-O.; Tranoy-Opalinski, I.; Roche, J.; Papot, S. *ChemMedChem* **2011**, *6* (6), 1006–1010.

(59) Grinda, M.; Clarhaut, J.; Tranoy-Opalinski, I.; Renoux, B.; Monvoisin, A.; Cronier, L.; Papot, S. *ChemMedChem* **2011**, *6* (12), 2137–2141.

(60) Nicolaou, K. C.; Rigol, S. *Angew. Chemie - Int. Ed.* **2019**, *58* (33), 11206–11241.

(61) Cazzamalli, S.; Dal Corso, A.; Widmayer, F.; Neri, D. *J. Am. Chem. Soc.* **2018**, *140* (5), 1617–1621.

(62) Lehar, S. M.; Pillow, T.; Xu, M.; Staben, L.; Kajihara, K. K.; Vandlen, R.; DePalatis, L.; Raab, H.; Hazenbos, W. L.; Hiroshi Morisaki, J.; Kim, J.; Park, S.; Darwish, M.; Lee, B.-C.; Hernandez, H.; Loyet, K. M.; Lupardus, P.; Fong, R.; Yan, D.; Chalouni, C.; Luis, E.; Khalfin, Y.; Plise, E.; Cheong, J.; Lyssikatos, J. P.; Strandh, M.; Koefoed, K.; Andersen, P. S.; Flygare, J. A.;

Wah Tan, M.; Brown, E. J.; Mariathasan, S. *Nature* **2015**, *527* (7578), 323–328.

(63) Dubowchik, G. M.; Firestone, R. A.; Padilla, L.; Willner, D.; Hofstead, S. J.; Mosure, K.; Knipe, J. O.; Lasch, S. J.; Trail, P. A. *Bioconjug. Chem.* **2002**, *13* (4), 855–869.

(64) Tiberghien, A. C.; Levy, J.-N.; Masterson, L. A.; Patel, N. V; Adams, L. R.; Corbett, S.; Williams, D. G.; Hartley, J. A.; Howard, P. W. *ACS Med. Chem. Lett.* **2016**, *7* (11), 983–987.

(65) Warnecke, A.; Kratz, F. *J. Org. Chem.* **2008**, *73* (4), 1546–1552.

(66) Sykes, B. M.; Hay, M. P.; Bohinc-Herceg, D.; Helsby, N. A.; O'Connor, C. J.; Denny, W. A. *J. Chem. Soc. Perkin Trans. 1* **2000**, No. 10, 1601–1608.

(67) P. Hay, M.; M. Sykes, B.; A. Denny, W.; J. O'Connor, C. *J. Chem. Soc. Perkin Trans. 1* **1999**, No. 19, 2759–2770.

(68) Amitay, Y.; Shmeeda, H.; Patil, Y.; Gorin, J.; Tzemach, D.; Mak, L.; Ohana, P.; Gabizon, A. *Pharm. Res.* **2016**, *33* (3), 686–700.

(69) Staben, L. R.; Koenig, S. G.; Lehar, S. M.; Vandlen, R.; Zhang, D.; Chuh, J.; Yu, S. F.; Ng, C.; Guo, J.; Liu, Y.; Fourie-O'Donohue, A.; Go, M.; Linghu, X.; Segraves, N. L.; Wang, T.; Chen, J.; Wei, B.; Phillips, G. D. L.; Xu, K.; Kozak, K. R.; Mariathasan, S.; Flygare, J. A.; Pillow, T. H. *Nat. Chem.* **2016**, *8* (12), 1112–1119.

(70) Xu, Y.; Chen, J.; Li, Y.; Peng, S.; Gu, X.; Sun, M.; Gao, K.; Fang, J. *Org. Biomol. Chem.* **2015**, *13* (9), 2634–2639.

(71) Park, S.; Kim, S. Y.; Cho, J.; Jung, D.; Seo, D.; Lee, J.; Lee, S.; Yun, S.; Lee, H.; Park, O.; Seo, B.; Kim, S.; Seol, M.; Woo, S. H.; Park, T. K. *Bioconjug. Chem.* **2019**, *30* (7), 1969–1978.

(72) Pei, Z.; Chen, C.; Chen, J.; Cruz-Chuh, J. Dela; Delarosa, R.; Deng, Y.; Fourie-O'Donohue, A.; Figueroa, I.; Guo, J.; Jin, W.; Khojasteh, S. C.; Kozak, K. R.; Latifi, B.; Lee, J.; Li, G.; Lin, E.; Liu, L.; Lu, J.; Martin, S.; Ng, C.; Nguyen, T.; Ohri, R.; Lewis Phillips, G.; Pillow, T. H.; Rowntree, R. K.; Stagg, N. J.; Stokoe, D.; Ulufatu, S.; Verma, V. A.; Wai, J.; Wang, J.; Xu, K.; Xu, Z.; Yao, H.; Yu, S. F.; Zhang, D.; Dragovich, P. S. *Mol. Pharm.* **2018**, *15* (9), 3979–3996.

(73) Pillow, T. H.; Schutten, M.; Yu, S.-F.; Ohri, R.; Sadowsky, J.; Poon, K. A.; Solis, W.; Zhong, F.; Del Rosario, G.; Go, M. A. T.; Lau, J.; Yee, S.; He, J.; Liu, L.; Ng, C.; Xu, K.; Leipold, D. D.; Kamath, A. V; Zhang, D.; Masterson, L.; Gregson, S. J.; Howard, P. W.; Fang, F.; Chen, J.; Gunzner-Toste, J.; Kozak, K. K.; Spencer, S.; Polakis, P.; Polson, A. G.; Flygare, J. A.; Junutula, J. R. *Mol. Cancer Ther.* **2017**, *16* (5), 871 LP – 878.

(74) Vlahov, I. R.; Qi, L.; Santhapuram, H. K. R.; Felten, A.; Parham, G. L.; Zou, N.; Wang, K.; You, F.; Vaughn, J. F.; Hahn, S. J.; Klein, H. F.; Kleindl, P. J.; Reddy, J.; Reno, D.; Nicoson, J.; Leamon, C. P. *Bioorg. Med. Chem. Lett.* **2020**, *30* (7), 126987.

(75) Shan, D.; Nicolaou, M. G.; Borchardt, R. T.; Wang, B. *J. Pharm. Sci.* **1997**, *86* (7), 765–767.

(76) Sykes, B. M.; Atwell, G. J.; Hogg, A.; Wilson, W. R.; O'Connor, C. J.; Denny, W. A. *J. Med. Chem.* **1999**, *42* (3), 346–355.

(77) Azoulay, M.; Tuffin, G.; Sallem, W.; Florent, J.-C. *Bioorg. Med. Chem. Lett.* **2006**, *16* (12), 3147–3149.

(78) Rossin, R.; van Duijnhoven, S. M. J.; ten Hoeve, W.; Janssen, H. M.; Kleijn, L. H. J.; Hoeben, F. J. M.; Versteegen, R. M.; Robillard, M. S. *Bioconjug. Chem.* **2016**, *27* (7), 1697–1706.

(79) Davies, S.; Oliveira, B. L.; Bernardes, G. J. L. *Org. Biomol. Chem.* **2019**, *17* (23), 5725–5730.

(80) Riber, C. F.; Smith, A. A. A.; Zelikin, A. N. *Adv. Healthc. Mater.* **2015**, *4* (12), 1887–1890.

(81) Jensen, E.; Bundgaard, H. *Int. J. Pharm.* **1991**, *71* (1), 117–125.

(82) Bundgaard , H. *Design of Prodrugs*; Elsevier: Amsterdam; New York; Oxford, 1985.

(83) Maag, H. Prodrugs of Carboxylic Acids. In *Prodrugs. Biotechnology: Pharmaceutical Aspects*; Springer US, 2007.

(84) Salam, R.; Chowdhury, S. M.; Marshall, S. R.; Gneid, H.; Busschaert, N. *Chem. Commun.* **2021**, *57* (97), 13122–13125.

(85) Nielsen, N. M.; Bundgaard, H. *Int. J. Pharm.* **1987**, *39* (1), 75–85.

(86) Hovgaard, L.; Brøndsted, H.; Buur, A.; Bundgaard, H. *Pharm. Res.* **1995**, *12* (3), 387–392.

(87) Wang, R. E.; Liu, T.; Wang, Y.; Cao, Y.; Du, J.; Luo, X.; Deshmukh, V.; Kim, C. H.; Lawson, B. R.; Tremblay, M. S.; Young, T. S.; Kazane, S. A.; Wang, F.; Schultz, P. G. *J. Am. Chem. Soc.* **2015**, *137* (9), 3229–3232.

(88) Wang, M.; Yan, J.; Li, C.; Wang, X.; Xiong, J.; Pan, D.; Wang, L.; Xu, Y.; Li, X.; Yang, M. *Eur. Polym. J.* **2020**, *123* (November 2019), 109462.

(89) Lee, M. H.; Sharma, A.; Chang, M. J.; Lee, J.; Son, S.; Sessler, J. L.; Kang, C.; Kim, J. S. *Chem. Soc. Rev.* **2018**, *47* (1), 28–52.

(90) Maiti, S.; Park, N.; Han, J. H.; Jeon, H. M.; Lee, J. H.; Bhuniya, S.; Kang, C.;

Kim, J. S. *J. Am. Chem. Soc.* **2013**, *135* (11), 4567–4572.

(91) Bej, R.; Ghosh, S. *Bioconjug. Chem.* **2019**, *30* (1), 101–110.

(92) Wang, Z.; Ling, L.; Xia, Q.; Li, X. *J. Drug Deliv. Sci. Technol.* **2019**, *53* (July), 101168.

(93) Santos, C. R.; Capela, R.; Pereira, C. S. G. P.; Valente, E.; Gouveia, L.; Pannecouque, C.; De Clercq, E.; Moreira, R.; Gomes, P. *Eur. J. Med. Chem.* **2009**, *44* (6), 2339–2346.

(94) Alouane, A.; Labruère, R.; Le Saux, T.; Schmidt, F.; Jullien, L. *Angew. Chemie Int. Ed.* **2015**, *54* (26), 7492–7509.

(95) Nuñez, S. A.; Yeung, K.; Fox, N. S.; Phillips, S. T. *J. Org. Chem.* **2011**, *76* (24), 10099–10113.

(96) Szalai, M. L.; Kevwitch, R. M.; McGrath, D. V. *J. Am. Chem. Soc.* **2003**, *125* (51), 15688–15689.

(97) Amir, R. J.; Pessah, N.; Shamis, M.; Shabat, D. *Angew. Chemie Int. Ed.* **2003**, *42* (37), 4494–4499.

(98) de Groot, F. M. H.; Albrecht, C.; Koekkoek, R.; Beusker, P. H.; Scheeren, H. W. *Angew. Chemie Int. Ed.* **2003**, *42* (37), 4490–4494.

(99) Erez, R.; Segal, E.; Miller, K.; Satchi-Fainaro, R.; Shabat, D. *Bioorg. Med. Chem.* **2009**, *17* (13), 4327–4335.

(100) Zang, C.; Wang, H.; Li, T.; Zhang, Y.; Li, J.; Shang, M.; Du, J.; Xi, Z.; Zhou, C. *Chem. Sci.* **2019**, *10* (39), 8973–8980.

(101) Park, S.; Kim, S. Y.; Cho, J.; Jung, D.; Seo, D.; Lee, J.; Lee, S.; Yun, S.; Lee, H.; Park, O.; Seo, B.; Woo, S. H.; Park, T. K. *Bioconjug. Chem.* **2019**, *30* (7), 1957–1968.

(102) Luo, X.; Pailla, S. K.; Gao, F.; Zheng, X.; Wang, R. *Tetrahedron* **2020**, *76* (9), 130926.

(103) Yang, Y.; Zhou, T.; Jin, M.; Zhou, K.; Liu, D.; Li, X.; Huo, F.; Li, W.; Yin, C. *J. Am. Chem. Soc.* **2020**, *142* (3), 1614–1620.

(104) Żądło-Dobrowolska, A.; Szczygieł, M.; Koszelewski, D.; Paprocki, D.; Ostaszewski, R. *Org. Biomol. Chem.* **2016**, *14* (38), 9146–9150.

(105) Šimon, P.; Tichotová, M.; García Gallardo, M.; Procházková, E.; Baszczyňski, O. *Chem. – A Eur. J.* **2021**, *27* (50), 12763–12775.

(106) Thioester, E.; In, C.; Prodrug, M.; For, D.; Antihypertensive, C. **2015**, *4* (1), 740–767.

(107) Frost, L.; Suryadevara, P.; Cannell, S. J.; Groundwater, P. W.; Hambleton, P. A.; Anderson, R. J. *Eur. J. Med. Chem.* **2016**, *109*, 206–215.

(108) Husser, C.; Pähler, A.; Seymour, M.; Kuhlmann, O.; Schadt, S.; Zell, M. *J. Pharm. Biomed. Anal.* **2018**, *152*, 143–154.

(109) Morrison, R. A.; Kripalani, K. J.; Marino, A. M.; Dean, A. V.; Migdalof, B. H.; Weinstein, S. H.; Jain, N. B.; Bathala, M. S.; Singhvi, S. M. *Biopharm. Drug Dispos.* **1997**, *18* (1), 25–39.

(110) Crinelli, R.; Zara, C.; Smietana, M.; Retini, M.; Magnani, M.; Fraternale, A. *Nutrients* **2019**, *11* (6).

(111) Fernández, M.; Shamsabadi, A.; Chudasama, V. *Chem. Commun.* **2020**, *56* (7), 1125–1128.

(112) Thomson, P.; Naylor, M. A.; Stratford, M. R. L.; Lewis, G.; Hill, S.; Patel, K. B.; Wardman, P.; Davis, P. D. *Bioorganic Med. Chem. Lett.* **2007**, *17* (15), 4320–4322.

(113) Van Der Vlies, A. J.; Hasegawa, U.; Hubbell, J. A. *Mol. Pharm.* **2012**, *9* (10), 2812–2818.

(114) Bakthavatsalam, S.; Sleeper, M. L.; Dharani, A.; George, D. J.; Zhang, T.; Franz, K. J. *Angew. Chemie Int. Ed.* **2018**, *57* (39), 12780–12784.

(115) Bakthavatsalam, S.; Wiangnak, P.; George, D. J.; Zhang, T.; Franz, K. J. *Bioorganic & Med. Chem. Lett.* **2020**, *30* (11), 127148.

(116) Rohde, M.; MØrk, N.; Håkansson, A. E.; Jensen, K. G.; Pedersen, H.; Dige, T.; JØrgensen, E. B.; Holm, R. *Results Pharma Sci.* **2014**, *4* (1), 19–25.

(117) Kahns, A. H.; Bundgaard, H. *Int. J. Pharm.* **1991**, *71* (1–2), 31–43.

(118) Bundgaard, H.; Buur, A.; Hansen, K. T.; Larsen, J. D.; Møss, J.; Olsen, L. *Int. J. Pharm.* **1988**, *45* (1–2), 47–57.

(119) Tenn, W. J.; French, N. L.; Nagorski, R. W. *Org. Lett.* **2001**, *3* (1), 75–77.

(120) Larsen, S. W.; Sidenius, M.; Ankersen, M.; Larsen, C. *Eur. J. Pharm. Sci.* **2003**, *20* (2), 233–240.

(121) Hamada, Y.; Ohtake, J.; Sohma, Y.; Kimura, T.; Hayashi, Y.; Kiso, Y. *Bioorganic Med. Chem.* **2002**, *10* (12), 4155–4167.

(122) Hamada, Y.; Matsumoto, H.; Yamaguchi, S.; Kimura, T.; Hayashi, Y.; Kiso, Y. *Bioorganic Med. Chem.* **2004**, *12* (1), 159–170.

(123) Wang, H.; Sobral, M. C.; Snyder, T.; Brudno, Y.; Gorantla, V. S.; Mooney, D. J. *Biomater. Sci.* **2020**, *8* (1), 266–277.

(124) Pavličková, V.; Jurášek, M.; Rimpelová, S.; Záruba, K.; Sedlák, D.; Šimková, M.; Kodr, D.; Staňková, E.; Fähnrich, J.; Rottnerová, Z.; Bartůněk, P.; Lapčík, O.; Drašar, P.; Ruml, T. *J. Mater. Chem. B* **2019**, *7* (36), 5465–5477.

(125) Zhang, H.; Liu, P. *Langmuir* **2019**, *35* (24), 8007–8014.

(126) Vergote, I.; Leamon, C. P. *Ther. Adv. Med. Oncol.* **2015**, *7* (4), 206–218.

(127) Fulcher, J. A.; Tamshen, K.; Wollenberg, A. L.; Kickhoefer, V. A.; Mrazek, J.; Elliott, J.; Ibarrondo, F. J.; Anton, P. A.; Rome, L. H.; Maynard, H. D.; Deming, T.; Yang, O. O. *Bioconjug. Chem.* **2019**, *30* (8), 2216–2227.

(128) Brandish, P. E.; Palmieri, A.; Antonenko, S.; Beaumont, M.; Benso, L.; Cancilla, M.; Cheng, M.; Fayadat-Dilman, L.; Feng, G.; Figueroa, I.; Firdos, J.; Garbaccio, R.; Garvin-Queen, L.; Gately, D.; Geda, P.; Haines, C.; Hseih, S.; Hodges, D.; Kern, J.; Knudsen, N.; Kwasnjuk, K.; Liang, L.; Ma, H.; Manibusan, A.; Miller, P. L.; Moy, L. Y.; Qu, Y.; Shah, S.; Shin, J. S.; Stivers, P.; Sun, Y.; Tomazela, D.; Woo, H. C.; Zaller, D.; Zhang, S.; Zhang, Y.; Zielstorff, M. *Bioconjug. Chem.* **2018**, *29* (7), 2357–2369.

(129) Lisitskiy, V. A.; Khan, H.; Popova, T. V.; Chubarov, A. S.; Zakharova, O. D.; Akulov, A. E.; Shevelev, O. B.; Zavjalov, E. L.; Koptyug, I. V.; Moshkin, M. P.; Silnikov, V. N.; Ahmad, S.; Godovikova, T. S. *Bioorganic Med. Chem. Lett.* **2017**, *27* (16), 3925–3930.

(130) Jourden, J. L. M.; Daniel, K. B.; Cohen, S. M. *Chem. Commun. (Camb).* **2011**, *47* (28), 7968–7970.

(131) Daniel, K. B.; Sullivan, E. D.; Chen, Y.; Chan, J. C.; Jennings, P. A.; Fierke, C. A.; Cohen, S. M. *J. Med. Chem.* **2015**, *58* (11), 4812–4821.

(132) Parveen, I.; Naughton, D. P.; Whish, W. J. D.; Threadgill, M. D. *Bioorganic Med. Chem. Lett.* **1999**, *9* (14), 2031–2036.

(133) Steiger, A. K.; Pardue, S.; Kevil, C. G.; Pluth, M. D. *J. Am. Chem. Soc.* **2016**, *138* (23), 7256–7259.

(134) Kularatne, S. A.; Wang, K.; Santhapuram, H. K. R.; Low, P. S. *Mol. Pharm.* **2009**, *6* (3), 780–789.

(135) Ferhati, X.; Salas-Cubero, M.; Garrido, P.; García-Sanmartín, J.; Guerreiro, A.; Avenoza, A.; Busto, J. H.; Peregrina, J. M.; Martínez, A.; Jiménez-Moreno, E.; Bernardes, G. J. L.; Corzana, F. *Org. Lett.* **2021**, *23* (21), 8580–8584.

(136) Tercel, M.; Atwell, G. J.; Yang, S.; Stevenson, R. J.; Botting, K. J.; Boyd, M.; Smith, E.; Anderson, R. F.; Denny, W. A.; Wilson, W. R.; Pruijn, F. B. *J. Med. Chem.* **2009**, *52* (22), 7258–7272.

(137) Zhang, X.; Zhao, Q.; Li, Y.; Duan, X.; Tang, Y. *Anal. Chem.* **2017**, *89* (10),

5503–5510.

(138) Race, P. R.; Lovering, A. L.; Green, R. M.; Ossor, A.; White, S. A.; Searle, P. F.; Wrighton, C. J.; Hyde, E. I. *J. Biol. Chem.* **2005**, *280* (14), 13256–13264.

(139) Peterson, F. J.; Mason, R. P.; Hovsepian, J.; Holtzman, J. L. *J. Biol. Chem.* **1979**, *254* (10), 4009–4014.

(140) Bryant, D. W.; McCalla, D. R.; Leeksma, M.; Laneuville, P. *Can. J. Microbiol.* **1981**, *27* (1), 81–86.

(141) Chevalier, A.; Zhang, Y.; Khdour, O. M.; Kaye, J. B.; Hecht, S. M. *J. Am. Chem. Soc.* **2016**, *138* (37), 12009–12012.

(142) GRAY, L. H.; CONGER, A. D.; EBERT, M.; HORNSEY, S.; SCOTT, O. C. *Br. J. Radiol.* **1953**, *26* (312), 638–648.

(143) Nielsen, O. S.; Horsman, M.; Overgaard, J. *Eur. J. Cancer* **2001**, *37* (13), 1587–1589.

(144) Nepali, K.; Lee, H. Y.; Liou, J. P. *J. Med. Chem.* **2019**, *62* (6), 2851–2893.

(145) Wardman, P. *Curr. Med. Chem.* **2012**, *8* (7), 739–761.

(146) Rami M Dubois L, P. N. K. A. V. van K. S. J. M. S. M. L. P. D. S. G. S. C. T. W. J. Y. *J Med Chem (ISSN 0022-2623, 1520-4804, 0022-2623print)* **2013**, *502*, 8512–8520.

(147) Hibbard, H. A. J.; Reynolds, M. M. *Bioorg. Chem.* **2019**, *93*, 103318.

(148) Sharma, K.; Sengupta, K.; Chakrapani, H. *Bioorg. Med. Chem. Lett.* **2013**, *23* (21), 5964–5967.

(149) Mahato, R.; Tai, W.; Cheng, K. *Adv. Drug Deliv. Rev.* **2011**, *63* (8), 659–670.

(150) Meng, Z.; Lv, Q.; Lu, J.; Yao, H.; Lv, X.; Jiang, F.; Lu, A.; Zhang, G. Prodrug Strategies for Paclitaxel. *International Journal of Molecular Sciences* . 2016.

(151) Ikeda, Y.; Hisano, H.; Nishikawa, Y.; Nagasaki, Y. *Mol. Pharm.* **2016**, *13* (7), 2283–2289.

(152) Karnthaler-Benbakka, C.; Groza, D.; Koblmüller, B.; Terenzi, A.; Holste, K.; Haider, M.; Baier, D.; Berger, W.; Heffeter, P.; Kowol, C. R.; Keppler, B. K. *ChemMedChem* **2016**, *11* (21), 2410–2421.

(153) Luger, K.; Mäder, A. W.; Richmond, R. K.; Sargent, D. F.; Richmond, T. J. *Nature* **1997**, *389* (6648), 251–260.

(154) RUIJTER, A. J. M. de; GENNIP, A. H. van; CARON, H. N.; KEMP, S.; KUILENBURG, A. B. P. van. *Biochem. J.* **2003**, *370* (3), 737–749.

(155) Naldi, M. Caratterizzazione Mediante HPLC-MS Di Modifiche Post-Trasduzionali Di Proteine Istoniche, alma, 2008.

(156) Haberland, M.; Montgomery, R. L.; Olson, E. N. *Nat. Rev. Genet.* **2009**, *10* (1), 32–42.

(157) Finnin, M. S.; Donigian, J. R.; Cohen, A.; Richon, V. M.; Rifkind, R. A.; Marks, P. A.; Breslow, R.; Pavletich, N. P. *Nature* **1999**, *401* (6749), 188–193.

(158) Lombardi, P. M.; Cole, K. E.; Dowling, D. P.; Christianson, D. W. *Curr. Opin. Struct. Biol.* **2011**, *21* (6), 735–743.

(159) Rajak, H.; Kumar, P.; Parmar, P.; Thakur, B. S.; Veerasamy, R.; Sharma, P. C.; Sharma, A. K.; Gupta, A. K.; Dangi, J. S. *Eur. J. Med. Chem.* **2012**, *53*, 390–397.

(160) McClure, J. J.; Li, X.; Chou, C. J. Chapter Six - Advances and Challenges of HDAC Inhibitors in Cancer Therapeutics. In *Advances in Cancer Research*; Tew, K. D., Fisher, P. B. B. T.-A. in C. R., Eds.; Academic Press, 2018; Vol. 138, pp 183–211.

(161) Khan, O.; La Thangue, N. B. *Immunol. Cell Biol.* **2012**, *90* (1), 85–94.

(162) Woster, P. M. *Methods Mol. Biol.* **2011**, *720*, 475–491.

(163) Giannini, G.; Vesci, L.; Battistuzzi, G.; Vignola, D.; Milazzo, F. M.; Guglielmi, M. B.; Barbarino, M.; Santaniello, M.; Fantò, N.; Mor, M.; Rivara, S.; Pala, D.; Taddei, M.; Pisano, C.; Cabri, W. *J. Med. Chem.* **2014**, *57* (20), 8358–8377.

(164) Cini, E.; Faltoni, V.; Petricci, E.; Taddei, M.; Salvini, L.; Giannini, G.; Vesci, L.; Milazzo, F. M.; Anastasi, A. M.; Battistuzzi, G.; De Santis, R. *Chem. Sci.* **2018**, *9* (31), 6490–6496.

(165) Skarbek, C.; Serra, S.; Maslah, H.; Rascol, E.; Labruère, R. *Bioorg. Chem.* **2019**, *91*, 103158.

(166) Berry, J. M.; Watson, C. Y.; Whish, W. J. D.; Threadgill, M. D. *J. Chem. Soc. - Perkin Trans. 1* **1997**, No. 8, 1147–1156.

(167) Tercel, M.; Lee, A. E.; Hogg, A.; Anderson, R. F.; Lee, H. H.; Siim, B. G.; Denny, W. A.; Wilson, W. R. *J. Med. Chem.* **2001**, *44* (21), 3511–3522.

(168) Hay, M. P.; Anderson, R. F.; Ferry, D. M.; Wilson, W. R.; Denny, W. A. *J. Med. Chem.* **2003**, *46* (25), 5533–5545.

(169) Ferrer, S.; Naughton, D. P.; Threadgill, M. D. *Tetrahedron* **2003**, *59* (19), 3437–3444.

(170) Winn, B. A.; Shi, Z.; Carlson, G. J.; Wang, Y.; Nguyen, B. L.; Kelly, E. M.; Ross 4th, R. D.; Hamel, E.; Chaplin, D. J.; Trawick, M. L.; Pinney, K. G. *Bioorg. Med. Chem. Lett.* **2017**, *27* (3), 636–641.

(171) O'Connor, L. J.; Cazares-Körner, C.; Saha, J.; Evans, C. N. G.; Stratford, M. R. L.; Hammond, E. M.; Conway, S. J. *Nat. Protoc.* **2016**, *11* (4), 781–794.

(172) Schmid, K. M.; Phillips, S. T. *J. Phys. Org. Chem.* **2013**, *26* (7), 608–610.

(173) Robbins, J. S.; Schmid, K. M.; Phillips, S. T. *J. Org. Chem.* **2013**, *78* (7), 3159–3169.

(174) Balaban, A. T.; Oniciu, D. C.; Katritzky, A. R. *Chem. Rev.* **2004**, *104* (5), 2777–2812.

(175) Klingler, F.-M.; Wichelhaus, T. A.; Frank, D.; Cuesta-Bernal, J.; El-Delik, J.; Müller, H. F.; Sjuts, H.; Göttig, S.; Koenigs, A.; Pos, K. M.; Pogoryelov, D.; Proschak, E. *J. Med. Chem.* **2015**, *58* (8), 3626–3630.

(176) Sun, S.; Oliveira, B. L.; Jiménez-Osés, G.; Bernardes, G. J. L. *Angew. Chem. Int. Ed. Engl.* **2018**, *57* (48), 15832–15835.

(177) Saito, G.; Swanson, J. A.; Lee, K.-D. *Adv. Drug Deliv. Rev.* **2003**, *55* (2), 199–215.

(178) Vesci, L.; Bernasconi, E.; Milazzo, F. M.; De Santis, R.; Gaudio, E.; Kwee, I.; Rinaldi, A.; Pace, S.; Carollo, V.; Giannini, G.; Bertoni, F. *Oncotarget* **2015**, *6* (8), 5735–5748.

(179) Milazzo, F. M.; Vesci, L.; Anastasi, A. M.; Chiapparino, C.; Rosi, A.; Giannini, G.; Taddei, M.; Cini, E.; Faltoni, V.; Petricci, E.; Battistuzzi, G.; Salvini, L.; Carollo, V.; De Santis, R. *Front. Oncol.* **2020**, *9*.

(180) Valeur, E.; Knerr, L.; Ölwegård-Halvarsson, M.; Lemurell, M. *Drug Discov. Today* **2017**, *22* (6), 841–847.

(181) Feng, J.; Handa, S.; Gallou, F.; Lipshutz, B. H. *Angew. Chemie Int. Ed.* **2016**, *55* (31), 8979–8983.

(182) Morita, K.; Suzuki, Z.; Hirose, H. *Bull. Chem. Soc. Jpn.* **1968**, *41* (1949), 2815.

(183) Basavaiah, D.; Rao, A. J.; Satyanarayana, T. *Chem. Rev.* **2003**, *103* (3), 811–892.

(184) Basavaiah, D.; Dharma Rao, P.; Suguna Hyma, R. *Tetrahedron* **1996**, *52* (24), 8001–8062.

(185) Bhowmik, S.; Batra, S. Applications of Morita-Baylis-Hillman Reaction to the Synthesis of Natural Products and Drug Molecules. *Current Organic*

Chemistry. 2014, pp 3078–3119.

(186) Sekgota, K. C.; Majumder, S.; Isaacs, M.; Mnkandhla, D.; Hoppe, H. C.; Khanye, S. D.; Kriel, F. H.; Coates, J.; Kaye, P. T. *Bioorg. Chem.* **2017**, *75*, 310–316.

(187) Ka, Y. L.; Seung, C. K.; Jae, N. K. *Bull. Korean Chem. Soc.* **2005**, *26* (7), 1109–1111.

(188) Familoni, O. B.; Klaas, P. J.; Lobb, K. A.; Pakade, V. E.; Kaye, P. T. *Org. Biomol. Chem.* **2006**, *4* (21), 3960–3965.

(189) O'Dell, D. K.; Nicholas, K. M. *J. Org. Chem.* **2003**, *68* (16), 6427–6430.

(190) Lee, K. Y.; Kim, T. H.; Kim, J. N. *Bull. Korean Chem. Soc.* **2004**, *25* (12), 1966–1968.

(191) Bakthadoss, M.; Sivakumar, N. *Synlett* **2011**, *2011* (09), 1296–1302.

(192) de Luna Freire, K. R.; Tormena, C. F.; Coelho, F. *Synlett* **2011**, *22* (14), 2059–2063.

(193) Aggarwal, V. K.; Patin, A.; Tisserand, S. *Org. Lett.* **2005**, *7* (13), 2555–2557.

(194) Majhi, T. P.; Neogi, A.; Ghosh, S.; Mukherjee, A. K.; Chattopadhyay, P. *Tetrahedron* **2006**, *62* (51), 12003–12010.

(195) Shang, Y.; Feng, Z.; Yuan, L.; Wang, S. *Tetrahedron* **2008**, *64* (24), 5779–5783.

(196) Mateus, C. R.; Feltrin, M. P.; Costa, A. M.; Coelho, F.; Almeida, W. P. *Tetrahedron* **2001**, *57* (32), 6901–6908.

(197) Mikami, K.; Okubo, Y. *Synlett* **2000**, *2000* (04), 491–492.

(198) Chen, P.-Y.; Chen, H.-M.; Chen, L.-Y.; Tzeng, J.-Y.; Tsai, J.-C.; Chi, P.-C.; Li, S.-R.; Wang, E.-C. *Tetrahedron* **2007**, *63* (13), 2824–2828.

(199) Krishna, P. R.; Reddy, P. S. *J. Comb. Chem.* **2008**, *10* (3), 426–435.

(200) Suarez del Villar, I.; Gradillas, A.; Domínguez, G.; Pérez-Castells, J. *Org. Lett.* **2010**, *12* (10), 2418–2421.

(201) Lee, J.; Singh, D.; Ha, H.-J. *Org. Biomol. Chem.* **2018**, *16* (43), 8048–8055.

(202) Pringle, W.; Sharpless, K. B. *Tetrahedron Lett.* **1999**, *40* (28), 5151–5154.

(203) Liu, Y.; Zheng, H.; Xu, D.; Xu, Z.; Zhang, Y. *Org. Prep. Proced. Int.* **2007**, *39* (2), 190–195.

(204) Darby, W. J.; DeMeio, R. H.; Bernheim, M. L. C.; Bernheim, F. *J. Biol. Chem.* **1945**, *158* (1), 67–69.

(205) Levinn, C. M.; Cerda, M. M.; Pluth, M. D. *Acc. Chem. Res.* **2019**, *52* (9), 2723–2731.

(206) Yang, X.; Ammeter, D.; Idowu, T.; Domalaon, R.; Brizuela, M.; Okunnu, O.; Bi, L.; Guerrero, Y. A.; Zhanel, G. G.; Kumar, A.; Schweizer, F. *Eur. J. Med. Chem.* **2019**, *175*, 187–200.

(207) Cohen, L. A.; Marks, P. A.; Rifkind, R. A.; Amin, S.; Desai, D.; Pittman, B.; Richon, V. M. *Anticancer Res.* **2002**, *22* (3), 1497–1504.

(208) Barltrop, J. A.; Schofield, P. *Tetrahedron Lett.* **1962**, *3* (16), 697–699.

(209) Barton, D. H. R.; Chow, Y. L.; Cox, A.; Kirby, G. W. *Tetrahedron Lett.* **1962**, *3* (23), 1055–1057.

(210) Engels, J.; Schlaeger, E. J. *J. Med. Chem.* **1977**, *20* (7), 907–911.

(211) Kaplan, J. H.; Forbush, B.; Hoffman, J. F. *Biochemistry* **1978**, *17* (10), 1929–1935.

(212) Young, D. D.; Lively, M. O.; Deiters, A. *J. Am. Chem. Soc.* **2010**, *132* (17), 6183–6193.

(213) Kneuttinger, A. C.; Straub, K.; Bittner, P.; Simeth, N. A.; Bruckmann, A.; Busch, F.; Rajendran, C.; Hupfeld, E.; Wysocki, V. H.; Horinek, D.; König, B.; Merkl, R.; Sterner, R. *Cell Chem. Biol.* **2019**, *26* (11), 1501-1514.e9.

(214) Palao, E.; Slanina, T.; Muchová, L.; Šolomek, T.; Vítek, L.; Klán, P. *J. Am. Chem. Soc.* **2016**, *138* (1), 126–133.

(215) Rodgers, Z. L.; Hughes, R. M.; Doherty, L. M.; Shell, J. R.; Molesky, B. P.; Brugh, A. M.; Forbes, M. D. E.; Moran, A. M.; Lawrence, D. S. *J. Am. Chem. Soc.* **2015**, *137* (9), 3372–3378.

(216) Umeda, N.; Takahashi, H.; Kamiya, M.; Ueno, T.; Komatsu, T.; Terai, T.; Hanaoka, K.; Nagano, T.; Urano, Y. *ACS Chem. Biol.* **2014**, *9* (10), 2242–2246.

(217) Klán, P.; Šolomek, T.; Bochet, C. G.; Blanc, A.; Givens, R.; Rubina, M.; Popik, V.; Kostikov, A.; Wirz, J. *Chem. Rev.* **2013**, *113* (1), 119–191.

(218) Hansen, M. J.; Velema, W. A.; Lerch, M. M.; Szymanski, W.; Feringa, B. L. *Chem. Soc. Rev.* **2015**, *44* (11), 3358–3377.

(219) Weinstain, R.; Slanina, T.; Kand, D.; Klán, P. *Chem. Rev.* **2020**, *120* (24), 13135–13272.

(220) Timko, B. P.; Dvir, T.; Kohane, D. S. *Adv. Mater.* **2010**, *22* (44), 4925–4943.

(221) Pan, P.; Svirskis, D.; Rees, S. W. P.; Barker, D.; Waterhouse, G. I. N.; Wu, Z. *J. Control. Release* **2021**, *338* (June), 446–461.

(222) Janssen, Y. M.; Van Houten, B.; Borm, P. J.; Mossman, B. T. *Lab. Invest.* **1993**, *69* (3), 261–274.

(223) Kobayashi, H.; Ogawa, M.; Alford, R.; Choyke, P. L.; Urano, Y. *Chem. Rev.* **2010**, *110* (5), 2620–2640.

(224) Aujard, I.; Benbrahim, C.; Gouget, M.; Ruel, O.; Baudin, J.-B.; Neveu, P.; Jullien, L. *Chem. – A Eur. J.* **2006**, *12* (26), 6865–6879.

(225) Horspool, W.; Lenci, F. *CRC Handbook of: Organic Photochemistry and Photobiology, Second Edition*; 2003.

(226) Kim, A.; Zhou, J.; Samaddar, S.; Song, S. H.; Elzey, B. D.; Thompson, D. H.; Ziaie, B. *Sci. Rep.* **2019**, *9* (1), 1395.

(227) Nazempour, R.; Zhang, Q.; Fu, R.; Sheng, X. Biocompatible and Implantable Optical Fibers and Waveguides for Biomedicine. *Materials* . 2018.

(228) Bisby, R. H.; Mead, C.; Morgan, C. G. *Photochem. Photobiol.* **2000**, *72* (1), 57–61.

(229) Baskaran, R.; Lee, J.; Yang, S.-G. *Biomater. Res.* **2018**, *22*, 25.

(230) Carling, C.-J.; Viger, M. L.; Nguyen Huu, V. A.; Garcia, A. V; Almutairi, A. *Chem. Sci.* **2015**, *6* (1), 335–341.

(231) Chandra, B.; Subramaniam, R.; Mallik, S.; Srivastava, D. K. *Org. Biomol. Chem.* **2006**, *4* (9), 1730–1740.

(232) Eom, T.; Yoo, W.; Kim, S.; Khan, A. *Biomaterials* **2018**, *185*, 333–347.

(233) Chu, Y.; Wu, X.; Wu, Y.; Liu, L.; Chen, Y. *J. Control. Release* **2017**, *259*, e182.

(234) Vickerman, B. M.; Zywot, E. M.; Tarrant, T. K.; Lawrence, D. S. *Nat. Rev. Chem.* **2021**, *5* (11), 816–834.

(235) Fomina, N.; Sankaranarayanan, J.; Almutairi, A. *Adv. Drug Deliv. Rev.* **2012**, *64* (11), 1005–1020.

(236) Wang, P. *Asian J. Org. Chem.* **2013**, *2* (6), 452–464.

(237) Treibs, A.; Kreuzer, F.-H. *Justus Liebigs Ann. Chem.* **1968**, *718* (1), 208–223.

(238) Quan, L.; Liu, S.; Sun, T.; Guan, X.; Lin, W.; Xie, Z.; Huang, Y.; Wang, Y.; Jing, X. *ACS Appl. Mater. Interfaces* **2014**, *6* (18), 16166–16173.

(239) Gao, J.; Chen, X.; Chen, S.; Meng, H.; Wang, Y.; Li, C.; Feng, L. *Anal. Chem.* **2019**, *91* (21), 13675–13680.

(240) Hesari, M.; Swanick, K. N.; Lu, J.-S.; Whyte, R.; Wang, S.; Ding, Z. *J. Am.*

Chem. Soc. **2015**, *137* (35), 11266–11269.

(241) Klfout, H.; Stewart, A.; Elkhalifa, M.; He, H. *ACS Appl. Mater. Interfaces* **2017**, *9* (46), 39873–39889.

(242) Sitkowska, K.; Feringa, B. L.; Szymański, W. *J. Org. Chem.* **2018**, *83* (4), 1819–1827.

(243) Goswami, P. P.; Syed, A.; Beck, C. L.; Albright, T. R.; Mahoney, K. M.; Unash, R.; Smith, E. A.; Winter, A. H. *J. Am. Chem. Soc.* **2015**, *137* (11), 3783–3786.

(244) DeCosta, D. P.; Pincock, J. A. *J. Am. Chem. Soc.* **1989**, *111* (24), 8948–8950.

(245) Alford, R.; Simpson, H. M.; Duberman, J.; Hill, G. C.; Ogawa, M.; Regino, C.; Kobayashi, H.; Choyke, P. L. *Mol. Imaging* **2009**, *8* (6), 7290.2009.00031.

(246) Umezawa, K.; Matsui, A.; Nakamura, Y.; Citterio, D.; Suzuki, K. *Chem. – A Eur. J.* **2009**, *15* (5), 1096–1106.

(247) Menges, N. *Comput. Theor. Chem.* **2015**, *1068*, 117–122.

(248) Pochorovski, I.; Knehans, T.; Nettels, D.; Müller, A. M.; Schweizer, W. B.; Caflisch, A.; Schuler, B.; Diederich, F. *J. Am. Chem. Soc.* **2014**, *136* (6), 2441–2449.

(249) Ponte, F.; Mazzone, G.; Russo, N.; Sicilia, E. *J. Mol. Model.* **2018**, *24* (7), 183.

(250) Lu, H.; Mack, J.; Yang, Y.; Shen, Z. *Chem. Soc. Rev.* **2014**, *43* (13), 4778–4823.

(251) Shah, M.; Thangaraj, K.; Soong, M.-L.; Wolford, L. T.; Boyer, J. H.; Politzer, I. R.; Pavlopoulos, T. G. *Heteroat. Chem.* **1990**, *1* (5), 389–399.

(252) Baruah, M.; Qin, W.; Basarić, N.; De Borggraeve, W. M.; Boens, N. *J. Org. Chem.* **2005**, *70* (10), 4152–4157.

(253) Leen, V.; Yuan, P.; Wang, L.; Boens, N.; Dehaen, W. *Org. Lett.* **2012**, *14* (24), 6150–6153.

(254) Zhao, N.; Xuan, S.; Byrd, B.; Fronczek, F. R.; Smith, K. M.; Vicente, M. G. H. *Org. Biomol. Chem.* **2016**, *14* (26), 6184–6188.

(255) Rohand, T.; Qin, W.; Boens, N.; Dehaen, W. *European J. Org. Chem.* **2006**, No. 20, 4658–4663.

(256) Rohand, T.; Baruah, M.; Qin, W.; Boens, N.; Dehaen, W. *Chem. Commun.* **2006**, No. 3, 266–268.

(257) Yu, C.; Wu, Q.; Wang, J.; Wei, Y.; Hao, E.; Jiao, L. *J. Org. Chem.* **2016**, *81*

(9), 3761–3770.

(258) Wang, J.; Boens, N.; Jiao, L.; Hao, E. *Org. Biomol. Chem.* **2020**, *18* (22), 4135–4156.

(259) Wakamiya, A.; Murakami, T.; Yamaguchi, S. *Chem. Sci.* **2013**, *4* (3), 1002–1007.

(260) Awuah, S. G.; Das, S. K.; D'Souza, F.; You, Y. *Chem. – An Asian J.* **2013**, *8* (12), 3123–3132.

(261) Matulis, V. E.; Ragoyja, E. G.; Ivashkevich, O. A. *Int. J. Quantum Chem.* **2020**, *120* (9), e26159.

(262) Lv, W.; Li, Y.; Li, F.; Lan, X.; Zhang, Y.; Du, L.; Zhao, Q.; Phillips, D. L.; Wang, W. *J. Am. Chem. Soc.* **2019**, *141* (44), 17482–17486.

(263) Rose, A.; Kumar, S. V; Swavey, S.; Erb, J. *Comput. Theor. Chem.* **2017**, *1118*, 107–114.

(264) Chibani, S.; Le Guennic, B.; Charaf-Eddin, A.; Laurent, A. D.; Jacquemin, D. *Chem. Sci.* **2013**, *4* (5), 1950–1963.

(265) Momeni, M. R.; Brown, A. *J. Phys. Chem. A* **2016**, *120* (16), 2550–2560.

(266) Jacquemin, D.; Planchat, A.; Adamo, C.; Mennucci, B. *J. Chem. Theory Comput.* **2012**, *8* (7), 2359–2372.

(267) Chibani, S.; Laurent, A. D.; Le Guennic, B.; Jacquemin, D. *J. Chem. Theory Comput.* **2014**, *10* (10), 4574–4582.

(268) Alberto, M. E.; De Simone, B. C.; Mazzone, G.; Quartarolo, A. D.; Russo, N. *J. Chem. Theory Comput.* **2014**, *10* (9), 4006–4013.

(269) Jacquemin, D.; Duchemin, I.; Blase, X. *J. Chem. Theory Comput.* **2015**, *11* (11), 5340–5359.

(270) Wen, J.; Han, B.; Havlas, Z.; Michl, J. *J. Chem. Theory Comput.* **2018**, *14* (8), 4291–4297.

(271) Turksoy, A.; Yildiz, D.; Akkaya, E. U. *Coord. Chem. Rev.* **2019**, *379*, 47–64.

(272) Feng, Z.; Jiao, L.; Feng, Y.; Yu, C.; Chen, N.; Wei, Y.; Mu, X.; Hao, E. *J. Org. Chem.* **2016**, *81* (15), 6281–6291.

(273) Kubota, Y.; Kimura, K.; Jin, J.; Manseki, K.; Funabiki, K.; Matsui, M. *New J. Chem.* **2019**, *43* (3), 1156–1165.

(274) Loudet, A.; Burgess, K. *Chem. Rev.* **2007**, *107* (11), 4891–4932.

(275) Bessette, A.; Auvray, T.; Désilets, D.; Hanan, G. S. *Dalt. Trans.* **2016**, *45* (18),

7589–7604.

(276) Kirk-Othmer. *Kirk-Othmer Encyclopedia of Chemical Technology*, 4th ed.; Kroschwitz M, J. H.-G., Ed.; 1991; Vol. 1.

(277) Singh, H. B.; Bharati, K. A. *Handbook of Natural Dyes and Pigments*; 2014.

(278) B.J., G. Synthesis and Physico-Chemical Studies of 1, 1'-Substituted Phenyl Cyclohexane, Saurashtra University, 2006.

(279) Rowe, R. C.; Sheskey, P. J.; Quinn, M. E. Coloring Agents. In *Handbook of Pharmaceutical Excipients*; 2009; pp 189–196.

(280) Allam, K. V. I.; Kumar, G. P. *Int. J. Pharm. Pharm. Sci.* **2011**, *3* (SUPPL. 3), 13–21.

(281) O'Banion, C. P.; Lawrence, D. S. *ChemBioChem* **2018**, *19* (12), 1201–1216.

(282) Downham, A.; Collins, P. *Int. J. Food Sci. Technol.* **2000**, *35* (1), 5–22.

(283) Yan, Y.; Chen, J.; Yang, Z.; Zhang, X.; Liu, Z.; Hua, J. *J. Mater. Chem. B* **2018**, *6* (45), 7420–7426.

(284) Yang, L.; Li, X.; Yang, J.; Qu, Y.; Hua, J. *ACS Appl. Mater. Interfaces* **2013**, *5* (4), 1317–1326.

(285) Zhang, X.; Yan, Y.; Hang, Y.; Wang, J.; Hua, J.; Tian, H. *Chem. Commun.* **2017**, *53* (42), 5760–5763.

(286) Qu, Y.; Zhang, X.; Wang, L.; Yang, H.; Yang, L.; Cao, J.; Hua, J. *RSC Adv.* **2019**, *6*, 22389–22394.

(287) Yang, H.; Han, C.; Zhu, X.; Liu, Y.; Zhang, K. Y.; Liu, S.; Zhao, Q.; Li, F.; Huang, W. *Adv. Funct. Mater.* **2016**, *26* (12), 1945–1953.

(288) Kuzmin, A. N.; Baev, A.; Kachynski, A. V.; Fisher, T. S.; Shakouri, A.; Prasad, P. N. *J. Appl. Phys.* **2011**, *110* (3).

(289) Clark, J. L.; Miller, P. F.; Rumbles, G. *J. Phys. Chem. A* **1998**, *102* (24), 4428–4437.

(290) Bloor, D.; Cross, G.; Sharma, P. K.; Elliott, J. A.; Rumbles, G. *J. Chem. Soc. Faraday Trans.* **1993**, *89* (22), 4013–4015.

(291) Bradford, M. M. *Anal. Biochem.* **1976**, *72* (1), 248–254.

(292) Barthel, B. L.; Rudnicki, D. L.; Kirby, T. P.; Colvin, S. M.; Burkhart, D. J.; Koch, T. H. *J. Med. Chem.* **2012**, *55* (14), 6595–6607.

(293) Frisch, M. J.; Trucks, G. W.; Schlegel, H. B.; Scuseria, G. E.; Robb, M. A.; Cheeseman, J. R.; Scalmani, G.; Barone, V.; Petersson, G. A.; Nakatsuji, H.;

Li, X.; Caricato, M.; Marenich, A. V; Bloino, J.; Janesko, B. G.; Gomperts, R.; Mennucci, B.; Hratchian, H. P.; Ortiz, J. V; Izmaylov, A. F.; Sonnenberg, J. L.; Williams-Young, D.; Ding, F.; Lipparini, F.; Egidi, F.; Goings, J.; Peng, B.; Petrone, A.; Henderson, T.; Ranasinghe, D.; Zakrzewski, V. G.; Gao, J.; Rega, N.; Zheng, G.; Liang, W.; Hada, M.; Ehara, M.; Toyota, K.; Fukuda, R.; Hasegawa, J.; Ishida, M.; Nakajima, T.; Honda, Y.; Kitao, O.; Nakai, H.; Vreven, T.; Throssell, K.; Montgomery Jr., J. A.; Peralta, J. E.; Ogliaro, F.; Bearpark, M. J.; Heyd, J. J.; Brothers, E. N.; Kudin, K. N.; Staroverov, V. N.; Keith, T. A.; Kobayashi, R.; Normand, J.; Raghavachari, K.; Rendell, A. P.; Burant, J. C.; Iyengar, S. S.; Tomasi, J.; Cossi, M.; Millam, J. M.; Klene, M.; Adamo, C.; Cammi, R.; Ochterski, J. W.; Martin, R. L.; Morokuma, K.; Farkas, O.; Foresman, J. B.; Fox, D. J. Gaussian˜16 {R}evision {C}.01. 2016.

(294) Petersson, G. A.; Al-Laham, M. A. *J. Chem. Phys.* **1991**, *94* (9), 6081–6090.

(295) Petersson, G. A.; Bennett, A.; Tensfeldt, T. G.; Al-Laham, M. A.; Shirley, W. A.; Mantzaris, J. *J. Chem. Phys.* **1988**, *89* (4), 2193–2218.

(296) Becke, A. D. *J. Chem. Phys.* **1993**, *98* (7), 5648–5652.

(297) Zhao, Y.; Truhlar, D. G. *Theor. Chem. Acc.* **2008**, *120* (1), 215–241.

(298) Adamo, C.; Barone, V. *J. Chem. Phys.* **1999**, *110* (13), 6158–6170.

(299) Yanai, T.; Tew, D. P.; Handy, N. C. *Chem. Phys. Lett.* **2004**, *393* (1), 51–57.

(300) Vydrov, O. A.; Scuseria, G. E. *J. Chem. Phys.* **2006**, *125* (23), 234109.

(301) Chai, J.-D.; Head-Gordon, M. *Phys. Chem. Chem. Phys.* **2008**, *10* (44), 6615–6620.

(302) Wachters, A. J. H. *J. Chem. Phys.* **1970**, *52* (3), 1033–1036.

(303) Dunning, T. H. *J. Chem. Phys.* **1989**, *90* (2), 1007–1023.

(304) Tomasi, J.; Mennucci, B.; Cammi, R. *Chem. Rev.* **2005**, *105* (8), 2999–3094.

(305) Bang, E.-K.; Gasparini, G.; Molinard, G.; Roux, A.; Sakai, N.; Matile, S. *J. Am. Chem. Soc.* **2013**, *135* (6), 2088–2091.

(306) Padilla, M. S.; Farley, C. A.; Chatkewitz, L. E.; Young, D. D. *Tetrahedron Lett.* **2016**, *57* (42), 4709–4712.

(307) Canaria, C. A.; Smith, J. O.; Yu, C. J.; Fraser, S. E.; Lansford, R. *Tetrahedron Lett.* **2005**, *46* (28), 4813–4816.